Università degli Studi di Cagliari

DOTTORATO DI RICERCA
SCIENZE E TECNOLOGIE CHIMICHE
Ciclo XXIX

FROM OXYGEN TO SELENIUM: NOVEL NEUTRAL RECEPTORS FOR ANION RECOGNITION AND SENSING

CHIM/03 Chimica Generale e Inorganica

Presentata da:	Arianna Casula
Coordinatore Dottorato	Prof. Stefano Enzo
Tutor	Prof.ssa Claudia Caltagirone

Esame finale anno accademico 2015 – 2016
Tesi discussa nella sessione d'esame marzo – aprile 2017




Università degli Studi di Cagliari

Università degli Studi di Sassari

DOTTORATO DI RICERCA

SCIENZE E TECNOLOGIE CHIMICHE

Ciclo XXIX

FROM OXYGEN TO SELENIUM: NOVEL NEUTRAL RECEPTORS FOR ANION RECOGNITION AND SENSING

CHIM/03 Chimica Generale e Inorganica

Presentata da:	Arianna Casula
Coordinatore Dottorato	Prof. Stefano Enzo
Tutor	Prof.ssa Claudia Caltagirone

Esame finale anno accademico 2015 – 2016

Tesi discussa nella sessione d'esame marzo – aprile 2017

Ho perso un pò la vista, molto l'udito. Alle conferenze non vedo le proiezioni e non sento bene. Ma penso più adesso di quando avevo vent'anni. Il corpo faccia quello che vuole. io non sono il corpo: io sono la mente.

Rita levi Montalcini

Impara da ieri, vivi oggi, spera per domani; la cosa più importante è non smettere mai di porti domande.

Albert Einstein

Io sono tra quelli che pensano che la Scienza abbia una grande Bellezza. Uno scienziato nel suo laboratorio non è solo un tecnico: è anche un bambino posto di fronte a fenomeni naturali che lo appassionano come un racconto di fiabe.

Marie Curie

Acknowledgements

Molte persone hanno preso parte a questo percorso appena concluso.
Il primo Ringraziamento va al mio Supervisore, la Prof. Claudia Caltagirone.
Tante sono le tappe importanti degli ultimi anni che a Lei si possono collegare: Il primo laboratorio all'inizio dell'Università, la prima Tesi, le prime informazioni per l'Erasmus, le prime Conferenze, le prime esperienze all'estero e infine il Dottorato.
Grazie per il supporto, la fiducia, la professionalità e l'incoraggiamento dimostrati in questi anni.
Per essere sempre stata un punto di riferimento stabile nel mio percorso, nei momenti di incertezza (benedetto selenio!) così come per i primi traguardi raggiunti; per essersi dimostrata non solo un competente e brillante capo, ma anche all'occorrenza una valente motivatrice (dai che abbiamo quasi finito!), un coach (dai che siamo nei tempi giusti!) e spesse volte anche un'ottima ascoltatrice per gli svariati dubbi e preoccupazioni!
Sicuramente è stata colei che più di tutti mi ha vista crescere sia come chimico che come persona nel corso di questi anni universitari. Grazie per tutto!

Come non ringraziare i Dottori Alessandra Garau, Greta De Filippo, Riccardo Montis e Alexandre Bettoschi sempre disponibili ogni volta che ne avevo bisogno.
Per aver preso parte costantemente al mio percorso con quel consiglio in più che fa la differenza, per gli incoraggiamenti, le critiche costruttive, per le esperienze condivise e per aver contribuito attivamente ognuno a proprio modo a farmi maturare come chimico e non solo.

Vorrei ringraziare inoltre il Prof. Guido Ennas per i tanti suggerimenti e incoraggiamenti di questi mesi, il Dott. Mariano Andrea Scorciapino per il suo prezioso aiuto in diverse fasi del progetto, per la sua capacità nel

trovare sempre l'esperimento NMR giusto che salvava la situazione e per i suoi immancabili "Vai Tranquilla che risolviamo!".

Un doveroso grazie ai Prof. Vito Lippolis e Francesco Isaia per la costante presenza nelle varie fasi del progetto, per le continue idee su come migliorarlo, per la professionalità e la disponibilità dimostrate.

Inoltre vorrei ringraziare il Prof. Simon J. Coles, i Dottori Peter Horton e Lucy Mapp (University of Southampton, UK), il Prof. Alexander Blake (University of Nottingham, UK) e il Prof Maciej Kubicki (Mickiewicz University, Poland) per le misure cristallografiche, il Prof. Claudio Santi (Università degli Studi di Perugia) per le misure NMR sul Selenio e la Prof.ssa Carla Bazzicalupi (Università degli Studi di Firenze) per i calcoli computazionali.

Un ringraziamento va anche a tutte le persone con le quali ho condiviso le giornate di laboratorio; al Sig. Antonio Sabeddu che ha costantemente fornito una colonna sonora diversa per ogni giorno dell'anno, per il suo immancabile aiuto e il buonumore contagioso; agli studenti e colleghi che hanno contribuito a questo lavoro di tesi e a tutte le persone con le quali ho lavorato in questi anni, in particolare Giada, Giulio, Marco e Giacomo, per aver contribuito a rendere unica ogni giornata passata in laboratorio.
Quante rassegne stampa, critiche cinematografiche, discorsi esistenziali, sedute dallo psicologo, coreografie e risate tra quelle mura!

Difficile trovare un gruppo di Ricerca migliore con il quale poter lavorare.

Sevilla, Sevilla de mi mi corazón! Quiero enviar un agradecimiento especial al grupo de investigación del Profesor José María Fernández-Bolaños Guzmán de la Universidad de Sevilla.
Gracias de corazón al Profesor Fernández-Bolaños, a la Profesora Inés Maya Castilla y al Dr. Oscar López-López por haberme permitido trabajar en su laboratorio, por haberme guiado paso a paso en cada fase del

proyecto con gran profesionalidad haciéndome sentir desde el principio una más del grupo. Gracias por ser no sólo óptimos jefes, sino además personas maravillosas.

Gracias a todas las personas con las que he compartido el laboratorio en Sevilla. A Paloma por su paciencia en enseñarme poco a poco los trucos de la química orgánica y responder cada vez a mis numerosas dudas y Lucía por sus diarias mini clases de español y por las risas en el laboratorio.
Un agradecimiento especial a Badi, Nazaret y Juan Carlos que desde el primer día me han ayudado siempre en todo; por haberme mimado con todas las delicias epañolas y marroquíes y haberme enseñado las maravillas de la ciudad; por haberme hecho sentir como en casa y por habernos hecho grandes amigos en tan poco tiempo.

Siempre en España, quiero agradecer al Profesor Ramón Martínez-Máñez de la Universidad Politécnica de Valencia y a su grupo de investigación, y en especial al Dr. Félix Sancenón Galarza.
Gracias por haberme permitido formar parte de vuestro prestigioso grupo de investigación y haberme provisto de todos los medios necesarios para llevar a cabo my proyecto.
Un agradecimiento especial a Toni, Maria Elena, Tania, Andy e Sameh, con los cuales he tenido la oportunidad de estar más tiempo durante mi estancia en Valencia. Gracias por la ayuda en el laboratirio, por los consejos y por la disponibilidad.

Un doveroso grazie ai miei compagni di avventure e disavventure di questo XXIX ciclo di Dottorato, Valentina, Nicola, Ilaria e Federica. Tra le mille scadenze, presentazioni, imprevisti, complotti e tanto altro, quanti attacchi d'ansia e quante risate abbiamo condiviso tutti insieme! Team che vince non si cambia!

Un grazie in più a Vale e Nico per essere stati parte dei "fantastici tre" e a Vale N. per la sua immancabile presenza! Per avermi sostenuta in ogni

momento perché si sa che i problemi diviso quattro si fanno più gestibili; per aver assecondato le mie tante idee sui famosi pranzi a tema, le zippolate, i cluedo, gli all you can eat, le excape room; per avermi riempita di caramelle e cioccolata al minimo segno di stress; per tutte le risate, le confidenze, le cospirazioni e le follie condivise in questi anni.
Non ci sono parole per descrivere la mia gratitudine, non potevo desiderare amici migliori.

Ultimi ma non per importanza i ringraziamenti alla mia Famiglia. Tante cose sono successe in questi anni ma mai il loro sostegno è venuto a mancare.

Grazie per essere da sempre i primi a credere in me.

“La presente tesi è stata prodotta durante la frequenza del corso di dottorato in Scienze e Tecnologie Chimiche dell’Università degli Studi di Cagliari, a.a. 2015/2016 - XXIX ciclo, con il sostegno di una borsa di studio finanziata dall’Università degli Studi di Cagliari con le risorse del P.O.R. SARDEGNA F.S.E. 2007-2013 - Obiettivo competitività regionale e occupazione, Asse IV Capitale umano, Linea di Attività l.3.1 “Finanziamento di corsi di dottorato finalizzati alla formazione di capitale umano altamente specializzato, in particolare per i settori dell’ICT, delle nanotecnologie e delle biotecnologie, dell'energia e dello sviluppo sostenibile, dell'agroalimentare e dei materiali tradizionali”.

Arianna Casula

Abstract

The present PhD thesis is based on the application of Supramolecular Chemistry principles for the design and development of a new series of compounds containing urea and selenourea moieties that can find application as receptors and chemosensor for anions selective detection. The aim of the project was to investigate and study the anion sensing and binding properties of these molecules in the presence of specific target anions of interest. Studies focussed on the possibility to tune the selectivity of these compounds for anions as a function of the different heteroatoms in the urea site, receptor structure steric hindrance and presence of particular activating electron withdrawing substituents.

These molecules were designed with the purpose to create optical systems able to selectively recognize anions in competitive media (like DMSO and pure water) when used as free receptors or embedded into micelles or silica nanoparticles.

Chapter 2 reports the study carried out on the new family of halogenated urea comprising receptors **L_1-L_{15}** with a set of anions of different geometry, size and acid/base nature (AcO^-, HCO_3^-, BzO^-, Cl^- and F^-) (Figure 1). The study was carried out by means of Single Crystal X-Ray diffraction, when possible, and ^{1}H-NMR spectroscopy titrations in DMSO-d_6 in order to verify the affinity of each receptors to these anions. The best results were obtained in the case of receptors **L_1-L_{15}** (in particular for the sensing of acetate) probably due the good combination between the electron withdrawing effect of the nitro group that makes more acidic the NHs protons of the urea group and its *para* position in the phenyl arm which limits the steric impedimental to the anion in the coordination site.

In Chapter 3, a new series of bis-urea receptors **L_{16}-L_{22}** is reported (Figure 2). The binding properties towards different anions ($H_2PO_4^-$, F^-, $HPpi^{3-}$,AcO^-, HCO_3^-, ADP, AMP, ATP, Mal^-, Glu^-, NO_3^-, CN^-, ClO_4^-, Cl^-, BzO^-) were studied by means of ^{1}H-NMR, UV/Visible and fluorescence spectroscopies and a remarkable affinity for phosphate species has been observed especially in the case of **L_{16}-L_{22}**. Indeed,these receptors work as fluorimetric (**L_{18}**) and colorimetric (**L_{21}**) sensors both able to recognize $HPpi^3$, even at naked eye, in DMSO and in pure water environment when they are embedded in CTAB micelles. Theoretical calculations and Single crystal X-Ray Diffraction experiments confirmed the binding properties observed.

Chapter 4 focuses on the comparison between bis-phenylurea and bisphenylthiourea receptors (**L_{23}-L_{24}**) with a new family of selenoureas (**L_{25}-L_{31}**) designed for anion selective recognition (Figure **4**3). The behaviour of these organoseleno compounds in the presence of anion species ($H_2PO_4^-$, AcO^-, Cl^- and BzO^-) was studied by means of ^{1}H-NMR spectroscopy. We investigated how the presence of Selenium atom, steric hindrance of the receptor and typology of anion used can affect the behaviour of the system leading to the formation of bi-coordinated and mono-coordinated host:guest adducts via hydrogen bond.

Finally, inspired by the interesting results obtained in Chapter 4, we decided to test the applicability of selenoureas **L_{26}**, **L_{27}** and **L_{32}** as optical sensors for anions (Figure 4). The study was carried out using an anionic set also including nucleophilic species (S^{2-}, CN^-, AcO^-, SO_3^{2-}, F^-, HCO_3^-, HSO_4^-, $H_2PO_4^-$, NO_3^-, Br^-, I^- ,ClO_4^-, BzO^-, OH^-, SCN^-, and Cit^{3-}) in order to verify the possibility to use these molecules as chemosensors. By means of ^{1}H,^{13}C and ^{77}Se-NMR, UV/Visible and fluorescence spectroscopies, and ESI-MS spectrometry a significant affinity for CN^- and S^{2-} species was found for receptor **L_{32}**. This molecule can be defined as the first example of a selenourea useful for both colorimetric and fluorimetric

anion sensing. This system acts as chemodosimeter for CN^- and S^{2-} in H_2O/MeCN 75:25 (v/v) and an increasing of the selectivity towards S^{2-} with respect to CN^- has been observed when it was imbedded into MCM-41 nanoparticles. In this case, **L_{32}** works as an ON-OFF fluorescent chemosensor for S^{2-} recognition in pure water.

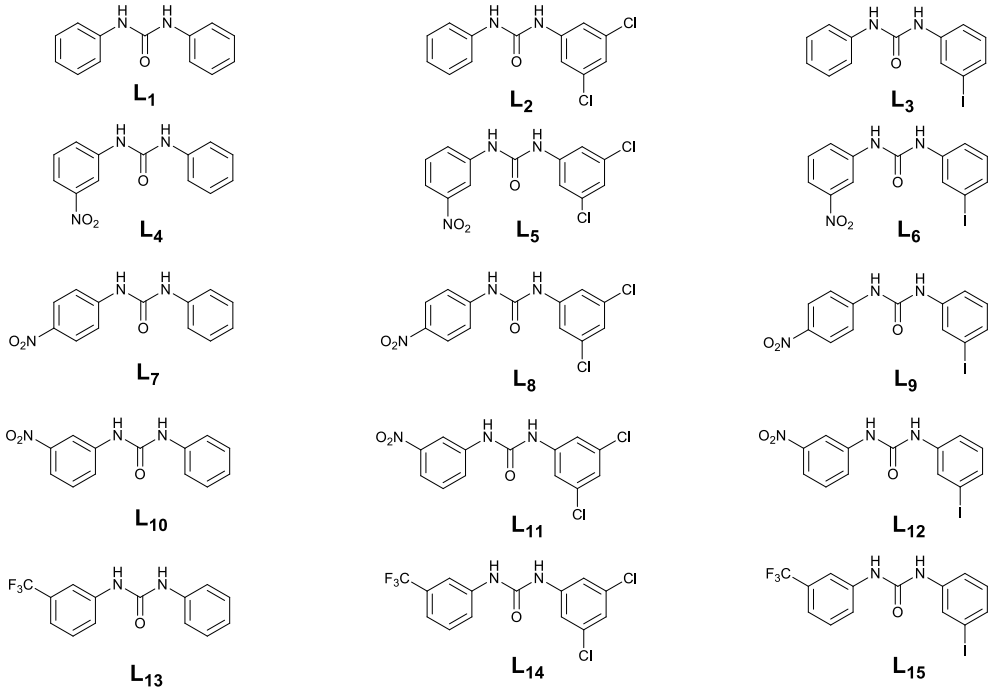

Figure 1 Summary of Receptors **$L_{1\text{-}15}$** studied in Chapter 2.

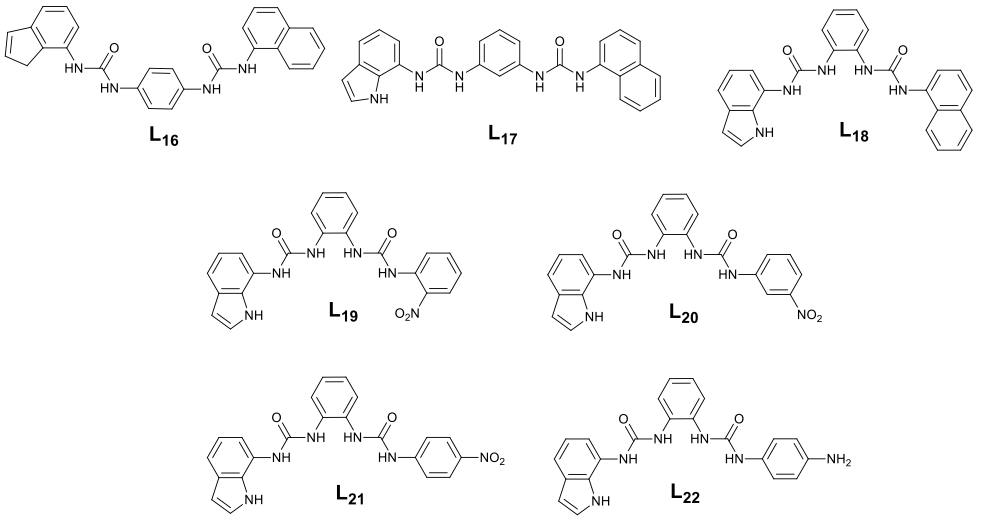

Figure 2 Summary of Receptors **$L_{16\text{-}22}$** studied in Chapter 3.

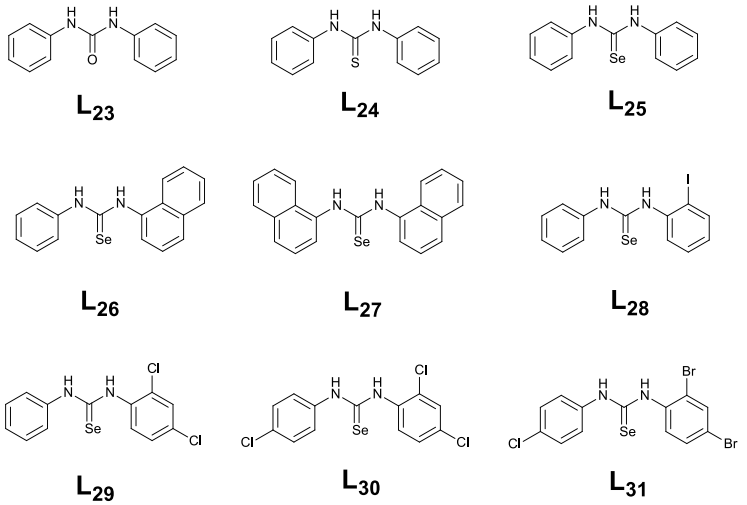

Figure 3 Summary of Receptors **$L_{23\text{-}31}$** studied in Chapter 4.

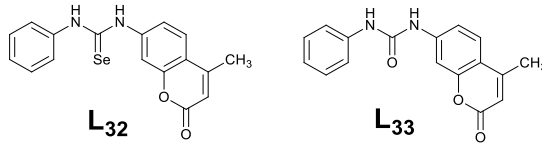

Figure 4 Summary of Receptors **$L_{32\text{-}33}$** studied in Chapter 5.

Contents

Chapter 1:

Introduction

1. Introduction

1.1 Supramolecular Chemistry

Supramolecular Chemistry is a significant area of the modern research that quickly developed in the last decades because of its multidisciplinarity involving chemistry, biology and physics.

The time line of Supramolecular chemistry roots can be collocated in the 19th century when important discoveries were the first signals of the existence of internal non-covalent interactions (Supramolecular interactions) between molecules. In 1893 Alfred Werner (Nobel Prize in 1913) introduced for the first time the concept of Coordination Chemistry [1,2] and in 1894 Emil Fisher (Nobel Prize in 1902) was able to explain the particular and specific interactions between enzyme and substrate with his new "Lock and Key" model.[3] Basically, this principle is based on the perfect complementary in terms of shape, size and geometry between an enzyme and a substrate that leads to a very specific interaction. Paul Ehrlich used this model in 1906 when he introduced the concept of biological receptor [4] and when James Watson and Francis Crick in 1953 discovered the double helix structure of DNA [5] originated from very specific hydrogen bonds connecting two strands of purine and pyrimidine bases, it was clear the importance of intermolecular forces in chemical and biological process.

Following these new discoveries, D.J. Cram,[6] C.J. Pedersen [7] and J.M. Lehn [8] in 1987 won the Nobel Prize for their pioneering job in this new area of chemistry. Furthermore, the Nobel Prize in Chemistry 2016 was awarded jointly to Jean-Pierre Sauvage, Sir J. Fraser Stoddart and Bernard L. Feringa for the design and

synthesis of molecular machines that we can consider another concrete application of the Supramolecular Chemistry principles.[9]

The result of these contribution led to a the first official definition of Supramolecular Chemistry as "the Chemistry of molecular assemblies and of intermolecular bond" [10] as "a chemistry beyond the molecule, bearing on the organised entities of higher complexity that result from the association of two or more chemical species held together by intermolecular forces" [11] such as H-bonding, hydrophobic interactions, π-π stacking and specific coordination properties of metal cations or metal complexes.

The consequence of the selective non-covalent interaction between receptor and substrate (host-guest interaction) is a new species called supramolecule with different structure and physical-chemical properties with respect to the two components.

Therefore, molecular recognition may be defined as the specific binding of a guest molecule with a host compound forming a host-guest complex (supramolecule) through non-covalent interaction.[12]

The key concepts in all fields of development in Supramolecular chemistry can be summarized in:

a) *Host-Guest complexation*: the interaction between host and guest entities required high degree of complementary in terms of shape, size and geometry.[13,14,15] The Host molecule generally presents convergent binding sites (hydrogen bond donor groups, Lewis bases) and cavity or pseudo cavity of adequate dimension and shape to accommodate a small guest molecule that, as opposed, shows divergent binding sites (hydrogen bond acceptor groups, Lewis acids).

b) *Templating, Molecular self-assembly and self-organization*: Templating refers to a synthetically efficient technique that uses a temporary or permanent inorganic or organic "helper" for the stepwise assembly of Supramolecular structures of higher complexity. [16] Self-assembly and self-organization are processes reversible and spontaneous, in which molecules interact with each other through non-covalent interaction and without external stimuli in order to form the supramolecule.

c) *Crystal engineering:* "the understanding of intermolecular interactions in the context of crystal packing and in the utilisation of such understanding in the design of new solids with desired physical and chemical properties". [17,18]

d) *Supramolecular transport:* it is the process that, taking advantage of host-guest recognition, permits the selective transport of a substrate from an aqueous source phase to an organic phase containing the appropriate receptor through a membrane. [19] In this sense the receptor may act as a mobile carrier for particular substrate target and this fact has a remarkable importance in lot of fields, particularly In biomedicine.

e) *Supramolecular sensors and devices:* they are system composed by a receptor, a possible spacer unit and a photoactive o redox-active group. The molecular recognition between the receptor and a specific substrate leads to a variation in the physical and/or chemical properties of the active unit. Therefore, the molecular sensor can translate the complexation event in a detectable analytical signal (change in pH, fluorescence or UV/Visible variation or electronic distribution). Examples of molecular devices are

"molecular machines" [20] able to perform easy mechanical movements and chemosensors. [21]

1.2 Anions recognition

The development of new receptors, sensors and transporters for anionic species results to be a rich area of research in Supramolecular chemistry due the ubiquitous role of the anion species in a lot of fields such as biology, industry, environment and medicine. [22,23]

They are essential for life because they are involved in almost every biochemical processes. Important biological molecules such as DNA or RNA are polyanionic at physiological pH. Phosphates, for example, are constituents of membrane lipids and are involved in many biological processes such as energy storage, gene regulation, muscle contraction, and signal transduction. [24,25] Bicarbonate and chloride take active part in the anion flux across cell membranes and the interruption of this flux can increment disease like cystic fibrosis, Dent's disease or osteoporosis.[26,27,28]

Fluoride plays an important beneficial aspect in dental health (fluoride containing toothpaste), but over exposure to fluoride (fluorosis) can have detrimental effects such as kidney failure and debilitating skeletal defects. [29]

In general, the constant monitoring of the anion cellular concentration is essential for the osmotic pressure regulation, signal transduction pathways activation and in the production of electrical signals.

Many anions, such as chromate, arsenate, nitrate, perchlorate, sulphate and sulphide, are included in the "Priority Pollutant list" reported by the European Community as they cause pollution problems in the environment. Nitrate and

phosphate, which are commonly used as fertilizers, can cause the eutrophication of the water while other anions are components of pesticides or they are part of industrial or nuclear fuels.

Because of the importance of the anionic species, it is clear why the development of new receptors, sensors and transporters for anion targets continues to be a research area of constant interest.[30,31,32,33]

However, the design of anion receptors is more complicated with respect to the metal ions analogue due to some of their properties:

a) *Size*: anions are larger than their isoelectronic cations therefore the receptor must be designed to have a cavity suitable for the size of the target anion. (Table 1.1)

Table 1.1 Comparison of the radii of isoelectronic cations and anions

Cation	Radius Å	Anion	Radius Å
Na^+	1.16	F^-	1.19
K^+	1.52	Cl^-	1.67
Rb^+	1.66	Br^-	1.82
Cs^+	1.81	I^-	2.06

b) *Charge*: Generally, they show a low charge to radius ratio that involves in a less functional electrostatic binding interaction than covalent bond established with the cations.

c) *Geometry*: anions have a wide range of shape and geometry that must be considered in the receptor design phase in order to guarantee the high degree of complementary between host and guest. (Figure 1.1)

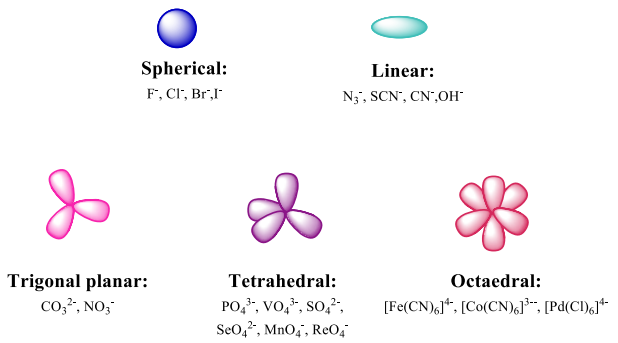

Figure 1.1 Geometries of anions

d) *pH dependence*: the anions negative charge can be influenced by variation of pH (because at low pH they can be protonated). For this reason the receptor must be able to work within the specific pH range of the anion target that they want recognise.

e) *Solvent*: the nature of the solvent plays a central role in the anion recognition. Anion binding is based on electrostatic interactions that occur between the receptor and the anion. However, this type of force can occur also between the solvent and the anion so an ideal receptor must compete with the solvent environment and with the counter cation too. For example, neutral receptor that only bind anion through hydrogen-bond interactions will be more competitive in aprotic organic solvent. In fact, protic solvent can establish strong hydrogen bonds with the anion and the receptor must compete with them to bind the anion and take their place.

f) *Hydrophobicity*: Following the Hofmeister series (Figure 1.2) it is clear that an increase of the anion hydrophobicity corresponds to a decrease of its aqueous solvation. Hydrophobic anions are generally bound more strongly in hydrophobic binding sites with respect to the hydrophilic ones and it is true the opposite combination (Hydrophilic anions in hydrophilic binding sites).

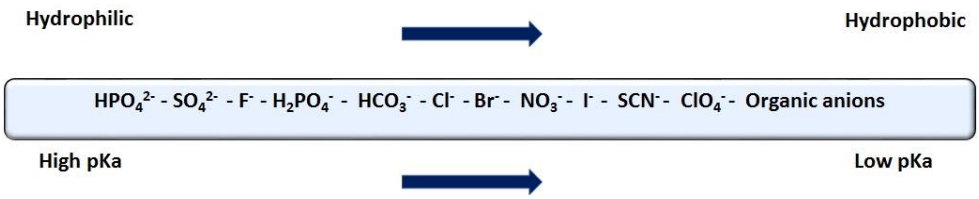

Figure 1.2 Hofmeister series

In order to design and synthesize a selective anion receptor, all the mentioned factors must be taken into account. Therefore, the choice of the noncovalent interaction used to complex the anion results to be very important in the design of the receptor. These interactions include basically electrostatic interactions, hydrogen bonding, halogen bonding, Lewis acids and a combination of these interactions.

The easiest way to bind an anionic species is to introduce one or more positive charge in the receptor structure to bind the anion target through ***electrostatic interactions.*** More positive is the charge of the system and, in theory, more strong and effective these interaction should be. However, the fact of introducing lot of charged groups can became a problem if these charges start to repel one other. To avoid this situation, in general, rigid moieties or cyclic units are widely used.

Another common way to complex anion targets is to use the ***hydrogen bonds***. Anions can be considered as electron pair donors and they interact with electron pair acceptors such as electron-positive hydrogen atom forming a hydrogen bond. Functional groups with this property are for example N-H or O-H widely employed in urea, amide or alcohol based receptors. If we substitute, as electron pair acceptors, the electron positive hydrogen atom in the hydrogen bond with a halogen atom, the resulting interaction is called ***halogen bond.*** Both in the case of hydrogen bond and halogen bond, it is very common to design receptor systems that show hydrogen or halogen atoms orientated in a correct, convergent manner to facilitate the complexation of a particular anion target depending on its size and geometry.

Finally, another way to bind anions is to use metal ions, which work as ***Lewis acids***. These electro-deficient groups are able to accept electron pairs from an anionic guest into their vacant orbitals.

All these kind of interactions can be used together in a synergic way to produce a very selective and efficient receptor for anions.

1.3 Classification of anion receptors

On the basis of the type of interactions previously mentioned, anion receptors can be divided into three groups:

a) Charged anion receptors*:*
   - *Ammonium based receptors*
   - *Guanidinium based receptors*
   - *Imidazolium and triazolium based receptors*

b) Neutral anion receptors*:*
   - *Amide based anion receptors*
   - *Urea and thiourea based anion receptors*

- *Alcohol based anion receptors*
- *Indole and pyrrole based anion receptors*

c) Metal and Lewis acid receptors

1.3.1 Charged anion receptors

As anions are negatively charged, an intuitive way to bind them is employ particular receptor systems that contain a positively charged unit like ammonium, guanidinium or imidazolium groups.

Ammonium based anion receptors

The ammonium groups have been widely used in the anion recognition chemistry. Ammonium based receptors can be easily generated via protonation of amines and they have the advantage that their synthesis show a wide range of synthetic pathway, allowing for a considerable diversity in terms of shape, size and charge.

Generally they show an efficient capacity to bind anion in organic an aqueous environment as a results of a combination of electrostatic and hydrogen-bond forces.

Bencini, Lippolis and co-workers have explored the effect of the aromatic linker between two [9]aneN_3 ammonium units in receptors **1**–**3**.[34] In aqueous environment these units are protonated and can interact with anions via hydrogen bonding and electrostatic interactions. By means of ^{1}H NMR and ^{31}P NMR measurements and potentiometric titrations, it was found that the three receptor have a selectivity for different anions. **1** shows an affinity for the selective recognition of triphosphate while **2** selectively binds diphosphate and **3** monophosphate in aqueous solutions over a wide pH range. These differences in selectivity can be attributed to the distance between the two macrocyclic units

depending on the dimension of the spacer unit in 1–3. Furthermore, **1** and **2** are also able to interact with the nucleotides ATP (adenosine triphosphate) and ADP (adenosine diphosphate) over inorganic phosphate species. **1** shows the highest associations with ATP and ADP probably due the presence of π stacking and hydrophobic interactions with the adenine units of the receptor.

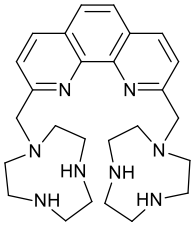

1

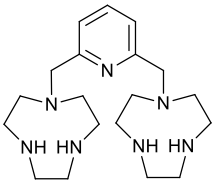

2

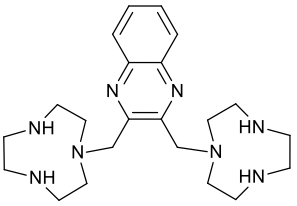

3

Bowman-James and co-workers studied the role of the positive charge on anion selective recognition in amide-amine based macrocyclies **4**-**9** by means of ^{1}H-NMR spectroscopy and X-Ray crystallography. [35]

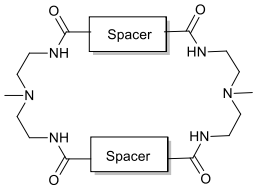

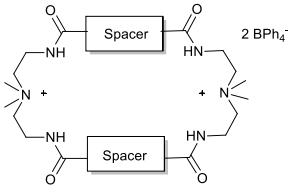

4

5

6

7

8

9

The ^{1}H-NMR titrations performed in DMSO-d_6 showed that charged receptors **7-9** revealed a higher affinity for anion species than the neutral precursors **4-6**.(Table 1.2).

Table 1.2 Binding constants Ka/M^{-1} of receptors 4-9 in DMSO-d_6 at 25°C. Receptors 7, 8, 9 are in the form of BPh_4^- salts.

Anions	**4**	**5**	**6**	**7^{2+}**	**8^{2+}**	**9^{2+}**
Cl^-	25	490	20	1700	56230	130
Br^-	20	515	<10	140	23990	>10
I^-	<10	<10	<10	100	160	>10
$H_2PO_4^-$	830	10 960	100	10 960	208 900[b]	900
HSO_4^-	795	107	<10	[a]	7945	1500
NO_3^-	<10	<10	<10	45	210	<10
ClO_4^-	<10	<10	<10	40	250	<10

[a] calculation complicated due to peak broadening after the addition of anion.
[b] At the upper limits for NMR determination.

The binding constants were obtained principally fitting the ^{1}H NMR curve with 1:1 binding stoichiometry apart from those for dihydrogen phosphate and hydrogen sulphate. The values reported in Table 1.2 indicate that the pyridine based receptor have a higher affinity in general than receptors with m-xylyl or thiophene spacer. This evidence may be attributed in part, to the pre- organising influence of pyridine moiety on the amide NH protons forming a cavity suitable for anion complexation.

X-Ray crystallography confirmed this evidence. In the structure of $\mathbf{7}^{2+}$ with chloride and hydrogen sulphate the anion is located outside the macrocyclic cavity and it interacts with only one amide NH proton while in the structure $\mathbf{8}^{2+}$ with iodide, the anion specie is coordinated by both amide NH groups around the pyridine fragment (Figure 1.3).

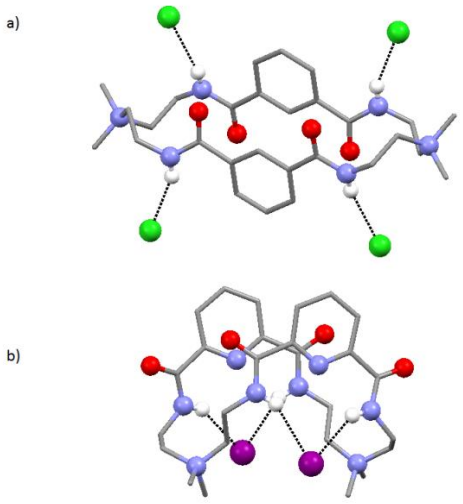

Figure 1.3 (a) Crystal structure of receptor $\mathbf{7}^{2+}\cdot 2Cl^{-}\cdot 2\cdot 66H_2O$. (b) Crystal structure of $\mathbf{8}^{2+}\cdot 2I^{-}\cdot 2H_2O$. Hydrogen bonds are shown as dashed lines while solvent molecules and non-coordinating hydrogens are omitted for clarity.

Guanidinium based anion receptors

The guanidinium group has several advantages in terms of applicability in the supramolecular chemistry. It common used for the selective recognition of oxo-anions via hydrogen bond and electrostatic interactions. This topic has been reviewed by De Mendoza and co-workers in Chemical *S*ociety Reviews. [36] A very interesting feature of the guanidinium moiety is the high basicity that guarantees that the group remains protonated over a wide pH range (pKa= 13.5).[37] Very

important is also the hydrogen donor sites orientation in the same direction that contributes to increase the selectivity for oxo-anions species.

Schmuck and co-workers have reported the synthesis and the anion binding properties of five new receptors **10-14** containing a guanidiniocarbonyl pyrrole moiety and a primary ammonium cation connected by flexible chain linkers .[38] The binding properties of **10-14** were studied by means of UV/Vis titrations in buffered water at pH 6 containing 10% DMSO with some N-acetyl amino acid carboxylates (Ala, Phe, Val, Glu, Asp) as well as sulfate and acetate. This study proved that a minimum linker length of four carbons is necessary to allow efficient anion binding by both positive charges. In fact, moving from the shortest bis-cations receptor to the longer receptor **12**, the stability constant for Phe increases from Ka = 1400 M^{-1} to Ka = 10 700 M^{-1} (for **10** and **12** respectively). For **13** and **14** the stability constants have a decrease with the same substrate (Ka = 4700 and 1850 M^{-1} for **13** and **14** respectively). This trend shows that not only unspecific Coulombic forces are involved in the complexation process but also specific ion pair interaction based on geometry and space orientation between receptor and anion target play a key rule.

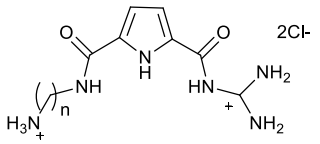

10 n= 2
11 n= 3
12 n= 4
13 n= 5

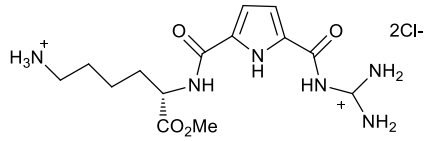

14

Kilburn and co-workers have reported the synthesis of new guanidinium receptors **15–17** as their hexafluorophosphate salts.[39] These receptors were

studied by ^{1}H-NMR spectroscopy and ITC (Isothermal calorimetry) using tetrabutylammonium acetate as anion target in DMSO. It was impossible calculate stability constants by ^{1}H-NMR technique due the broadening of the NH protons but stability data of 6900, 5300 and 22 000 M^{-1} for **15** , **16** and **17** respectively were founded for the complex with acetate by ITC measurements. The study showed that compound **17** has a remarkable affinity to recognize acetate anion compared to the other receptors due to, presumably, the presence of the pyridine moiety that causes a higher degree of pre-organisation in this system.

17 was also performed by ITC in 10% water-DMSO mixture and 30% water-DMSO mixture giving stability constants for acetate of 3900 and 480 M^{-1} respectively.

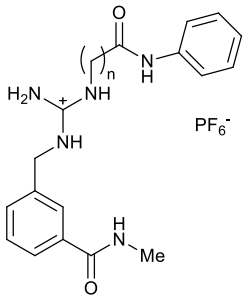

15 n= 1
16 n= 2

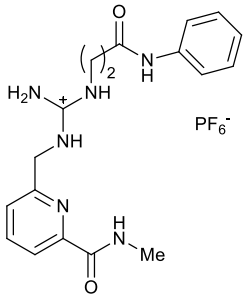

17

Imidazolium and triazolium based anion receptors

Imidazolium groups takes advantage in terms of anion complexation, of the presence of CH moieties which allow the combination of electrostatic interaction and $^{+}CH\cdots A^{-}$ hydrogen bond instead the commonly $^{+}NH\cdots A^{+}$ hydrogen bond. This fact comports a very useful feature, namely pH-independent binding. Kim and co-authors have reported the synthesis and the anion properties of the

imidazolium–anthracene cyclophane based receptor **18**. This system is able to recognize in an efficient way GTP (Guanosine-5'-triphosphate), a very important biological target, and I- over other anions in a 100% aqueous solution of pH 7.4 via fluorescence quenching. [40]

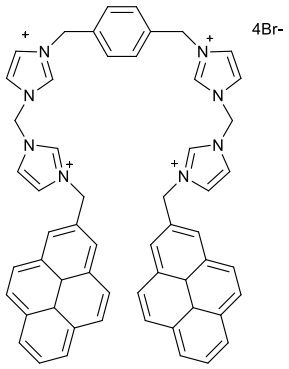

18

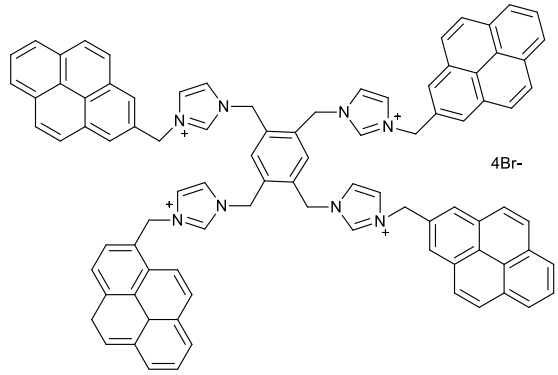

19

These performances can be attributed to the strong $^{+}CH\cdots A^{-}$ hydrogen bond. Recently, Yoon and co-workers described the first example of imidazolium-based fluorescent receptor **19** for Dmyo-inositol1,4,5-trisphosphate(IP_3).[41] The selective recognition of IP_3 is very interesting due the important role played by this specie as a secondary messenger in intracellular signal transduction events. The interaction between **19** and IP_3 leads to a dramatic quenched of the excimer emission of **19** (486nm) in DMSO− HEPES buffer (1:9, v/v) environment. This evidence can be attributed to the formation of a 1:1 complex with IP_3 while other phosphorylated species (pyrophosphate, ATP, and other IP compounds for example) did not induce a significant change in the emission.

Flood and co-workers synthesized the PMMA copolymer **20** with triazole containing appendages capable of binding anions through C−H···anion hydrogen bonding. [42] ^{1}H NMR experiments in $CDCl_2$ showed that **20** is able to extract selectively tetrapropylammonium chloride from water to dichloromethane more effectively than a pure PMMA polymer. This affinity probably originated from the hydrogen bonding to the triazole CH, which is strongly polarized due to the presence of the three nitrogen atoms in the ring and therefore serves as a good hydrogen bond donor.

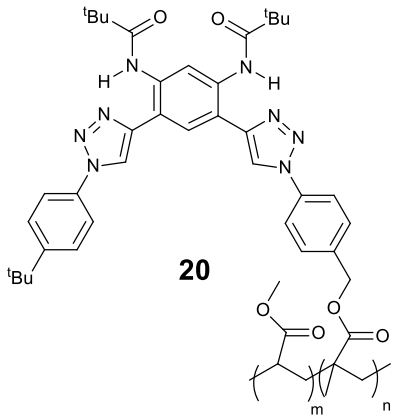

20

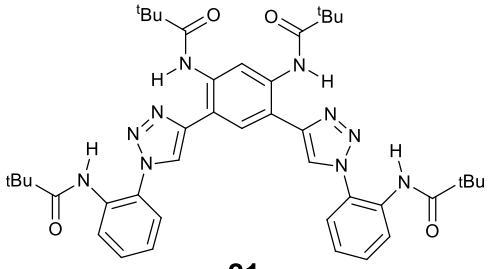

21

Another triazole based foldamer receptor **21** was reported by Shang et colleagues. [43] ^{1}H NMR titrations with TBA chloride in CD_2Cl_2 showed that **20** can recognize chloride anions via CH hydrogen bonding to the triazoles, but the amide functionalities were found not to participate in the anion binding event. Moreover the chloride transport ability of this receptor was investigated using the halide-sensitive dye lucigenin encapsulated in EYPC (L-α-phosphatidylcholine) vesicles and confirmed the chloride transport ability of **21**. A mobile carrier mechanism was suggested by the absence of conductance signals in patch clamp experiments.

1.3.2 Neutral anion receptors

Amide based anion receptors

Thordarson and co-workers have reported the synthesis of pyromellitamide **22**. [44] This molecule is able to form one dimensional columnar stacks in solid state through hydrogen-bonding network. **22** was performed in acetone-d_6 and the study showed a capacity of bind different small anions with the binding strength decreasing in the order chloride > acetate > bromide > nitrate ≈ iodide with 2:1 complexes forming with negative cooperativity. The receptor forms self-assembled gels in non-polar solvents presumably through the same hydrogen-bonding network of the solid state. The interaction between the receptor and the anion guest led to the dissociation of the gel. The time it takes for anions to collapse the gel correlates qualitatively with the anion affinity trend reported above: chloride led to the fastest collapse (within a few tens of seconds) and iodide the slowest (up to one hour). These evidences may be probably used in the future in biomedical field.

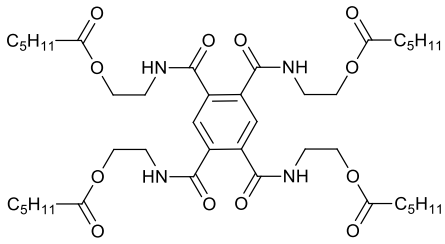

22

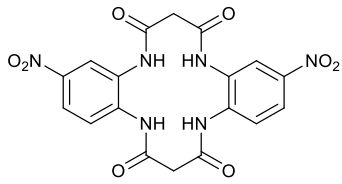

23

Lin and co-workers have designed the receptor **23**. [45,46] This molecule was studied by means of UV-Vis and ^{1}H NMR titration experiments in DMSO or DMSO-d_6 and through theoretical studies. The results of this work showed a high selectivity for the recognition of fluoride anion over acetate, dihydrogen phosphate, chloride, bromide and iodide. Therefore, the recognize process is very interesting because of the colour change of the receptor caused by the interaction with fluoride. The interaction may be attributed to the hydrogen-binding and not to a deprotonation as confirmed by the fact that tetrabutylammonium hydroxide did not involve any change in the colour of the solution of **23**.

Urea, Thiourea based anion receptors

Urea and thiourea groups have been widely studied as anion receptor moieties due their features to provide two hydrogen bond donor that point in the same direction and which are appropriately spacial orientated to interact with a range of anionic target species including Y-shape ones such as nitrates, phosphates and oxo-anions. Their synthetic accessibility and the possibility to tune the NH acidity in an easy way contribute to make these groups very useful in supramolecular chemistry.[47]

Fabbrizzi and co-workers have reported the synthesis and the anion binding properties of simple monoureas **24**-**26**.[48,49,50,51,52] The study of receptor **24** was carried out through UV-Vis experiments in acetonitrile and ^{1}H NMR titrations in DMSO-d_6 and it displayed a remarkable coordination affinity of **24** for oxoanions with the formation of 1:1 complex with benzoate and acetate with good stability constants (log K_a of 6.62 and 6.61 respectively). It is particular the case of fluoride that forms a 1:1 complex with **24** with the higher constant (log K_a 7.38) while the

addition of the second equivalent leads to the deprotonation of **24** and the formation of $[HF_2]^-$.[48,49,50,51,52] This deprotonation is also observed by pale yellow to red colorimetric change that is not observed upon the addition of the other anions tested (AcO^-, BzO^-,$H_2PO_4^-$, NO_2^-, HSO_4^- and NO_3^-) which form hydrogen-bonded complexes. A similar behaviour was observed for the more acid receptor **25** that was deprotonated in acetonitrile by acetate and di-hydrogen phosphate as well as fluoride.[49] These studies have explained the connection between the deprotonation of the receptor and its acidity and the stability of $[HF_2]^-$ species.

To confirm the importance of the tuneable NH acidity in urea groups, Fabbrizzi and colleagues have demonstrated that the bis-naphthalimide receptor **26** in DMSO could be doubly deprotonated by fluoride and hydroxyl groups (blue colour change) but only monodeprotonated by acetate and by an excess of di-hydrogen phosphate (resulting in a red colour) and could not be deprotonated by less basic anions. [50]

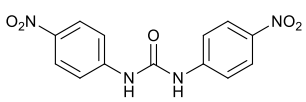

24

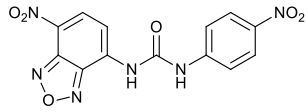

25

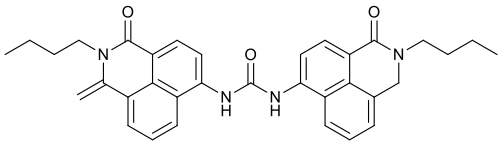

26

Peng and co-workers studied the photophysical properties of a new phenyl urea benzoxazole fluorescent anion sensor **27** obtained by the condensation of 2-(20-aminophenyl)benzoxazole with phenyl isocyanate.[53]

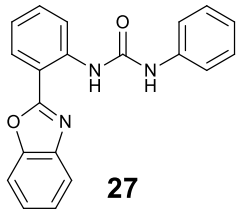

27

The excitation at 336 nm led **27** to an excited-state intramolecular proton transfer (ESIPT) (Scheme 1.1).The emission spectrum shows two bands: a blue fluorescence emission and a yellow fluorescence due to tautomer formation for the ESIPT. In DMSO environment, fluoride causes deprotonation as confirmed by UV-Vis spectroscopy with a formation of a new red-shifted band at 386 nm and fluorescence spectroscopy with the formation of a new band at 495 nm and decrease of the tautomer emission. The disappearance of the urea NH protons in the ^{1}H-NMR spectra has been also displayed. Upon addition of acetate, instead, an isosbestic point at 330 nm is observed. This point indicates the formation of a new coordinated specie formed through via urea NH hydrogen bonds. During the fluorescence titration of **27** with acetate, the spectra show a decrease of the tautomer emission band accompanied by an increase of the normal emission band. This is probably due to a change in conformation of the receptor, i.e. a twist of the phenyl–benzoxazole unit induced by the strong acetate–urea hydrogen bond (Scheme 1.1).

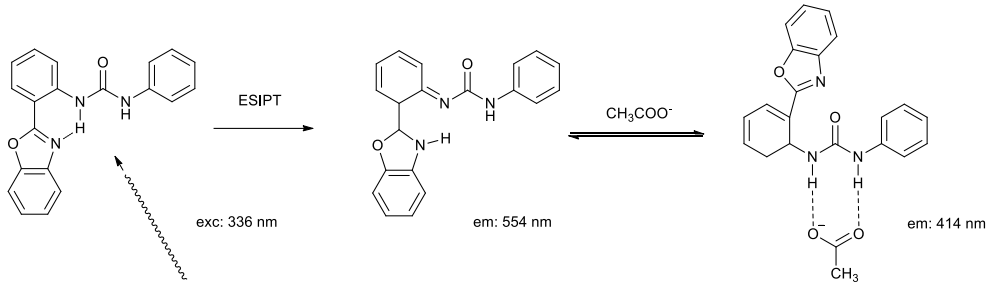

Scheme 1.1 Change in conformation of receptor **27** upon ESIPT and acetate coordination.

The study of **27** with a range of other anions has also been investigated and its result leads to a good affinity for the dihydrogen phosphate that causes changes in the UV-Vis and fluorescence spectrum of the receptor. The absorbance and the blue emission intensities in fluorescence increase upon addition of this anion indicating the formation of the dihydrogen phosphate–urea hydrogen bond complex. The tautomer emission band does not change probably because of the urea NHs and the oxygen of dihydrogen phosphate are not strong enough to compete with the intramolecular hydrogen bonds and to inhibit the ESIPT process.

Gunnlaugsson and co-workers have synthesised urea functionalised phenanthroline receptor **28** that can be used as sensor for the selective recognition of chloride.[54] The anion binding of this receptor was performed in acetronitrile with several anions of different shape and geometry (like fluoride, bromide, acetate and dihydrogen phosphate). Only bromide did not cause any change in the fluorescence properties of **28** while the rest of the anions studied led to a quenching of the emission band of the receptor because of the anion photoinduced electron transfer (PET).

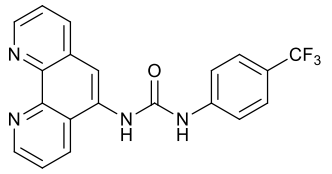

28

Different result were observed for chloride that, instead, caused an increase in the fluorescence emission. The reason of this opposite behaviour can be connected with the spherical shape of chloride. This anion tend to generate a 2:1 complex with **28** respect the common 1:1 complex and this different stoichiometry inhibits the PET quenching from the trifluoro-*p*-tolyl group to the *phen* fluorophore.

Gunnlaugsson and co-workers have investigated the anion recognition capacity of the pyridyl-based bis-amidothiourea **29** to sense AMP and ADP over ATP in DMSO/water (4:1, v/v).[55] This molecule acts as colorimetric sensor (due the presence of two NO_2 moieties) for AMP and ADP but also $HP_2O_7^{3-}$. The interaction between these anion species and **29** results in the formation of a new absorption band at 425nm and a colour change of the solution from colourless to yellow. The authors suggested that both hydrogen bonding and deprotonation are involved in the recognition process. The same group has also improved the performance of this kind of system in aqueous environment synthesizing a similar receptor **28**. The structural differences between **29** and **30** are the presence of two CF_3 groups and a glycol chain in order to improve the solubility in water. Also 30 is able to sense AMP in EtOH/ H2O (1:1, v/v).[56]

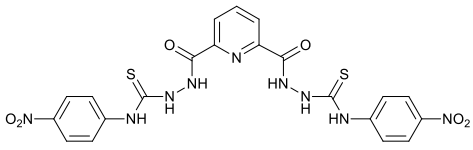

29

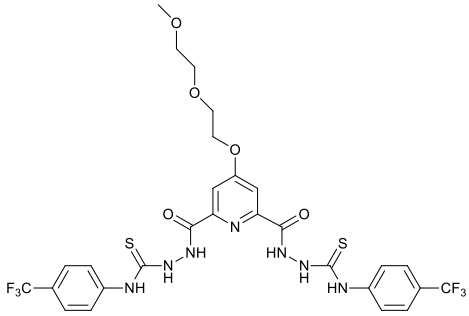

30

Espinosa and Molina have recently reported two new bis-urea based system **31** and **32** for the recognition of $HP_2O_7^{3-}$ designed to be used as chemosensor in competitive media. In particular this study performed the receptors in a mixed MeCN/H_2Omedium.[57]

Receptor **31**, which presents two urea-functionalized arms connected to p-nitrophenyl rings, shows a high affinity for hydrogenpyrophosphate in MeCN/H_2O (70:30, v/v). A modest increase of the absorption bands of the recptor in the region 370−400nm was observed, resulting in a color change from colorless to yellow. System **32** bearing two photoactive pyrenyl rings, acts as a highly selective fluorescent molecular probe for hydrogen pyrophosphate anions in both acetonitrile and in MeCN/H_2O (85:15, v/v). This receptor exhibits three emission bands attributed to the monomer (at 394 and 416 nm) and to excimer emission at (416 nm). Different behaviours in MeCN and MeCN/H_2O (85:15, v/v) are observed. In the first case, the addition of the anion causes the disappearance of the excimer band and simultaneously the intensity increase of the monomer band due the formation of the 1:1 complex. Interestingly, in MeCN/H_2O (85:15, v/v) a strong increase of the excimer emission band is

observed, while the monomer emission bands remain almost unaffected, and the stoichiometry of the complex changes to 1:2.

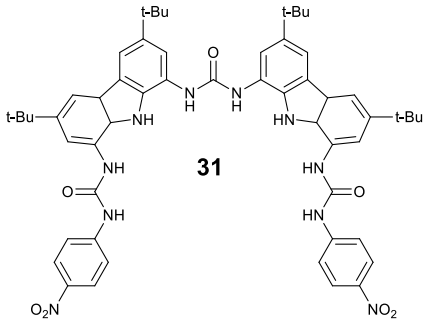

31

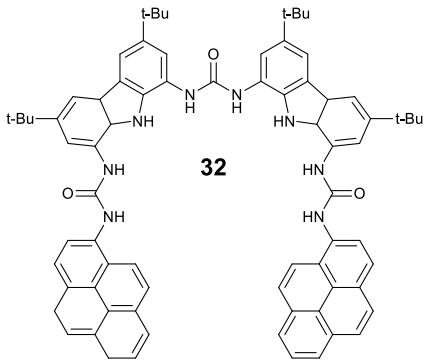

32

Martínez-Máñez and co-workers, in collaboration with Rurack, have investigated the synthesis and the anion complexation properties of two new azo dye derivatives, **33** and **34** containing a urea and a thiourea moiety, respectively. [58]

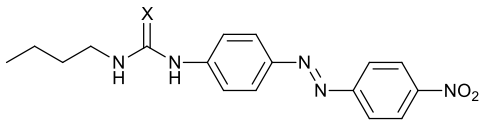

33 X= O
34 X= S

The two receptors displayed an intense yellow absorption band in acetonitrile at around 400 nm attributed to a charge-transfer process from the electron donor groups (urea and thiourea moieties) to the electron acceptor nitro group. The receptors were studied with a set of anions including acetate, benzoate, dihydrogen phosphate, chloride and fluoride. A bathochromic shift of 40 nm was observed for all the anions (exclude fluoride) with a concomitant colour change from yellow to pale orange. For fluoride, instead, a deprotonation was observed through the appearance of an absorption band at 580 nm and a blue colour variation of the solution. The stability constants, calculated by UV-Vis titrations

in acetonitrile are reported in Table 1.3 and as expected high affinities were observed according with the intrinsic acidity of the protons of the binding site and the basicity of the anions.

Table 1.3 Binding constants (M^{-1}) for receptors **33** - **34** measured by UV/Vis titrations.

	AcO^-	BzO^-	$H_2PO_4^-$	Cl^-
33	27100 ± 600	13200 ± 200	3900 ± 300	370 ± 110
34	60000 ± 4000	41000 ± 2000	7400 ± 600	1250 ± 50

Furthermore, receptor **34** can work also as sensor for carbon dioxide. The blue solution of **34** after the interaction with fluoride (deprotonated receptor) turns yellow if left open to the air due to dissolution of carbon dioxide in the solution. Proton NMR studies, carried out in acetonitrile, suggested the formation of a complex in which the thiourea moiety is hydrogen-bonding HCO_3^- formed through a reaction between traces of water and carbon dioxide in the presence of basic fluoride.

Wu and co-workers have synthesized a simple pyridylurea receptor **35**. The main particularity of this system is that it assembles into a hexameric capsule, directed by the coordination of six copper(II) ions, which can englobe sulphate anions with six urea groups.[59] The resulting system sulphate-**35** was generated by the reaction of $CuSO_4$ $5H_2O$ with 3 equivalents of the receptor in DMF. Single crystal X-Ray structure shows the presence of two different kind of copper (II), designated [Cu1] and [Cu2]. The [Cu1] moieties are octahedrally coordinated by six **35** molecules forming two opposing, inversion related C3-symmetric clefts. The sulfate specie is located within a cavity formed by two such complex units and coordinated by six urea groups, and the capsules further extend into a one

dimension chain (Figure 1.4). The [Cu2], instead, are coordinated by two ligands and two DMF molecules in a Jahn-Teller distorted octahedral geometry.

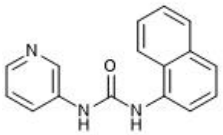

35

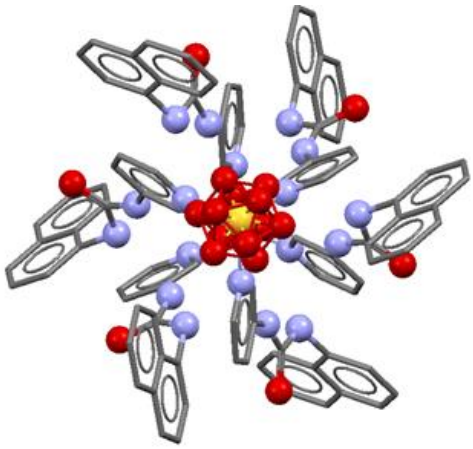

Figure 1.4 Structure of receptor **35** and sulfate encapsulation by multiple hydrogen bonds from six urea moieties in the $[SO_4(\mathbf{35})_6]^{2-}$ capsule (copper ions and hydrogen atoms are omitted for clarity).

Continuing their work on receptors containing multiple urea groups, Wu and co-workers have also reported tetra- and hexa-urea ligands **36** [60] and **37** [61] incorporating repeating bisurea units.

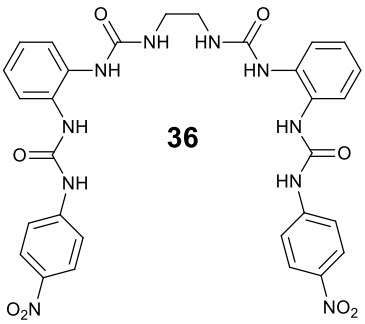

36

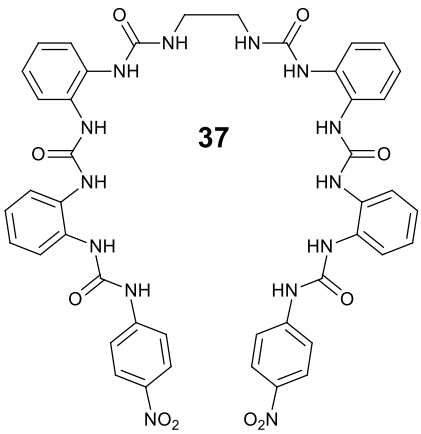

37

The focal aspect of these systems is their spacial disposition in solid state. Receptor **36** displays a dinuclear triple helix structure on coordination of phosphate anions in which three ligands are disposed around two PO_4^{3-} centres (Figure 1.5 a). Each anion unit is bound through twelve hydrogen bonds of three different receptor molecule. On the other hand, in solid state receptor **37** is able to encapsulate a number of different chloride and bromide salts forming different tridimensional structure depending on the counterion of the anion specie studied. A 'molecular barrel' complex was obtained with treatment of **37** with tetraethylammonium chloride (TEACl) (Figure 1.5 b). Two receptors dimerise by weak $CH\cdots O_2N$– hydrogen bond interactions, and two of these associated dimers encapsulate three TEA^+ cations. The urea NH groups point outside the cavity so a number of chloride anions are associated on the external surface of the barrel. Increasing the dimension of the counterion, from tetraetylammonium to tetrapropylammonium, the diameter of the barrel is wider and the length is shorter. However, moving to tetrabutylammonium chloride (TBACl) a helical foldamer-type structure was formed in which one receptor molecule is threaded around two chloride anions.

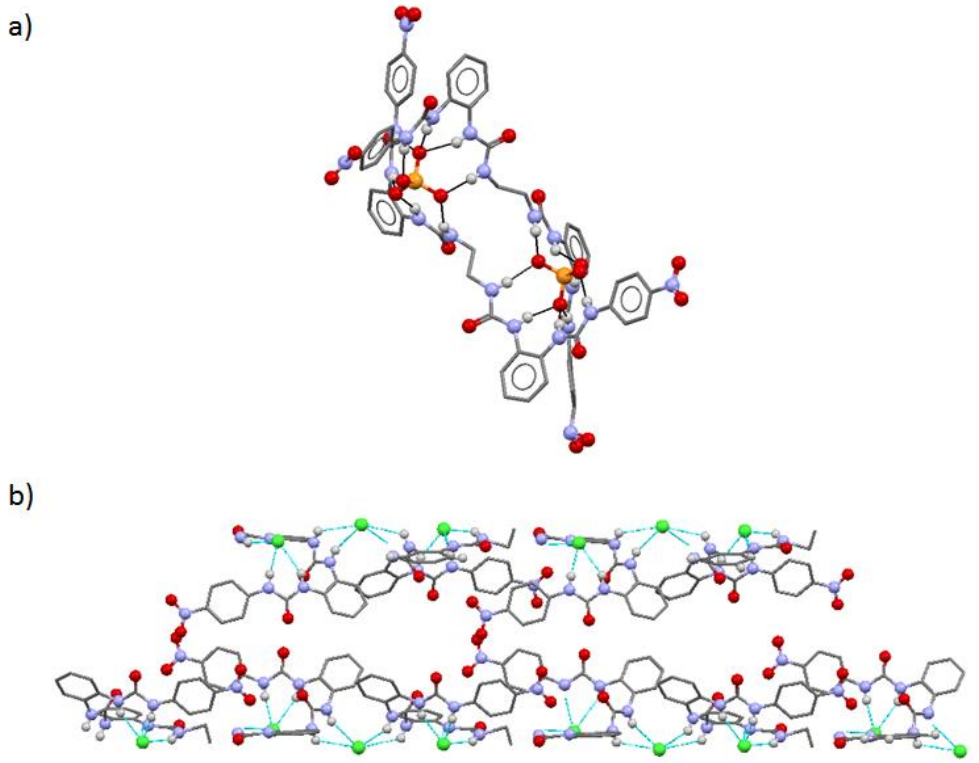

Figure 1.5 Crystal structure of (a) helix formed by receptor **36** and PO_4^{3-}; (b) molecular barrel formed by receptor **37** and Cl^-. Solvent molecules, non-coordinating hydrogen atoms and counterions have been omitted for clarity for both structures.

Costero and co-workers have reported the synthesis and the anion binding properties of homo- and heteroditopic bisthioureas based receptors **38** and **39** designed to binding in a selective way α,ω dicarboxylates.[62] The thiourea derivatives can adopt different conformations in solution as confirmed by NOESY experiments; in particular, **38** assumes the Z,Z conformation, while **39** adopts a Z,E conformation, as shown in Figure 1.6.

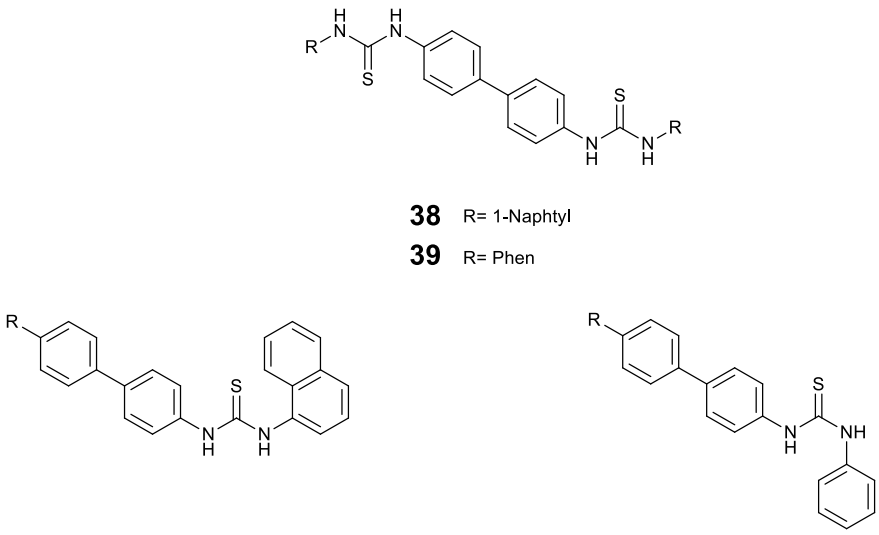

Figure 1.6 Receptors **38** and **39** and their main conformations in DMSO-d_6 solution.

The affinity for α,ω dicarboxylates (oxalate, succinate, adipate) was investigated by means of UV-Vis titration techniques in DMSO. The receptors displayed different attitude in forming complexes with different stoichiometry ratio depending on the conformations assumed by the receptors in solution. **38** was found to form 1 : 1 complexes with all the anions studied, while **39** formed 2 : 1 complexes. In the case of **39**, an excess of anion caused the deprotonation of the receptor, but an experiment carried out using a less basic acetate, deprotonation was not observed. In this case, both of the NH groups of the thioureas were involved in the complexation with acetate with the receptor changing conformation Figure 1.7.

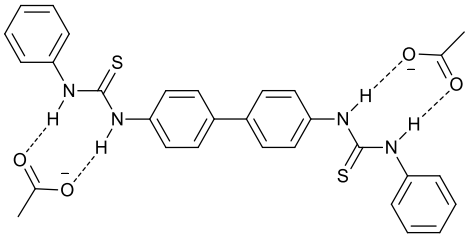

Figure 1.7 Structural proposal for the complex of **39** and two equivalents of acetate.

In the supramolecular chemistry systems based on urea and thiourea fragment, it is possible introduce also the selenourea moiety. This kind of substrate should be a good hydrogen bond donor group even if only calculated data on selenoureas NH acidity are available. [63]

Selenoureas show interesting features useful for designing receptors for anion binding:

a) Selenium has similar properties to sulfur but, because of its larger atomic radius, it is more polarizable and softer than sulfur and this evidence makes it capable to accommodate more negative charge.
b) Due the high polarizability of Selenium, selenourea NH protons should be more acid with respect to NH protons of thiourea and urea and for this reason, selenourea-based receptors should be stronger hydrogen bonding donors than the analogue receptor with oxygen and sulfur.
c) Due the low oxidation potential of Selenium, selenocompounds are very reactive.

Very few examples have been reported in the literature so far of receptors of this nature for the anion recognition even if a large number of organoselenium compounds has been recently reported as fluorescent probes for both metal ions and anions as well as neutral species. [64]

Indole and Pyrrole based anion receptors

Both pyrrole and indole contain a single hydrogen bond donor group. The anion complexation chemistry of pyrrole has been widely studied,[65] the anion complexation chemistry of indole, instead, is still largely unexplored. [66] Jeong and co-workers have investigated the anion complexation properties of led the acyclic receptors **40** and **41**.[67] The study was performed in a polar media DMSO/0.1–0.2% water and it resulted in a very interesting ability of **40** and **41** to recognize oxoanions with binding constants strongly dependent on the number of hydrogen bond donors present. Stability constants of both receptors with acetate, dihydrogen phosphate and pyrophosphate, increase in the order AcO^- < $H_2PO_4^-$ < $HPpi^{3-}$ with compound **41** showing a higher binding affinity (Ka > 5 10^6 M^{-1}) for pyrophosphate than **40** (Ka > 5.2 10^5 M^{-1}).

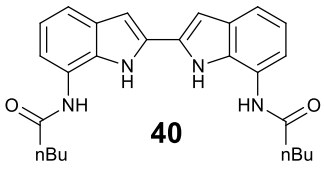

40

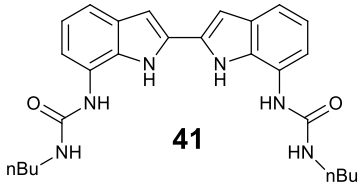

41

Kim and colleagues have reported the study on the indolocarbazole trimer receptor **42** that is able to form enantiomeric helix upon the binding of sulfate within the cavity.[68] Receptor **42** shows strong affinity to the chiral adenosine 3',5'-cyclic monophosphate (cAMP) (Ka = 1.1 10^4 M^{-1}) in a mixed 1:9:90 H_2O: CD_2Cl_2:CD_3CN media solvent mixture. CD spectroscopy in MeCN (containing 1% water) showed that the helix formed between **42** and cAMP is dissociated by the addition of CF_3COOH due to protonation of the phosphate group and that this dissociation could be reversed by the addition of the base DABCO (1,4-diazabicyclo[2.2.2]octane), which regenerated cAMP phosphate. These results

are very remarkable in the optic of the development of responsive chiroptical molecular switches.

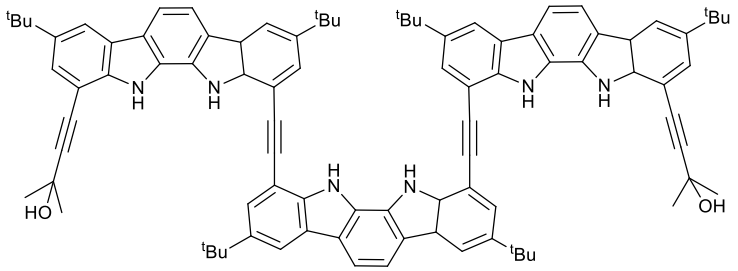

42

Beer and co-workers synthesized the preorganized indolo[2,3-a]carbazole based receptor **43** that have displayed a high affinity for the selective recognition of benzoate in acetone with a stability constant of log Ka = 5.4. [69] The interaction between **43** and the anion target led to a quenching in the fluorescence of the free receptor, while fluoride and chloride cause a significant improvement in the emission of **43**. In the same way, Gale and co-workers have shown that the dicarbazolyl urea **44** can sense benzoate in DMSO/0.5% H_2O via fluorescence quenching. [70] In Figure 1.8 the X-Ray structure of the 1:1 complex between **42** and this anion bound to the four hydrogen bonds is reported.

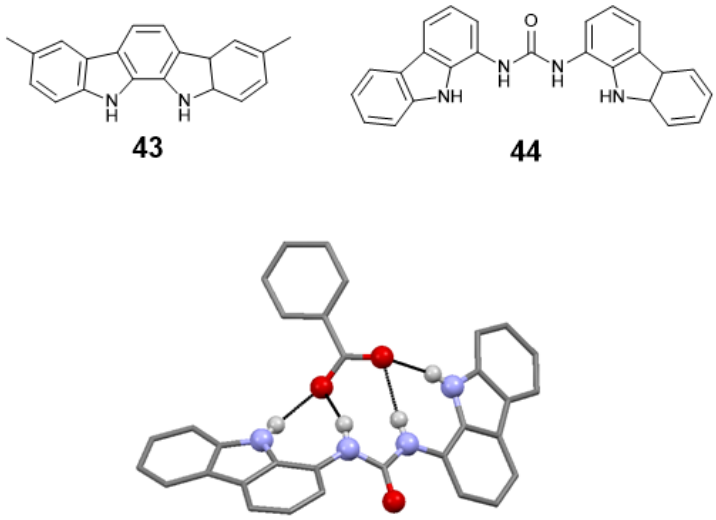

Figure 1.8 Receptors **43** and **44**. X-ray crystal structure of **44** with BzO^-. TBA counterions and non-coordinating hydrogen atoms are omitted for clarity.

Sessler and co-workers have reported the synthesis and anion coordination properties of new acyclic pyrrole receptors based **45** and **46**. Receptor **45** that presents a central phenyl ring in place of the pyridine was synthesised as well as a receptor in which the configuration of the amide linkages is reversed (**48**). [71] The anion binding capacities of these systems were studied by UV-Vis spectrophotometric titrations in dichloroethane and ^{1}H-NMR titrations in $CDCl_3$. Receptor **45** showed an affinity for carboxylates (acetate and benzoate), nitrite and cyanide anions (strongest interaction with benzoate, Ka= 43000 M^{-1} in dichloroethane) while receptor **46** binds acetate selectively (13900 M^{-1} in the same solvent) and receptor **47** resulted to be no selective with the anions of the set studied. These results confirm the important role of the pyridine nitrogen atom in stabilizing the receptor in a conformation that favours anion complexation. Interestingly receptor **48** in which the amide bonds are reversed

has completely different substrate selectivity, being selective for chloride (805 M^{-1} in dichloroethane).

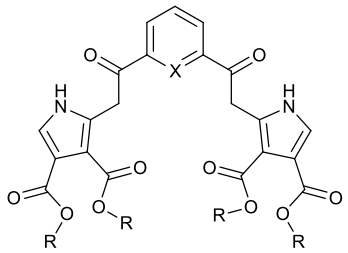

45 R= CH_2CH_3; X=N

46 R= $CH_2CH_2C(CH_3)_3$; X=N

47 R= CH_2CH_3; X=CH

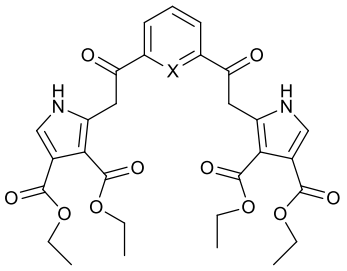

48

Archibald, Boyle, and co-workers have reported the synthesis of a calix[4]phyrin-(1,1,1,1) decorated with a 4-isothiocyanatophenyl group **49**. [72]

Using a nitro group instead of the isothiocyanato moiety, the receptor **50** was obtained. **50** was investigated by means of ^{1}H-NMR spectroscopy. Affinity for fluoride (although weakly Ka = 63.9 M^{-1}) over the other halides (Ka <1 M^{-1}) in CD_2Cl_2 at 293 K was observed. This selective interaction with fluoride is confirmed also by UV-Vis spectrometry where an addition of fluoride to **50** causes an hypsochromic shift of the maximum of the absorbance (433 nm vs. 458 nm for free **49**) accompanied by a decrease of the molar extinction coefficient value at 458 nm (11200 M^{-1} cm^{-1} vs. 14400 M^{-1} cm^{-1} for free **50**), while for the other halides no significant variation in the UV-Vis spectra was observed. Receptor **49** was coupled to Tentagel beads bearing amines to afford modified solid supports to obtained compound **51**.

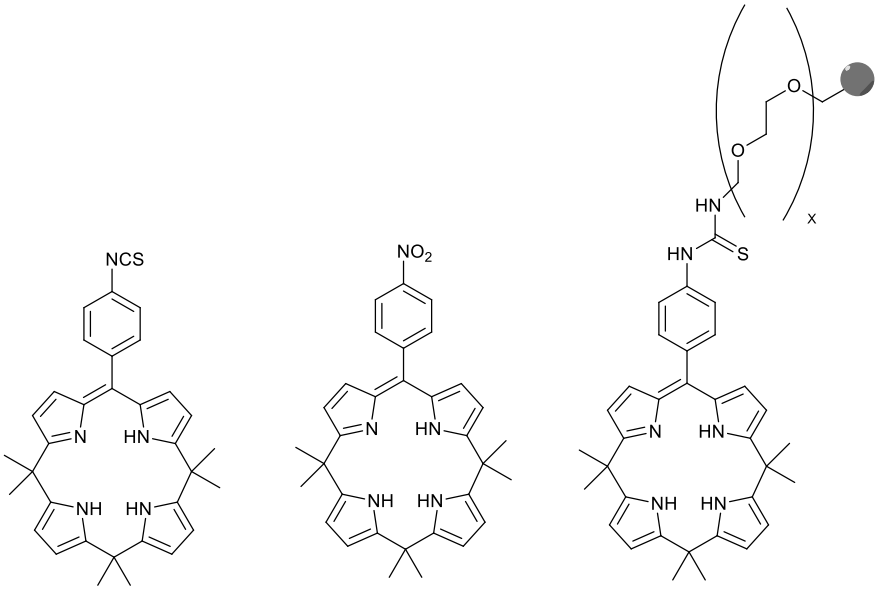

49 **50** **51**

Alcohol based anion receptors

Hydroxyl groups have been employed by a number of research groups in recent years due their involvement in many natural processes and due their great capacity as hydrogen-bonding donor. Precautions must be taken in order to avoid the deprotonation in presence of basic anions in organic solution.

Lee and his group designed a new fluorescent chemosensor **52** sensible for phosphate recognition .[73] **52** showed a fluorescent emission in DMF at 330 nm and around 500 nm attributed to the enol form and keto form, respectively. The addition of dihydrogen phosphate led to a quenching of the fluorescence emission for both bands and a slight red-shift. These evidences can be attributed to the formation of intermolecular hydrogen bond between the anion and the hydroxyl groups of the free receptor. Fluoride causes, instead, deprotonation of the receptor as confirmed by the formation of a new emission band at 450 nm.

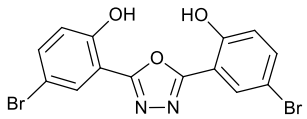

52

Lewis acids based anion receptors

Caltagirone and Lippolis have reported the anion complexation properties of the unsatured copper(II) complex of ligand **53** previously reported as a fluorescent sensor for zinc(II) ions. [74,75]

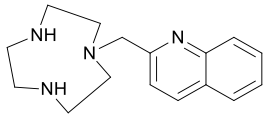

53

This ligand has been investigated in MeCN and H_2O by UV/Vis titration. This resulted in a high affinity of **53** for the selective recognition of CN^- and I^- anions. The interaction with I^- was found to follow a 1:1 binding stoichiometry (log Ka = 4.8 $\pm$ 0.1 in MeCN and log Ka = 2.4 $\pm$ 0.1 H_2O) with a colour change from cyan to green (Figure 1.9).The interaction with CN^- resulted to be a mix of 1:1 and 1:2 receptor: anion complexes in MeCN while in water media the formation of the 1:1 CN^- complex was very stable with an high stability constant (Log Ka > 7). The spectral changes upon the addition of CN^- led to a specific colour variation depending on the solvent and the stoichiometry of the complex formed (Figure 1.9). In MeCN the transition from 1:1 to 1:2 complex results in a clear colour change from cyan (only receptor) to dark blue (1 equivalent of CN^-) to pink (2 equivalents of CN^-). Crucially, this report represents the first example of CN^- sensing by a Cu(II) complex without removal of the Cu(II) centre from the receptor complex.

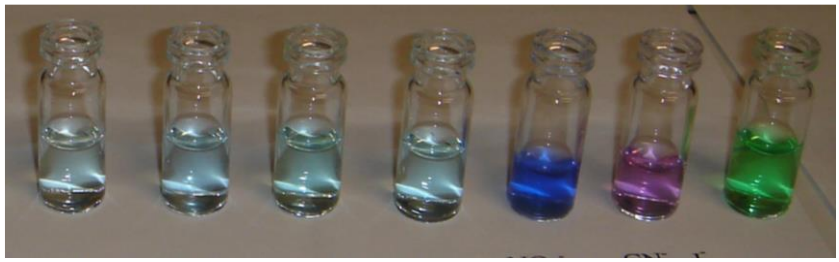

Figure 1.9 Colour change of receptor **53** in MeCN. From left to right: free receptor, +1Eq. F^-, +1Eq. Cl^-,+1Eq. Br^-, +1Eq. CN^-, +2Eq. CN^-, +1Eq. I^-. The image is reported according to Ref. 74.

1.4 Molecular sensor

According to the definition of IUPAC, a chemical sensor is a device that transforms chemical information , ranging from the concentration of a specific sample to total composition analysis into an analytically useful signal (change in pH, light emission or electronic distribution).[76]

On the base of the IUPAC definition, a chemical sensor is a macroscopic device but following the modern principles of supramolecular chemistry, an analogue of chemical sensor can be obtained for the molecular world. [77,78,79]

This approach is well known as “bottom-up” approach where the design starts from the molecular level to reach a resolution unachievable with a classic “top-down” method. The result of these interactions are a supramolecular species that are usually named molecular sensor or chemosensor to distinguish them from chemical sensor. [80,81,82]

Same specific properties must be possessed by a molecular sensor:

- The sensor should be specific and selective to one or to a small number of substrates of interest.
- The interaction between host and guest (receptor and analyte) should be fast and reversible.
- The sensor should be stable over a long time period in order to guarantee the data reproducibility.
- The sensor should be cheap and easy to synthesize.

The molecular sensor is composed of a receptor or binding subunit (which is the unit able to bind the analyte) and an active unit or signalling unit (which is the part that changes its physical properties after the interaction between the receptor and the substrate, generally separated by a spacer (Figure 1.10).

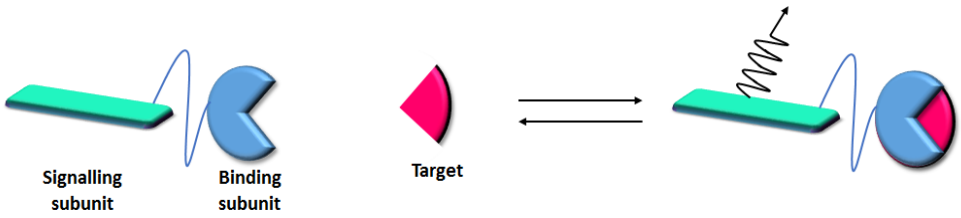

Figure 1.10 General scheme of a molecular sensor

The sensor are classified according to the principles of signal transduction in:

- Optical sensors
- Electrochemical sensors
- Electrical sensors
- Magnetic sensors
- Thermometric sensors

In particular, this thesis will be focused on the development of optical sensors able to change its photophysical features due the interaction with anions.

1.4.1 Optical anion sensors

With the terms of optical anion sensors, we referred to all the systems that are able to change their photophysical properties following the recognition of a substrate target. This kind of receptors is commonly divided into fluorescent sensors, if the active unit is a fluorophore and calorimetrical sensors, if the active unit is a cromophore.

1.4.1.1 Fluorescent chemosensors

Photoinduced Electron Transfer (PET)

This kind of process has been well studied and used in the anions and cations sensing chemistry. [83,84] Generally, fluorescence process is observed when an excited electron passes from the excited state to the ground state by releasing the excess of energy radioactively. A photoinduced electron transfer (PET) involved systems where the receptor and the fluorophore are connected by a spacer that keeps the two fragments together but separated. This process depends on the relative energies of the fluorophore molecular orbital and the receptor. The HOMO of the receptor ($HOMO_R$) is energetically collocated between the HOMO and LUMO of the fluorophore ($HOMO_F$ and $LUMO_F$). The excitation causes a series of photoinduced transfers. The first one takes place from the $HOMO_R$ to the $SOMO\text{-}1_{F*}$ followed by an electron transfer from the $SOMO_{F*}$ to the $SOMO_R$.

The result of these combinations is a fluorescence quenching that occurs due the transition from the excited to the ground state of the fluorophore takes place following a non-radiactive path.[85] The system is in an OFF state. In the case of $HOMO_R$ or receptor-substrate, is lower than that of $HOMO_F$ and $LUMO_F$, PET can not take place so the releasing occurs in a radiative way. This fact involves in an increase of the emission intensity: the system is in an ON state.

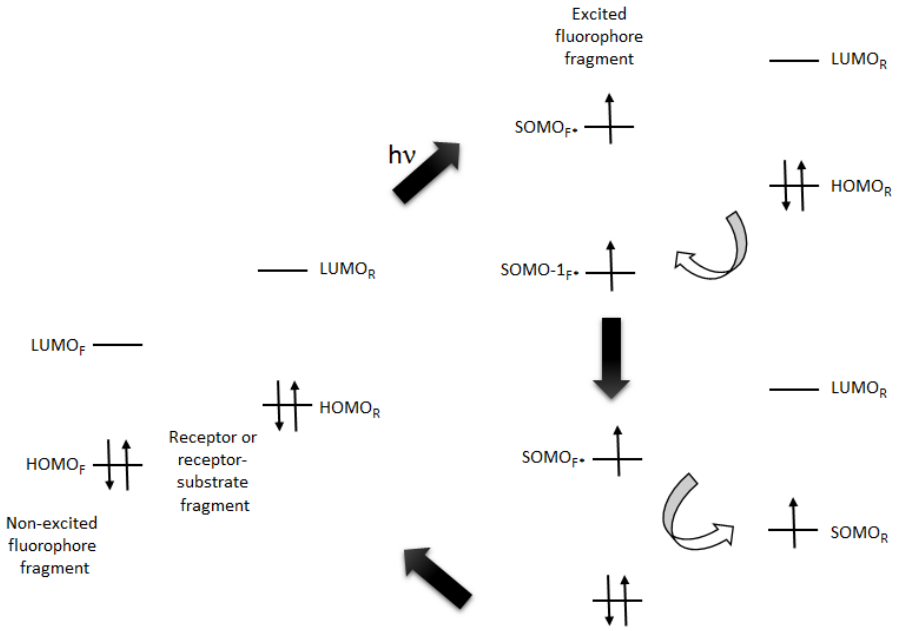

Figure 1.11 Simplified PET process with the participation of the $HOMO_F$ and $LUMO_F$ of the non-excited fluorophore fragment and the $HOMO_R$ of the receptor or receptor-substrate moiety.

A Comparable process can happen when the $LUMO_R$ shows an energy between the $HOMO_F$ and $LUMO_F$. In this case a PET from $SOMO_{F*}$ to the $LUMO_R$ can occur, followed by another second PET from the $SOMO_R$ to the SOMO-1_{F*}. Also in this case the de-excitation is a non radiatve process and the system is in an OFF state.

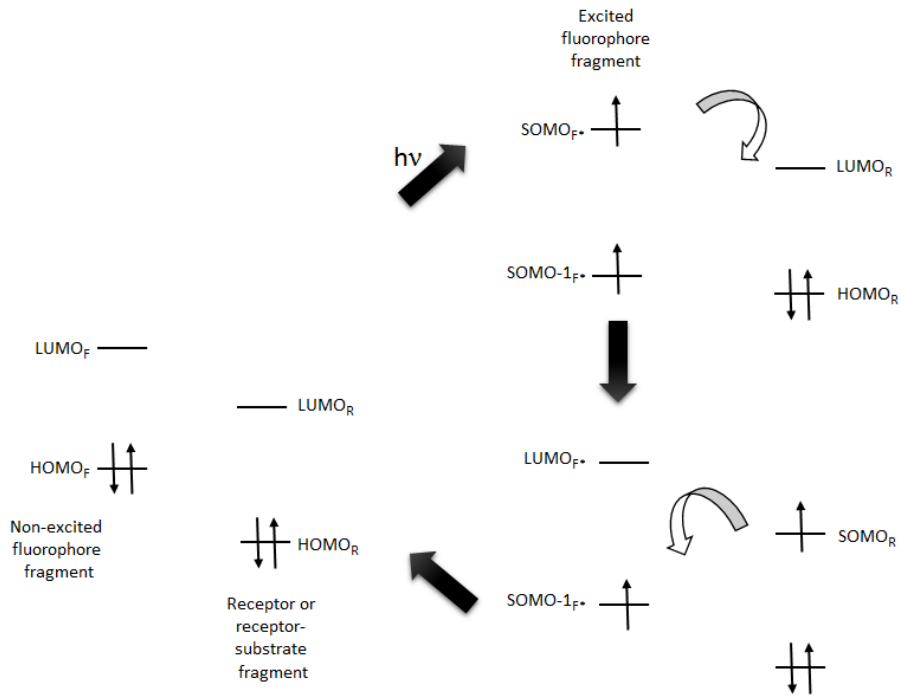

Figure 1.12 Simplified PET process with the participation of the $HOMO_F$ and $LUMO_F$ of the non-excited fluorophore fragment and the $LUMO_R$ of the receptor or receptor-substrate moiety.

Shao reported the synthesis and anion affinity of a BODIPY based fluorescent receptor **54**. [86] This ON-OFF-ON PET based system can act as an efficient fluorescent switch modulated by fluoride and hydrogensulfate anions. By means of UV-Vis, fluorescence and ^{1}H-NMR spectroscopies it was found that the addition of fluoride to a solution of the receptor in MeCN led to the loss of the NH proton while no significant change in absorption and emission was observed for the other anions studied. The emission titrations experiments of **54** in MeCN with increasing amount of fluoride causes the quenching of the free ligand emission band at 518 nm with a little blue shift. This evidence can be attributed to both the PET (photo-induced electron transfer) process and the ICT (internal

charge transfer, where a charge moves from a site of the molecule to another site in the same molecule) process as schematize in Figure 1.13.

Based on the deprotonation mechanism, recovery of the deprotonated sensor should be possible using the hydrogensulfate as "recovering reagent". The result of this work puts in evidence that this kind of system is a great base to the design of anions sensors as multifunctional logic switching devices.

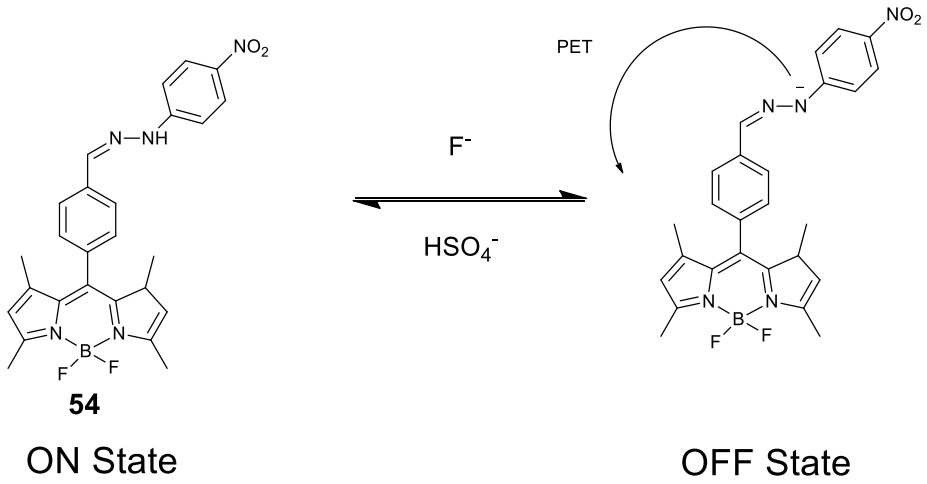

Figure 1.13 Proposed interaction mode of receptor **54** with fluoride and hydrogensulfate.

Pang and co-workers have proposed the synthesis and the binding properties of the receptor **55** sensible to malate anion (MA).[87] The receptor shows an N-Boc protected amine alcohol fragments connected to a central acridine spacer and can be used a as a fluorescent enantioselective sensor for MA.

In order to investigate the binding properties, the receptor was studied by means of fluorescence and UV-Visible spectroscopies in MeCN. No changes in the absorption spectra of **55** upon addition of carboxylate anions were found while

a remarkable variation in emission intensity of the free receptor was observed only in the case of L- and D- malate anion with respect to the other anionic species studied.

55 shows an emission band centred at 423nm (λ_{exc}= 356 nm) that, upon addition of MA, increase in intensity. This evidence can be explained with the fluorescence turn-on capacity of the oxygen atoms of the receptor to inhibiting the photoinduced-electron-transfer (PET).[88 89 90]

In addition, **55** is able to discriminate the two MA enantiomers because the same equivalents of D- MA cause a more intense increase in the fluorescence intensity of the free ligand emission band than the addition of L- MA as reported in Figure 1.14.

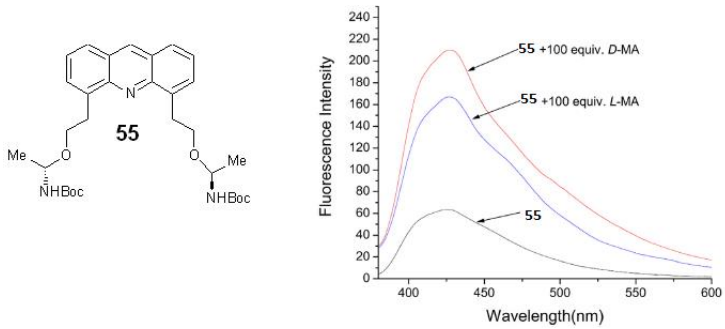

Figure 1.14 Structure of receptor **55** and fluorescent spectra of **55** with 100 equivalents of L- and M- MA.

Moreover, ^{1}H-NMR experiments were recorded to explain the mechanism of the enantioselective recognition ability of **55** to L- and D- MA and these studies resulted in a proposed interaction modes reported in Figure 1.15.

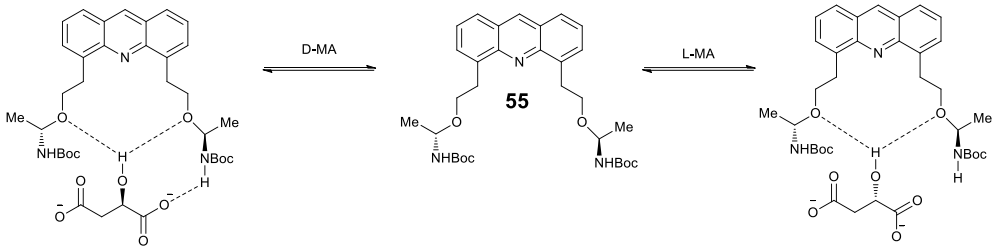

Figure 1.15 Proposed interaction modes of receptor **55** with D- and L- MA.

Electron Energy Transfer (EET)

Another mechanism that may be responsible for the fluorescence quenching by certain molecular entities is the Electron Energy Transfert (EET). [91,92] This process can occur when $HOMO_R$ and the $LUMO_R$ of the receptor are energetically positioned between the $HOMO_F$ and $LUMO_F$ of the fluorophore. After the excitation, a simultaneous exchange of two electrons from the $SOMO_{F*}$ and from $HOMO_R$ to the $LUMO_R$ and to $SOMO\text{-}1_{F*}$ respectively followed by an electron transfer from $SOMO_{R*}$ to $SOMO\text{-}1_{R*}$ of the receptor can take place. The double electron exchange restores the fluorophore to its ground state following a non-radiative process therefore resulting in a fluorescence quenching. This decay results in a non-radiative path so the final evidence is a quenching of the emission intensity and the system is in an OFF state.

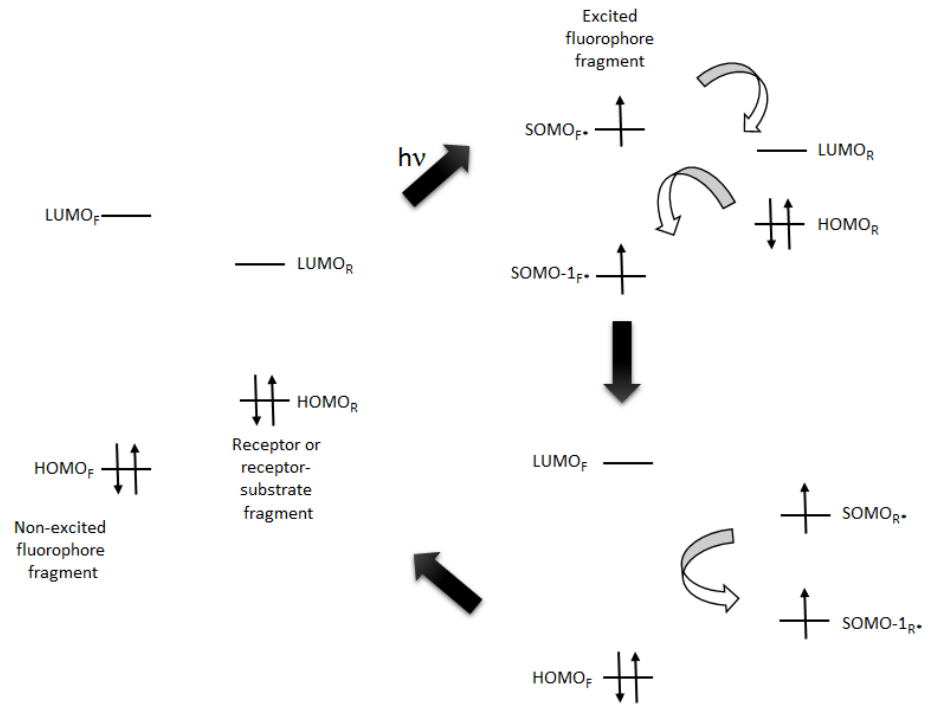

Figure 1.16 Simplified EET process with the participation of the $HOMO_F$ and $LUMO_F$ of the non-excited fluorophore and both $LUMO_R$ and $HOMO_R$ of the receptor or receptor-substrate moiety.

Excited State Proton Transfer (ESPT)

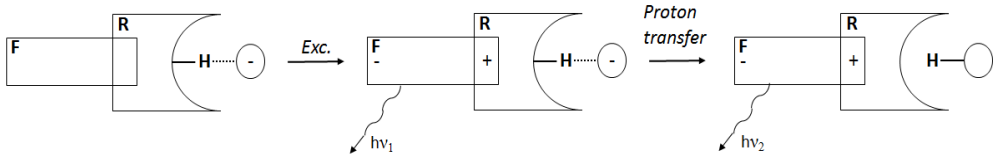

Figure 1.17 Mechanism of Excited State Proton Transfer.

According to this further mechanism, ESPT, the unit receptor-anion localised near the fluorophore can stabilize the positive charge of the latter in the excited state (that shows an emission energy $h\nu_1$) and it is able to promote an

intermolecular proton transfer to the anion followed by a new fluorescence emission of $h\nu_2$ energy.

Hamilton and Choi reported the synthesis and the anion binding study of the macrocycle **56** able to recognize $H_2PO_4^-$ over other anions in a mixed DMSO:1,4 dioxane (1:1, v/v) media via a dual-channel fluorescence emission. The mechanism of the receptor is based on the ESPT principle. [93]

The binding of all tetrahedral anions studied causes an increase in the fluorescence intensity and a red shift of the peak maximum presumably due to the stabilization of the fluorophore excited state relative to the ground state on anion binding. Only upon addition of dihydrogen phosphate, a new emission band red shifted in respect to the emission of the free receptor appears. This evidence can be attributed with the second emission channel opening deriving from the proton transfer from the fluorophore excited state.

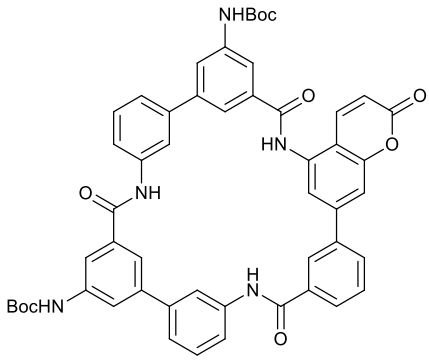

56

Fluorescence Resonance Energy Transfer (FRET)

If the donor emission spectrum overlaps the absorption spectrum of the acceptor, several vibronics transitions have the same energy level so a FRET may occurs. The fluorescence resonance energy transfer is a non-radiative transfer of excitation energy between a donor and an acceptor groups that is widely adopted in the analyte detection chemistry.

Hamachi and co-workers have reported the design and the properties of the dual-emission chemosensors **57** and **58**. These receptors are able to detect nucleoside polyphosphates and they are based on a new mechanism involving binding-induced recovery of FRET. [94]

Their structure shows a coumarine and a xanthene ring moieties as a FRET donor and acceptor respectively. In absence of ATP the xanthene part of the chemosensors adopts a non-conjugated form, so the chemosensors display the typical blue emission from the coumarine.

The presence of a nucleoside polyphosphate, instead, results in a structural change of the system that brings about a large spectral overlap between the two fluorophores. This involves a new strong green emission from the xanthene due to the significant enhancement of the FRET efficiency. The proposal mechanism is showed in Figure 1.18.

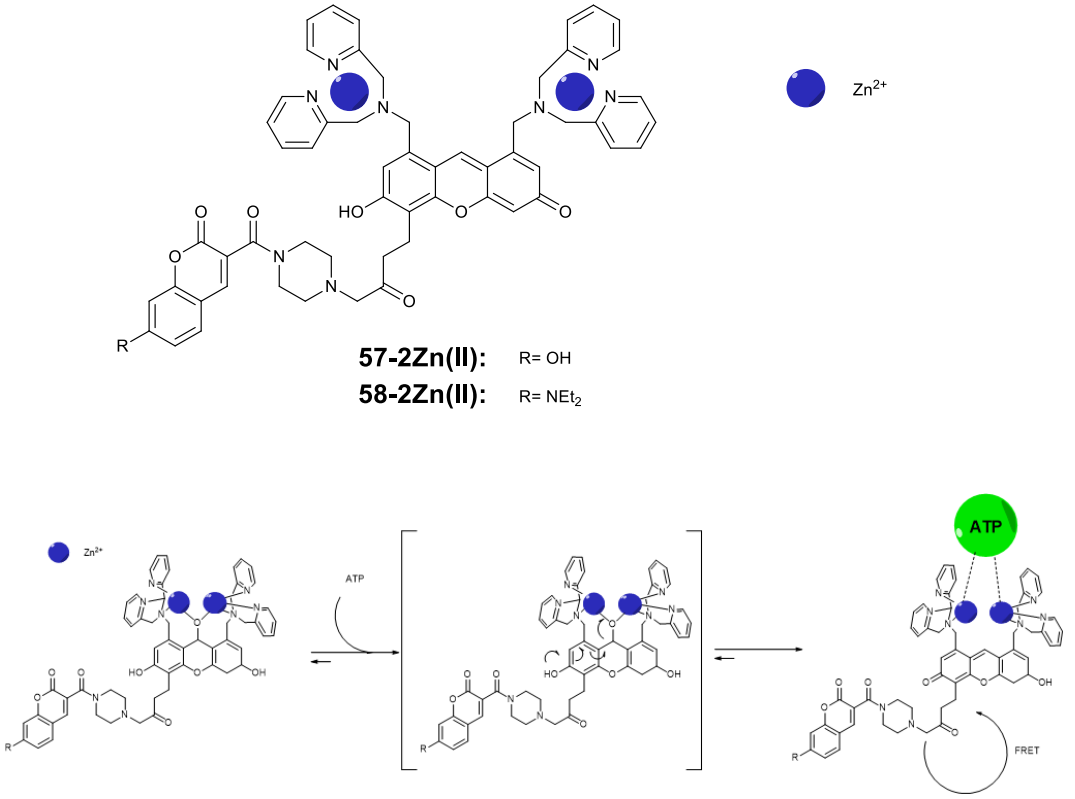

Figure 1.18 Representation of the dual-emission sensing of ATP with the chemosensors.

Monomer-excimer formation

The formation of an excimer can occur between fluorophores characterised by high π delocalization. An excimer can be defined as a complex formed by interaction of a fluorophore in the excited state with a fluorophore of the same structure in the ground state. [92] If these two units are connected by a flexible receptor, the complexation with the anion may cause variation in the structural conformation of the system and bring the fluorophores in close proximity. The emission spectra of the excimer is red-shifted with respect to that of the monomer, and in many cases, the dual emission of the monomer and the

excimer is observed. A schematic representation of the substrate-induced excimer formation is shown in Figure 1.19.

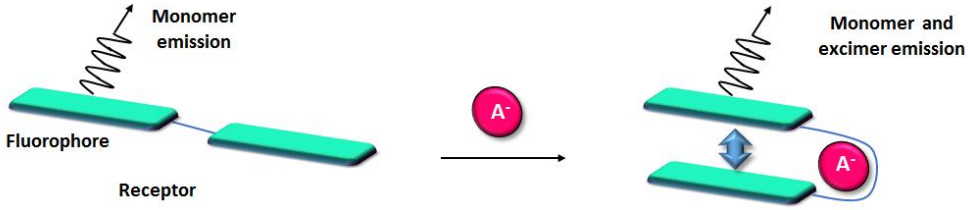

Figure 1.19 Chemosensor composed of a flexible coordinating subunit and two flat fluorophores. The coordination with a substrate induces spatial proximity between the fluorophore moieties and dual emission from the monomer and the excimer.

Teramae at al. designed the pyrene based charge receptor **59**. They studied the properties and the anion affinity of this system in methanol and as result a particular affinity of the receptor to form a 2:1 receptor: anion complex was found with pyrophosphate. [95] The emission band at 370-450 nm attributed to the pyrene monomer quenches upon addition of Ppi anion. Simultaneously, a structureless band at 476 nm, assigned to the formation of an intermolecular excimer in 2:1 complex, is observed (Figure 1.20).

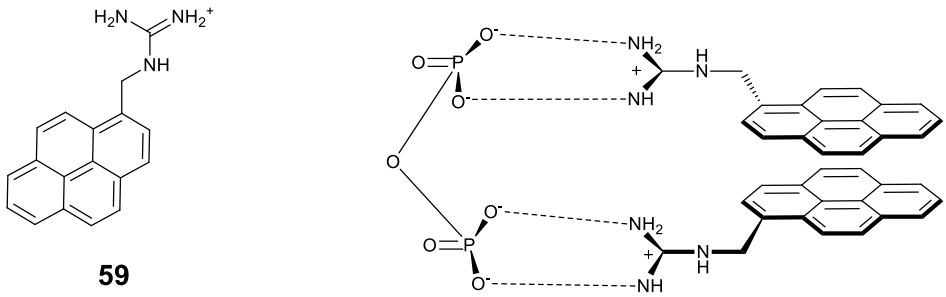

Figure 1.20 Formation of complex between **59** and pyrophosphate anion.

1.4.1.2 Colorimetric chemosensors

The anion recognition using colorimetric sensors involves a variation in the absorption properties of the free receptor bearing a cromophoric fragment that can be qualitatively detected even to the naked eye. The interaction between the receptor with the anion species causes a variation in relative energy between the HOMO and LUMO orbitals that leads to a change of the cromophore colour. This chromatic change can be caused by the formation of the complex with an opportune anion or by the deprotonation of the receptor by an anion sufficiently basic.

Gunnlaugsson et al. studied colorimetric hydrazine-based naphthalimide sensors **60** and **61.** [96] For use in aqueous solution. Titration in DMSO of **61** showed an absorption band at 441 nm and a smaller shoulder at 560 nm, which upon addition of anions, (AcO^-,$H_2PO_4^-$ and F^-) increased in intensity simultaneously with the formation of new band at 350 nm (isosbestic points at 465 and 380 nm). The results of these interactions led to a colorimetric naked eye visible changes from yellow to purple solution. In order to evaluate the capacity of sensing of **60** and **61** in more competitive environment, the same UV-Vis titrations were carried out in 1:1 (v/v) $E_tOH–H_2O$ buffered solutions at pH 7.1 and pH 7.3 for **60** and **61** respectively with no variation in the spectral and colour changes described in DMSO. These data were fitted to obtain the stability of the complexes of **60** with AcO^-, F^- and $H_2PO_4^-$ (log β = 3.4, 2.2 and 1 respectively) in mixed aqueous media.

Also the urea-based sensors **62**, **63** and **64** were able to bind anions such as AcO^- ,$H_2PO_4^-$ and F^- even if only in aprotic solvents like DMSO. [97] Also in this case, the three sensors act as colorimetric sensor for the anions above mentioned (Figure 1.21).

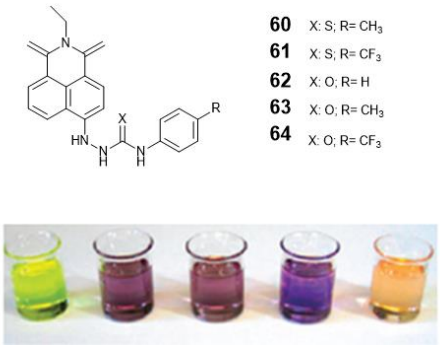

Figure 1.21 Structures of receptor **60-64.** Colour variation of **64** solutions in DMSO upon addition of anions. From left to right: free receptor, +1Eq. AcO^-, +1Eq. $H_2PO_4^-$, +1Eq. F^-, +F^-(excess). The image is reported according to Ref. 97**.**

Additionally, ^1H NMR titrations in DMSO-d_6 demonstrated that AcO^- was recognised through 'pure' hydrogen bonding while the interactions for $H_2PO_4^-$ and F^- involve a full or partial deprotonation (Through NMR data, the stability constants reported in Table 1.4 were found.

Table 1.4 Binding constants (Log β/M^{-1}) for receptors **62 - 64** measured by ^1H-NMR titrations.

Receptor	AcO^-	$H_2PO_4^-$	F^{-a}
62	4.19 ± 0.03	2.86 ± 0.04	-
63	3.99 ± 0.06	[a]	-
64	4.26 ± 0.06	3.49 ± 0.02	-

[a] The binding profile was too complicated to allow for accurate determination of log β.

Bhattacharya and co-workers reported the synthesis and anion sensing properties of the receptor **65** that acted as a colorimetric probe for cyanide and fluoride. [98] The interaction between **65** and F^- or CN^- in MeCN/5% DMSO results in a clear colour change from yellow to, respectively, blue or red due to an intramolecular charge-transfer (ICT) process (Figure 1.22a). Increasing the polarity of the solvent, moving from MeCN:DMSO media to water, the system is only able to recognize cyanide because of the more higher degree of hydration of fluoride with respect to cyanide in water.[99]

Another example of a colorimetric sensor for both cyanide and fluoride is one study reported by Akkaya and collaborators, who showed that the BODIPY based receptor **66** shows a remarkable affinity for sense F^- and CN^- in chloroform with a strong colorimetric variation as shown in Figure 1.22b. [100]

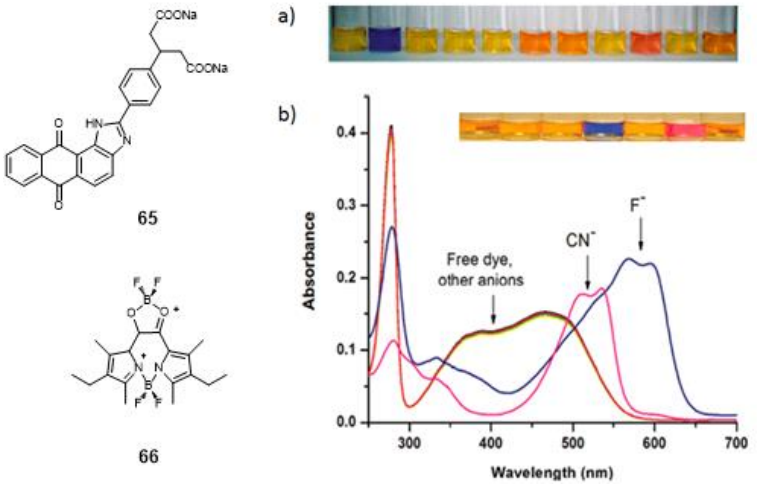

Figure 1.22 Structures of receptor **65** and **66**. a) Changes in colour of receptor **65** in a mixed MeCN/5% DMSO media upon addition of 50 Eq. of different anions. From left to right: free receptor, F^-, Cl^-, Br^-,I^-, AcO^-, $H_2PO_4^-$, NO_3^-, CN^-, ClO_4^-, HSO_4^-. b) Absorption variation spectra of **66** in chloroform upon addition Fluoride and Cyanide. Inset: naked-eye chromatic change of **66** with different anions; from left to right: free receptor, +1Eq. $H_2PO_4^-$, +1Eq. N_3^-, +1Eq. F^-, +1Eq. I^-, +1Eq. I^-, +1Eq. CN^-, +1Eq. OH^-. All graph and images are reported according to Ref. 98 and 100.

1.5 Aim of the thesis

The receptors that will be described in the next chapters are reported in Figure 1.23. The importance of the supramolecular chemistry and the anion sensing in different areas of interest has been introduced in the previous paragraphs. A wide number of receptors based essentially on the hydrogen bond interaction for anion species are constantly designed and synthesized because of the fundamental interest towards anions. Among them, the urea moiety is the most largely employed due to its easy synthesis and due the presence of NH acid protons oriented in a convergent way able to interact with the anion through hydrogen bond.

The work described in this thesis focusses on the design, the synthesis and the study of a new series of molecules containing the urea moiety that are able to act as receptors for anions, or, when suitably functionalised, as fluorescent and UV-Visible chemosensors for the selective recognition of anion target species in competitive media in free state or when embedded in micelles or nanoparticles systems.

Our purpose was to investigate how and how much the variation of heteroatom in the urea site (moving from Oxygen to Sulfur to Selenium) can influence the anion binding capacity of the receptors.

The anion binding abilities of the proposed receptors have been studied by means of ^{1}H-NMR, ^{13}C-NMR, ^{77}Se-NMR, UV-Visible and fluorescence spectroscopies and X-Ray crystallography, where possible, in order to investigate their applicability as colorimetric and fluorescent sensors.

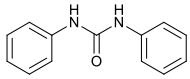

L_1

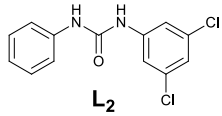

L_2

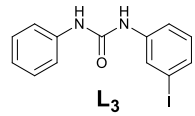

L_3

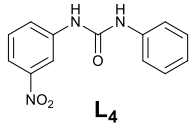

L_4

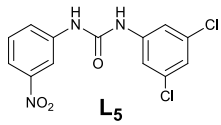

L_5

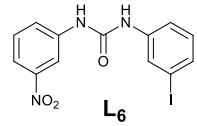

L_6

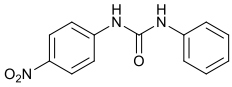

L_7

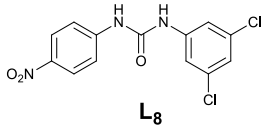

L_8

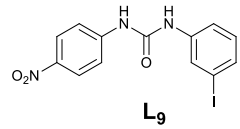

L_9

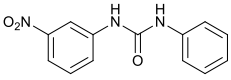

L_{10}

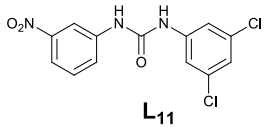

L_{11}

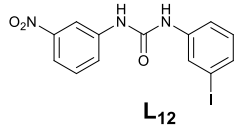

L_{12}

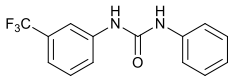

L_{13}

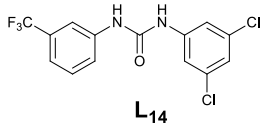

L_{14}

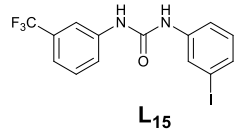

L_{15}

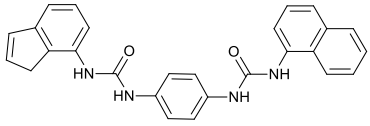

L_{16}

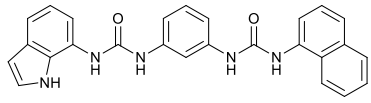

L_{17}

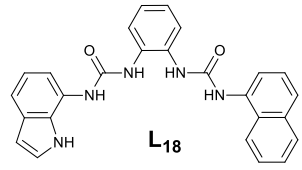

L_{18}

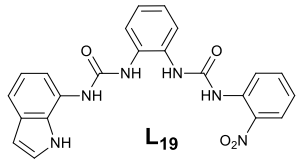

L_{19}

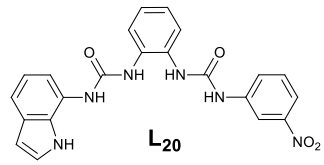

L_{20}

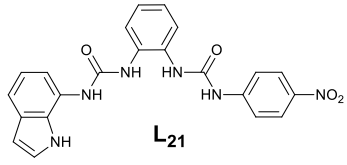

L_{21}

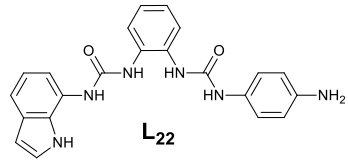

L_{22}

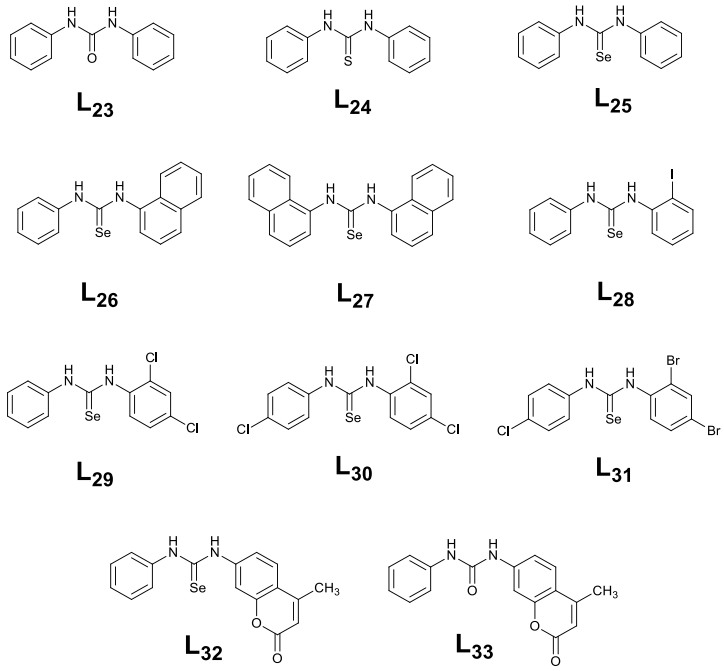

Figure 1.23 Receptors discussed in the thesis.

References

1. A. Werner, N. L. i. C., 1966,256-269.

2. Bowman-James, K., Alfred Werner revisited: the coordination chemistry of anions. *Accounts of chemical research* **2005,** *38* (8), 671-678.

3. Fischer, E., Ueber den Einfluss der Konfiguration auf die Wirkung der Enzyme III. *Berichte der deutschen chemischen Gesellschaft* **1895,** *28* (2), 1429-1438.

4. P. Ehrlich, N. L. P. o. M., 1967, 304-320.

5. J. Watson, F. C., Nobel Lecture: Physiology or Medicine, 1962.

6. Cram, D. J., Nobel Lectures in Chemistry (1981–1990). World Scientific Publishing Co, Singapore 1992, 419.

7. Pedersen, C.; Malmström, B., Nobel Lectures, Chemistry 1981–1990. World Scientific Publishing Co. Singapore: 1992.

8. Lehn, J., Nobel Lectures in Chemistry (1981–1990). *World Scientific Publishing Co, Singapore* **1992**, 474.

9. Lehn, J. M., Supramolecular chemistry—scope and perspectives molecules, supermolecules, and molecular devices (Nobel Lecture). *Angewandte Chemie International Edition in English* **1988,** *27* (1), 89-112.

10. J.M. Lehn, P. A. C., 1978, 50, 871.

11. K.B. Mertes, J. M. L., in Comprehensive Coordination Chemistry, Eds. G. Wilkinson, R.D. Gillard, J.A. McClevety, Pergamon Press, Oxford, 1987, Vol. 2, Ch. 21.3.

12. J.M. Lehn, N. L., 1987.

13. Curtis, N.; Melson, G., Coordination Chemistry of Macrocyclic Compounds. *Plenum Press, New York* **1979**, 230.

14. Lehn, J. M., Cryptates: the chemistry of macropolycyclic inclusion complexes. *Accounts of Chemical Research* **1978,** *11* (2), 49-57.

15. Dietrich, B.; Lehn, J.; Sauvage, J.; Blanzat, J., Cryptates—X: Syntheses et proprietes physiques de systemes diaza-polyoxa-macrobicycliques. *Tetrahedron* **1973,** *29* (11), 1629-1645.

16. Lehn, J.-M., *Supramolecular chemistry*. Vch, Weinheim: 1995; Vol. 1.

17. Desiraju, G. R.; Parshall, G. W., Crystal engineering: the design of organic solids. *Materials science monographs* **1989,** *54*.

18. Desiraju, G. R., Crystal engineering: a holistic view. *Angewandte Chemie International Edition* **2007,** *46* (44), 8342-8356.

19. J.M. Lehn, S., 1985, 227, 849.

20. J.P. Sauvage, J. F. S., B.L. Feringa, Nobel Lecture, Chemistry, 2016.

21. Engle, J. M.; Carroll, C. N.; Johnson, D. W.; Haley, M. M., Synthesis and optoelectronic properties of 2, 6-bis (2-anilinoethynyl) pyridine scaffolds. *Chemical Science* **2012,** *3* (4), 1105-1110.

22. Gale, P. A.; Garcia-Garrido, S. E.; Garric, J., Anion receptors based on organic frameworks: highlights from 2005 and 2006. *Chemical Society Reviews* **2008,** *37* (1), 151-190.

23. Gale, P. A.; Quesada, R., Anion coordination and anion-templated assembly: Highlights from 2002 to 2004. *Coordination Chemistry Reviews* **2006,** *250* (23–24), 3219-3244.

24. Adams, R. L. P. K., J.T.;Leader,D.P.TheBiochemistryof the Nucleic Acids, 10th ed.; Chapman and Hall: New York, 1986.

25. Egli, M.; Saenger, W., *Principles of nucleic acid structure*. Springer Science & Business Media: 2013.

26. Anderson, M. P.; Gregory, R. J., Demonstration that CFTR is a chloride channel by alteration of its anion selectivity. *Science* **1991,** *253* (5016), 202.

27. Devuyst, O.; Christie, P. T.; Courtoy, P. J.; Beauwens, R.; Thakker, R. V., Intra-renal and subcellular distribution of the human chloride channel, CLC-5, reveals a pathophysiological basis for Dent's disease. *Human molecular genetics* **1999,** *8* (2), 247-257.

28. Kornak, U.; Kasper, D.; Bösl, M. R.; Kaiser, E.; Schweizer, M.; Schulz, A.; Friedrich, W.; Delling, G.; Jentsch, T. J., Loss of the ClC-7 chloride channel leads to osteopetrosis in mice and man. *Cell* **2001,** *104* (2), 205-215.

29. Kaminsky, L. S.; Mahoney, M. C.; Leach, J.; Melius, J.; Miller, M. J., Fluoride: benefits and risks of exposure. *bone* **1990,** *14* (16), 17.

30. Gale, P. A.; García-Garrido, S. E.; Garric, J., Anion receptors based on organic frameworks: highlights from 2005 and 2006. *Chemical Society Reviews* **2008,** *37* (1), 151-190.

31. Gale, P. A.; Quesada, R., Anion coordination and anion-templated assembly: Highlights from 2002 to 2004. *Coordination chemistry reviews* **2006,** *250* (23), 3219-3244.

32. Sessler, J. L.; Gale, P. A.; Cho, W.-S., *Anion receptor chemistry*. Royal Society of Chemistry: 2006.

33. Bianchi, A.; Bowman-James, K.; García-España, E., *Supramolecular chemistry of anions*. Wiley-vch New York: 1997; Vol. 62.

34. Bazzicalupi, C.; Bencini, A.; Giorgi, C.; Valtancoli, B.; Lippolis, V.; Perra, A., Exploring the Binding Ability of Polyammonium Hosts for Anionic Substrates: Selective Size-Dependent Recognition of Different Phosphate Anions by Bis-macrocyclic Receptors. *Inorganic Chemistry* **2011,** *50* (15), 7202-7216.

35. Hossain, M. A.; Kang, S. O.; Kut, J. A.; Day, V. W.; Bowman-James, K., Influence of Charge on Anion Receptivity in Amide-Based Macrocycles. *Inorganic Chemistry* **2012,** *51* (8), 4833-4840.

36. Blondeau, P.; Segura, M.; Perez-Fernandez, R.; de Mendoza, J., Molecular recognition of oxoanions based on guanidinium receptors. *Chemical Society Reviews* **2007,** *36* (2), 198-210.

37. Schwesinger, R., Extremely Strong, Non-Ionic Bases: Synthesis and Applications. *Chemischer Informationsdienst* **1986,** *17* (7).

38. Schmuck, C.; Bickert, V., Oxoanion Binding by Flexible Guanidiniocarbonyl Pyrrole−Ammonium Bis-Cations in Water. *The Journal of Organic Chemistry* **2007,** *72* (18), 6832-6839.

39. Fitzmaurice, R. J.; Gaggini, F.; Srinivasan, N.; Kilburn, J. D., Carboxylate binding in polar solvents using pyridylguanidinium salts. *Organic & Biomolecular Chemistry* **2007,** *5* (11), 1706-1714.

40. Ahmed, N.; Shirinfar, B.; Geronimo, I.; Kim, K. S., Fluorescent Imidazolium-Based Cyclophane for Detection of Guanosine-5′-triphosphate and I– in Aqueous Solution of Physiological pH. *Organic Letters* **2011,** *13* (20), 5476-5479.

41. Jung, J. Y.; Jun, E. J.; Kwon, Y.-U.; Yoon, J., Recognition of myo-inositol 1,4,5-trisphosphate using a fluorescent imidazolium receptor. *Chemical Communications* **2012,** *48* (64), 7928-7930.

42. McDonald, K. P.; Qiao, B.; Twum, E. B.; Lee, S.; Gamache, P. J.; Chen, C.-H.; Yi, Y.; Flood, A. H., Quantifying chloride binding and salt extraction with poly(methyl methacrylate) copolymers bearing aryl-triazoles as anion receptor side chains. *Chemical Communications* **2014,** *50* (87), 13285-13288.

43. Shang, J.; Si, W.; Zhao, W.; Che, Y.; Hou, J.-L.; Jiang, H., Preorganized Aryltriazole Foldamers as Effective Transmembrane Transporters for Chloride Anion. *Organic Letters* **2014,** *16* (15), 4008-4011.

44. Webb, J. E. A.; Crossley, M. J.; Turner, P.; Thordarson, P., Pyromellitamide Aggregates and Their Response to Anion Stimuli. *Journal of the American Chemical Society* **2007,** *129* (22), 7155-7162.

45. Shang, X.-F.; Xu, X.-F.; Lin, H.; Shao, J.; Lin, H.-K., Efficient fluoride-selective receptor: experiment and theory. *Journal of Inclusion Phenomena and Macrocyclic Chemistry* **2007,** *58* (3-4), 275-281.

46. Shang, X. F.; Xu, X. F.; Lin, H.; Shao, J.; Lin, H. K., Studies on synthesis and anion recognition properties of (3′-nitrobenzo)[2, 3-d]-(3 ″-nitrobenzo)[9, 10-d]-1, 4, 8, 11-tetraazacyclotetradecane-5, 7, 12, 14-tetraone. *Journal of Molecular Recognition* **2007,** *20* (2), 139-144.

47. Harris, K.; Atwood, J.; Steed, J., Encyclopedia of Supramolecular Chemistry. Atwood, JL, Steed, JW, Eds: 2004.

48. Boiocchi, M.; Del Boca, L.; Gómez, D. E.; Fabbrizzi, L.; Licchelli, M.; Monzani, E., Nature of Urea−Fluoride Interaction: Incipient and Definitive Proton Transfer. *Journal of the American Chemical Society* **2004,** *126* (50), 16507-16514.

49. Boiocchi, M.; Del Boca, L.; Esteban-Gómez, D.; Fabbrizzi, L.; Licchelli, M.; Monzani, E., Anion-Induced Urea Deprotonation. *Chemistry – A European Journal* **2005,** *11* (10), 3097-3104.

50. Esteban-Gómez, D.; Fabbrizzi, L.; Licchelli, M., Why, on Interaction of Urea-Based Receptors with Fluoride, Beautiful Colors Develop. *The Journal of Organic Chemistry* **2005,** *70* (14), 5717-5720.

51. Amendola, V.; Boiocchi, M.; Fabbrizzi, L.; Palchetti, A., What Anions Do Inside a Receptor's Cavity: A Trifurcate Anion Receptor Providing Both Electrostatic and Hydrogen-Bonding Interactions. *Chemistry–A European Journal* **2005,** *11* (19), 5648-5660.

52. Amendola, V.; Esteban-Gómez, D.; Fabbrizzi, L.; Licchelli, M., What Anions Do to N−H-Containing Receptors. *Accounts of Chemical Research* **2006,** *39* (5), 343-353.

53. Wu, Y.; Peng, X.; Fan, J.; Gao, S.; Tian, M.; Zhao, J.; Sun, S., Fluorescence Sensing of Anions Based on Inhibition of Excited-State Intramolecular Proton Transfer. *The Journal of Organic Chemistry* **2007,** *72* (1), 62-70.

54. Dos Santos, C. M.; McCabe, T.; Gunnlaugsson, T., Selective fluorescent sensing of chloride. *Tetrahedron letters* **2007,** *48* (18), 3135-3139.

55. Duke, R. M.; O'Brien, J. E.; McCabe, T.; Gunnlaugsson, T., Colorimetric sensing of anions in aqueous solution using a charge neutral, cleft-like, amidothiourea receptor: tilting the balance between hydrogen bonding and deprotonation in anion recognition. *Organic & biomolecular chemistry* **2008,** *6* (22), 4089-4092.

56. Duke, R. M.; McCabe, T.; Schmitt, W.; Gunnlaugsson, T., Recognition and Sensing of Biologically Relevant Anions in Alcohol and Mixed Alcohol–Aqueous Solutions Using Charge Neutral Cleft-Like Glycol-Derived Pyridyl–Amidothiourea Receptors. *The Journal of Organic Chemistry* **2012,** *77* (7), 3115-3126.

57. Sanchez, G.; Espinosa, A.; Curiel, D.; Tarraga, A.; Molina, P., Bis(carbazolyl)ureas as Selective Receptors for the Recognition of Hydrogenpyrophosphate in Aqueous Media. *The Journal of Organic Chemistry* **2013,** *78* (19), 9725-9737.

58. Ros-Lis, J. V.; Martínez-Máñez, R.; Sancenón, F.; Soto, J.; Rurack, K.; Weißhoff, H., Signalling Mechanisms in Anion-Responsive Push-Pull Chromophores: The Hydrogen-Bonding, Deprotonation and Anion-Exchange Chemistry of Functionalized Azo Dyes. *European Journal of Organic Chemistry* **2007,** *2007* (15), 2449-2458.

59. Yang, Z.; Wu, B.; Huang, X.; Liu, Y.; Li, S.; Xia, Y.; Jia, C.; Yang, X.-J., Sulfate encapsulation in a metal-assisted capsule based on a mono-pyridylurea ligand. *Chemical Communications* **2011,** *47* (10), 2880-2882.

60. Li, S.; Jia, C.; Wu, B.; Luo, Q.; Huang, X.; Yang, Z.; Li, Q.-S.; Yang, X.-J., A Triple Anion Helicate Assembled from a Bis(biurea) Ligand and Phosphate Ions. *Angewandte Chemie International Edition* **2011,** *50* (25), 5721-5724.

61. Li, S.; Wei, M.; Huang, X.; Yang, X.-J.; Wu, B., Ion-pair induced self-assembly of molecular barrels with encapsulated tetraalkylammonium cations based on a bis–trisurea stave. *Chemical Communications* **2012,** *48* (25), 3097-3099.

62. Costero, A. M.; Gaviña, P.; Rodríguez-Muñiz, G. M.; Gil, S., Relationship between ligand conformations and complexation properties in ditopic biphenyl thioureas. *Tetrahedron* **2007,** *63* (33), 7899-7905.

63. Bian, G.; Yang, S.; Huang, H.; Zong, H.; Song, L.; Fan, H.; Sun, X., Chirality sensing of tertiary alcohols by a novel strong hydrogen-bonding donor–selenourea. *Chemical Science* **2016,** *7* (2), 932-938.

64. Panda, S.; Panda, A.; Zade, S. S., Organoselenium compounds as fluorescent probes. *Coordination Chemistry Reviews* **2015,** *300*, 86-100.

65. Gale, P. A., Amide-and urea-based anion receptors. *Encyclopedia of Supramolecular Chemistry* **2004,** *31*.

66. Gale, P. A., Synthetic indole, carbazole, biindole and indolocarbazole-based receptors: applications in anion complexation and sensing. *Chemical Communications* **2008,** (38), 4525-4540.

67. Lee, J.-Y.; Lee, M.-H.; Jeong, K.-S., Synthesis and binding properties of anion receptors containing multiple hydrogen bond donors. *Supramolecular Chemistry* **2007,** *19* (4-5), 257-263.

68. Kim, J.-i.; Juwarker, H.; Liu, X.; Lah, M. S.; Jeong, K.-S., Selective sulfate binding induces helical folding of an indolocarbazole oligomer in solution and solid state. *Chemical Communications* **2010,** *46* (5), 764-766.

69. Curiel, D.; Cowley, A.; Beer, P. D., Indolocarbazoles: a new family of anion sensors. *Chemical communications* **2005,** (2), 236-238.

70. Hiscock, J. R.; Caltagirone, C.; Light, M. E.; Hursthouse, M. B.; Gale, P. A., Fluorescent carbazolylurea anion receptors. *Organic & biomolecular chemistry* **2009,** *7* (9), 1781-1783.

71. Sessler, J. L.; Barkey, N. M.; Pantos, G. D.; Lynch, V. M., Acyclic pyrrole-based anion receptors: design, synthesis, and anion-binding properties. *New Journal of Chemistry* **2007,** *31* (5), 646-654.

72. Jha, S. C.; Lorch, M.; Lewis, R. A.; Archibald, S. J.; Boyle, R. W., Isothiocyanato-calix [4] phyrin-(1, 1, 1, 1): a useful intermediate for the synthesis of derivatised anion sensors. *Organic & biomolecular chemistry* **2007,** *5* (12), 1970-1974.

73. Kim, T. H.; Lee, C.-H.; Kwak, C. G.; Choi, M. S.; Park, W. H.; Lee, T. S., Bis (2-hydroxyphenyl)-1, 3, 4-oxadiazole derivative for anion sensing and fluorescent patterning. *Molecular Crystals and Liquid Crystals* **2007,** *463* (1), 255/[537]-261/[543].

74. Tetilla, M. A.; Aragoni, M. C.; Arca, M.; Caltagirone, C.; Bazzicalupi, C.; Bencini, A.; Garau, A.; Isaia, F.; Laguna, A.; Lippolis, V., Colorimetric response to anions by a "robust" copper (ii) complex of a [9] aneN 3 pendant arm derivative: CN− and I− selective sensing. *Chemical Communications* **2011,** *47* (13), 3805-3807.

75. Mameli, M.; Aragoni, M. C.; Arca, M.; Atzori, M.; Bencini, A.; Bazzicalupi, C.; Blake, A. J.; Caltagirone, C.; Devillanova, F. A.; Garau, A., Synthesis and coordination properties of quinoline pendant arm derivatives of [9] aneN3 and [9] aneN2S as fluorescent zinc sensors. *Inorganic chemistry* **2009,** *48* (19), 9236-9249.

76. Adam, H.; Stanislaw, G.; Folke, I., Chemical sensors definitions and classification. *Pure Appl. Chem* **1991,** *63*, 1274-1250.

77. Pinalli, R.; Nachtigall, F. F.; Ugozzoli, F.; Dalcanale, E., Supramolecular sensors for the detection of alcohols. *Angewandte Chemie International Edition* **1999,** *38* (16), 2377-2380.

78. Atwood, J. L.; Lehn, J.-M., *Comprehensive supramolecular chemistry*. Pergamon: 1996.

79. Fabrizzi, L., A special issue on 'Luminescent Sensors'. *Coord. Chem. Rev* **2000,** *205*, 1-232.

80. Janata, J.; Josowicz, M.; Vanýsek, P.; DeVaney, D. M., Chemical sensors. *Analytical Chemistry* **1998,** *70* (12), 179-208.

81. Bakker, E.; Bühlmann, P.; Pretsch, E., Carrier-based ion-selective electrodes and bulk optodes. 1. General characteristics. *Chemical Reviews* **1997,** *97* (8), 3083-3132.

82. Bühlmann, P.; Pretsch, E.; Bakker, E., Carrier-based ion-selective electrodes and bulk optodes. 2. Ionophores for potentiometric and optical sensors. *Chemical Reviews* **1998,** *98* (4), 1593-1688.

83. De Silva, A. P.; Gunaratne, H. N.; Gunnlaugsson, T.; Huxley, A. J.; McCoy, C. P.; Rademacher, J. T.; Rice, T. E., Signaling recognition events with fluorescent sensors and switches. *Chemical Reviews* **1997,** *97* (5), 1515-1566.

84. Sauvage, J.-P., *Transition metals in supramolecular chemistry*. John Wiley & Sons: 2008; Vol. 21.

85. Martinez-Manez, R.; Sancenón, F., Fluorogenic and chromogenic chemosensors and reagents for anions. *Chemical Reviews* **2003,** *103* (11), 4419-4476.

86. Li, Q.; Yue, Y.; Guo, Y.; Shao, S., Fluoride anions triggered "OFF–ON" fluorescent sensor for hydrogen sulfate anions based on a BODIPY scaffold that works as a molecular keypad lock. *Sensors and Actuators B: Chemical* **2012,** *173*, 797-801.

87. Li, Q.; Xu, K.; Song, P.; Dai, Y.; Yang, L.; Pang, X., Novel enantioselective fluorescent sensors for malate anion based on acridine. *Dyes and Pigments* **2014,** *109*, 169-174.

88. Liu, H. L.; Peng, Q.; Wu, Y. D.; Chen, D.; Hou, X. L.; Sabat, M.; Pu, L., Highly Enantioselective Recognition of Structurally Diverse α-Hydroxycarboxylic Acids using a Fluorescent Sensor. *Angewandte Chemie International Edition* **2010,** *49* (3), 602-606.

89. Xu, K.-x.; Jiao, S.-y.; Yao, W.-y.; Kong, H.-j.; Zhang, J.-l.; Wang, C.-j., Syntheses and highly enantioselective fluorescent recognition of α-hydroxyl/amino carboxylic acid anions in protic solutions. *Sensors and Actuators B: Chemical* **2013,** *177*, 384-389.

90. Xu, K.-X.; Yang, L.-R.; Wang, Y.-X.; Zhao, J.; Wang, C.-J., Synthesis and enantioselective fluorescent sensors for amino acid derivatives based on BINOL. *Supramolecular Chemistry* **2010,** *22* (10), 563-570.

91. Fabbrizzi, L.; Licchelli, M.; Pallavicini, P.; Parodi, L.; Taglietti, A., *Fluorescent sensors for and with transition metals*. Chichester, UK: Wiley: 1999; Vol. 5.

92. de Silva, A. P.; Gunaratne, H. Q. N.; Gunnlaugsson, T.; Huxley, A. J. M.; McCoy, C. P.; Rademacher, J. T.; Rice, T. E., Signaling Recognition Events with Fluorescent Sensors and Switches. *Chemical Reviews* **1997,** *97* (5), 1515-1566.

93. Choi, K.; Hamilton, A. D., A dual channel fluorescence chemosensor for anions involving intermolecular excited state proton transfer. *Angewandte Chemie International Edition* **2001,** *40* (20), 3912-3915.

94. Kurishita, Y.; Kohira, T.; Ojida, A.; Hamachi, I., Rational Design of FRET-Based Ratiometric Chemosensors for in Vitro and in Cell Fluorescence Analyses of Nucleoside Polyphosphates. *Journal of the American Chemical Society* **2010,** *132* (38), 13290-13299.

95. Nishizawa, S.; Kato, Y.; Teramae, N., Fluorescence sensing of anions via intramolecular excimer formation in a pyrophosphate-induced self-assembly of a pyrene-functionalized guanidinium receptor. *Journal of the American Chemical Society* **1999,** *121* (40), 9463-9464.

96. Gunnlaugsson, T.; Kruger, P. E.; Jensen, P.; Tierney, J.; Ali, H. D. P.; Hussey, G. M., Colorimetric "naked eye" sensing of anions in aqueous solution. *The Journal of organic chemistry* **2005,** *70* (26), 10875-10878.

97. Ali, H. D. P.; Kruger, P. E.; Gunnlaugsson, T., Colorimetric 'naked-eye'and fluorescent sensors for anions based on amidourea functionalised 1, 8-naphthalimide structures: anion recognition via either deprotonation or hydrogen bonding in DMSO. *New Journal of Chemistry* **2008,** *32* (7), 1153-1161.

98. Kumari, N.; Jha, S.; Bhattacharya, S., Colorimetric probes based on anthraimidazolediones for selective sensing of fluoride and cyanide ion via intramolecular charge transfer. *The Journal of organic chemistry* **2011,** *76* (20), 8215-8222.

99. Housecroft, C. E. S., A. G. Inorganic Chemistry, 3rd ed.; Pearson Education Ltd.: Harlow, 2008.

100. Guliyev, R.; Ozturk, S.; Sahin, E.; Akkaya, E. U., Expanded Bodipy Dyes: Anion Sensing Using a Bodipy Analog with an Additional Difluoroboron Bridge. *Organic Letters* **2012,** *14* (6), 1528-1531.

Chapter 2:

Synthesis and anion binding studies of a family of simple asymmetric urea receptors

2. Synthesis and anion binding studies of a family of simple asymmetric urea receptors

2.1 Introduction

Urea and thiourea functional groups have been widely studied as anion receptor moieties because of their synthetic accessibility and their ability to interact with the guests through space-oriented, strong hydrogen-bonds. [1]

Many urea-based receptors with a wide range of substituents are reported in the literature. Among them, halogens are quickly expanding their applicability as functional groups because of their electron withdrawing nature that can contribute to modify the NH protons acidity and their possibility to interact with the anion guests *via* halogen bond. [2,3]

Taylor and co-workers have reported a family of urea based receptors for anion recognition that shows iodoperfluoro-benzoate groups (**67**a-b, **68**a-b, **69**a-b, **70**a-b and **71**a-b). [4] UV/Visible, ^{1}H-NMR and ^{19}F-NMR experiments confirmed the good affinity of these receptors to halides and oxoanions guests in CD_3CN and suggested a 1:1 binding stoichiometry for all receptors-anion complexes. The introduction of halogen atoms in the receptor scaffold confers halide selectivity to receptors that have high affinity for Y-shaped anions, without negating the strength of the interactions with oxoanions. Moreover, these systems are able to interact with anion species *via* halogen bond.

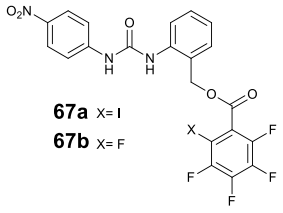

67a X= I
67b X= F

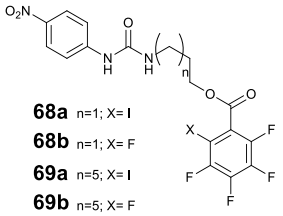

68a n=1; X= I
68b n=1; X= F
69a n=5; X= I
69b n=5; X= F

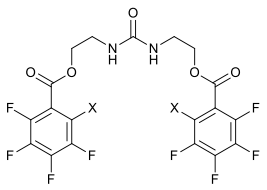

70a X= I
70b X= F

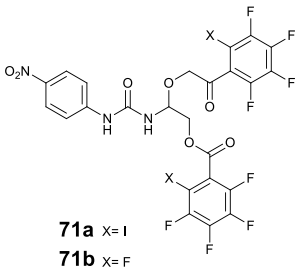

71a X= I
71b X= F

The incorporation of perfluorinated benzoates as controls that do not participate in halogen bonding [5,6,7] (**67b**, **68b**, **69b**, **70b** and **71b**) in fact led to a decrease in the halides affinity of the receptors as demonstrated by the evidence of the symmetrical urea receptor **70a** that displays the affinity constant for the binding of halides 30 times greater than observed with **70b**, where no halogen bond donor group is present.

Das and colleagues studied two simple urea based *para*-halo substituted (Iodo and fluoro for **72** and **73**, respectively) acyclic receptors as anion receptors. [8]

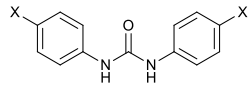

72 X= I
73 X= F

The solution-state anion binding properties of **72** and **73** have been investigated by ^{1}H-NMR titration experiments with halides and oxyanions in DMSO-d_6.

Both the receptors showed strong interactions with F^-, HCO_3^- and CH_3COO^-, as observed also in the solid-state, whereas both of them have been found to be less effective in the interaction with other anions such as Cl^-, Br^- ,I^-, NO_3^-, HSO_4^- and $H_2PO_4^-$.

In Table 2.1 are reported the stability constants of **72** and **73** with F^-, HCO_3^- and CH_3COO^- in 1:1 and 2:1 receptor: anion stoichiometry.

Table 2.1 Association constants in Log K_a (M^{-1}) of **72** and **73** with different anions in DMSO-d_6 at 298 K.

Receptor	Anion	Log $Ka_{1:1}$	Log $Ka_{1:2}$
72	F^-	4.95	8.37
72	AcO^-	3.69	6.34
72	HCO_3^-	5.16	9.06
73	F^-	4.40	8.24
73	AcO^-	3.66	6.53
73	HCO_3^-	3.32	6.79

The higher values of log Ka calculated for receptor **72** are associated with the attitude of this receptor to interact with the anion species through a synergetic activity of hydrogen and halogen bond as confirmed by evidences found in the solid state (Figure 2.1).

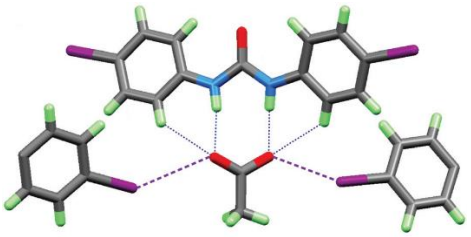

Figure 2.1 Ball-and-stick representation of complex of receptor **72** with CH_3COO^- along the crystallographic a-axis: hydrogen and halogen bonding are highlighted. The image is reported according to Ref. 8.

We decided to synthetise a new family of simple asymmetric phenyl-based ureas **L_1**-**L_{15}** for anion recognition. The **L_1**, **L_4**, **L_7**, **L_{10}**, and **L_{13}** receptors have been chosen as reference molecules for each serie of receptors, to evaluate the change in anion binding properties due to the halogen substitution (the synthesis of **L_1**, **L_4**, **L_7**, **L_{10}**, and **L_{13}** is already reported in literature). [9,10,11,12]

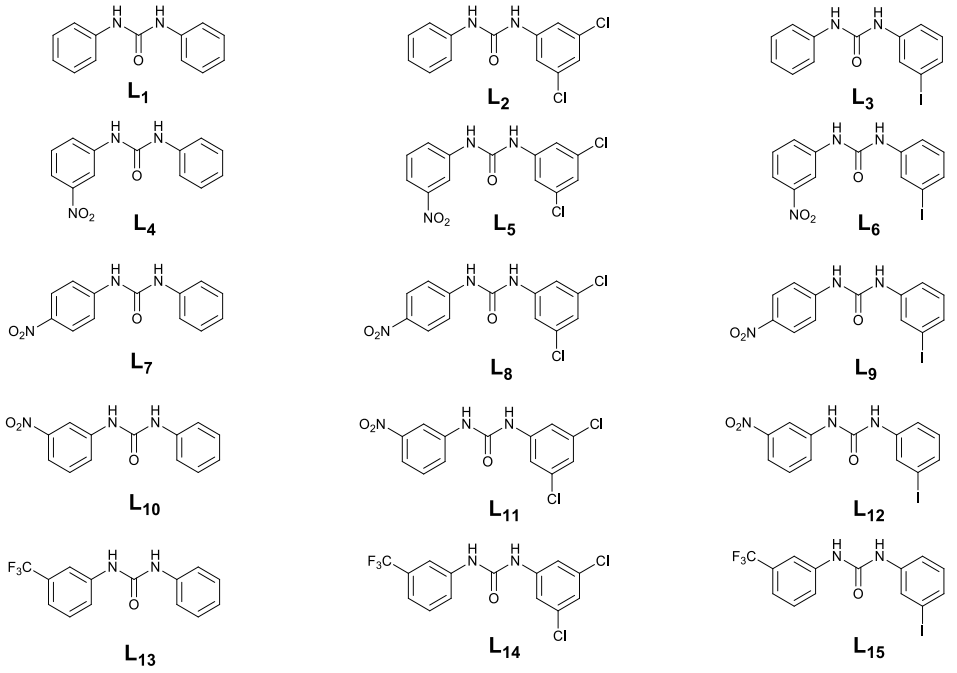

These receptors show two phenyl arms: one with iodo and chloro substituents in different position in a phenyl ring (*ortho* and *para* for chloro groups and *ortho* for iodo one) and the other phenyl ring with a nitro and trifluoromethyl sites.

These different combinations of substituents in both of the phenyl arms were chosen in order to evaluate how different halogens in different positions on the phenyl ring can affect the anion binding ability of the receptors.

We tested ligands **L_1-L_{15}** with a set including a Y-shape (AcO^- and BzO^-), spherical (Cl^- and F^-) and tetrahedral ($H_2PO_4^-$) anions by means of ^{1}H-NMR spectroscopy and, when possible, Single Crystal X-Ray diffraction.

2.2 Synthesis

Receptors **L_1-L_{15}** were designed and successfully synthesized according to the Scheme 2.1, Scheme 2.2 and Scheme 2.3. The synthesis is based on a simple nucleophilic addition between an isocyanate (phenyl isocyanate, nitro-phenyl isocyanate and trifluoromethyl-phenyl isocyanate for receptors **L_1-L_3**, **L_4-L_{12}** and **L_{13}-L_{15}** respectively) and a suitable amine (aniline, 2,4-dichloroaniline and 2-iodoaniline). As mentioned in the introduction of this chapter, the synthesis of receptors **L_1**, **L_4**, **L_7**, **L_{10}**, and **L_{13}** is already known in the literature. [9,10,11,12] After two hours of reflux in DCM, all the products were obtained as solid by precipitation without any other purification steps in a wide variable yield range depending on the substituents introduced in the systems (20- 96%).

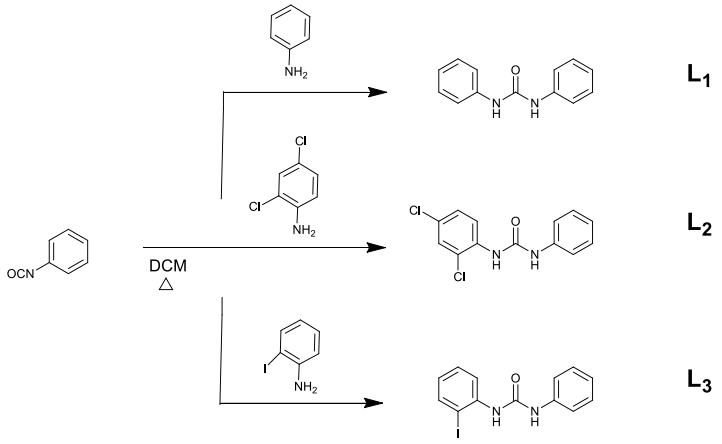

Scheme 2.1 Reaction scheme adopted for the synthesis of **L_1**, **L_2** and **L_3**.

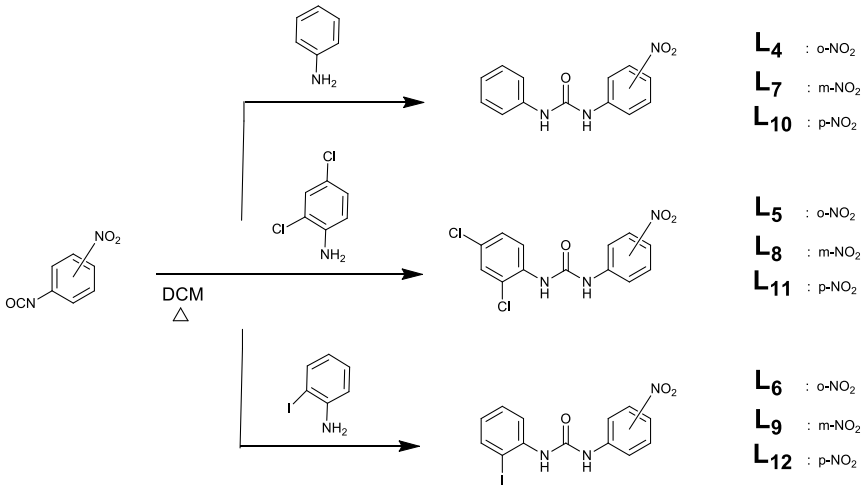

Scheme 2.2 Reaction scheme adopted for the synthesis of L_4-L_{12}.

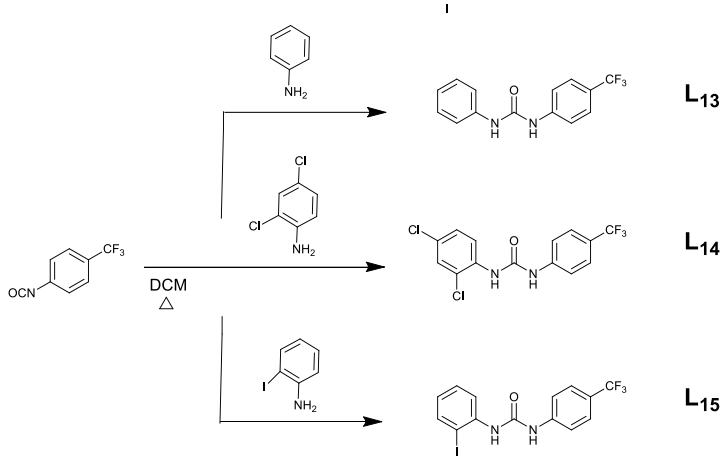

Scheme 2.3 Reaction scheme adopted for the synthesis of L_{13}, L_{14} and L_{15}.

2.3 Single Crystal X-Ray Diffraction

Despite many attempts to crystallize adducts of all the receptors with several anion guests, we were able to isolate samples suitable for single crystal X-ray diffraction only for the adduct **L_6** with BzO^- while single crystals of the free receptors **L_1, L_2, L_5, L_8, L_{11}, L_{14}** and **L_{15}** were obtained more easily.

Receptor **L_1** crystallizes in the orthorhombic crystal system (space group: $Pna2_1$). The asymmetric unit contains only one independent **L_1** receptor unit (Z' = 1). The two phenyl moieties of the receptor adopt a staggered conformation with respect to the plane of ureidic site (Figure 2.2a). Adjacent receptor molecules are connected *via* N-H…O hydrogen bond interactions between the Oxygen atom in the carbonyl site of one receptor and the two NH sites of another ligand unit (N-H…O distances are in the range 1.94(3)-2.12(3) Å while the angle NHO is in the range of 142.7(2)-142.6(2)°).These interactions cause the formation of a mono-dimensional chain as shown in Figure 2.2a and b along the direction [100] and [010] respectively. This space arrangement is common in the structures of urea derivative due the strong nature and directionality of NH…O hydrogen bonds. [13,14] Figure 2.2c shows the arrangement of different mono-dimensional chains of **L_1** along the [010] and [001] axis connected *via* weak C-H…O and C-H…N interactions (C-H…O and C-H…N distances are in the range 2.71(2)-2.81(2) Å) between the C-H aromatic hydrogens of the phenyl moiety of one receptor and the Oxygen and Nitrogen atoms of the urea group of another receptor in another chain.

The structure data of intermolecular distances and angle found for receptor **L_1** are in agreement with the observations reported in the literature for this substrate. [10]

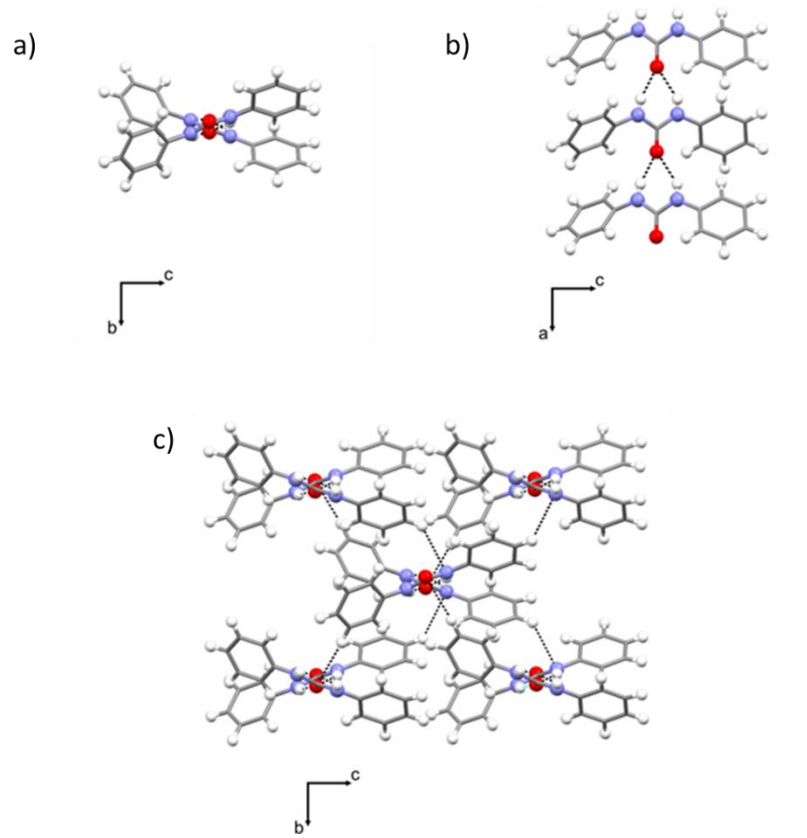

Figure 2.2 X-Ray crystal structure of receptor **L_1**. (a) mono-dimensional N-H...O chains viewed along the [100] direction; (b) N-H...O mono-dimensional chains viewed along the [010] direction (c) portion of the crystal packing of **L_1** viewed along the [100] direction.

Two polymorphic structures **$L_{2\alpha}$** and **$L_{2\beta}$** of receptor **L_2** were obtained by slow evaporation of a DMSO saturated solution of the receptor. The two forms differ only for the number of the receptor molecules in the asymmetric unit (two and one units for **$L_{2\alpha}$** and **$L_{2\beta}$**, respectively). Both polymorphic forms crystallize in the same triclinic crystal system (space group: P1) (see Table 2.4).

The two receptor molecules in the asymmetric unit of **$L_{2\alpha}$** (Z'=2) show the same arrangement previously discussed for the structure of **L_1**. The different units 1

and 2 (Figure 2.3a) interact *via* N-H…O hydrogen bond (N-H…O distances are in the range 2.045(4)-2.130(4) Å while the angle NHO is in the range of 144.1(4)-145.0(4)°) forming two independent mono-dimensional chains propagating along the [100] direction of the crystal lattice (Figure 2.3b). These are connected each other along the [001] direction by a set of weak C-H…Cl interactions (C-H…Cl intermolecular distances are in the range 2.94(1)-2.99(1) Å) as shown in Figure 2.3b. Receptor units of the same chain are connected *via* C-H…O, C-H…N and C-H…Cl interactions along the crystallographic axis [010] (C-H…O, C-H…N and C-H…Cl intermolecular distances are in the range 2.75(4)-3.02(4) Å, 2.98(1)-3.31(2) Å and 3.04(3)-3.41(3) Å respectively) (see Figure 2.3c).

The asymmetric unit of the polymorphic form $\mathbf{L_{2\beta}}$ contains only one independent receptor molecule (Z′ = 1). Also in this case the receptor molecules form a mono-dimensional chain developing along the [100] direction where receptor units interact each other *via* N-H…O hydrogen bond interaction (N-H…O distances are in the range 2.045(2)-2.074(2) Å while the angle NHO is in the range of 145.3(3)-145.0(3)°) (see Figure 2.3d). Adjacent mono-dimensional chains communicate *via* C-H…Cl and C-H…O intermolecular interactions along the crystallographic directions axes [010] and [001] as displayed in Figure 2.3f.

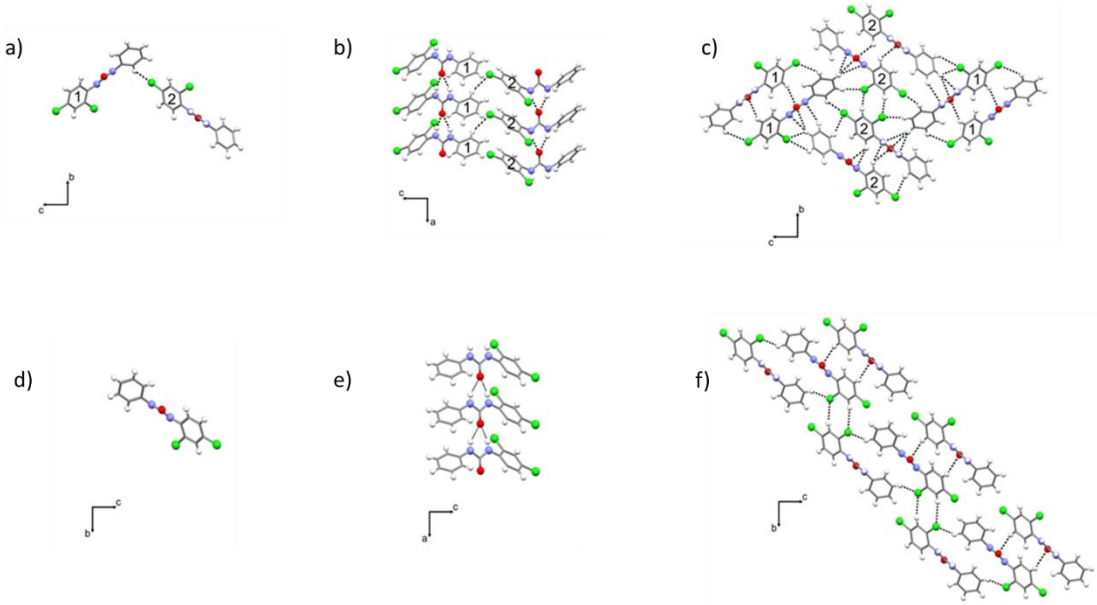

Figure 2.3 X-Ray crystal structure of the polymorphic $\mathbf{L_{2\alpha}}$ and $\mathbf{L_{2\beta}}$. (a) mono-dimensional N-H...O chain in the structure of $\mathbf{L_{2\alpha}}$ viewed along the [100] direction (b) mono-dimensional N-H...O chain in the structure of $\mathbf{L_{2\alpha}}$ viewed along the [010] direction (c) crystal packing of of $\mathbf{L_{2\alpha}}$ viewed along the [100] direction. (d) mono-dimensional N-H...O chain in the structure of $\mathbf{L_{2\beta}}$ viewed along the [100] direction (e) mono-dimensional N-H...O chain in the structure of $\mathbf{L_{2\beta}}$ viewed along the [010] direction (f) crystal packing of of $\mathbf{L_{2\beta}}$ viewed along the [100] direction. The two symmetry independent molecules 1 and 2 of $\mathbf{L_{2\alpha}}$ a are also indicated.

Crystals of receptor $\mathbf{L_5}$ were obtained by slow evaporation from saturated solution of the receptor in MeCN and MeOH. This receptor crystallizes in the monoclinic crystal system (space group: $P2_1/n$) with an asymmetric unit that contains only one independent $\mathbf{L_5}$ receptor molecule (Z' = 1). The $\mathbf{L_5}$ molecules form mono-dimensional N-H…O chains propagating along the [100] direction as displayed in Figure 2.4a. Different receptor units interact *via* N-H…O intermolecular hydrogen bond interactions (N-H…O distances are in the range

2.09(5)-2.24(5) Å, while the angle NHO is around 145(3)°), forming mono-dimensional urea chains analogous to those described above (Figures 2.4 a and b). These are connected via set of C-H…Cl and C-H…O interactions (C-H…Cl and C-H…O distances are in the range 2.95(5) Å and 2.38(5) Å respectively) to adjacent mono-dimensional chains along the [010] and [001] directions, forming the three-dimensional packing (Figure 2.4c).

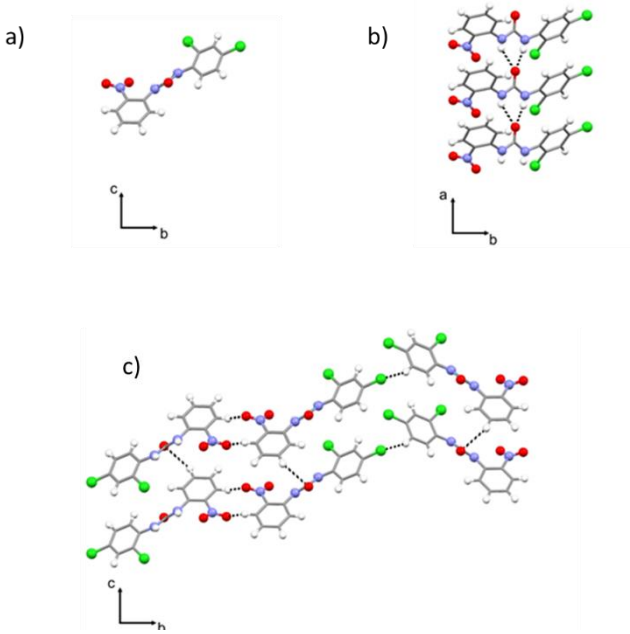

Figure 2.4 X-Ray crystal structure of the polymorphic **L_5**. (a) mono-dimensional N-H...O chains viewed along the [100] direction; (b) N-H...O mono-dimensional chains viewed along the [001] direction (c) portion of the crystal packing of **L_5** viewed along the [100] direction.

Crystals for the adduct of **L_6** with benzoate were obtained by slow evaporation of a saturated MeCN solution of **L_6** containing an excess of the TBABzO salt.

[(**L_6**)(BzO)(TBA)], that is characterized by a 1:1 receptor/anion molar ratio, crystallizes in the monoclinic crystal system (space group: $P2_1/n$). The

asymmetric unit of the adduct contains one independent **L_6** receptor unit and one BzO^- anion balanced by one TBA^+ cation (Z′ = 4). The nitro and iodo groups point in opposite directions probably to minimize the steric hindrance. The anion interacts *via* a bifurcated N-H...O hydrogen bond involving only one carbonyl Oxygen and the second to form a weaker C-H…O hydrogen bond (N-H...O distances are in the range 1.92(4)-2.10(4) Å while the angle NHO is in the range of 143.0(3)°). The benzoate unit is further stabilized by a C-H…O interaction involving an aromatic proton of the nitro-phenyl moiety and the other Oxygen atom of BzO^- (C-H...O distances is 2.10(4) Å).

This evidence could be possibly explained considering the higher acidity of the aromatic protons of the nitro-phenyl arm with respect to the iodo-phenyl one. Moreover, in this conformation, the presence of the iodine atom in *ortho* position in the aromatic ring makes its protons unenviable to the anion coordination.

The guest units interact with different receptor molecules also *via* C-H…O interactions involving one aromatic proton of the nitro-phenyl fragment with an Oxygen atom of the nitro group of a receptor unit (C-H...O distances are 2.64 Å respectively) (see Figure 2.5b). The asymmetric unit repetitions results in a staggered space packing as shown in Figure 2.5c.

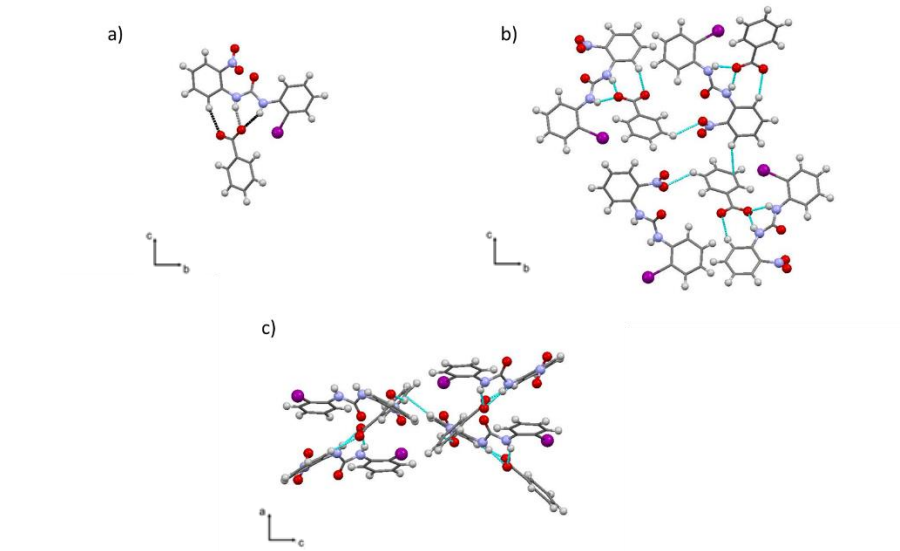

Figure 2.5 X-Ray crystal structure of the adduct of **L_6** with BzO^-. (a) View of the host:guest interaction of **$L_{6\text{-}BzO}$**; (b) View of the interactions of the benzoate units in the crystal system. (c) View of the staggered space crystal packing of **$L_{6\text{-}BzO}$**.

Two samples suitable for single crystal X-ray diffraction of receptor **L_8** were isolated. The crystals were obtained from crystallization made from different conditions: the "pure" form of **L_8** and its solvated form **$L_{8\text{-}DMSO}$** were obtained by slow evaporation from a saturated solution of the receptor in MeOH and in DMSO:MeCN mixture, respectively for **L_8** and **$L_{8\text{-}DMSO}$**.

Receptor **L_8** crystallizes in the orthorhombic crystal system (space group: $Pna2_1$) with the asymmetric unit that shows only one independent receptor molecule (Z' = 1). Similarly to the structures described above, the receptor molecules are connected via N-H...O hydrogen bonds (N-H…O intermolecular distances of 2.292(2) Å and 2.857(2) Å respectively, while the angle NHO are 132.7(2)° and 127.3(1)°) to form one-dimensional chains developing along the [001] direction

(Figure 2.6 b). These chains are then connected to adjacent chain via set of N-H...O and C-H...O hydrogen bonds involving the nitro groups (N-H...O distances are in the range 2.42(3)-2.79(3) Å, C-H...O distances are in the range 2.34(3)-2.61(3) Å) and a set of weak C-H...Cl interactions (C-H...Cl distances are in the range 2.92(4)-3.41(4) Å), generating the resulting three dimensional packing (Figure 2.6 c).

The solvated form of receptor $\mathbf{L_{8\text{-}DMSO}}$ crystallizes in the triclinic crystal system (space group: P1) with the asymmetric unit that shows only one independent receptor molecule (Z' = 1).

In the case of $\mathbf{L_{8\text{-}DMSO}}$ the formation of typical urea-urea molecular arrangements is inhibited by the presence of DMSO molecules which strongly interact with the NH groups by strong N-H...O hydrogen bonds (N-H…O intermolecular distances are in the range 1.869(2)-2.254(2) Å while the angle NHO is around 158.7(2)°), preventing any formation of the 1-D chains observed in the majority of the structures. DMSO molecules bridges adjacent receptor molecules along the [110] (Figure 2.6e) and along the [1-10] direction via C-H...O hydrogen bonds involving the nitro groups and the methyl groups (C-H...O intermolecular interactions are in the range 2.503(2)- 2.891(2) Å). The receptors molecules are connected along the [001] direction via two set of weak interactions, C-H...O and C-H...Cl involving the nitro groups and chlorides (C-H…Cl intermolecular distances are in the range 2.791(5)-2.921(5) Å) to for the 2-D plane reported in figure 2.6e. These planes are then bridged by DMSO molecules along the [1-10] direction to form the 3-D packing.

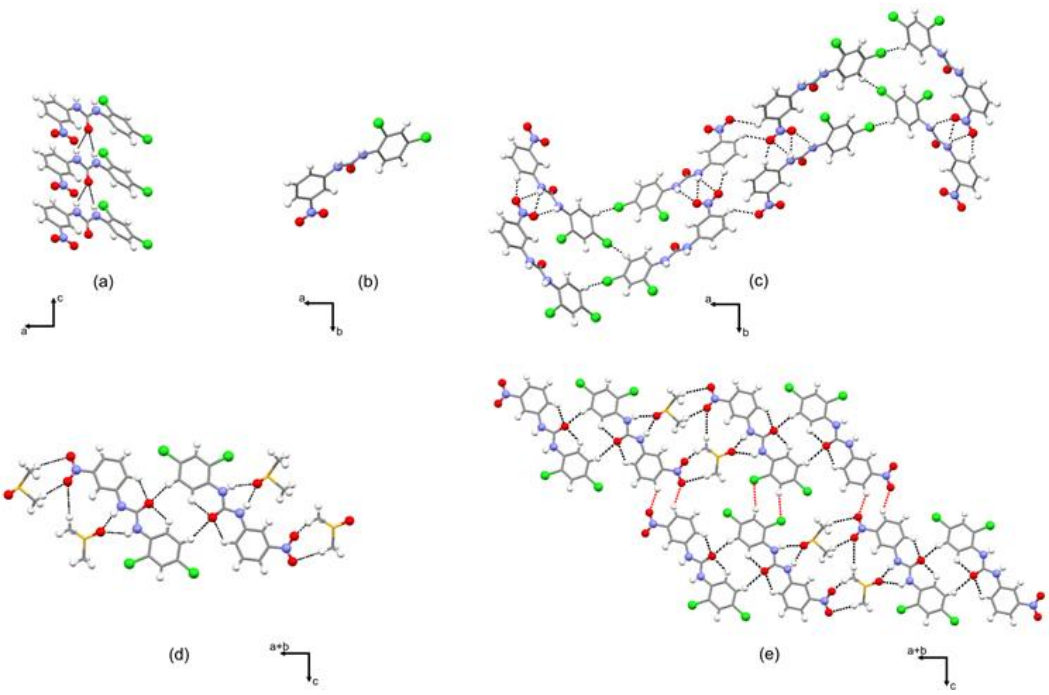

Figure 2.6 Crystal structure **L_8**, mono-dimensional N-H...O chains viewed along the [010] direction. (b) Crystal structure **L_8**, mono-dimensional N-H...O chains viewed along the [100] direction. (c) Portion of the crystal packing of **L_8** viewed along the [001] direction. (d) DMSO-receptor interactions in the structure of **$L_{8\text{-}DMSO}$** (e) 2-D portion of the crystal packing of **$L_{8\text{-}DMSO}$**: 2-D planes.

Crystals of the solvated form of receptor **L_{11}** were obtained by slow evaporation from a saturated solution of the receptor in DMF:MeCN (1:1, v/v) mixture. The solvated form **$L_{11\text{-}DMF}$** crystallizes in the monoclinic crystal system (space group: $P2_1/n$) with the asymmetric unit that shows only one independent receptor unit with a molecule of DMF ($Z' = 1$) as shown in Figure 2.7a. The receptor molecules

interact *via* a C-H…O interaction involving the Oxygen atom of the nitro group and C-H aromatic protons of another receptor unit (C-H…O intermolecular distances are in the range 2.613(3)-2.645(3) Å) and *via* weak hydrogen bond between the Oxygen atom of the carbonyl group of a receptor molecule and the C-H aromatic protons of the adjacent receptors (C-H…O intermolecular distances are in the range 2.491(3)-2.512(3) Å) (see Figure 2.7b). In Figure 2.7c, it is also possible to note the staggered space arrangement in the packing of **$L_{11\text{-DMF}}$**.

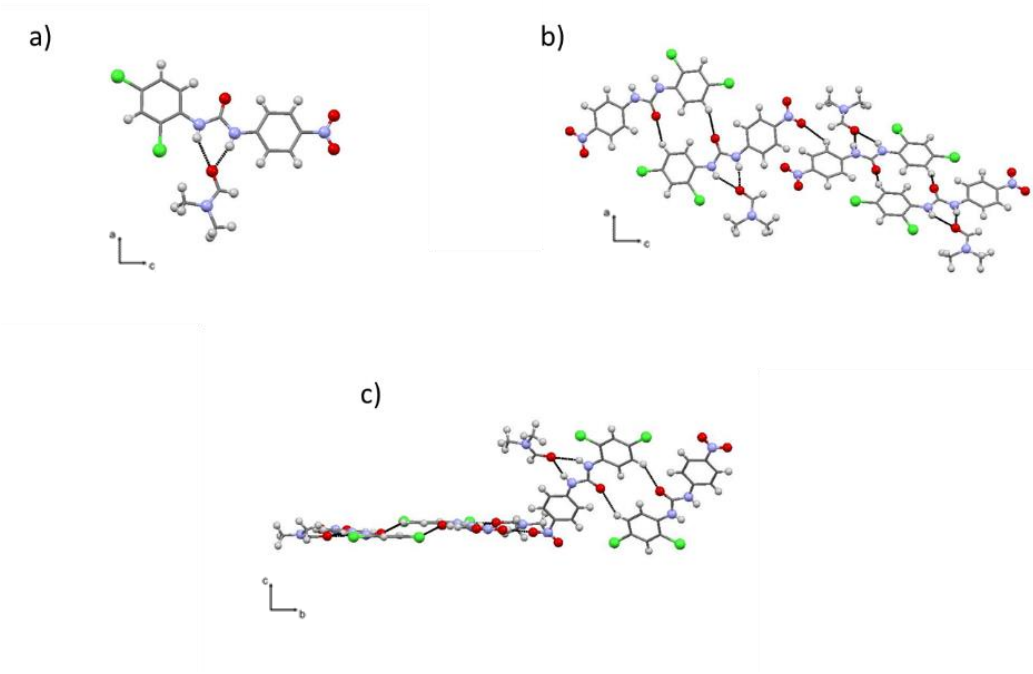

Figure 2.7 X-Ray crystal structure of the solvated form **$L_{11\text{-DMF}}$**. (a) View of the interaction between **L_{11}** a solvent molecule (b) Crystal packing of **$L_{11\text{-DMF}}$**. (c) View of the space arrangement of **$L_{11\text{-DMF}}$**.

Crystals of receptor **L_{14}** were obtained by slow evaporation from a saturated solution of the receptor in MeCN.

This receptor crystallizes in the monoclinic crystal system (space group: Pc). The asymmetric unit, shown in Figure 2.8a, contains two independent receptor units (Z'=2) (N-H…O intermolecular distances of 1.96(2)-2.40(2) Å while the NHO angle is 142.2(3)° and 142.7(3)° for the receptor unit 1 and 2 respectively).

Each receptor unit forms a mono-dimensional chain along the crystallographic axis [100] as shown in Figure 2.8b. The two independent chains (figure 2.8a) are connected to adjacent chains along the [100] and [010] directions uniquely by a set of C-H...F and C-H...Cl weak interactions (C-H…Cl intermolecular distances are 2.92(3) Å, C-H…F intermolecular distances are 2.64(1) Å) as shown Figure 2.8c.

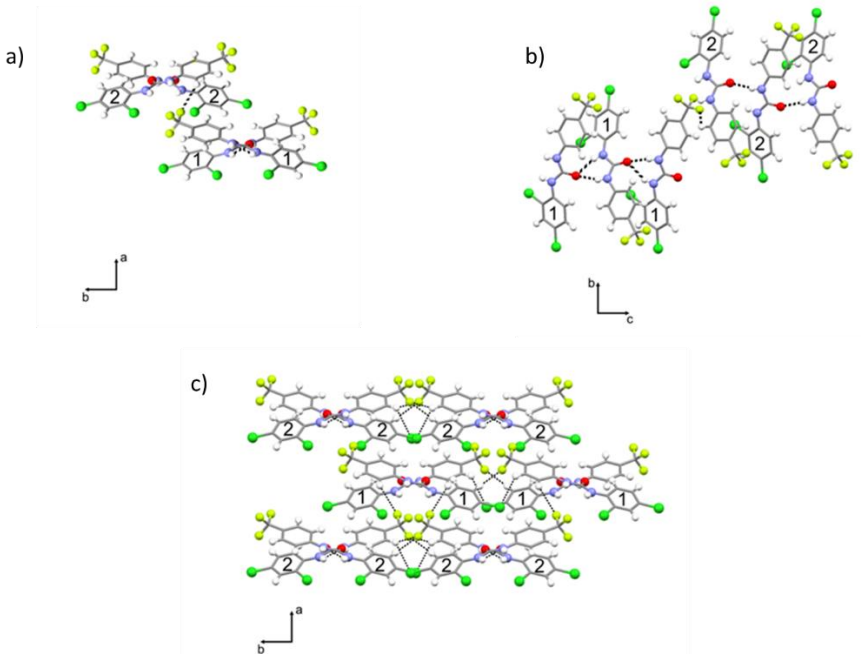

Figure 2.8 (a) Representation of the two independent mono-dimensional N-H...O chains 1 and 2 viewed along the [001] direction. (b) Representation of the two independent mono-dimensional N-H...O chains 1 and 2 viewed along the [100] direction. (c) Crystal packing of **L_{14}** viewed along the [001] direction.

Crystals of receptor **L_{15}** were obtained by slow evaporation from a saturated MeCN solution of the receptor. **L_{15}** crystallizes in the orthorhombic crystal system (space group: $Pca2_1$). The asymmetric unit contains one independent receptor unit (Z'=1) able to form a mono-dimensional chain *via* N-H…O hydrogen bond (N-H…O intermolecular distances are in the range 2.06(1)-2.14(1) Å while the NHO angle is in around 145(1)°) as shown in Figures 2.9a and b. Figure 2.9c displays a very interesting aspect in this crystal structure: the presence of halogen bond interaction between iodine atom of a receptor unit and an Oxygen atom of the carbonyl groups of another receptor molecule (distance of 3.50 Å). The iodine atom of a receptor molecule also interacts with the aromatic protons of another receptor unit (C-H…I intermolecular distances are in the range 3.21(2)-3.26(2) Å) (see Figure 2.9c).

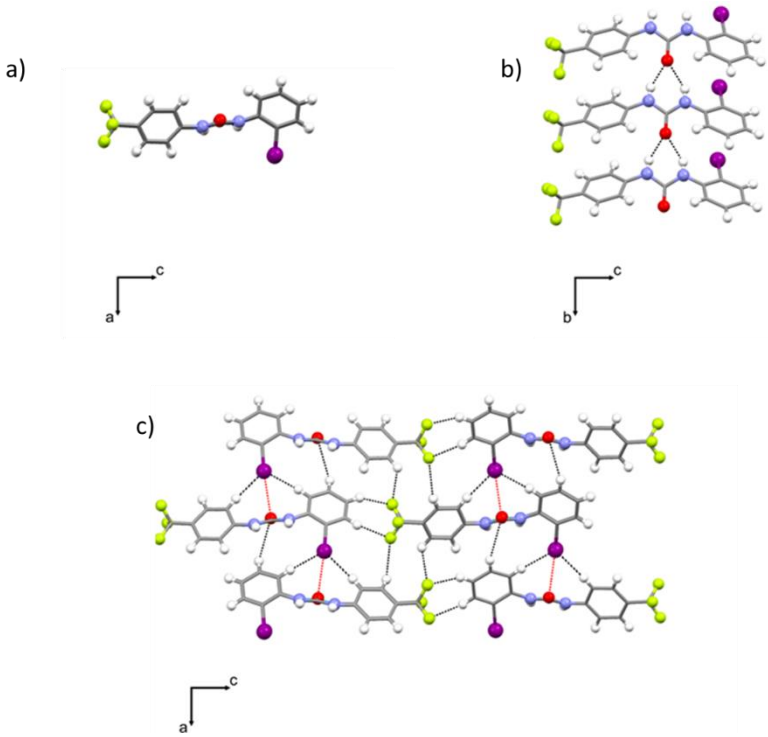

Figure 2.9 X-Ray crystal structure of **L_{15}**. (a) Representation of the mono-dimensional N-H...O chain viewed along the [010] direction. (b) mono-dimensional N-H...O chain viewed along the [100] direction. (c) Crystal packing of **L_{15}** viewed along the [010] direction. Halogen bonding are indicated as red dotted lines.

2.4 ^{1}H-NMR Spectroscopy

In order to evaluate the anion binding ability of the receptors, ^{1}H-NMR titrations were carried out in DMSO-d_6. The EQNMR program [15] was used to calculate stability constants from the ^{1}H-NMR titration curves obtained fitting the data to a 1:1 binding model as shown in Table 2.2.

Table 2.2 Association constants (M^{-1}) for the equilibrium reactions of **L_1–L_{15}** with the tetrabutylammonium salts of the anion considered in DMSO-d_6 at 300 K.

Receptor	$H_2PO_4^-$	Cl^-	F^-	AcO^-	BzO^-
L_1	1117.0 ± 1.7%	34.5 ± 0.1%	Deprot. [a]	2765.0 ± 1.2%	364 ± 9.3%
L_2	231.0 ± 2.5%	17.7 ± 3.6%	Deprot. [a]	445.0 ± 11.0%	136± 1.7%
L_3	174.0 ± 6.0%	<10	Deprot. [a]	277.0 ± 0.6%	100 ± 1.3%
L_4	684.0 ± 5.9%	<10	Deprot. [a]	1283.0 ± 3.5%	314 ± 5.9%
L_5	[b]	<10	Deprot. [a]	Deprot. [a]	123.3 ± 5.9%
L_6	[b]	<10	Deprot. [a]	218.0 ± 3.9%	87.3 ± 11.0%
L_7	[b]	57.8 ± 1.8%	Deprot. [a]	9620.0 ± 3.8%	3322.0 ± 1.8%
L_8	[b]	35.2 ± 7.8%	Deprot. [a]	1883.0 ± 8.1%	567.0 ± 0.9%
L_9	[b]	20.6 ± 2.3%	Deprot. [a]	1611.0 ± 4.3%	425.0 ± 2.8%
L_{10}	[b]	68.6 ± 2.9%	Deprot. [a]	13467.0 ± 2.3%	3513.0 ± 19.3%

Receptor	$H_2PO_4^-$	Cl^-	F^-	AcO^-	BzO^-
L_{11}	[b]	36.8 ± 0.7%	Deprot. [a]	6833.0 ± 30.0%	780.0 ± 1.7%
L_{12}	[b]	26.2 ± 6.2%	Deprot. [a]	1470.0 ± 5.6%	681.0 ± 1.6%
L_{13}	871.9 ± 32%	52.2 ± 3.3%	Deprot. [a]	2608.0 ± 17%	1980.0 ± 6.4%
L_{14}	[b]	33 ± 4.8%	Deprot. [a]	642.0 ± 4.8%	514.0 ± 11.0%
L_{15}	[b]	14 ± 8.3%	Deprot. [a]	583.5 ± 23.0%	301.0 ± 1.8%

[a] The NH signals disappeared after the addition of one equivalent of anion. [b] Experimental evidence suggests strong interaction.

2.4.1 ^{1}H-NMR titrations of receptors L_1-L_3

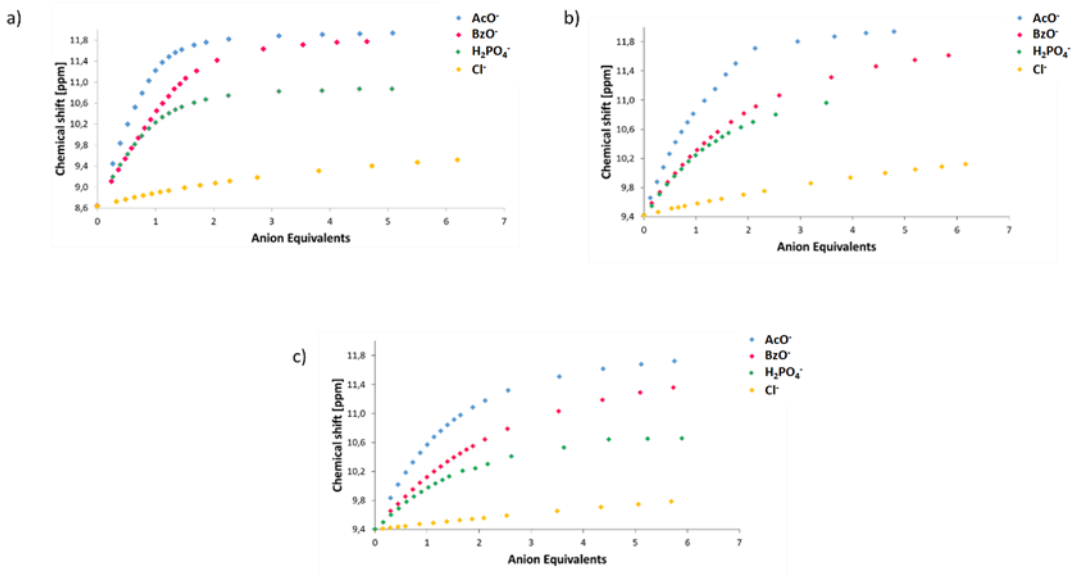

Figure 2.10 Changes of the ^{1}H-NMR shift for the NH protons upon addition of increasing amounts of the anionic guests to a DMSO-d_6 solution of **L_1** (a), **L_2** (b), and **L_3** (c).

Figure 2.10 shows the ^{1}H-NMR trends of the NH (localized on the non-halogenated phenyl ring side) chemical shift of the receptors **L_1**-**L_3** *versus* the anion equivalents added. By means of COSY (Correlation Spectroscopy) bidimensional NMR experiment it was possible to attribute the correct chemical shift value for each NH proton in the asymmetrical receptors **L_2** and **L_3**: the signal of the NH proton in close proximity of the phenyl moiety is downfield shifted with respect to the signal of the NH proton near the 2,4-dichloro phenyl and the 2-iodophenyl fragments for **L_2** and **L_3** respectively. Stability constants calculated following both NH proton signals were comparable so we decided to follow the chemical shift of the NH proton signal in close proximity of the phenyl moiety.

As it possible to note in Figure 2.10, moving from **L_1** to **L_3** the titration curves have a neat inflection point in the case of **L_1** (Figure 2.10a) while for the other two receptors (Figures 2.10b and c) the inflection point is less marked. This evidence easily explains the higher stability constants determined for **L_1** with respect to **L_2** and **L_3** for the anionic guests studied.

These results are in agreement with the steric hindrance degree of the three receptors increasing in the order **L_3>L_2>L_1** The presence of the chlorine or iodine atom in *ortho* position of the halogenated phenyl ring with respect to the urea function, for **L_2** and **L_3** respectively, partially obstructs the anion access to the coordination site of the receptor. Several anion binding studies for receptor **L_1** are reported in literature, in particular for carboxylates recognition. [11,12]

The stability constants obtained for the equilibrium of **L_1** with acetate and benzoate at 300 K are consistent with the values reported by Leito and co-workers at 298K.[12] The slight values difference is probably connected with the difference in the temperature at which the experiments were conducted (300 K in our case and 298 K on the case of Leito's group).

2.4.2 ^{1}H-NMR titrations of receptors L_4-L_6

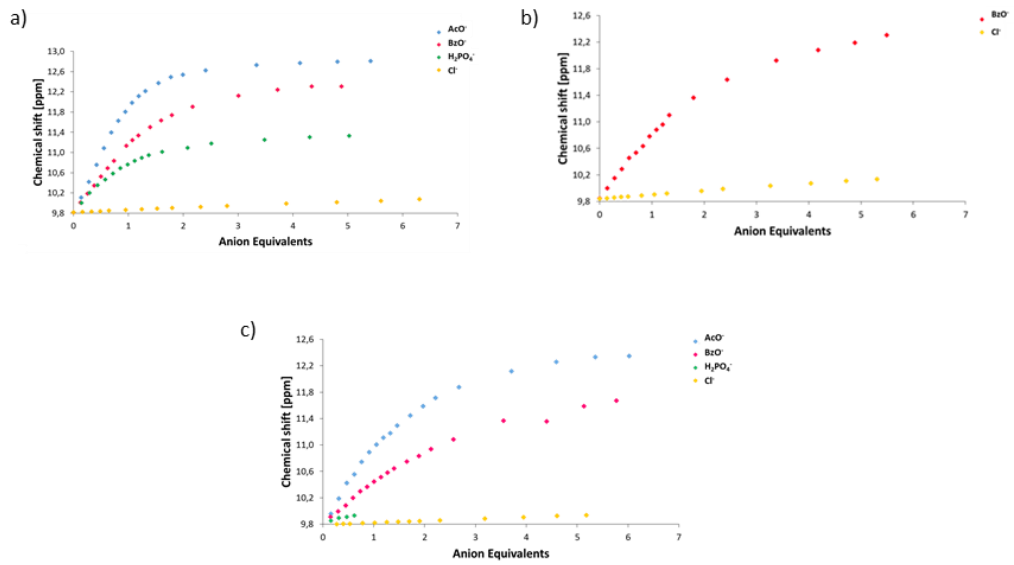

Figure 2.11 Changes of the ^{1}H-NMR shift for the NH protons upon addition of increasing amounts of the anionic guests to a DMSO-d_6 solution of **L_4** (a), **L_5** (b), and **L_6** (c).

In the set **L_4-L_6** the presence of the nitro group in *ortho* position with respect to the central urea function in addition to the presence of the chlorine and iodine atoms in the halogenated phenyl rings causes a decrease in the calculated stability constants values. This evidence can be explained in terms of steric effects. As previously shown in Figure 2.6 the nitro group is in close proximity of the urea function and it could obstruct the anion coordination. AcO^- and $H_2PO_4^-$ cause deprotonation of the receptor **L_5** presumably because of the electronic effect of the nitro group in *ortho* position that affects the NH proton acidity.

2.4.3 ^{1}H-NMR titrations of receptors L_7-L_9

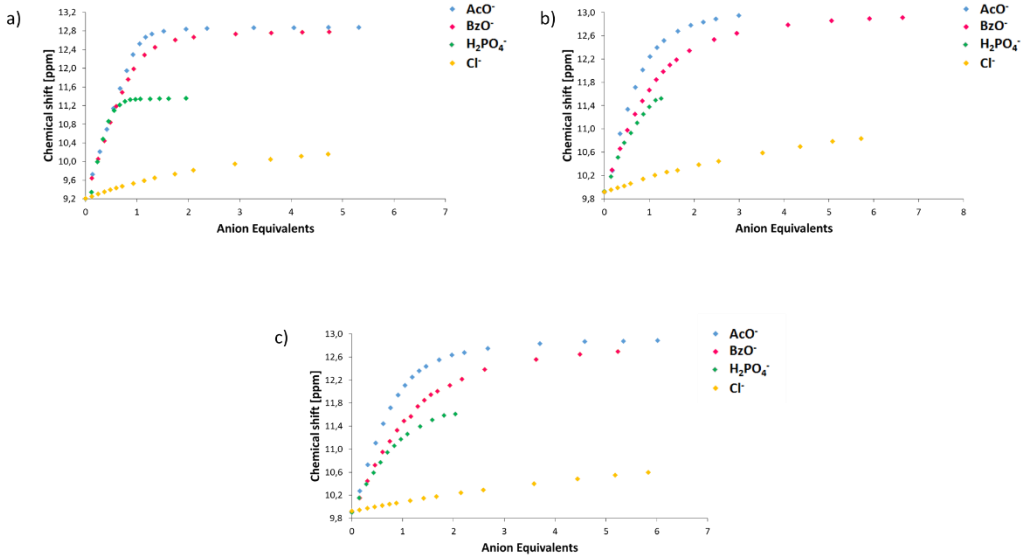

Figure 2.12 Changes of the ^{1}H-NMR shift for the NH protons upon addition of increasing amounts of the anionic guests to a DMSO-d_6 solution of **L_7** (a), **L_8** (b), and **L_9** (c).

In the set of receptors **L_7-L_9** , The titration curves have a neat inflection point in the case of **L_7** (Figura 2.12a). The stability constants increase with respect to the previously set **L_4-L_6** probably due the *meta* position of the nitro group that permits an easier anion access in the proximity of the urea site. Receptor **L_7** was studied by means of UV-Visible spectroscopy and ^{1}H-NMR by Ciarrocchi [9] and Leito respectively. [11,12] Also in this case the values reported in this thesis are in agreement with the literature.

2.4.4 ^{1}H-NMR titrations of receptors L_{10}-L_{12}

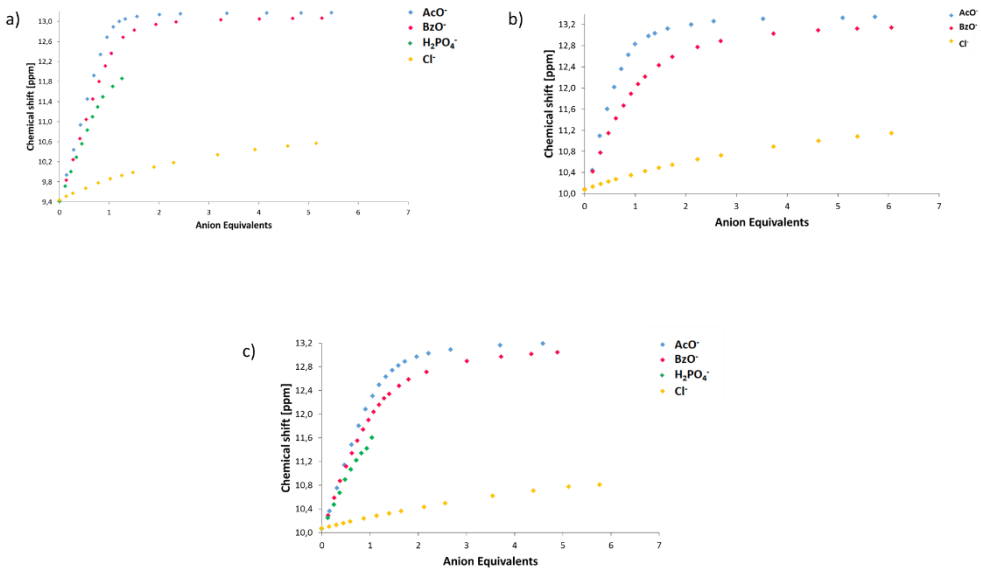

Figure 2.13 Changes of the ^{1}H-NMR shift for the NH protons upon addition of increasing amounts of the anionic guests to a DMSO-d_6 solution of **L_{10}** (a), **L_{11}** (b), and **L_{12}** (c).

The receptor series **L_{10}-L_{12}** shows the higher values of stability constants among all the receptors containing a nitro group functionalization. In particular receptor **L_{10}**, already known in the literature, displays a good affinity for acetate as confirmed by the value of stability constant > 10^4 M^{-1}. [16] The reasons that lead to an increasing in the anion coordination attitude of these receptors are of steric and electronic natures. First, the nitro group in *para* position decreases the steric hindrance with respect to the active urea function allowing an easier access of the anion in the pseudo cavity of the receptors also for bigger anion like benzoate. On the other hand, the *para* position of the electron withdrawing nitro group influences in a positive way the coordination properties of the ligands increasing the urea NH protons acidity.

2.4.5 1H-NMR titrations of receptors L_{13}-L_{15}

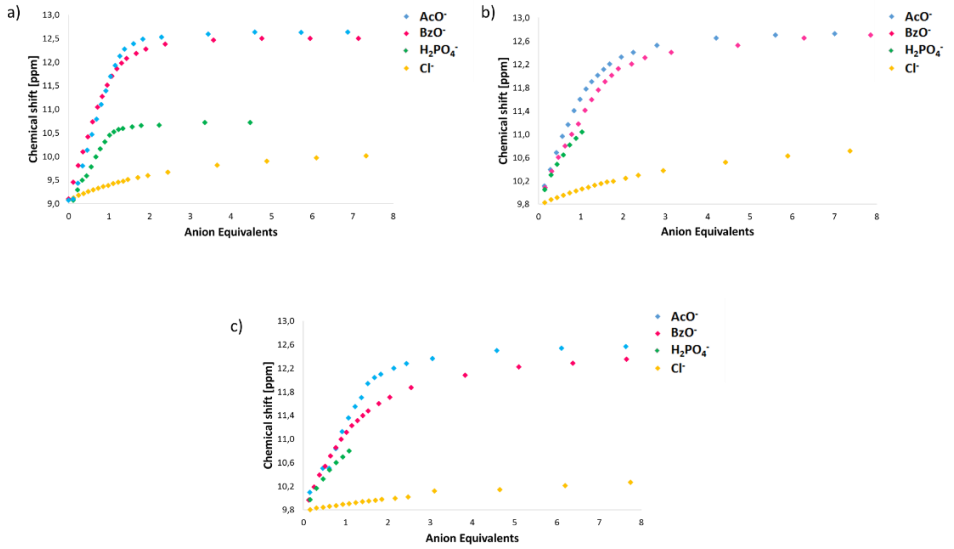

Figure 2.14 Changes of the ^{1}H-NMR shift for the NH protons upon addition of increasing amounts of the anionic guests to a DMSO-d_6 solution of **L_{13}** (a), **L_{14}** (b), and **L_{15}** (c).

The anion binding activity along this series is consistent with the trends previously described for the other receptors. The stability constants decrease from **L_{13}** to **L_{15}** because of the steric hindrance of the halogen in the phenyl ring. By Comparing the stability constant value of receptor **L_{15}** (14.0 ± 8.3% Ka/M^{-1} , 583.5 ± 23% Ka/M^{-1} , 301.0 ± 1.8% Ka/M^{-1} for Cl^-, AcO^- and BzO^- respectively) with **L_3**, receptor without substituents in the no-halogenated phenyl ring (174.0 ± 6% Ka/M^{-1} , <10 Ka/M^{-1} , 277.5 ± 0.6% Ka/M^{-1}, 100.0 ±1.3% Ka/M^{-1} for $H_2PO_4^-$, Cl^-, AcO^- and BzO^- respectively) and **L_{12}**, receptor with a nitro group in place of the tri-fluoromethy unit (26.2 ± 6.2% Ka/M^{-1}, 1470.0 ± 5.6% Ka/M^{-1}, 681.0 ±1.8% Ka/M^{-1} for Cl^-, AcO^- and BzO^- respectively) it is possible to define the increasing anion affinity in the order **L_3** < **L_{15}** < **L_{12}**.This evidence is in agreement with the lower acidity of the NHs protons in the "nude" (without any substituents in the

no-halogenated ring) receptor **L_3** with respect to receptors **L_{15}** and **L_{12}**. On the other hand, between receptors **L_{15}** and **L_{12}**, the lower ability to bind anion of receptor **L_{15}** is connected with the lower electron withdrawing nature of the CF_3 group with respect to the NO_2 group. The same behaviour can be found for the series **L_1**-**L_{10}**-**L_{13}** and **L_2**-**L_{11}**-**L_{14}**.

2.5 Conclusion

In conclusion, we have synthetized and studied by means of ^{1}H-NMR spectroscopy and single crystal X-Ray diffraction, the asymmetric urea-based receptors **L_1**-**L_{15}** that present two phenyl rings functionalised with halogens, nitro and trifluoromethyl substituents. The results showed that, in order to improve the selectivity in terms of anion recognition, an equilibria between the kind of the activating substituents, their steric hindrance and position in the receptor structure must be found. The series of ligands **L_{10}**-**L_{12}** with a nitro group in *para* position in the no-halogenated phenyl ring showed the best attitude to recognize anions with respect to the other series due the positive electron withdrawing effect of the nitro group in *para* position of the phenyl arm. The presence of the halogenated substituents in the other aromatic ring did not cause an improvement in the anion binding attitude of the receptors probably because the *ortho* halogenated position obstructed the anion access to the coordination site. Moreover, halogen bonds were not observed (except in the solid state for **L_{15}**) so a different insertion of the halogenated functionalizations that promotes the anion complexation also *via* halogen bond must be designed for the future.

2.6 Experimental methods

All reactions were performed in oven-dried glassware under a slight positive pressure of Nitrogen. 1H-NMR (400 MHz, 500MHz) and 13C NMR (100 MHz, 125MHz) spectra were determined on a Varian INOVA-400 spectrometer, and Varian INOVA-500 spectrometer. Chemical shifts for 1H NMR are reported in parts per million (ppm), calibrated to the residual solvent peak set, with coupling constants reported in Hertz (Hz). The following abbreviations are used for spin multiplicity: s = singlet, d = doublet, t = triplet, m = multiplet . Chemical shifts for 13C NMR are reported in ppm, relative to the central line of a septet at δ = 39.52 ppm for deuteriodimethylsulfoxide. Infrared (IR) spectra were recorded on a NICOLET 5700 FT-IR spectrophotometer and reported in wavenumbers (cm−1). All solvents and starting materials were purchased from commercial sources where available. Proton NMR titrations were performed by adding aliquots of the putative anionic guest (as the TBA salt, 0.075 M) in a solution of the receptor (0.005M) in DMSO-d6/0.5% water to a solution of the receptor (0.005M).

2.6.1 Synthetic procedure

Synthesis of L_2

A solution of 2,4-dichloroaniline (0.320 g , 2.00 mmol) in DCM (10 ml) was added dropwise to a solution of isocyanate-benzene (0.240 g, 2.00 mmol), in DCM (15ml). The mixture was refluxed overnight and then it was filtered to give the desired compound as a grey solid. Yield 30% (0.170g, 0,60mmol); M.p.: 212°C; ^{1}H-NMR (400 MHz,DMSO- *d_6*, 300 K): δH: 9.42 (s, 1H); 8.38 (s, 1H); 8.20 (d, J = 8 Hz, 1H); 7.62 (s, 1H); 7.46 (d, J = 8.0 Hz, 2H); 7.38 (d, J = 8 Hz, 1H); 7.30 (t, J = 8 Hz, 2H); 7.00 (t, J = 8 Hz, 1H); ^{13}C-NMR (125 MHz, DMSO- *d_6*, 298 K), δC: 151.96, 139.23, 135.23, 128.86, 128.49, 127.58, 126.03, 122.55, 122.24, 122.05, 118.25. IR: (KBr, cm^{-1}): $\bar{\nu}$ CO: 1653 (CO stretching); $\bar{\nu}$ NH: 3280 (NH urea stretching).

Synthesis of L_3

A solution of 2-iodoaniline (0.470g , 2.14 mmol) in DCM (10 ml) was added dropwise to a solution of isocyanate-benzene (0.250 g, 2.14 mmol), in DCM (10ml). The mixture was refluxed overnight and then it was filtered to give the desired compound as a grey solid. Yield 74% (0.530g, 1.58 mmol); M.p.: 200°C; ^{1}H-NMR (400 MHz,DMSO- d_6, 300 K): δH: 9.40 (s, 1H); 7.88 (s, 1H); 7.82 (d, J = 8 Hz, 2H); 7.46 (d, J = 8 Hz, 2H); 7.34 (t, J = 8.0 Hz, 1H); 7.29 (t, J = 8 Hz, 2H); 6.98 (t, J = 8 Hz, 1H); 6.84 (t, J = 8 Hz, 1H); ^{13}C-NMR (125 MHz, DMSO-d_6, 298 K), δC: 152.35, 139.84, 139.59, 138.89, 128.80, 128.53, 124.98, 123.05, 121.98, 118.20, 91.27. IR: (KBr, cm^{-1}): $\bar{\nu}$ CO: 1641 (CO stretching); $\bar{\nu}$ NH: 3278 (NH urea stretching).

Synthesis of L_5

A solution of 2,4-dichloroaniline (0.35g , 2.15 mmol) in DCM (10 ml) was added dropwise to a solution of 1-isocyanate-2-nitrobenzene (0.35 g, 2.15mmol), in DCM (10ml). The mixture was refluxed overnight and then it was filtered and then washed in DCM to give the desired compound as a white solid. Yield 30% (0.65g, 0.65 mmol); M.p.: 221°C; ^{1}H-NMR (400 MHz,DMSO- d_6, 300 K): δH: 9.85 (s,1H); 9.31 (s, 1H); 8.06 (d, J= 8 Hz, 2H); 7.98 (d, J = 8 Hz, 1H); 7.71 (t, J = 8.0 Hz, 1H); 7.66 (s, 1H); 7.41 (d, J = 8 Hz, 1H); 7.27 (t, J = 8 Hz, 1H); ^{13}C-NMR (100 MHz, DMSO- d_6, 300K), δC: 147.80; 134.33; 132.50; 131.26; 130.25; 129.43; 128.53; 128.19; 126.24; 122.86; 119.84. IR: (KBr, cm^{-1}): $\bar{\nu}$ CO: 1652 (CO stretching); $\bar{\nu}$ NH: 3331 (NH urea stretching).

Synthesis of L_6

A solution of 2-iodoaniline (0.470g , 2.15 mmol) in DCM (10 ml) was added dropwise to a solution of 1-isocyanate-2-nitrobenzene (0.350 g, 2.15mmol), in DCM (10ml). The mixture was refluxed overnight and then it was filtered and then washed in DCM to give the desired compound as a white solid. Yield 58% (0.480g, 1.25 mmol); M.p.: 192°C; ^{1}H-NMR (400 MHz,DMSO- d_6, 300 K): δH: 9.80 (s, 1H); 9.02 (s, 1H); 8.15 (d, J = 8 Hz, 1H); 8.06 (d, J = 8 Hz, 1H); 7.88 (d, J= 8 Hz, 1H); 7.70 (t, J = 8 Hz, 1H); 7.61 (d, J = 8.0 Hz, 1H); 7.38 (t, J = 8Hz, 1H); 7.24 (t, J = 8 Hz, 1H); 6.94 (t, J = 8 Hz, 1H); ^{13}C-NMR (125 MHz, DMSO- d_6, 298K), δC:152.33, 139.4, 138.97, 138.57, 134.60, 134.22, 128.60, 126.45, 125.60, 125.20, 123.21, 122.61, 94.01. IR: (KBr, cm^{-1}): $\bar{\nu}$ CO: 1651 (CO stretching); $\bar{\nu}$ NH: 3331 (NH urea stretching).

Synthesis of L_8

A solution of 1-isocyanate-3-nitrobenzene (0.220g , 1.34 mmol) in DCM (10 ml) was added dropwise to a solution of 2,4-dichloroaniline (0.210g, 1.34mmol), in DCM (10ml). The mixture was refluxed overnight and then it was filtered and washed in DCM to give the desired compound as a white solid. Yield 67% (0.290g, 0.90 mmol); M.p.: 217°C; ^{1}H-NMR (400 MHz,DMSO- d_6, 298 K): δH: 9.93 (s, 1H); 8.51 (s, 1H); 8.57 (s, 1H); 8.17 (d, J = 8 Hz, 1H); 7.86 (d, J = 8 Hz, 1H); 7.69 (d, J = 8.0 Hz, 1H); 7.65 (s, 1H); 7.59 (t, J = 8 Hz, 1H); 7.41 (d, J = 8 Hz, 1H); ^{13}C-NMR (100 MHz, DMSO- d_6, 298K), δC: 152.10; 148.17; 140.69; 134.96; 130.20; 128.61; 127.67; 126.63; 124.27; 123.31; 122.65; 116.62; 112.12. IR: (KBr, cm^{-1}): $\bar{\nu}$ CO: 1678(CO stretching); $\bar{\nu}$ NH: 3385 (NH urea stretching).

Synthesis of L_9

A solution of 2-iodoaniline (0.470g , 2.14 mmol) in DCM (10ml) was added dropwise to a solution of 1-isocyanate-3-nitrobenzene (0.280g, 1.78mmol), in DCM (10ml). The mixture was stirred overnight and then it was filtered and washed in DCM to give the desired compound as a white solid. Yield 56% (0.370g, 0.97 mmol); M.p.: 231°C; ^{1}H-NMR (500 MHz,DMSO- d_6, 300K): δH: 9.90 (s, 1H); 8.04 (s, 1H); 8.56 (s, 1H); 7.80-7.89 (m, 3H); 7.73 (d, J = 8.0 Hz, 1H); 7.59 (t, J = 8 Hz, 1H); 7.37 (t, J = 8 Hz, 1H); 6.89 (t, J = 8 Hz, 1H); ^{13}C-NMR (100 MHz, DMSO- d_6, 300K), δC: 152.99; 147.99; 141.58; 140.06; 139.62; 130.82; 129.31; 126.30; 124.82; 124.22; 117.08; 112.72. IR: (KBr, cm^{-1}): $\bar{\nu}$ CO: 1646 (CO stretching); $\bar{\nu}$ NH: 3294 (NH urea stretching).

Synthesis of L_{11}

A solution of 1-isocyanate-4-nitrobenzene (0.260g , 1.58 mmol) in DCM (10 ml) was added dropwise to a solution of 2,4-dichloroaniline (0.260g, 1.58mmol), in DCM (10ml). The mixture was stirred overnight at room temperature and then it was filtered and washed in DCM to give the desired compound as a yellow solid. Yield 51% (0.260g, 0.80 mmol); M.p.: >250°C; ^{1}H-NMR (500 MHz,DMSO- d_6, 300K): δH: 10.08 (s, 1H); 8.59 (s, 1H); 7.21 (d, J = 8 Hz, 2H); 8.16 (d, J = 8.0 Hz, 1H); 7.70 (d, J = 8 Hz, 2H); 7.66 (s, 1H); 7.42 (d, J = 8 Hz, 1H). ^{13}C-NMR (100 MHz, DMSO- d_6, 298K), δC: 151.85, 146.23, 141.20, 134.85, 128.63, 127.55, 126.78, 125.12, 123.49, 122.74, 117.61 . IR: (KBr, cm^{-1}): $\bar{\nu}$ CO: 1735 (CO stretching); $\bar{\nu}$ NH: 3373 (NH urea stretching).

Synthesis of L_{12}

A solution of 1-isocyanate-4-nitrobenzene (0.260g , 1.58 mmol) in DCM (10 ml) was added dropwise to a solution of 2-iodoaniline (0.350g, 1.58mmol), in DCM (10ml). The mixture was refluxed for one hour and then it was stirred overnight at room temperature. It was filtered and washed in DCM to give the desired compound as a yellow solid. Yield 57% (0.350g, 0.91 mmol); M.p.: 219°C; ^{1}H-NMR (500 MHz,DMSO- d_6, 298K): δH: 10.04 (s, 1H); 8.10 (s, 1H); 8.18 (d, J = 8 Hz, 2H); 7.84 (d, J = 8 Hz, 1H); 7.76 (d, J = 12.0 Hz, 1H); 7.68 (d, J = 8 Hz, 2H); 7.35 (t, J = 8 Hz, 1H); 6.87 (t, J = 8 Hz, 1H); 7.70 (d, J = 8 Hz, 2H); 7.66 (s, 1H); 7.42 (d, J = 8 Hz, 1H). ^{13}C-NMR (125 MHz, DMSO-d_6, 298K), δC: 151.94, 146.20, 141.06, 139.08, 138.97, 128.59, 125.78, 125.17, 123.58, 117.50, 92.16. IR: (KBr, cm^{-1}): $\bar{\nu}$ CO: 1641 (CO stretching); $\bar{\nu}$ NH: 3288 (NH urea stretching).

Synthesis of L_{14}

A solution of 1-isocyanate-4-(trifluoromethyl)benzene (0.250g , 1.34 mmol) in DCM (10ml) was added dropwise to a solution of 2,4-dchloroaniline (0.210g, 1.34 mmol), in DCM (10ml). The mixture was stirred overnight at room temperature. It was filtered and washed in DCM to give the desired compound as a white solid. Yield 71% (0.37g, 1.06 mmol); M.p.: 216°C; ^{1}H-NMR (500 MHz,DMSO- d_6, 298K): δH: 9.80 (s, 1H); 8.49 (s, 1H); 8.17 (d, J = 8 Hz, 2H); 7.63-7.68 (m, 3H); 7.40 (d, J = 8 Hz, 2H);^{13}C-NMR (100 MHz, DMSO- d_6, 298K), δC: 154.92, 146.11, 137.99, 131.65, 130.71, 129.62, 129.23, 129.20, 126.01, 125.36, 121.05,94.99.

Synthesis of L_{15}

A solution of 1-isocyanate-4-(trifluoromethyl)benzene (0.250 g , 1.34 mmol) in DCM (10 ml) was added dropwise to a solution of 2-iodoaniline (0.290 g, 1.34 mmol), in DCM (10ml). The mixture was stirred overnight at room temperature. It was filtered and washed in DCM to give the desired compound as a grey solid. Yield 74% (0.400g, 0.99 mmol); M.p.: 211°C; ^{1}H-NMR (500 MHz,DMSO- d_6, 300K): δH: 9.78 (s, 1H); 8.22 (s, 1H); 7.86 (d, J = 8 Hz, 1H); 7.81 (d, J = 8 Hz, 1H); 7.62-7.70 (m, 4H); 7.37 (t, J = 8 Hz, 1H); 6.88 (t, J = 8 Hz, 1H); ^{13}C-NMR (100 MHz, DMSO- d_6, 298K), δC: 152.18, 143.32, 139.47, 138.91, 128.55, 126.06, 126.03, 125.99, 123.38, 117.85, 91.77.

2.6.2 ^{1}H-NMR titrations

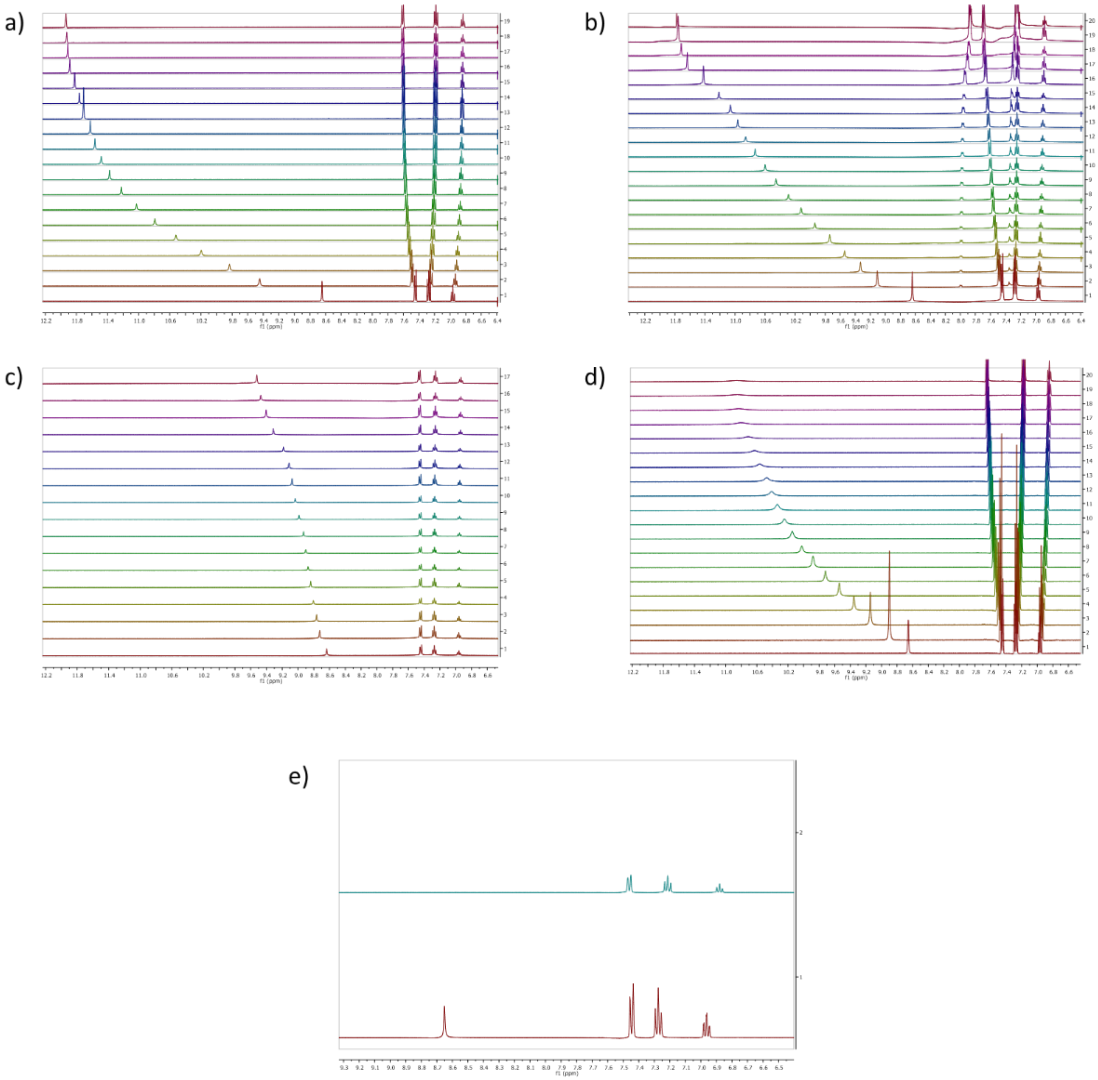

Figure 2.15 Changes in the ^{1}H-NMR spectra of **L_1** (0.005M) upon addition of increasing amounts of AcO^- (a), BzO^- (b), Cl^- (c) , $H_2PO_4^-$ (d) and F^- (e) (0.075M) in DMSO.

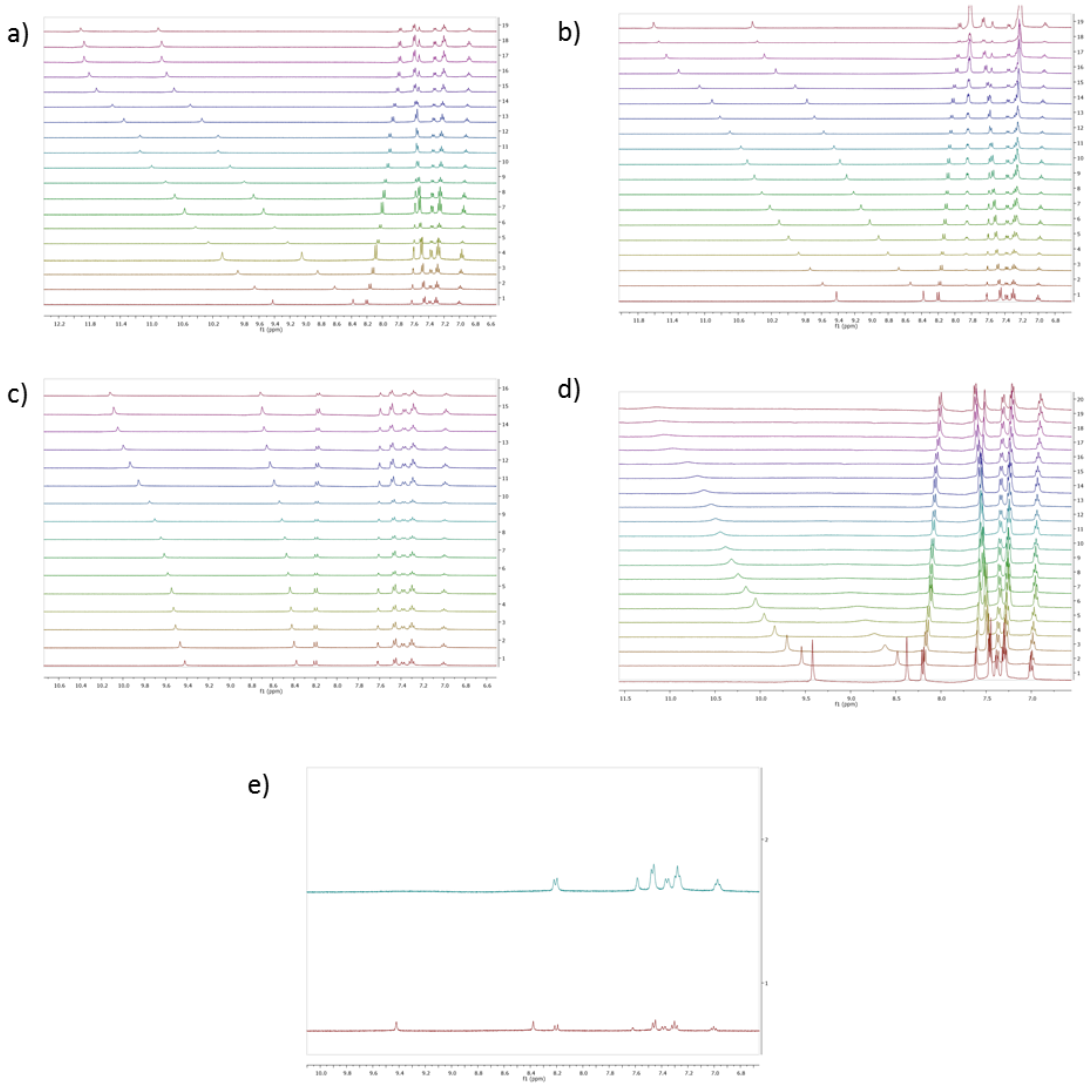

Figure 2.16 Changes in the ^{1}H-NMR spectra of **L_2** (0.005M) upon addition of increasing amounts of AcO^- (a), BzO^- (b), Cl^- (c) , $H_2PO_4^-$ (d) and F^- (e) (0.075M) in DMSO.

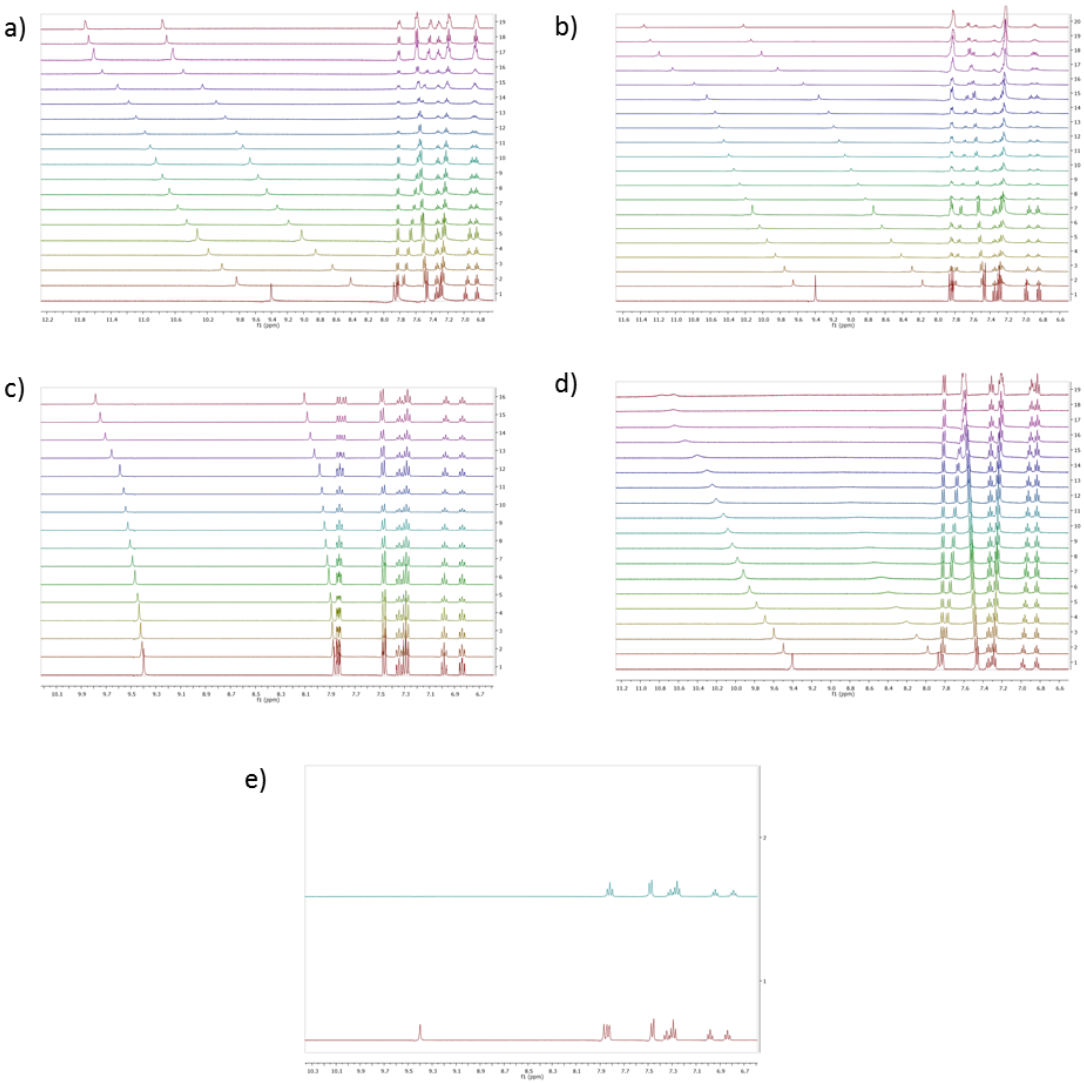

Figure 2.17 Changes in the ^{1}H-NMR spectra of $\mathbf{L_3}$ (0.005M) upon addition of increasing amounts of AcO^- (a), BzO^- (b), Cl^- (c) , $H_2PO_4^-$ (d) and F^- (e) (0.075M) in DMSO

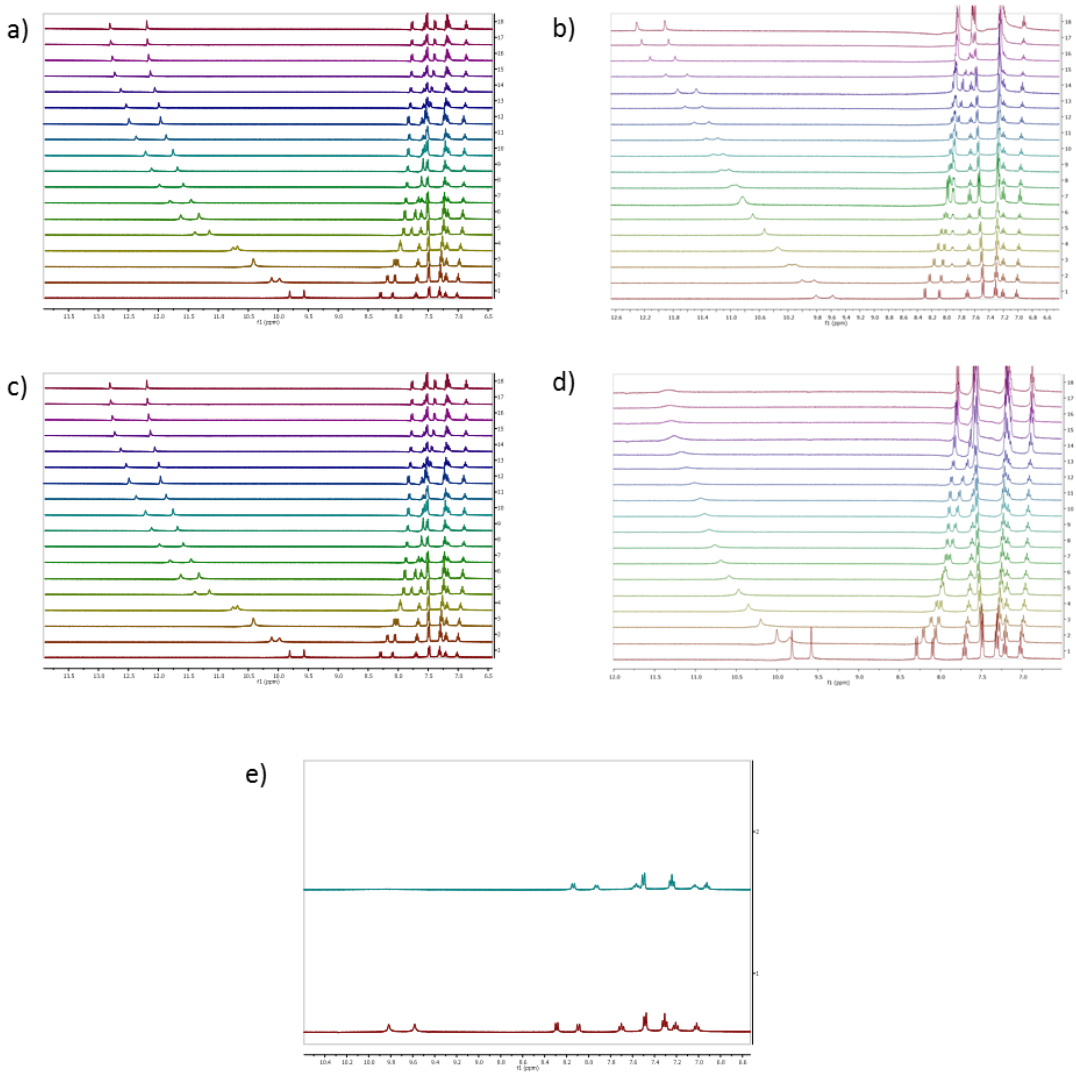

Figure 2.18 Changes in the ^{1}H-NMR spectra of **L_4** (0.005M) upon addition of increasing amounts of AcO^- (a), BzO^- (b), Cl^- (c) , $H_2PO_4^-$ (d) and F^- (e) (0.075M) in DMSO.

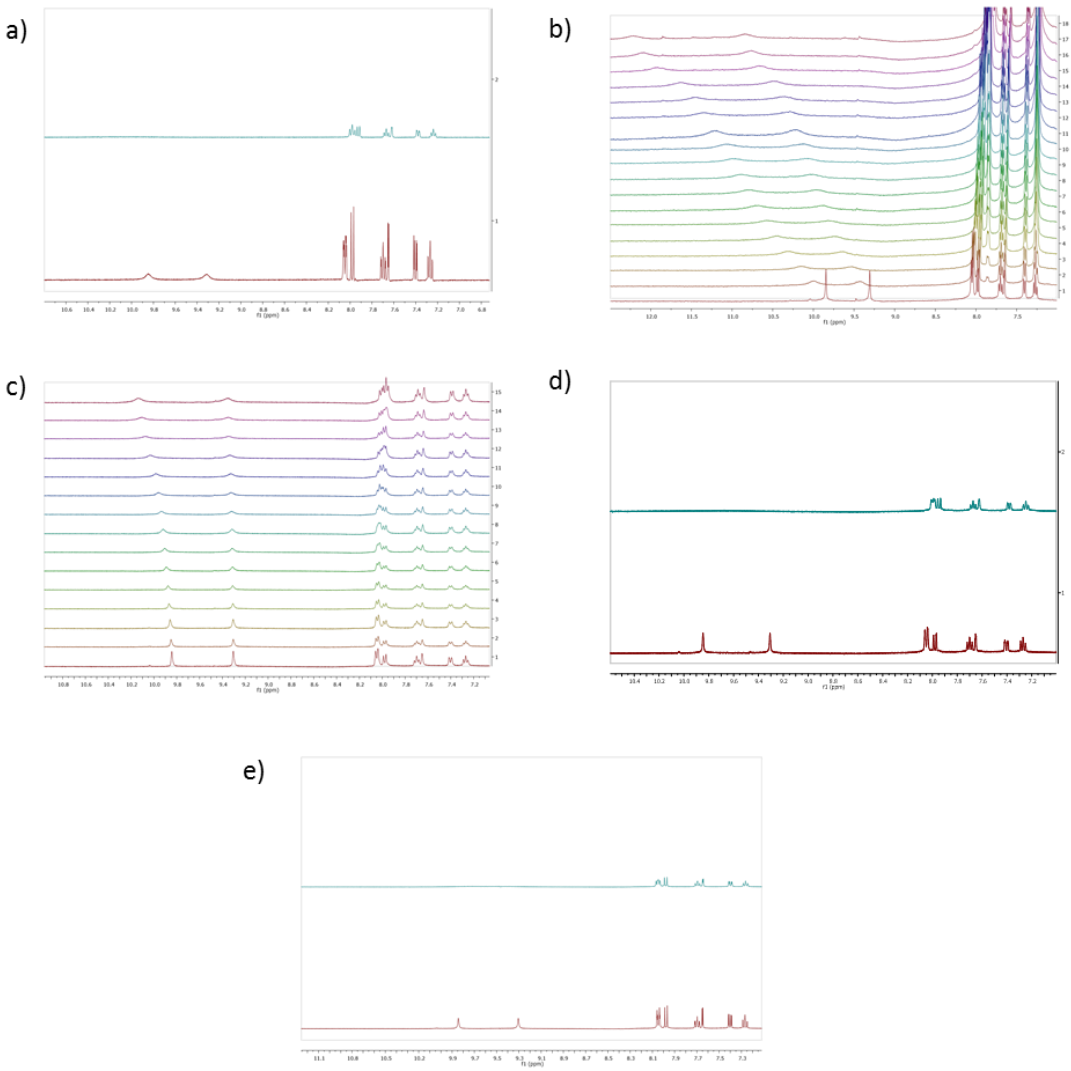

Figure 2.19 Changes in the ^{1}H-NMR spectra of **L_5** (0.005M) upon addition of increasing amounts of AcO^- (a), BzO^- (b), Cl^- (c) , $H_2PO_4^-$ (d) and F^- (e) (0.075M) in DMSO.

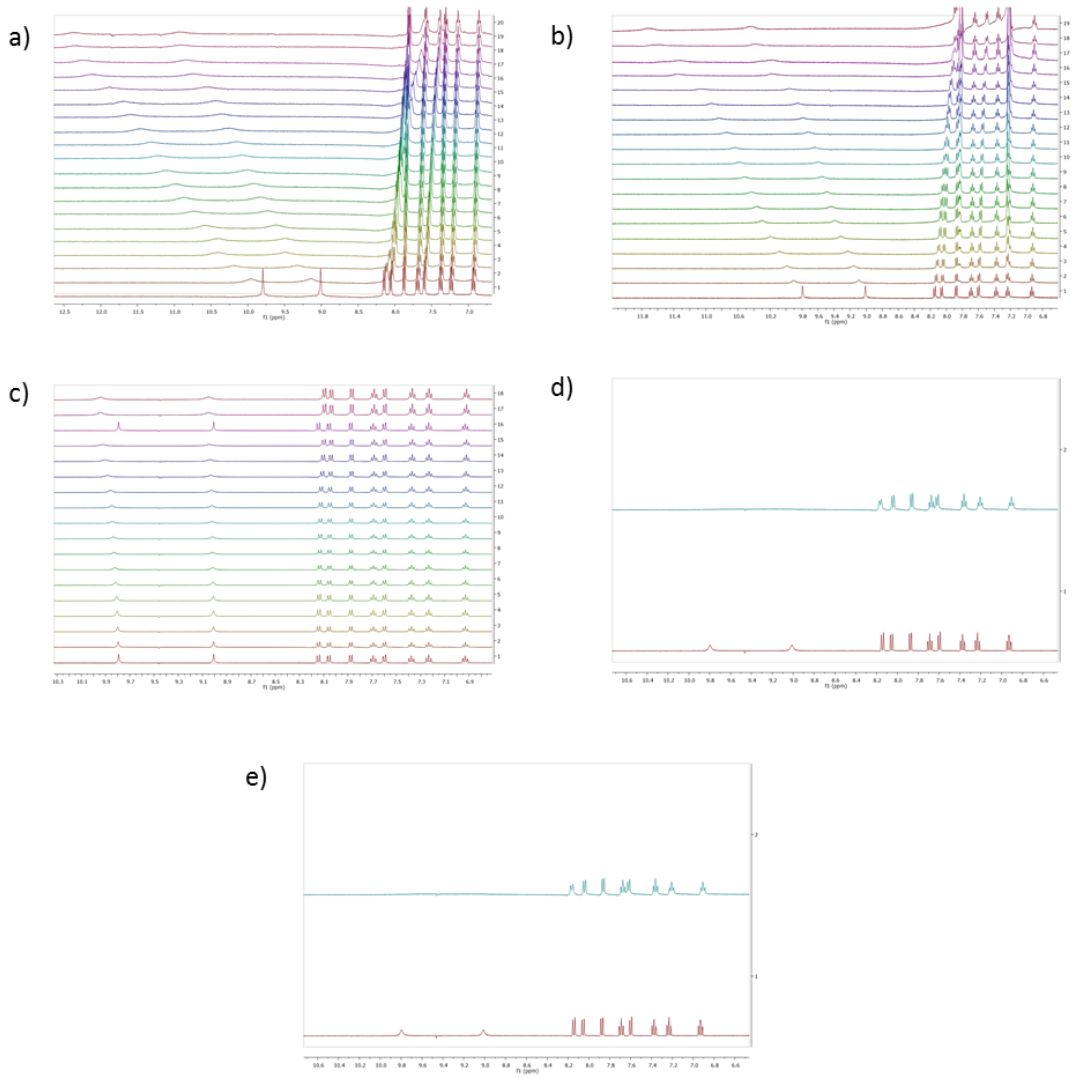

Figure 2.20 Changes in the ^{1}H-NMR spectra of **L_6** (0.005M) upon addition of increasing amounts of AcO^- (a), BzO^- (b), Cl^- (c) , $H_2PO_4^-$ (d) and F^- (e) (0.075M) in DMSO.

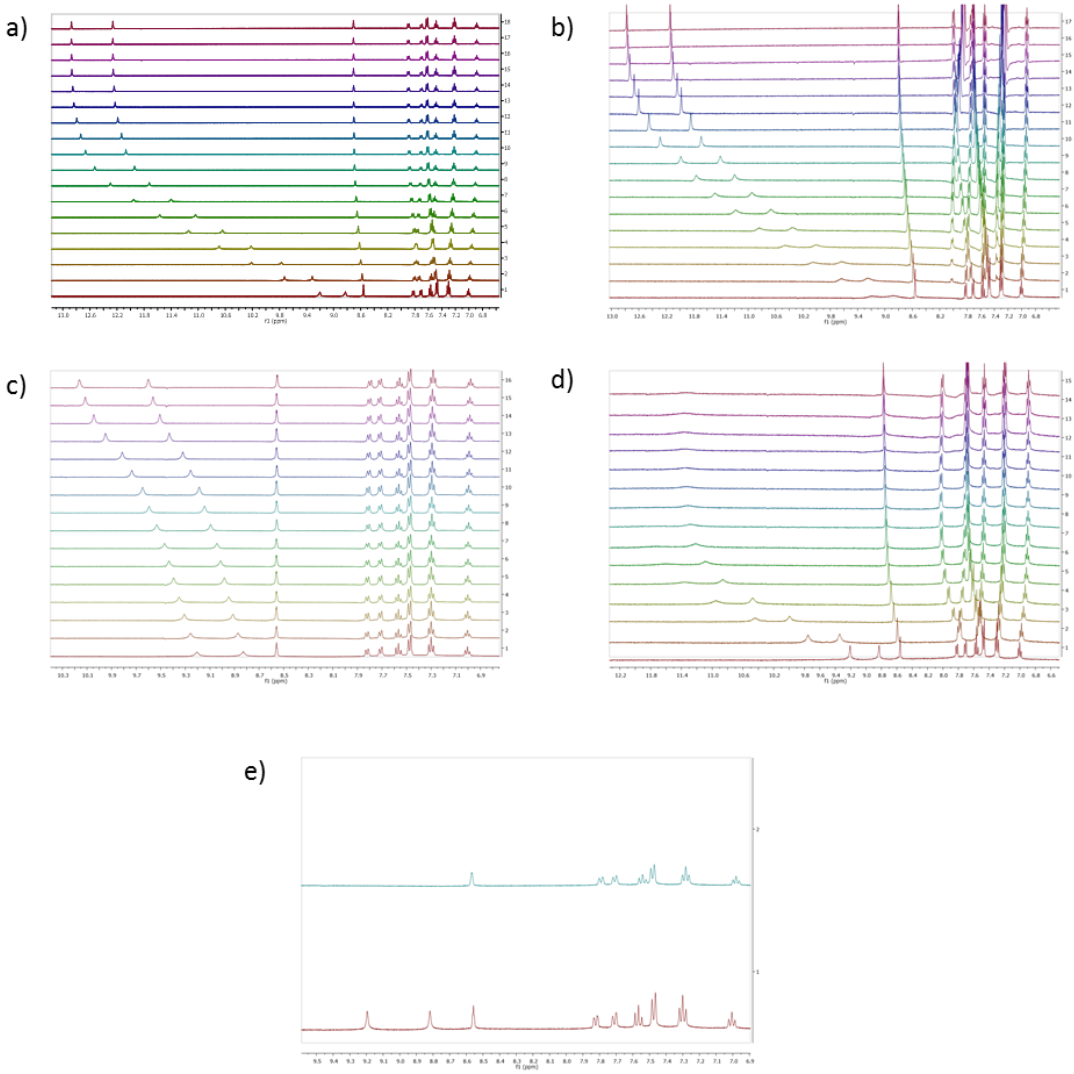

Figure 2.21 Changes in the ^{1}H-NMR spectra of **L_7** (0.005M) upon addition of increasing amounts of AcO^- (a), BzO^- (b), Cl^- (c) , $H_2PO_4^-$ (d) and F^- (e) (0.075M) in DMSO.

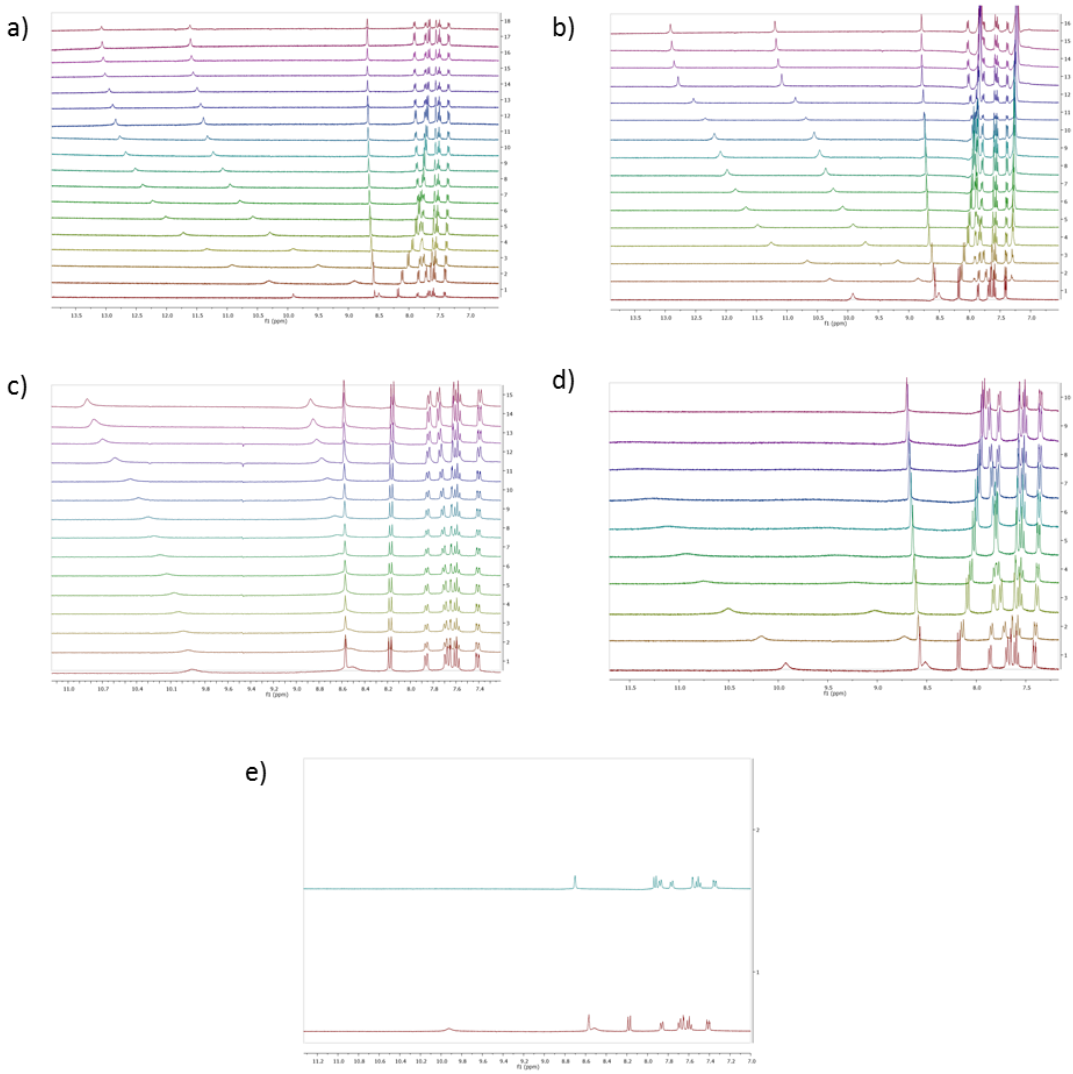

Figure 2.22 Changes in the ^{1}H-NMR spectra of **L_8** (0.005M) upon addition of increasing amounts of AcO^- (a), BzO^- (b), Cl^- (c) , $H_2PO_4^-$ (d) and F^- (e) (0.075M) in DMSO.

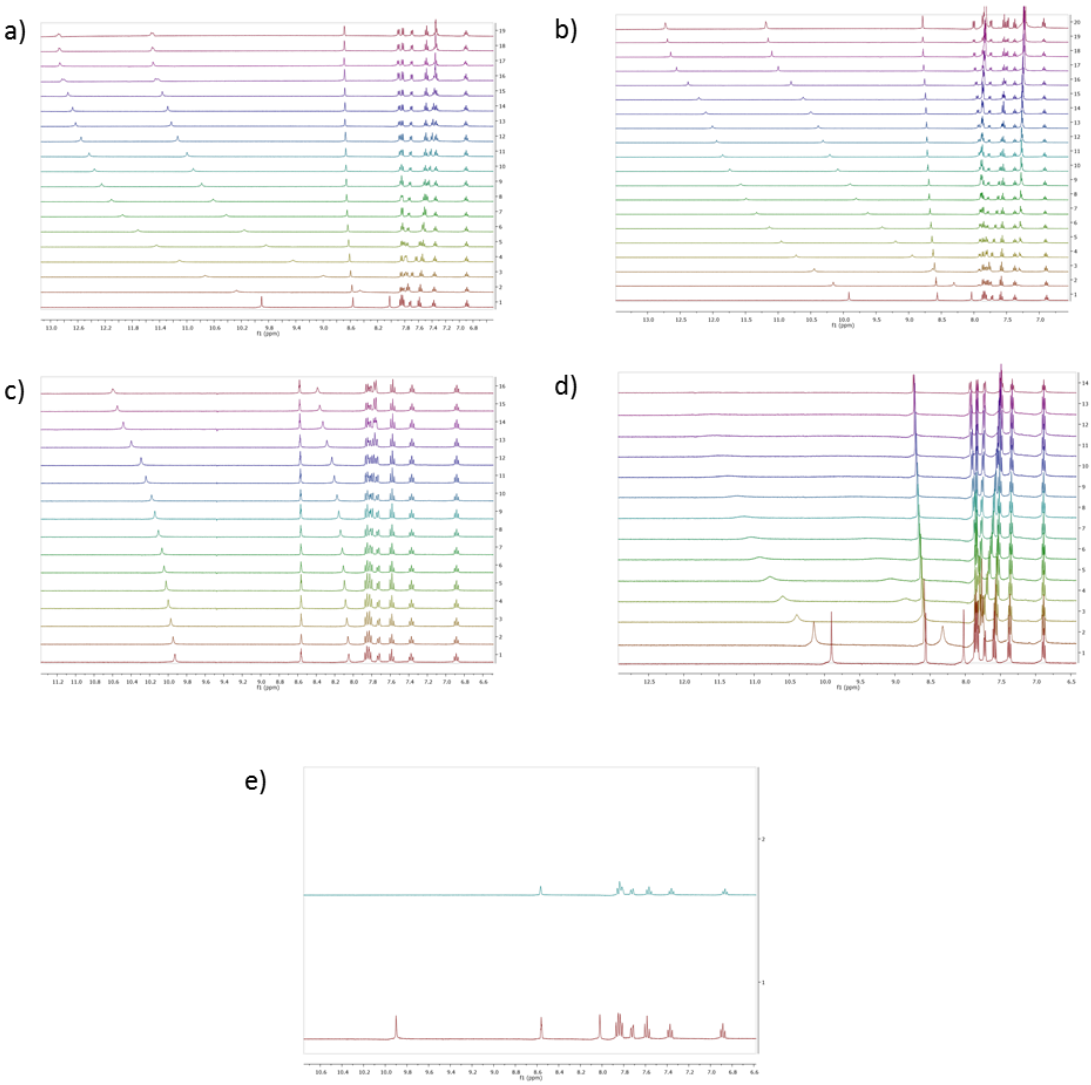

Figure 2.23 Changes in the ^{1}H-NMR spectra of **L_9** (0.005M) upon addition of increasing amounts of AcO^- (a), BzO^- (b), Cl^- (c) , $H_2PO_4^-$ (d) and F^- (e) (0.075M) in DMSO.

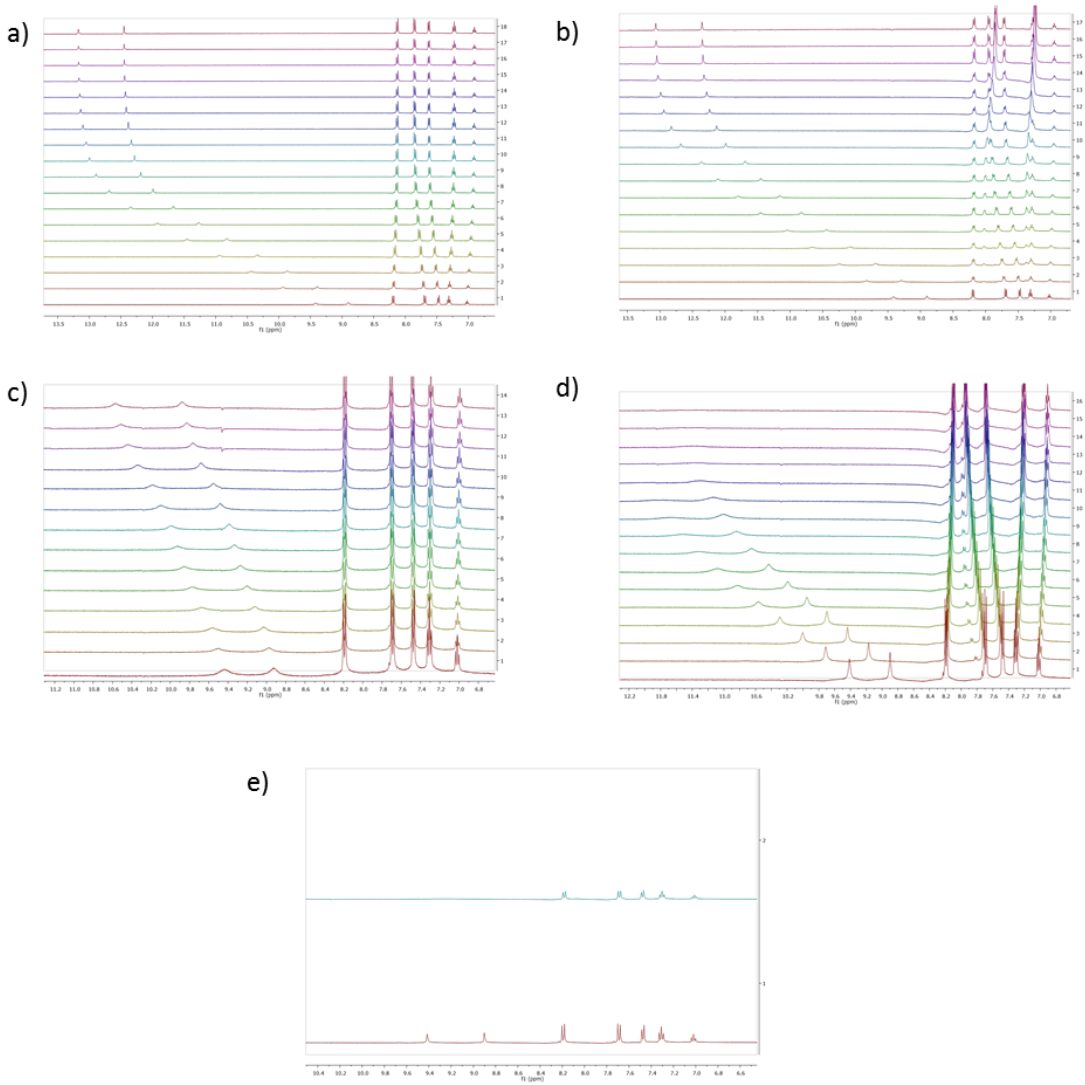

Figure 2.24 Changes in the ^{1}H-NMR spectra of **L_{10}** (0.005M) upon addition of increasing amounts of AcO^- (a), BzO^- (b), Cl^- (c) , $H_2PO_4^-$ (d) and F^- (e) (0.075M) in DMSO.

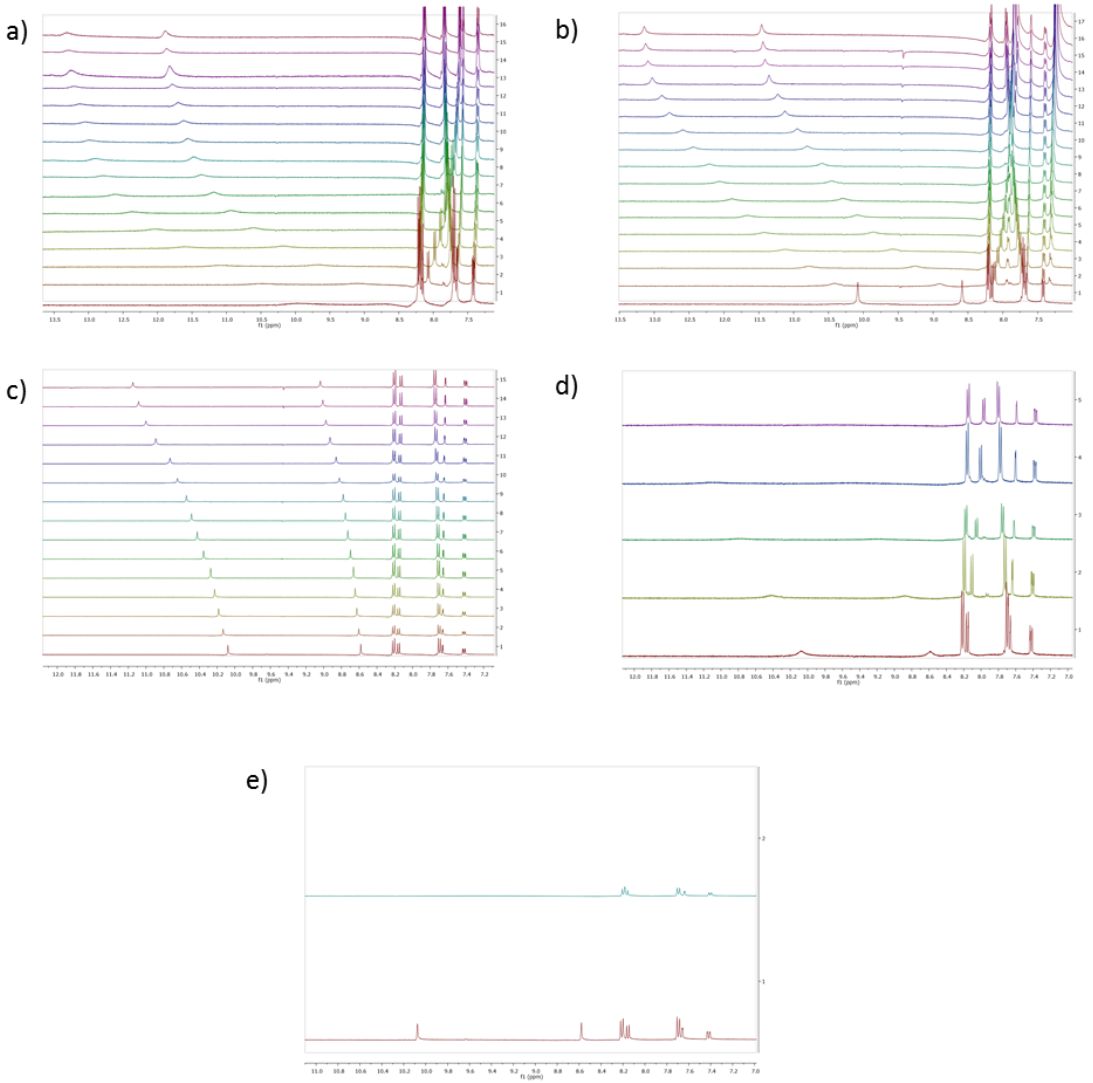

Figure 2.25 Changes in the ^{1}H-NMR spectra of **L_{11}** (0.005M) upon addition of increasing amounts of AcO^- (a), BzO^- (b), Cl^- (c) , $H_2PO_4^-$ (d) and F^- (e) (0.075M) in DMSO.

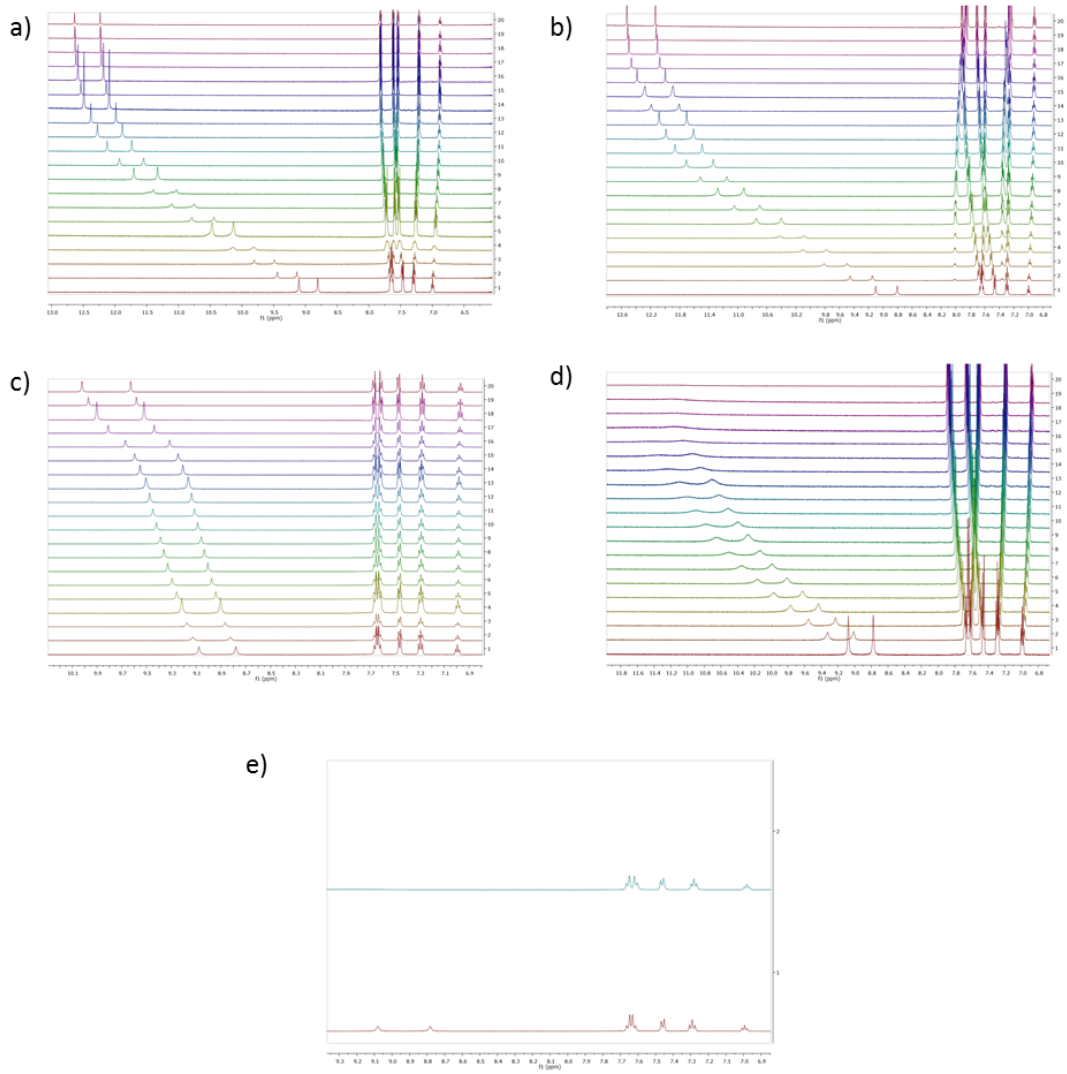

Figure 2.26 Changes in the ^{1}H-NMR spectra of **L_{13}** (0.005M) upon addition of increasing amounts of AcO^- (a), BzO^- (b), Cl^- (c) , $H_2PO_4^-$ (d) and F^- (e) (0.075M) in DMSO.

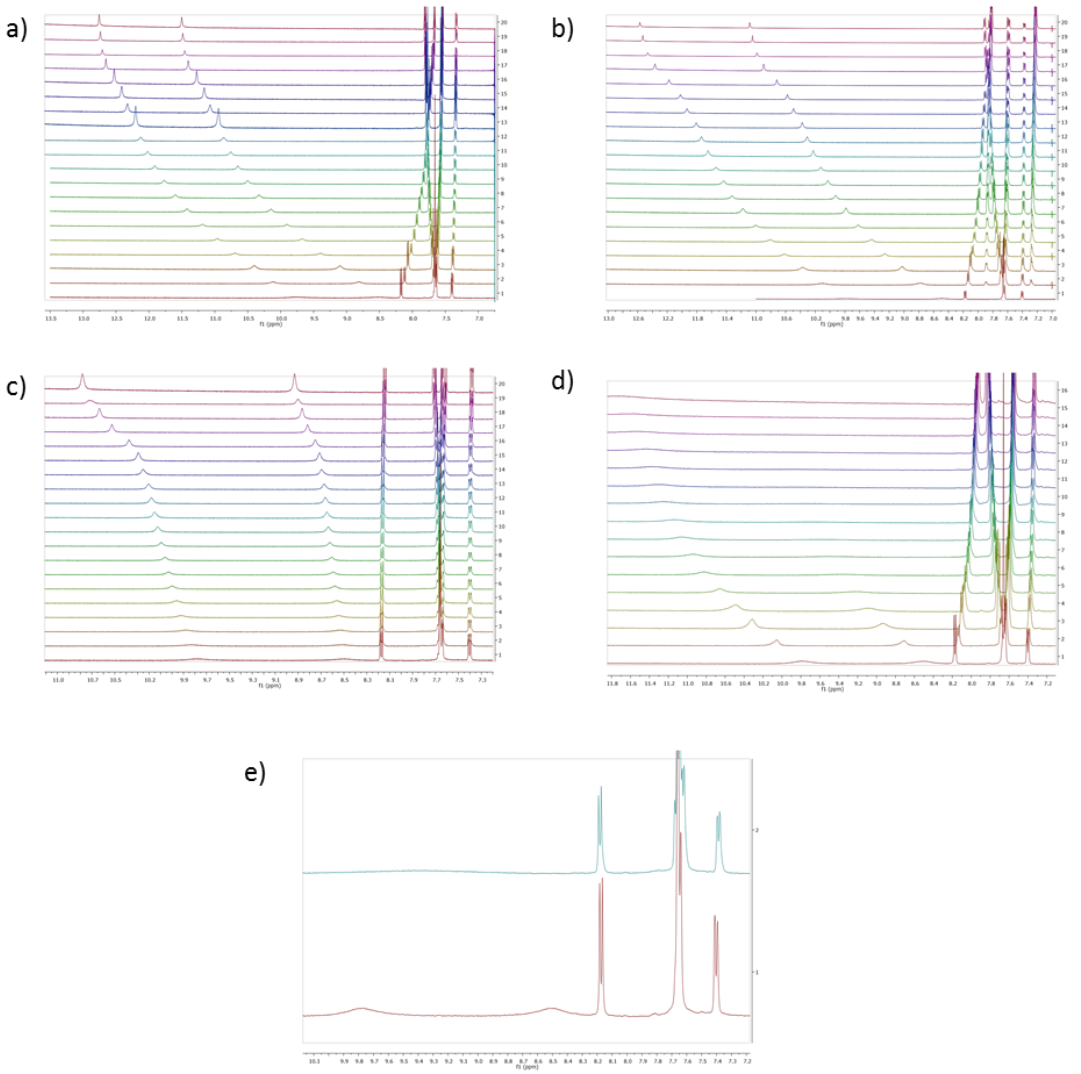

Figure 2.27 Changes in the ^{1}H-NMR spectra of **L_{14}** (0.005M) upon addition of increasing amounts of AcO^- (a), BzO^- (b), Cl^- (c) , $H_2PO_4^-$ (d) and F^- (e) (0.075M) in DMSO.

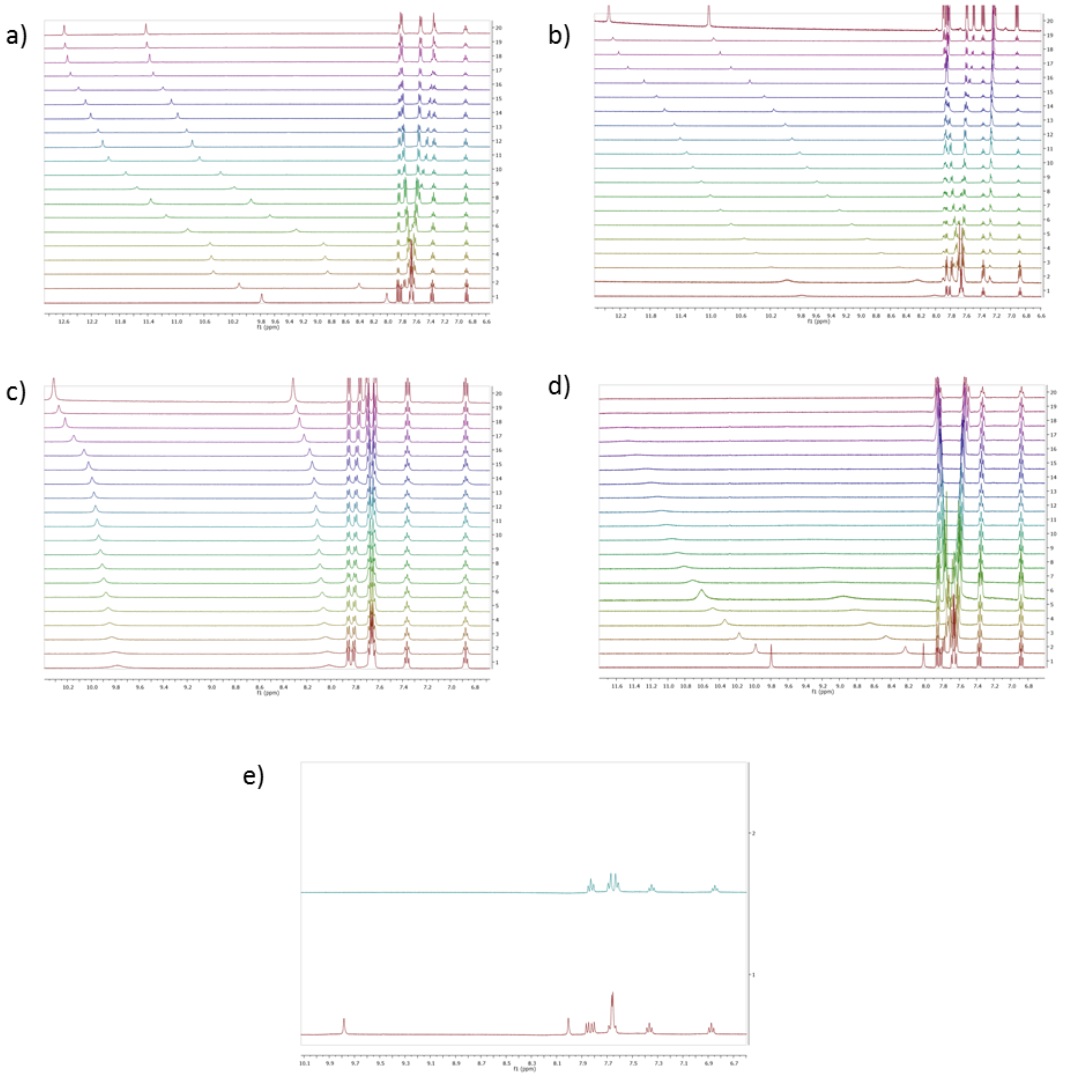

Figure 2.28 Changes in the ^{1}H-NMR spectra of **L_{15}** (0.005M) upon addition of increasing amounts of AcO^- (a), BzO^- (b), Cl^- (c) , $H_2PO_4^-$ (d) and F^- (e) (0.075M) in DMSO.

2.6.3 Proton NMR titration fitting

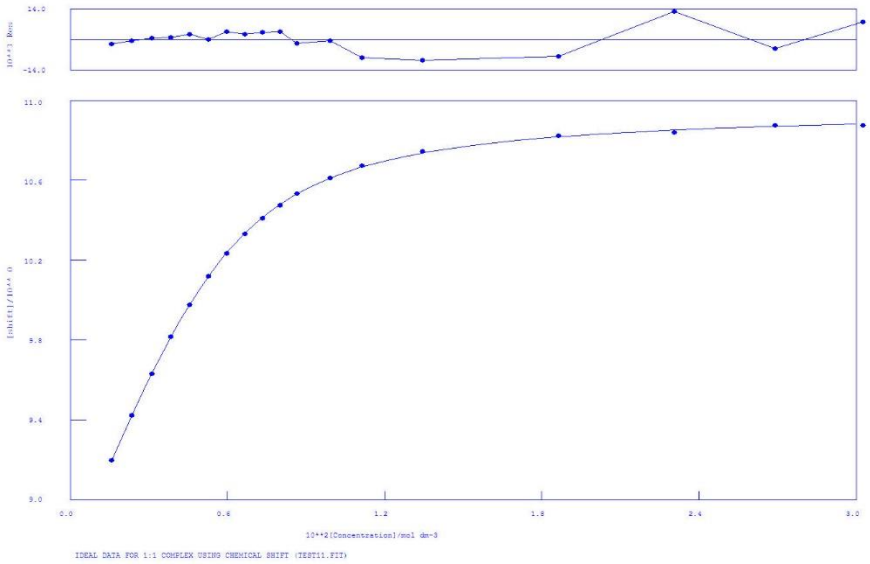

IDEAL DATA FOR 1:1 COMPLEX USING CHEMICAL SHIFT (TEST11.FIT)

Reaction: M + L = ML

FILE: TEST11.FIT

IDEAL DATA: K1 = 63.091; DELTA M = 20.0; DELTA ML = 120.0

File prepared by M. J. Hynes, October 22 2000

NO. A PARAMETER DELTA ERROR CONDITION DESCRIPTION

1 1 1.11684E+03 2.000E-01 1.879E+01 7.107E+00 K1

2 1 8.68885E+00 2.000E-01 5.656E-03 2.173E+00 SHIFT M

3 1 1.09610E+01 1.000E+00 4.211E-03 5.117E+00 SHIFT ML

0RMS ERROR = 5.90E-03 MAX ERROR = 1.27E-02 AT OBS.NO. 16

RESIDUALS SQUARED = 5.22E-04

RFACTOR = 0.0522 PERCENT

Figure 2.29 Titration of receptor **L_1** with TBA-H_2PO_4 in DMSO-d_6/0.5% H_2O

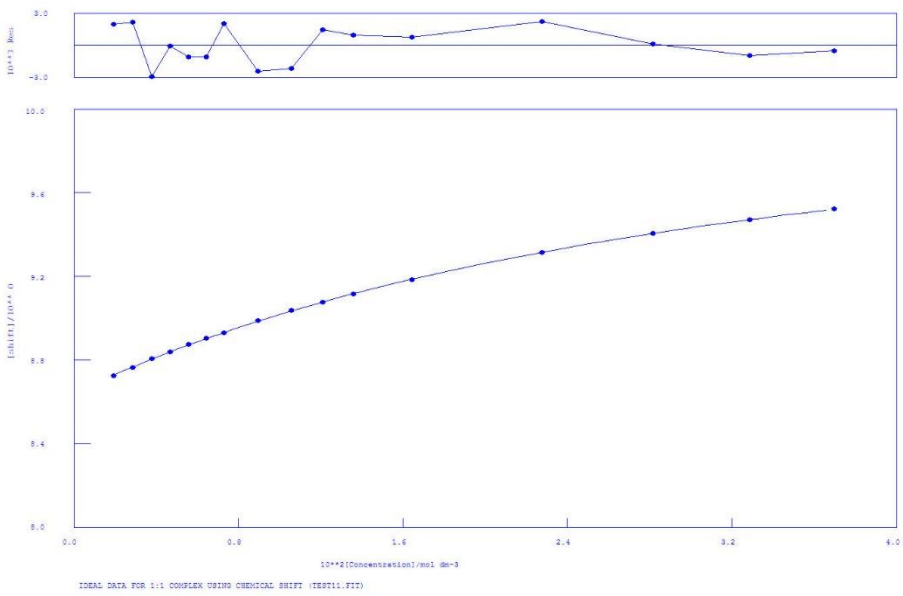

IDEAL DATA FOR 1:1 COMPLEX USING CHEMICAL SHIFT (TEST11.FIT)

Reaction: M + L = ML

FILE: TEST11.FIT

IDEAL DATA: K1 = 63.091; DELTA M = 20.0; DELTA ML = 120.0

File prepared by M. J. Hynes, October 22 2000

NO.	A	PARAMETER	DELTA	ERROR	CONDITION	DESCRIPTION
1	1	3.44820E+01	2.000E-01	5.887E-01	1.012E+02	K1
2	1	8.64165E+00	2.000E-01	1.597E-03	6.955E+00	SHIFT M
3	1	1.02756E+01	1.000E+00	1.307E-02	7.094E+01	SHIFT ML

0RMS ERROR = 1.84E-03 MAX ERROR = 2.95E-03 AT OBS.NO. 3

RESIDUALS SQUARED = 4.41E-05

RFACTOR = 0.0183 PERCENT

Figure 2.30 Titration of receptor **L_1** with TBA-Cl in DMSO-d_6/0.5% H_2O

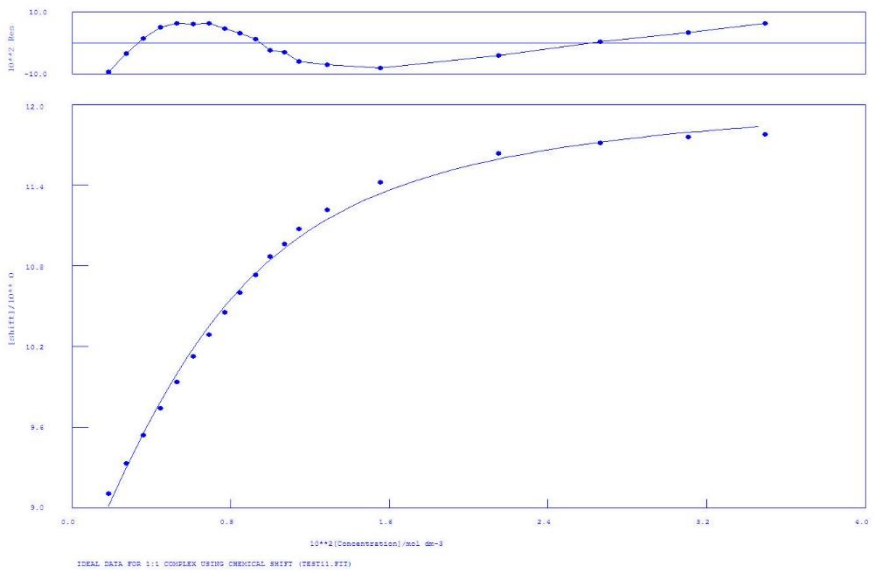

IDEAL DATA FOR 1:1 COMPLEX USING CHEMICAL SHIFT (TEST11.FIT)

Reaction: M + L = ML

FILE: TEST11.FIT

IDEAL DATA: K1 = 63.091; DELTA M = 20.0; DELTA ML = 120.0

File prepared by M. J. Hynes, October 22 2000

NO.	A	PARAMETER	DELTA	ERROR	CONDITION	DESCRIPTION
1	1	3.64299E+02	2.000E-01	3.378E+01	1.363E+01	K1
2	1	8.37050E+00	2.000E-01	5.142E-02	3.289E+00	SHIFT M
3	1	1.21770E+01	1.000E+00	6.001E-02	8.675E+00	SHIFT ML

0RMS ERROR = 5.65E-02 MAX ERROR = 9.38E-02 AT OBS.NO. 1

RESIDUALS SQUARED = 5.10E-02

RFACTOR = 0.4852 PERCENT

Figure 2.31 Titration of receptor **L_1** with TBA-BzO in DMSO-d_6/0.5% H_2O

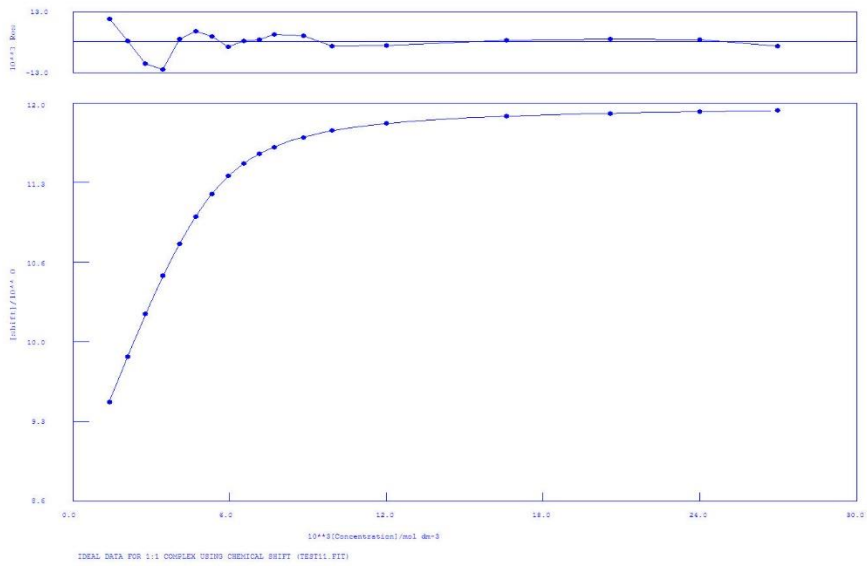

IDEAL DATA FOR 1:1 COMPLEX USING CHEMICAL SHIFT (TEST11.FIT)

Reaction: M + L = ML

FILE: TEST11.FIT

IDEAL DATA: K1 = 63.091; DELTA M = 20.0; DELTA ML = 120.0

File prepared by M. J. Hynes, October 22 2000

NO.	A	PARAMETER	DELTA	ERROR	CONDITION	DESCRIPTION
1	1	2.76468E+03	2.000E-01	3.315E+01	5.087E+00	K1
2	1	8.64075E+00	2.000E-01	4.752E-03	1.629E+00	SHIFT M
3	1	1.19870E+01	1.000E+00	3.019E-03	4.178E+00	SHIFT ML

0RMS ERROR = 5.03E-03 MAX ERROR = 1.17E-02 AT OBS.NO. 4

RESIDUALS SQUARED = 3.80E-04

RFACTOR = 0.0409 PERCENT

Figure 2.32 Titration of receptor **L_1** with TBA-AcO in DMSO-d_6/0.5% H_2O

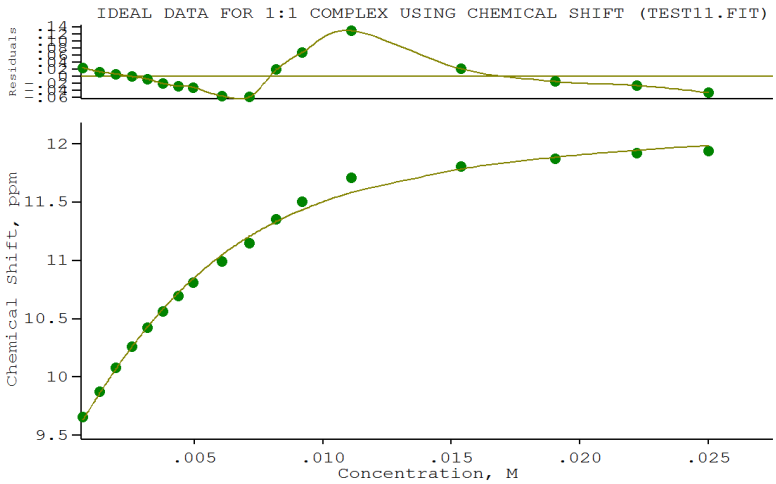

IDEAL DATA FOR 1:1 COMPLEX USING CHEMICAL SHIFT (TEST11.FIT)

Reaction: Sn + L = Sn(L)

FILE: TEST11.FIT (Measured shift is on 119Sn)

IDEAL DATA: K1 = 63.091; DELTA M = 20.0; DELTA ML = 120.0

File prepared by M. J. Hynes, October 22 2000

NO.	A	PARAMETER	DELTA	ERROR	CONDITION	DESCRIPTION
1	1	4.45422E+02	2.000E-01	4.808E+01	1.173E+01	K1
2	1	9.38494E+00	2.000E-01	3.755E-02	2.563E+00	SHIFT Sn
3	1	1.22714E+01	1.000E+00	5.688E-02	8.140E+00	SHIFT Sn(L)

0RMS ERROR = 4.98E-02 MAX ERROR = 1.30E-01 AT OBS.NO. 13

RESIDUALS SQUARED = 3.48E-02

RFACTOR = 0.4111 PERCENT

Figure 2.33 Titration of receptor **L_2** with n TBA-AcO in DMSO-d_6/0.5% H_2O.

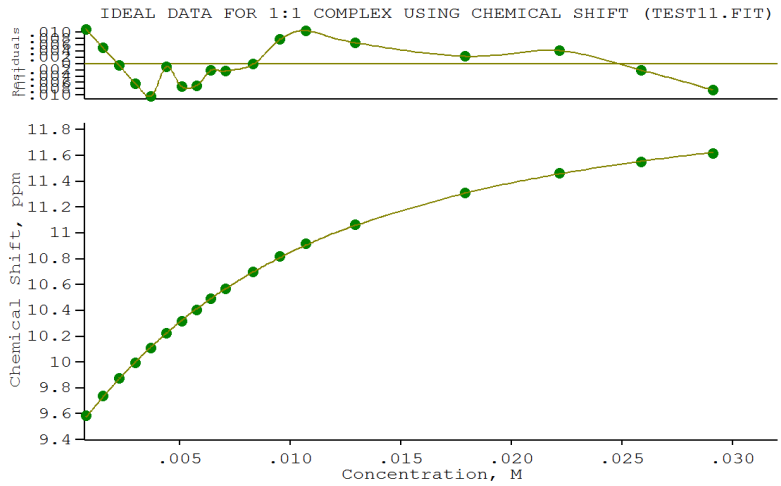

IDEAL DATA FOR 1:1 COMPLEX USING CHEMICAL SHIFT (TEST11.FIT)

Reaction: Sn + L = Sn(L)

FILE: TEST11.FIT (Measured shift is on 119Sn)

IDEAL DATA: K1 = 63.091; DELTA M = 20.0; DELTA ML = 120.0

File prepared by M. J. Hynes, October 22 2000

NO.	A	PARAMETER	DELTA	ERROR	CONDITION	DESCRIPTION
1	1	1.35841E+02	2.000E-01	2.338E+00	2.650E+01	K1
2	1	9.40463E+00	2.000E-01	5.413E-03	4.270E+00	SHIFT Sn
3	1	1.22693E+01	1.000E+00	1.427E-02	1.679E+01	SHIFT Sn(L)

0RMS ERROR = 6.91E-03 MAX ERROR = 1.09E-02 AT OBS.NO. 1

RESIDUALS SQUARED = 7.16E-04

RFACTOR = 0.0594 PERCENT

Figure 2.34 Titration of receptor **L_2** with TBA-BzO in DMSO-d_6/0.5% H_2O.

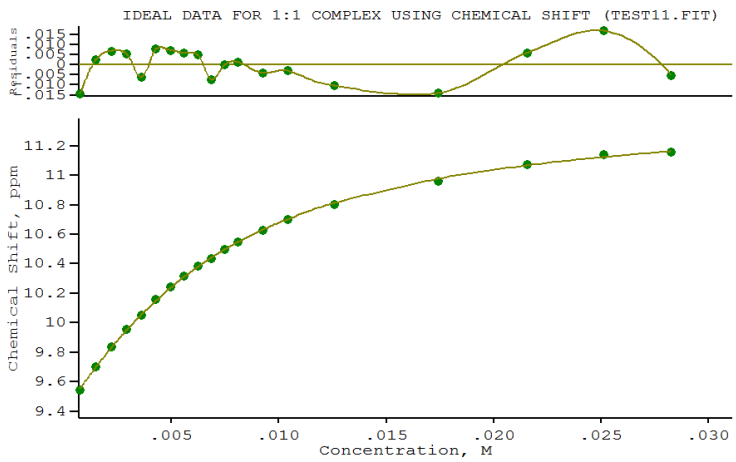

IDEAL DATA FOR 1:1 COMPLEX USING CHEMICAL SHIFT (TEST11.FIT)

Reaction: Sn + L = Sn(L)

FILE: TEST11.FIT (Measured shift is on 119Sn)

IDEAL DATA: K1 = 63.091; DELTA M = 20.0; DELTA ML = 120.0

File prepared by M. J. Hynes, October 22 2000

NO.	A	PARAMETER	DELTA	ERROR	CONDITION	DESCRIPTION
1	1	2.31118E+02	2.000E-01	5.720E+00	1.741E+01	K1
2	1	9.39794E+00	2.000E-01	6.902E-03	3.629E+00	SHIFT Sn
3	1	1.14772E+01	1.000E+00	1.215E-02	1.092E+01	SHIFT Sn(L)

0RMS ERROR = 8.72E-03 MAX ERROR = 1.68E-02 AT OBS.NO. 18

RESIDUALS SQUARED = 1.22E-03

RFACTOR = 0.0766 PERCENT

Figure 2.35 Titration of receptor **L_2** with TBA-H_2PO_4 in DMSO-d_6/0.5% H_2O.

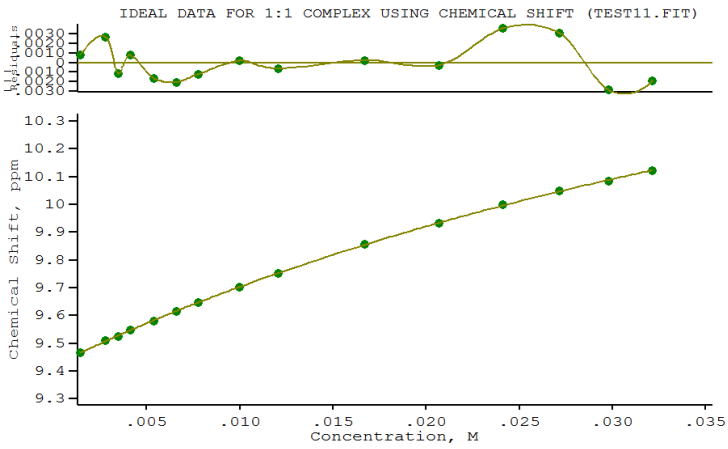

IDEAL DATA FOR 1:1 COMPLEX USING CHEMICAL SHIFT (TEST11.FIT)

Reaction: Sn + L = Sn(L)

FILE: TEST11.FIT (Measured shift is on 119Sn)

IDEAL DATA: K1 = 63.091; DELTA M = 20.0; DELTA ML = 120.0

File prepared by M. J. Hynes, October 22 2000

NO.	A	PARAMETER	DELTA	ERROR	CONDITION	DESCRIPTION
1	1	1.77453E+01	2.000E-01	6.329E-01	3.408E+02	K1
2	1	9.41978E+00	2.000E-01	1.672E-03	6.737E+00	SHIFT Sn
3	1	1.14303E+01	1.000E+00	4.521E-02	2.845E+02	SHIFT Sn(L)

0RMS ERROR = 2.09E-03 MAX ERROR = 3.57E-03 AT OBS.NO. 12

RESIDUALS SQUARED = 5.25E-05

RFACTOR = 0.0192 PERCENT

Figure 2.36 Titration of receptor **L_2** with TBA-Cl in DMSO-d_6/0.5% H_2O.

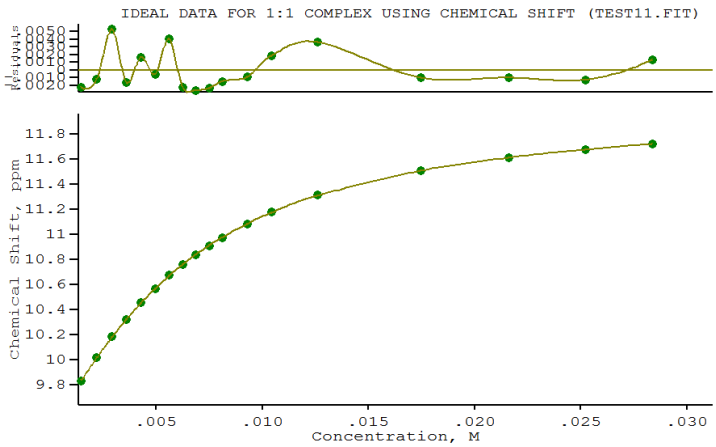

IDEAL DATA FOR 1:1 COMPLEX USING CHEMICAL SHIFT (TEST11.FIT)

Reaction: Sn + L = Sn(L)

FILE: TEST11.FIT (Measured shift is on 119Sn)

IDEAL DATA: K1 = 63.091; DELTA M = 20.0; DELTA ML = 120.0

File prepared by M. J. Hynes, October 22 2000

NO.	A	PARAMETER	DELTA	ERROR	CONDITION	DESCRIPTION
1	1	2.76457E+02	2.000E-01	1.766E+00	2.004E+01	K1
2	1	9.41093E+00	2.000E-01	2.716E-03	4.996E+00	SHIFT Sn
3	1	1.20699E+01	1.000E+00	3.370E-03	1.073E+01	SHIFT Sn(L)

0RMS ERROR = 2.56E-03 MAX ERROR = 5.30E-03 AT OBS.NO. 3

RESIDUALS SQUARED = 9.86E-05

RFACTOR = 0.0215 PERCENT

Figure 2.37 Titration of receptor **L_3** with TBA-AcO in DMSO-d_6/0.5% H_2O.

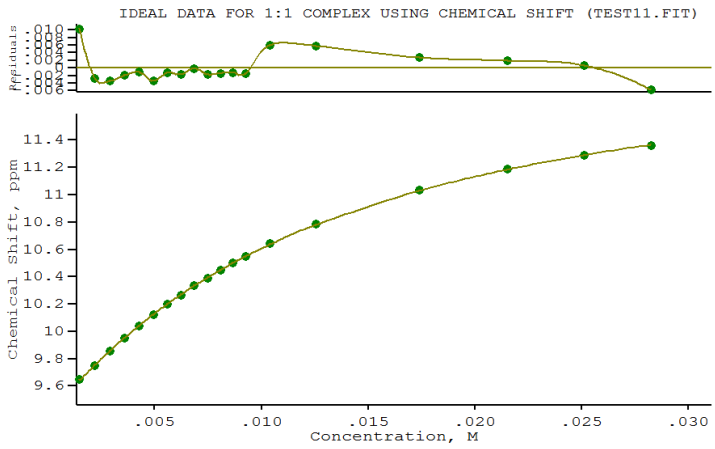

IDEAL DATA FOR 1:1 COMPLEX USING CHEMICAL SHIFT (TEST11.FIT)

Reaction: Sn + L = Sn(L)

FILE: TEST11.FIT (Measured shift is on 119Sn)

IDEAL DATA: K1 = 63.091; DELTA M = 20.0; DELTA ML = 120.0

File prepared by M. J. Hynes, October 22 2000

NO.	A	PARAMETER	DELTA	ERROR	CONDITION	DESCRIPTION
1	1	1.00145E+02	2.000E-01	1.288E+00	4.645E+01	K1
2	1	9.38549E+00	2.000E-01	3.846E-03	6.970E+00	SHIFT Sn
3	1	1.21635E+01	1.000E+00	1.163E-02	2.694E+01	SHIFT Sn(L)

0RMS ERROR = 4.10E-03 MAX ERROR = 1.02E-02 AT OBS.NO. 1

RESIDUALS SQUARED = 2.69E-04

Figure 2.38 Titration of receptor **L_3** with TBA-BzO in DMSO-d_6/0.5% H_2O.

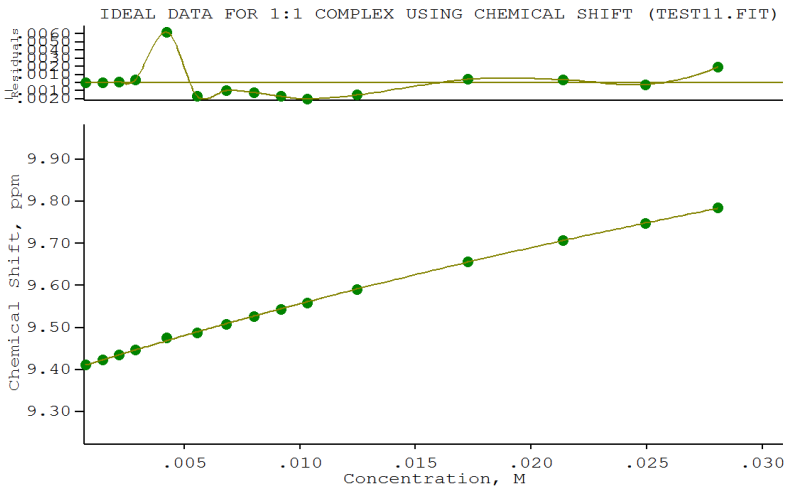

IDEAL DATA FOR 1:1 COMPLEX USING CHEMICAL SHIFT (TEST11.FIT)

Reaction: Sn + L = Sn(L)

FILE: TEST11.FIT (Measured shift is on 119Sn)

IDEAL DATA: K1 = 63.091; DELTA M = 20.0; DELTA ML = 120.0

File prepared by M. J. Hynes, October 22 2000

NO.	A	PARAMETER	DELTA	ERROR	CONDITION	DESCRIPTION
1	1	9.98714E+00	2.000E-01	1.014E+00	7.904E+02	K1
2	1	9.39788E+00	2.000E-01	1.423E-03	5.330E+00	SHIFT Sn
3	1	1.12061E+01	1.000E+00	1.414E-01	7.187E+02	SHIFT Sn(L)

0RMS ERROR = 2.19E-03 MAX ERROR = 6.23E-03 AT OBS.NO. 5

RESIDUALS SQUARED = 5.74E-05

RFACTOR = 0.0205 PERCENT

Figure 2.39 Titration of receptor **L_3** with TBA-Cl in DMSO-d_6/0.5% H_2O.

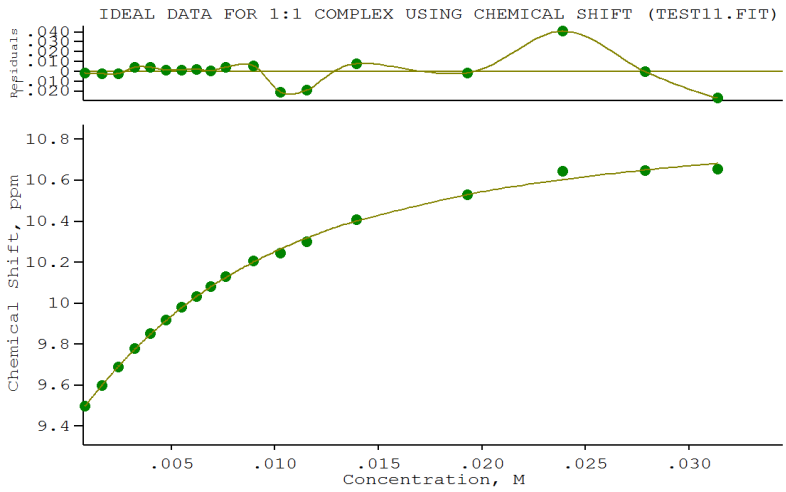

IDEAL DATA FOR 1:1 COMPLEX USING CHEMICAL SHIFT (TEST11.FIT)

Reaction: Sn + L = Sn(L)

FILE: TEST11.FIT (Measured shift is on 119Sn)

IDEAL DATA: K1 = 63.091; DELTA M = 20.0; DELTA ML = 120.0

File prepared by M. J. Hynes, October 22 2000

NO.	A	PARAMETER	DELTA	ERROR	CONDITION	DESCRIPTION
1	1	1.73662E+02	2.000E-01	1.037E+01	1.954E+01	K1
2	1	9.38712E+00	2.000E-01	1.196E-02	3.843E+00	SHIFT Sn
3	1	1.09569E+01	1.000E+00	2.363E-02	1.214E+01	SHIFT Sn(L)

0RMS ERROR = 1.49E-02 MAX ERROR = 4.10E-02 AT OBS.NO. 16

RESIDUALS SQUARED = 3.35E-03

RFACTOR = 0.1347 PERCENT

Figure 2.40 Titration of receptor **L_3** with TBA-H_2PO_4 in DMSO-d_6/0.5% H_2O.

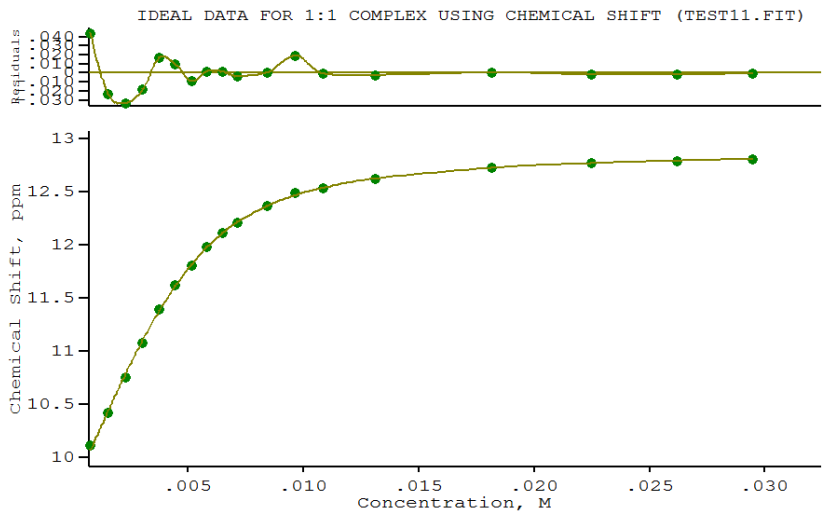

IDEAL DATA FOR 1:1 COMPLEX USING CHEMICAL SHIFT (TEST11.FIT)

Reaction: Sn + L = Sn(L)

FILE: TEST11.FIT (Measured shift is on 119Sn)

IDEAL DATA: K1 = 63.091; DELTA M = 20.0; DELTA ML = 120.0

File prepared by M. J. Hynes, October 22 2000

NO.	A	PARAMETER	DELTA	ERROR	CONDITION	DESCRIPTION
1	1	1.28298E+03	2.000E-01	4.444E+01	5.790E+00	K1
2	1	9.66853E+00	2.000E-01	1.400E-02	1.746E+00	SHIFT Sn
3	1	1.29117E+01	1.000E+00	1.213E-02	4.543E+00	SHIFT Sn(L)

0RMS ERROR = 1.79E-02 MAX ERROR = 4.41E-02 AT OBS.NO. 1

RESIDUALS SQUARED = 4.80E-03

RFACTOR = 0.1366 PERCENT

Figure 2.41 Titration of receptor **L_4** with TBA-AcO in DMSO-d_6/0.5% H_2O.

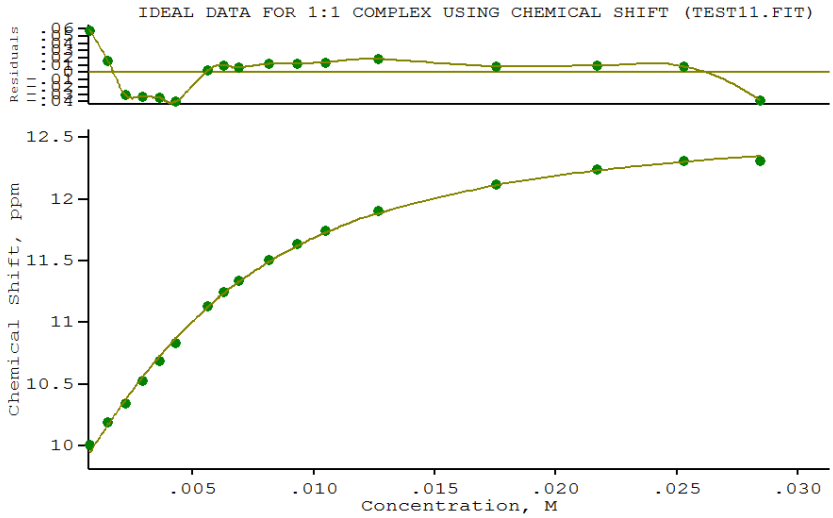

IDEAL DATA FOR 1:1 COMPLEX USING CHEMICAL SHIFT (TEST11.FIT)

Reaction: Sn + L = Sn(L)

FILE: TEST11.FIT (Measured shift is on 119Sn)

IDEAL DATA: K1 = 63.091; DELTA M = 20.0; DELTA ML = 120.0

File prepared by M. J. Hynes, October 22 2000

NO.	A	PARAMETER	DELTA	ERROR	CONDITION	DESCRIPTION
1	1	3.14013E+02	2.000E-01	1.849E+01	1.348E+01	K1
2	1	9.70879E+00	2.000E-01	2.138E-02	2.754E+00	SHIFT Sn
3	1	1.27073E+01	1.000E+00	3.558E-02	9.251E+00	SHIFT Sn(L)

0RMS ERROR = 2.82E-02 MAX ERROR = 5.81E-02 AT OBS.NO. 1

RESIDUALS SQUARED = 1.11E-02

RFACTOR = 0.2260 PERCENT

Figure 2.42 Titration of receptor **L_4** with TBA-BzO in DMSO-d_6/0.5% H_2O.

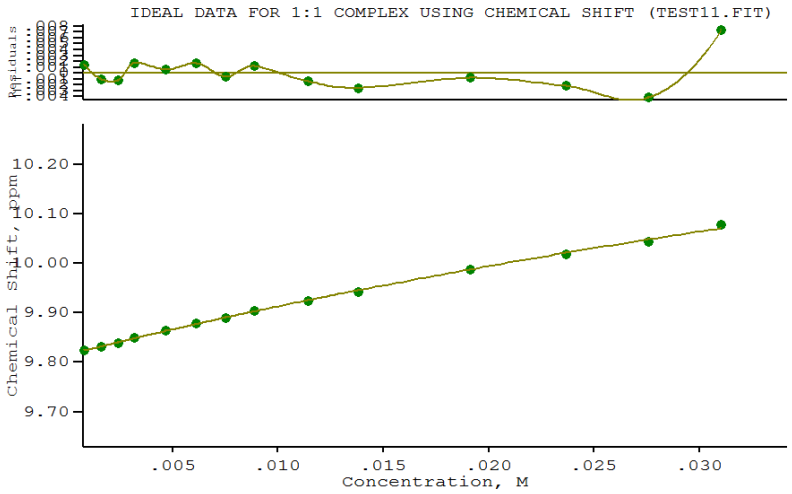

IDEAL DATA FOR 1:1 COMPLEX USING CHEMICAL SHIFT (TEST11.FIT)

Reaction: Sn + L = Sn(L)

FILE: TEST11.FIT (Measured shift is on 119Sn)

IDEAL DATA: K1 = 63.091; DELTA M = 20.0; DELTA ML = 120.0

File prepared by M. J. Hynes, October 22 2000

NO. A PARAMETER DELTA ERROR CONDITION DESCRIPTION

1 1 1.04370E+01 2.000E-01 1.696E+00 4.437E+02 K1

2 1 9.81482E+00 2.000E-01 1.832E-03 4.353E+00 SHIFT Sn

3 1 1.08877E+01 1.000E+00 1.300E-01 3.996E+02 SHIFT Sn(L)

0RMS ERROR = 2.98E-03 MAX ERROR = 7.36E-03 AT OBS.NO. 14

RESIDUALS SQUARED = 9.75E-05

RFACTOR = 0.0266 PERCENT

Figure 2.43 Titration of receptor **L_4** with TBA-Cl in DMSO-d_6/0.5% H_2O.

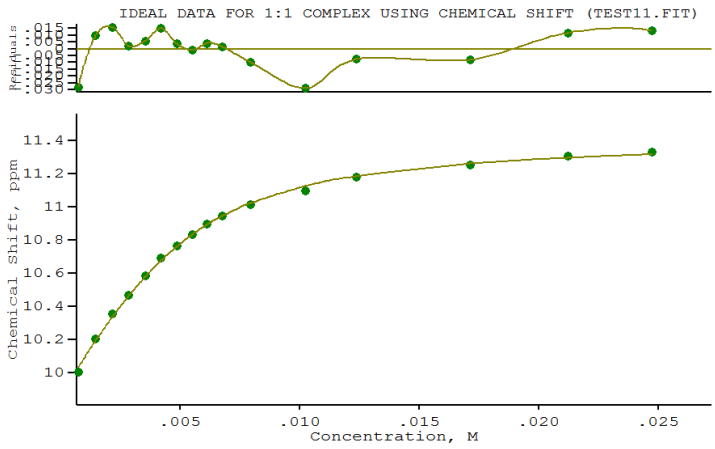

IDEAL DATA FOR 1:1 COMPLEX USING CHEMICAL SHIFT (TEST11.FIT)

Reaction: Sn + L = Sn(L)

FILE: TEST11.FIT (Measured shift is on 119Sn)

IDEAL DATA: K1 = 63.091; DELTA M = 20.0; DELTA ML = 120.0

File prepared by M. J. Hynes, October 22 2000

NO.	A	PARAMETER	DELTA	ERROR	CONDITION	DESCRIPTION
1	1	6.83902E+02	2.000E-01	4.026E+01	9.142E+00	K1
2	1	9.85802E+00	2.000E-01	1.208E-02	2.309E+00	SHIFT Sn
3	1	1.14189E+01	1.000E+00	1.436E-02	6.528E+00	SHIFT Sn(L)

0RMS ERROR = 1.48E-02 MAX ERROR = 2.90E-02 AT OBS.NO. 12

RESIDUALS SQUARED = 2.83E-03

RFACTOR = 0.1230 PERCENT

Figure 2.44 Titration of receptor **L_4** with TBA-H_2PO_4 in DMSO-d_6/0.5% H_2O.

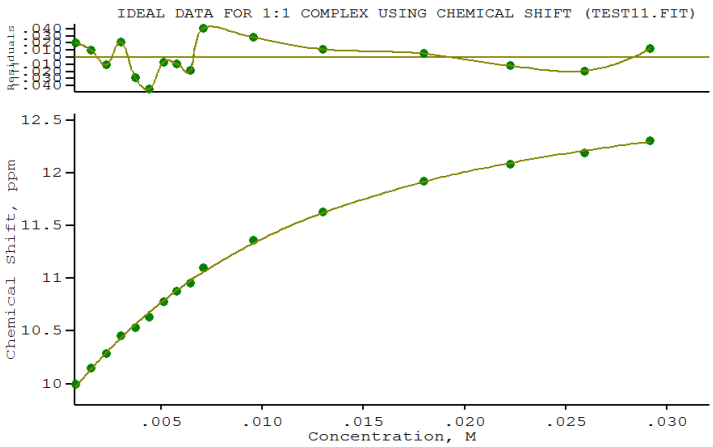

IDEAL DATA FOR 1:1 COMPLEX USING CHEMICAL SHIFT (TEST11.FIT)

Reaction: Sn + L = Sn(L)

FILE: TEST11.FIT (Measured shift is on 119Sn)

IDEAL DATA: K1 = 63.091; DELTA M = 20.0; DELTA ML = 120.0

File prepared by M. J. Hynes, October 22 2000

NO.	A	PARAMETER	DELTA	ERROR	CONDITION	DESCRIPTION
1	1	1.23340E+02	2.000E-01	7.324E+00	2.805E+01	K1
2	1	9.79417E+00	2.000E-01	1.934E-02	4.257E+00	SHIFT Sn
3	1	1.30967E+01	1.000E+00	5.771E-02	1.794E+01	SHIFT Sn(L)

0RMS ERROR = 2.44E-02 MAX ERROR = 4.47E-02 AT OBS.NO. 6

RESIDUALS SQUARED = 7.71E-03

RFACTOR = 0.1977 PERCENT

Figure 2.45 Titration of receptor **L_5** with TBA-BzO in DMSO-d_6/0.5% H_2O.

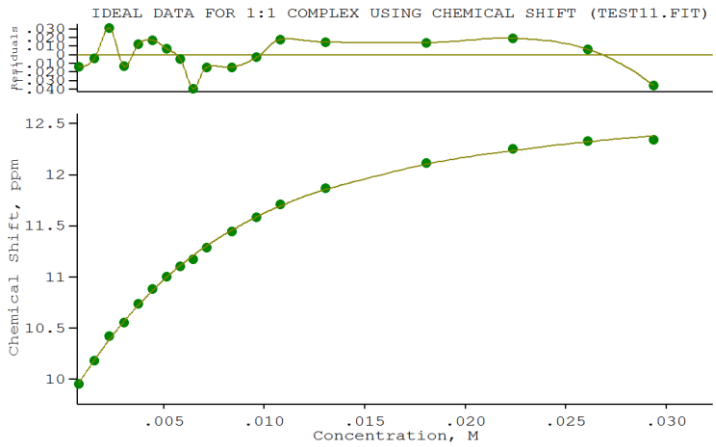

IDEAL DATA FOR 1:1 COMPLEX USING CHEMICAL SHIFT (TEST11.FIT)

Reaction: Sn + L = Sn(L)

FILE: TEST11.FIT (Measured shift is on 119Sn)

IDEAL DATA: K1 = 63.091; DELTA M = 20.0; DELTA ML = 120.0

File prepared by M. J. Hynes, October 22 2000

NO.	A	PARAMETER	DELTA	ERROR	CONDITION	DESCRIPTION
1	1	2.18417E+02	2.000E-01	8.495E+00	1.718E+01	K1
2	1	9.72247E+00	2.000E-01	1.666E-02	3.700E+00	SHIFT Sn
3	1	1.28629E+01	1.000E+00	2.858E-02	1.055E+01	SHIFT Sn(L)

0RMS ERROR = 2.04E-02 MAX ERROR = 3.90E-02 AT OBS.NO. 9

RESIDUALS SQUARED = 6.22E-03

RFACTOR = 0.1645 PERCENT

Figure 2.46 Titration of receptor **L_6** with TBA-AcO in DMSO-d_6/0.5% H_2O.

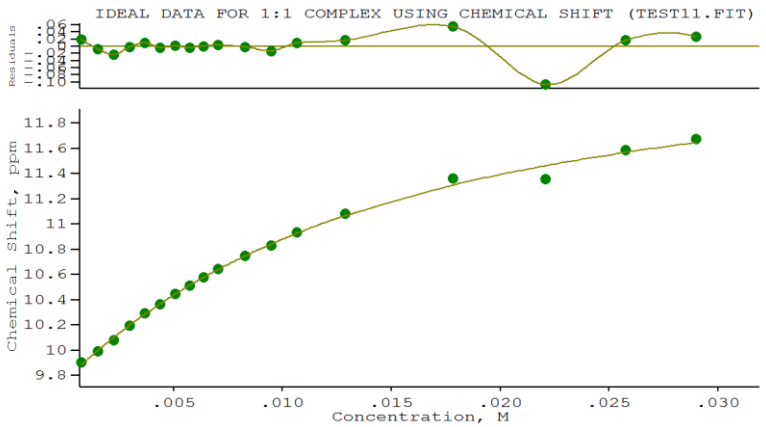

IDEAL DATA FOR 1:1 COMPLEX USING CHEMICAL SHIFT (TEST11.FIT)

Reaction: Sn + L = Sn(L)

FILE: TEST11.FIT (Measured shift is on 119Sn)

IDEAL DATA: K1 = 63.091; DELTA M = 20.0; DELTA ML = 120.0

File prepared by M. J. Hynes, October 22 2000

NO.	A	PARAMETER	DELTA	ERROR	CONDITION	DESCRIPTION
1	1	8.73511E+01	2.000E-01	9.640E+00	4.076E+01	K1
2	1	9.76564E+00	2.000E-01	2.571E-02	4.835E+00	SHIFT Sn
3	1	1.24887E+01	1.000E+00	1.053E-01	2.697E+01	SHIFT Sn(L)

0RMS ERROR = 3.39E-02 MAX ERROR = 1.07E-01 AT OBS.NO. 16

RESIDUALS SQUARED = 1.73E-02

RFACTOR = 0.2890 PERCENT

Figure 2.47 Titration of receptor **L_6** with TBA-BzO in DMSO-d_6/0.5% H_2O.

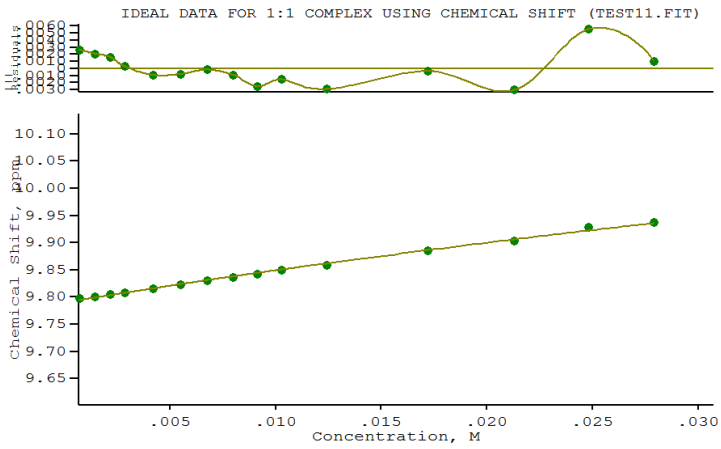

IDEAL DATA FOR 1:1 COMPLEX USING CHEMICAL SHIFT (TEST11.FIT)

Reaction: Sn + L = Sn(L)

FILE: TEST11.FIT (Measured shift is on 119Sn)

IDEAL DATA: K1 = 63.091; DELTA M = 20.0; DELTA ML = 120.0

File prepared by M. J. Hynes, October 22 2000

NO.	A	PARAMETER	DELTA	ERROR	CONDITION	DESCRIPTION
1	1	8.04109E+00	2.000E-01	1.960E+00	5.083E+02	K1
2	1	9.78964E+00	2.000E-01	1.494E-03	4.637E+00	SHIFT Sn
3	1	1.06063E+01	1.000E+00	1.553E-01	4.585E+02	SHIFT Sn(L)

0RMS ERROR = 2.50E-03 MAX ERROR = 5.56E-03 AT OBS.NO. 14

RESIDUALS SQUARED = 7.51E-05

RFACTOR = 0.0227 PERCENT

Figure 2.48 Titration of receptor **L_6** with TBA-Cl in DMSO-d_6/0.5% H_2O.

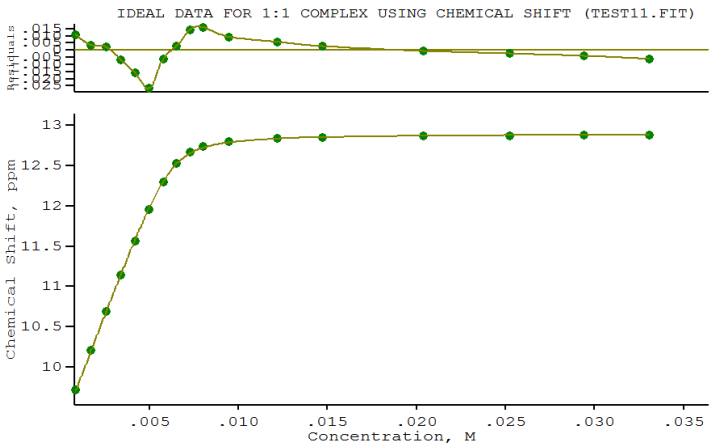

IDEAL DATA FOR 1:1 COMPLEX USING CHEMICAL SHIFT (TEST11.FIT)

Reaction: Sn + L = Sn(L)

FILE: TEST11.FIT (Measured shift is on 119Sn)

IDEAL DATA: K1 = 63.091; DELTA M = 20.0; DELTA ML = 120.0

File prepared by M. J. Hynes, October 22 2000

NO.	A	PARAMETER	DELTA	ERROR	CONDITION	DESCRIPTION
1	1	9.62012E+03	2.000E-01	3.647E+02	2.472E+00	K1
2	1	9.20627E+00	2.000E-01	8.486E-03	1.132E+00	SHIFT Sn
3	1	1.28932E+01	1.000E+00	5.352E-03	2.513E+00	SHIFT Sn(L)

0RMS ERROR = 1.15E-02 MAX ERROR = 2.67E-02 AT OBS.NO. 6

RESIDUALS SQUARED = 1.86E-03

RFACTOR = 0.0862 PERCENT

Figure 2.49 Titration of receptor **L_7** with TBA-AcO in DMSO-d_6/0.5% H_2O.

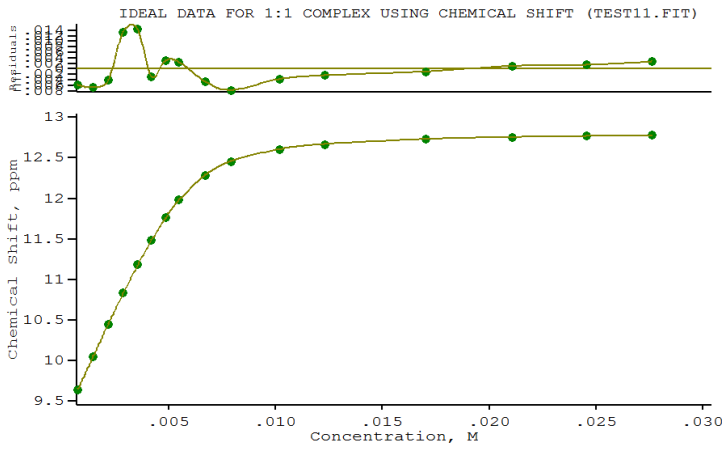

IDEAL DATA FOR 1:1 COMPLEX USING CHEMICAL SHIFT (TEST11.FIT)

Reaction: Sn + L = Sn(L)

FILE: TEST11.FIT (Measured shift is on 119Sn)

IDEAL DATA: K1 = 63.091; DELTA M = 20.0; DELTA ML = 120.0

File prepared by M. J. Hynes, October 22 2000

NO.	A	PARAMETER	DELTA	ERROR	CONDITION	DESCRIPTION
1	1	3.32249E+03	2.000E-01	6.053E+01	3.786E+00	K1
2	1	9.22086E+00	2.000E-01	4.920E-03	1.349E+00	SHIFT Sn
3	1	1.28250E+01	1.000E+00	4.130E-03	3.364E+00	SHIFT Sn(L)

0RMS ERROR = 6.88E-03 MAX ERROR = 1.45E-02 AT OBS.NO. 5

RESIDUALS SQUARED = 6.15E-04

RFACTOR = 0.0525 PERCENT

Figure 2.50 Titration of receptor **L_7** with TBA-BzO in DMSO-d_6/0.5% H_2O.

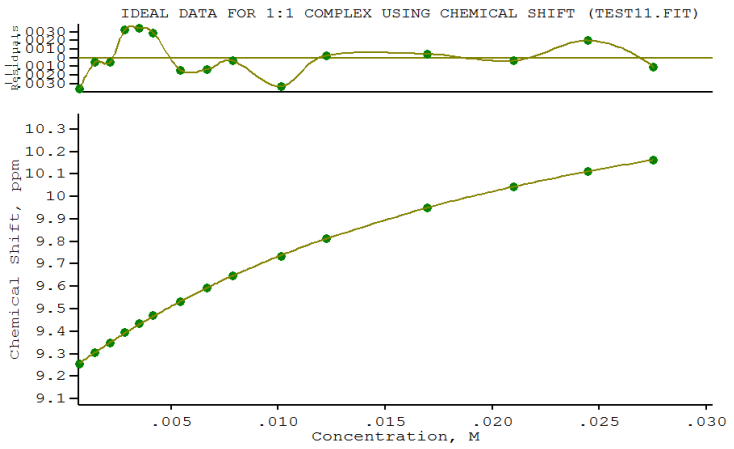

IDEAL DATA FOR 1:1 COMPLEX USING CHEMICAL SHIFT (TEST11.FIT)

Reaction: Sn + L = Sn(L)

FILE: TEST11.FIT (Measured shift is on 119Sn)

IDEAL DATA: K1 = 63.091; DELTA M = 20.0; DELTA ML = 120.0

File prepared by M. J. Hynes, October 22 2000

NO.	A	PARAMETER	DELTA	ERROR	CONDITION	DESCRIPTION
1	1	5.78254E+01	2.000E-01	1.066E+00	6.500E+01	K1
2	1	9.20951E+00	2.000E-01	1.646E-03	4.243E+00	SHIFT Sn
3	1	1.08449E+01	1.000E+00	1.294E-02	4.906E+01	SHIFT Sn(L)

0RMS ERROR = 2.32E-03 MAX ERROR = 3.61E-03 AT OBS.NO. 1

RESIDUALS SQUARED = 6.47E-05

RFACTOR = 0.0215 PERCENT

Figure 2.51 Titration of receptor **L_7** with TBA-Cl in DMSO-d_6/0.5% H_2O.

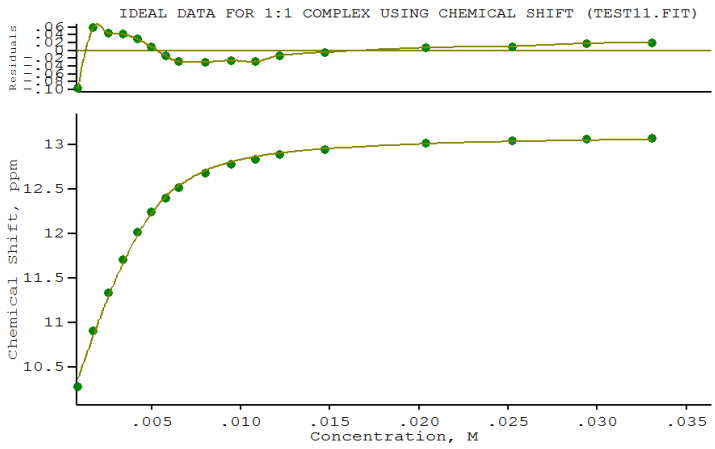

IDEAL DATA FOR 1:1 COMPLEX USING CHEMICAL SHIFT (TEST11.FIT)

Reaction: Sn + L = Sn(L)

FILE: TEST11.FIT (Measured shift is on 119Sn)

IDEAL DATA: K1 = 63.091; DELTA M = 20.0; DELTA ML = 120.0

File prepared by M. J. Hynes, October 22 2000

NO.	A	PARAMETER	DELTA	ERROR	CONDITION	DESCRIPTION
1	1	1.88324E+03	2.000E-01	1.530E+02	4.317E+00	K1
2	1	9.86701E+00	2.000E-01	3.540E-02	1.613E+00	SHIFT Sn
3	1	1.31134E+01	1.000E+00	2.210E-02	3.390E+00	SHIFT Sn(L)

0RMS ERROR = 3.96E-02 MAX ERROR = 9.69E-02 AT OBS.NO. 1

RESIDUALS SQUARED = 2.20E-02

RFACTOR = 0.2906 PERCENT

Figure 2.52 Titration of receptor **L_8** with TBA-AcO in DMSO-d_6/0.5% H_2O.

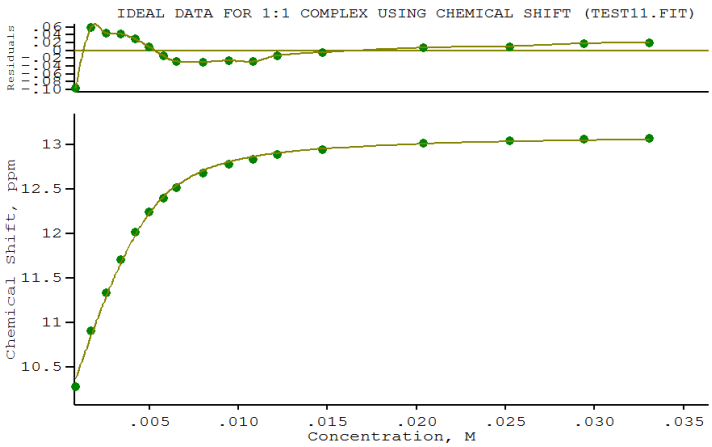

IDEAL DATA FOR 1:1 COMPLEX USING CHEMICAL SHIFT (TEST11.FIT)

Reaction: Sn + L = Sn(L)

FILE: TEST11.FIT (Measured shift is on 119Sn)

IDEAL DATA: K1 = 63.091; DELTA M = 20.0; DELTA ML = 120.0

File prepared by M. J. Hynes, October 22 2000

NO.	A	PARAMETER	DELTA	ERROR	CONDITION	DESCRIPTION
1	1	5.66580E+02	2.000E-01	4.901E+00	7.914E+00	K1
2	1	9.89989E+00	2.000E-01	4.582E-03	2.542E+00	SHIFT Sn
3	1	1.31101E+01	1.000E+00	4.075E-03	5.096E+00	SHIFT Sn(L)

0RMS ERROR = 5.13E-03 MAX ERROR = 1.25E-02 AT OBS.NO. 6

RESIDUALS SQUARED = 3.68E-04

RFACTOR = 0.0388 PERCENT

Figure 2.53 Titration of receptor **L_8** with TBA-BzO in DMSO-d_6/0.5% H_2O.

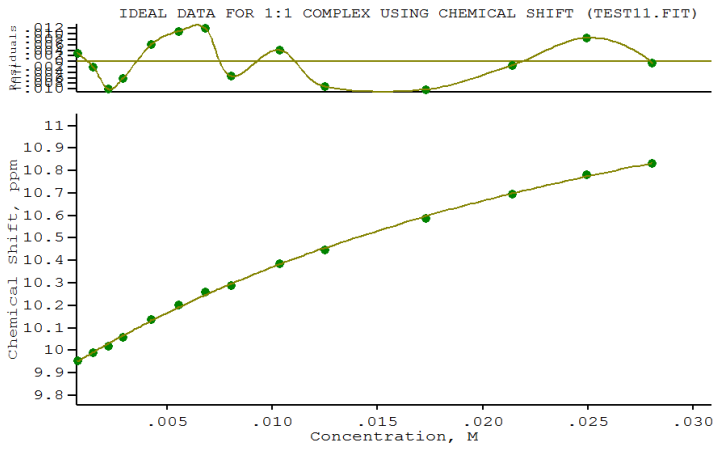

IDEAL DATA FOR 1:1 COMPLEX USING CHEMICAL SHIFT (TEST11.FIT)

Reaction: Sn + L = Sn(L)

FILE: TEST11.FIT (Measured shift is on 119Sn)

IDEAL DATA: K1 = 63.091; DELTA M = 20.0; DELTA ML = 120.0

File prepared by M. J. Hynes, October 22 2000

NO.	A	PARAMETER	DELTA	ERROR	CONDITION	DESCRIPTION
1	1	3.52281E+01	2.000E-01	2.754E+00	1.163E+02	K1
2	1	9.90971E+00	2.000E-01	5.941E-03	4.519E+00	SHIFT Sn
3	1	1.18504E+01	1.000E+00	8.268E-02	9.332E+01	SHIFT Sn(L)

0RMS ERROR = 8.35E-03 MAX ERROR = 1.20E-02 AT OBS.NO. 7

RESIDUALS SQUARED = 7.67E-04

RFACTOR = 0.0716 PERCENT

Figure 2.54 Titration of receptor **L_8** with TBA-Cl in DMSO-d_6/0.5% H_2O.

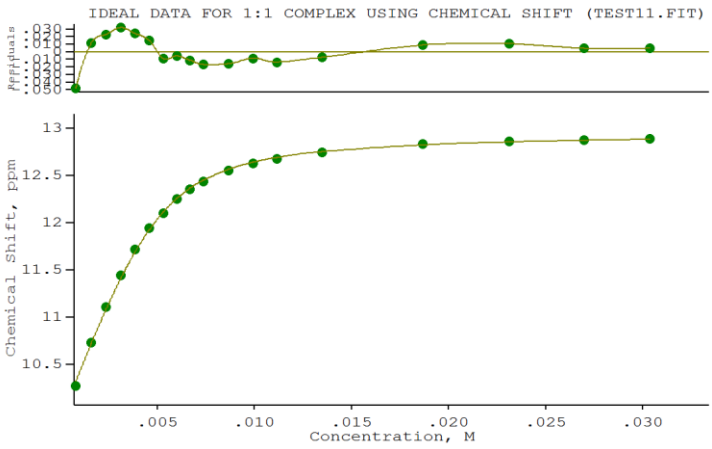

IDEAL DATA FOR 1:1 COMPLEX USING CHEMICAL SHIFT (TEST11.FIT)

Reaction: Sn + L = Sn(L)

FILE: TEST11.FIT (Measured shift is on 119Sn)

IDEAL DATA: K1 = 63.091; DELTA M = 20.0; DELTA ML = 120.0

File prepared by M. J. Hynes, October 22 2000

NO.	A	PARAMETER	DELTA	ERROR	CONDITION	DESCRIPTION
1	1	1.61078E+03	2.000E-01	6.847E+01	5.026E+00	K1
2	1	9.89695E+00	2.000E-01	1.669E-02	1.647E+00	SHIFT Sn
3	1	1.29539E+01	1.000E+00	1.233E-02	4.011E+00	SHIFT Sn(L)

0RMS ERROR = 2.02E-02 MAX ERROR = 4.83E-02 AT OBS.NO. 1

RESIDUALS SQUARED = 6.13E-03

RFACTOR = 0.1517 PERCENT

Figure 2.55 Titration of receptor **L$_9$** with TBA-AcO in DMSO-d_6/0.5% H_2O.

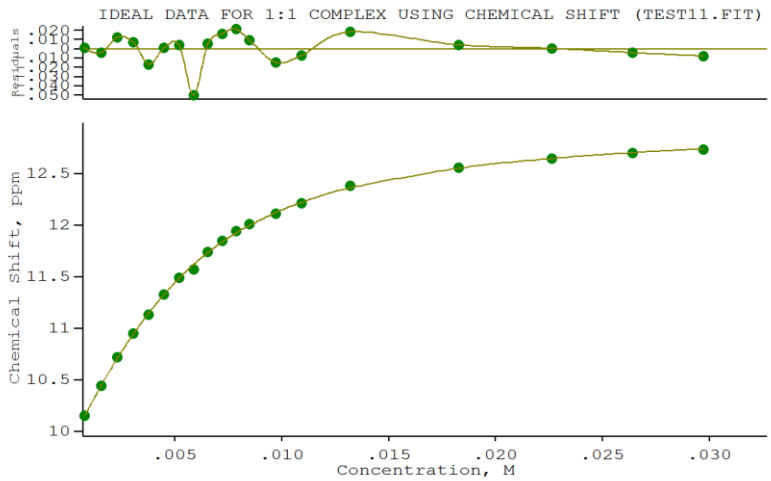

IDEAL DATA FOR 1:1 COMPLEX USING CHEMICAL SHIFT (TEST11.FIT)

Reaction: Sn + L = Sn(L)

FILE: TEST11.FIT (Measured shift is on 119Sn)

IDEAL DATA: K1 = 63.091; DELTA M = 20.0; DELTA ML = 120.0

File prepared by M. J. Hynes, October 22 2000

NO.	A	PARAMETER	DELTA	ERROR	CONDITION	DESCRIPTION
1	1	4.24704E+02	2.000E-01	1.206E+01	1.094E+01	K1
2	1	9.82957E+00	2.000E-01	1.378E-02	2.819E+00	SHIFT Sn
3	1	1.30093E+01	1.000E+00	1.612E-02	7.162E+00	SHIFT Sn(L)

0RMS ERROR = 1.68E-02 MAX ERROR = 4.95E-02 AT OBS.NO. 8

RESIDUALS SQUARED = 4.51E-03

RFACTOR = 0.1312 PERCENT

Figure 2.56 Titration of receptor **L9** with TBA-BzO in DMSO-d_6/0.5% H_2O.

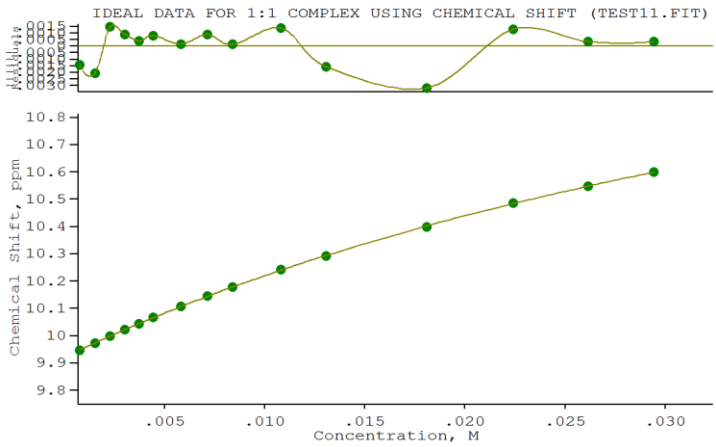

IDEAL DATA FOR 1:1 COMPLEX USING CHEMICAL SHIFT (TEST11.FIT)

Reaction: Sn + L = Sn(L)

FILE: TEST11.FIT (Measured shift is on 119Sn)

IDEAL DATA: K1 = 63.091; DELTA M = 20.0; DELTA ML = 120.0

File prepared by M. J. Hynes, October 22 2000

NO.	A	PARAMETER	DELTA	ERROR	CONDITION	DESCRIPTION
1	1	2.06199E+01	2.000E-01	4.739E-01	1.994E+02	K1
2	1	9.92164E+00	2.000E-01	9.883E-04	4.753E+00	SHIFT Sn
3	1	1.17890E+01	1.000E+00	2.675E-02	1.675E+02	SHIFT Sn(L)

0RMS ERROR = 1.50E-03 MAX ERROR = 3.17E-03 AT OBS.NO. 12

RESIDUALS SQUARED = 2.71E-05

RFACTOR = 0.0132 PERCENT

Figure 2.57 Titration of receptor **L9** with TBA-Cl in DMSO-d_6/0.5% H_2O.

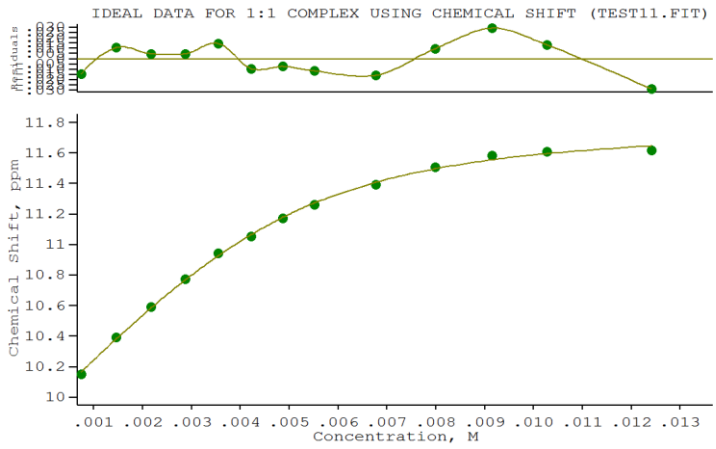

IDEAL DATA FOR 1:1 COMPLEX USING CHEMICAL SHIFT (TEST11.FIT)

Reaction: Sn + L = Sn(L)

FILE: TEST11.FIT (Measured shift is on 119Sn)

IDEAL DATA: K1 = 63.091; DELTA M = 20.0; DELTA ML = 120.0

File prepared by M. J. Hynes, October 22 2000

NO.	A	PARAMETER	DELTA	ERROR	CONDITION	DESCRIPTION
1	1	1.26813E+03	2.000E-01	1.439E+02	1.936E+01	K1
2	1	9.93110E+00	2.000E-01	1.406E-02	1.802E+00	SHIFT Sn
3	1	1.18207E+01	1.000E+00	3.048E-02	1.712E+01	SHIFT Sn(L)

0RMS ERROR = 1.75E-02 MAX ERROR = 2.91E-02 AT OBS.NO. 11

RESIDUALS SQUARED = 3.05E-03

RFACTOR = 0.1380 PERCENT

Figure 2.58 Titration of receptor **L9** with TBA-H_2PO_4 in DMSO-d_6/0.5% H_2O.

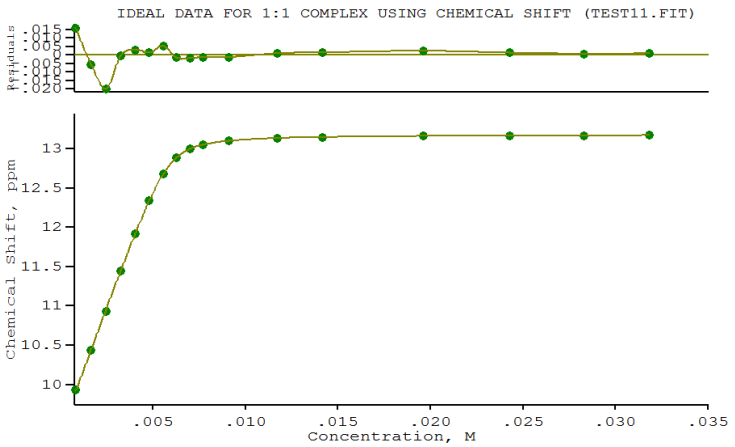

IDEAL DATA FOR 1:1 COMPLEX USING CHEMICAL SHIFT (TEST11.FIT)

Reaction: Sn + L = Sn(L)

FILE: TEST11.FIT (Measured shift is on 119Sn)

IDEAL DATA: K1 = 63.091; DELTA M = 20.0; DELTA ML = 120.0

File prepared by M. J. Hynes, October 22 2000

NO.	A	PARAMETER	DELTA	ERROR	CONDITION	DESCRIPTION
1	1	1.34674E+04	2.000E-01	3.088E+02	2.073E+00	K1
2	1	9.38001E+00	2.000E-01	5.567E-03	1.155E+00	SHIFT Sn
3	1	1.31826E+01	1.000E+00	2.994E-03	2.008E+00	SHIFT Sn(L)

0RMS ERROR = 7.30E-03 MAX ERROR = 1.99E-02 AT OBS.NO. 3

RESIDUALS SQUARED = 7.47E-04

RFACTOR = 0.0533 PERCENT

Figure 2.59 Titration of receptor **L_{10}** with TBA-AcO in DMSO-d_6/0.5% H_2O.

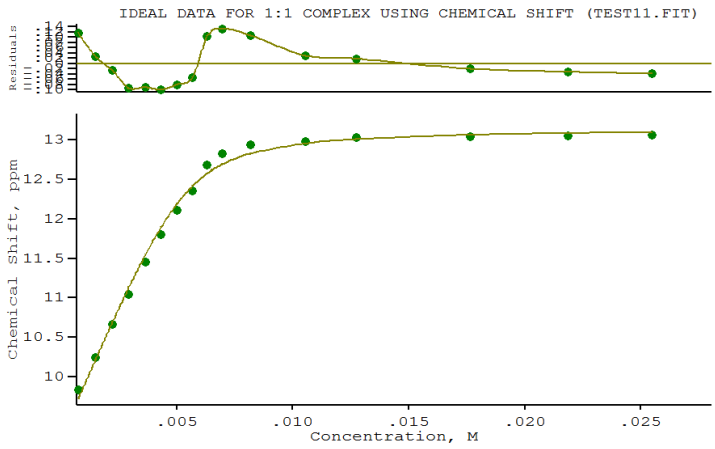

IDEAL DATA FOR 1:1 COMPLEX USING CHEMICAL SHIFT (TEST11.FIT)

Reaction: Sn + L = Sn(L)

FILE: TEST11.FIT (Measured shift is on 119Sn)

IDEAL DATA: K1 = 63.091; DELTA M = 20.0; DELTA ML = 120.0

File prepared by M. J. Hynes, October 22 2000

NO.	A	PARAMETER	DELTA	ERROR	CONDITION	DESCRIPTION
1	1	3.51345E+03	2.000E-01	6.787E+02	4.122E+00	K1
2	1	9.19697E+00	2.000E-01	6.436E-02	1.332E+00	SHIFT Sn
3	1	1.31551E+01	1.000E+00	5.377E-02	3.778E+00	SHIFT Sn(L)

0RMS ERROR = 8.57E-02 MAX ERROR = 1.33E-01 AT OBS.NO. 10

RESIDUALS SQUARED = 9.55E-02

RFACTOR = 0.6374 PERCENT

Figure 2.60 Titration of receptor **L_{10}** with TBA-BzO in DMSO-d_6/0.5% H_2O.

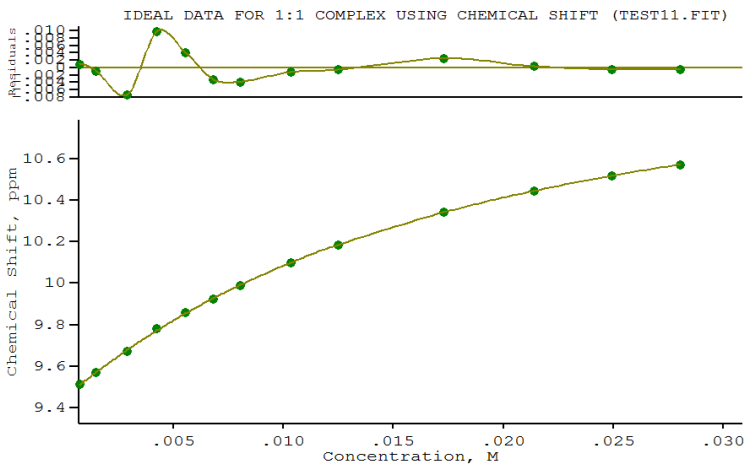

IDEAL DATA FOR 1:1 COMPLEX USING CHEMICAL SHIFT (TEST11.FIT)

Reaction: Sn + L = Sn(L)

FILE: TEST11.FIT (Measured shift is on 119Sn)

IDEAL DATA: K1 = 63.091; DELTA M = 20.0; DELTA ML = 120.0

File prepared by M. J. Hynes, October 22 2000

NO.	A	PARAMETER	DELTA	ERROR	CONDITION	DESCRIPTION
1	1	6.86374E+01	2.000E-01	2.005E+00	5.327E+01	K1
2	1	9.44784E+00	2.000E-01	3.647E-03	4.122E+00	SHIFT Sn
3	1	1.12343E+01	1.000E+00	2.065E-02	3.940E+01	SHIFT Sn(L)

0RMS ERROR = 4.52E-03 MAX ERROR = 9.94E-03 AT OBS.NO. 4

RESIDUALS SQUARED = 2.04E-04

RFACTOR = 0.0395 PERCENT

Figure 2.61 Titration of receptor **L_{10}** with TBA-Cl in DMSO-d_6/0.5% H_2O.

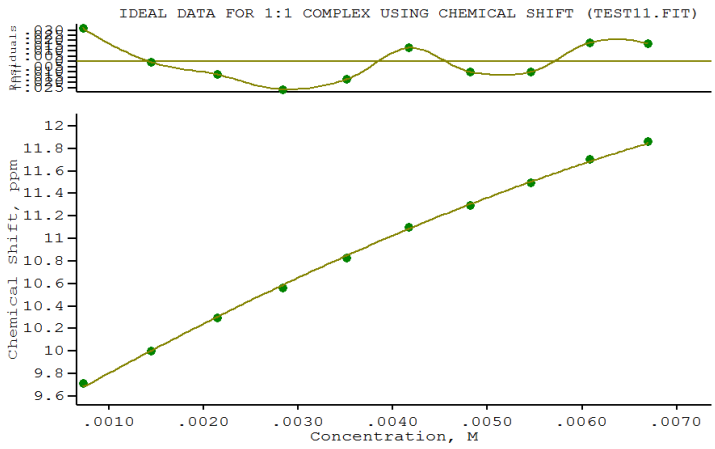

IDEAL DATA FOR 1:1 COMPLEX USING CHEMICAL SHIFT (TEST11.FIT)

Reaction: Sn + L = Sn(L)

FILE: TEST11.FIT (Measured shift is on 119Sn)

IDEAL DATA: K1 = 63.091; DELTA M = 20.0; DELTA ML = 120.0

File prepared by M. J. Hynes, October 22 2000

NO.	A	PARAMETER	DELTA	ERROR	CONDITION	DESCRIPTION
1	1	4.91024E+02	2.000E-01	6.424E+02	8.147E+03	K1
2	1	9.33994E+00	2.000E-01	3.136E-02	1.003E+01	SHIFT Sn
3	1	1.38328E+01	1.000E+00	1.657E+00	8.539E+03	SHIFT Sn(L)

0RMS ERROR = 2.12E-02 MAX ERROR = 3.17E-02 AT OBS.NO. 1

RESIDUALS SQUARED = 3.14E-03

RFACTOR = 0.1625 PERCENT

Figure 2.62 Titration of receptor **L_{10}** with TBA-H_2PO_4 in DMSO-d_6/0.5% H_2O.

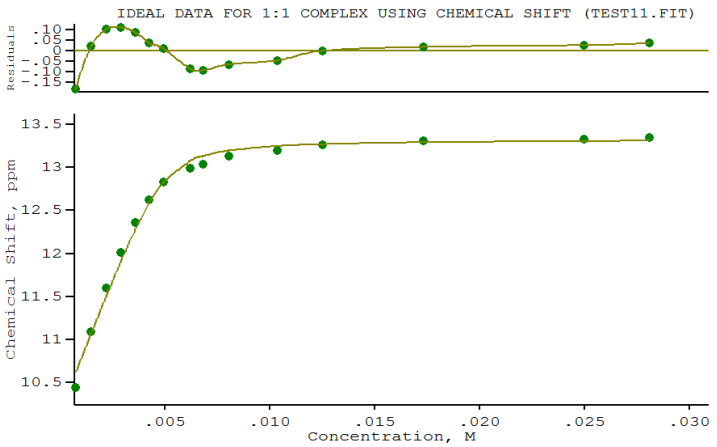

IDEAL DATA FOR 1:1 COMPLEX USING CHEMICAL SHIFT (TEST11.FIT)

Reaction: Sn + L = Sn(L)

FILE: TEST11.FIT (Measured shift is on 119Sn)

IDEAL DATA: K1 = 63.091; DELTA M = 20.0; DELTA ML = 120.0

File prepared by M. J. Hynes, October 22 2000

NO. A PARAMETER DELTA ERROR CONDITION DESCRIPTION

1 1 6.83335E+03 2.000E-01 2.048E+03 2.655E+00 K1

2 1 1.01667E+01 2.000E-01 6.916E-02 1.256E+00 SHIFT Sn

3 1 1.33255E+01 1.000E+00 4.320E-02 2.436E+00 SHIFT Sn(L)

0RMS ERROR = 8.67E-02 MAX ERROR = 1.79E-01 AT OBS.NO. 1

RESIDUALS SQUARED = 9.03E-02

RFACTOR = 0.6156 PERCENT

Figure 2.63 Titration of receptor **L_{11}** with TBA-AcO in DMSO-d_6/0.5% H_2O.

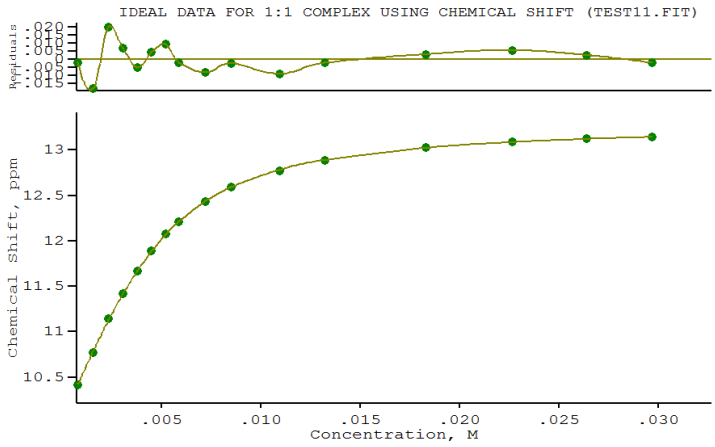

IDEAL DATA FOR 1:1 COMPLEX USING CHEMICAL SHIFT (TEST11.FIT)

Reaction: Sn + L = Sn(L)

FILE: TEST11.FIT (Measured shift is on 119Sn)

IDEAL DATA: K1 = 63.091; DELTA M = 20.0; DELTA ML = 120.0

File prepared by M. J. Hynes, October 22 2000

NO.	A	PARAMETER	DELTA	ERROR	CONDITION	DESCRIPTION
1	1	7.80352E+02	2.000E-01	1.317E+01	6.720E+00	K1
2	1	1.00187E+01	2.000E-01	8.024E-03	2.191E+00	SHIFT Sn
3	1	1.33029E+01	1.000E+00	7.127E-03	4.597E+00	SHIFT Sn(L)

0RMS ERROR = 9.35E-03 MAX ERROR = 2.01E-02 AT OBS.NO. 3

RESIDUALS SQUARED = 1.14E-03

RFACTOR = 0.0691 PERCENT

Figure 2.64 Titration of receptor **L_{11}** with TBA-BzO in DMSO-d_6/0.5% H_2O.

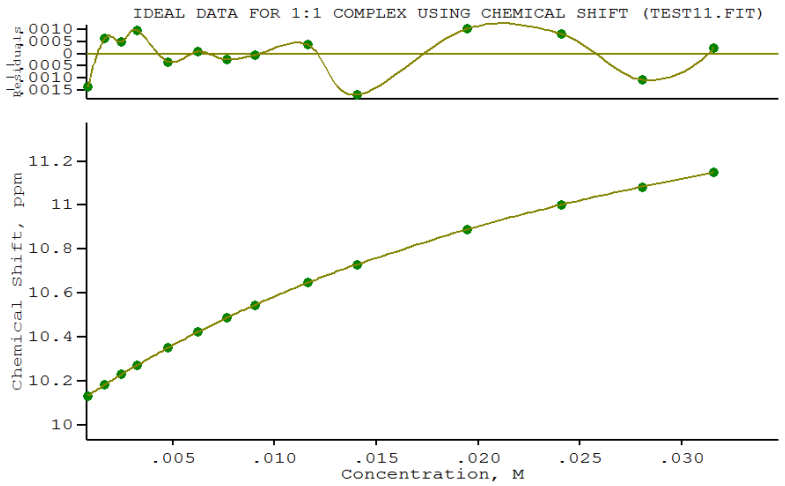

IDEAL DATA FOR 1:1 COMPLEX USING CHEMICAL SHIFT (TEST11.FIT)

Reaction: Sn + L = Sn(L)

FILE: TEST11.FIT (Measured shift is on 119Sn)

IDEAL DATA: K1 = 63.091; DELTA M = 20.0; DELTA ML = 120.0

File prepared by M. J. Hynes, October 22 2000

NO.	A	PARAMETER	DELTA	ERROR	CONDITION	DESCRIPTION
1	1	3.67713E+01	2.000E-01	2.611E-01	9.059E+01	K1
2	1	1.00812E+01	2.000E-01	6.842E-04	4.453E+00	SHIFT Sn
3	1	1.21520E+01	1.000E+00	7.321E-03	7.073E+01	SHIFT Sn(L)

0RMS ERROR = 9.41E-04 MAX ERROR = 1.71E-03 AT OBS.NO. 10

RESIDUALS SQUARED = 9.75E-06

RFACTOR = 0.0079 PERCENT

Figure 2.65 Titration of receptor **L_{11}** with TBA-Cl in DMSO-d_6/0.5% H_2O

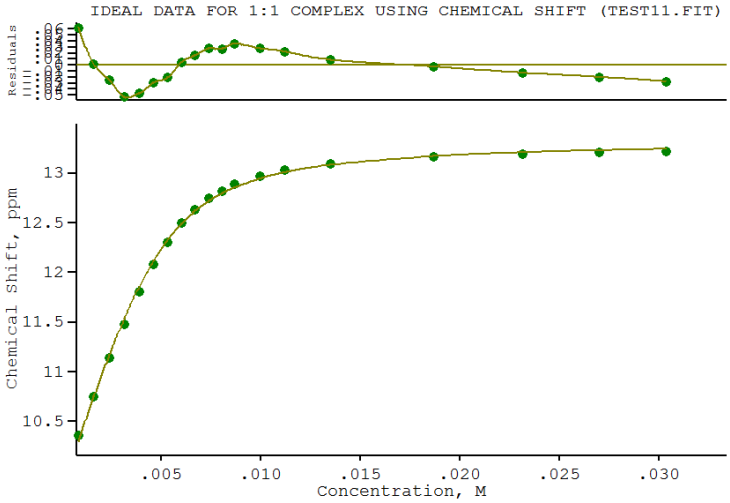

IDEAL DATA FOR 1:1 COMPLEX USING CHEMICAL SHIFT (TEST11.FIT)

Reaction: Sn + L = Sn(L)

FILE: TEST11.FIT (Measured shift is on 119Sn)

IDEAL DATA: K1 = 63.091; DELTA M = 20.0; DELTA ML = 120.0

File prepared by M. J. Hynes, October 22 2000

NO.	A	PARAMETER	DELTA	ERROR	CONDITION	DESCRIPTION
1	1	1.47054E+03	2.000E-01	8.194E+01	5.473E+00	K1
2	1	9.82093E+00	2.000E-01	2.660E-02	1.707E+00	SHIFT Sn
3	1	1.33345E+01	1.000E+00	1.995E-02	4.325E+00	SHIFT Sn(L)

0RMS ERROR = 3.22E-02 MAX ERROR = 6.28E-02 AT OBS.NO. 1

RESIDUALS SQUARED = 1.66E-02

RFACTOR = 0.2383 PERCENT

Figure 2.66 Titration of receptor **L_{12}** with TBA-AcO in DMSO-d_6/0.5% H_2O.

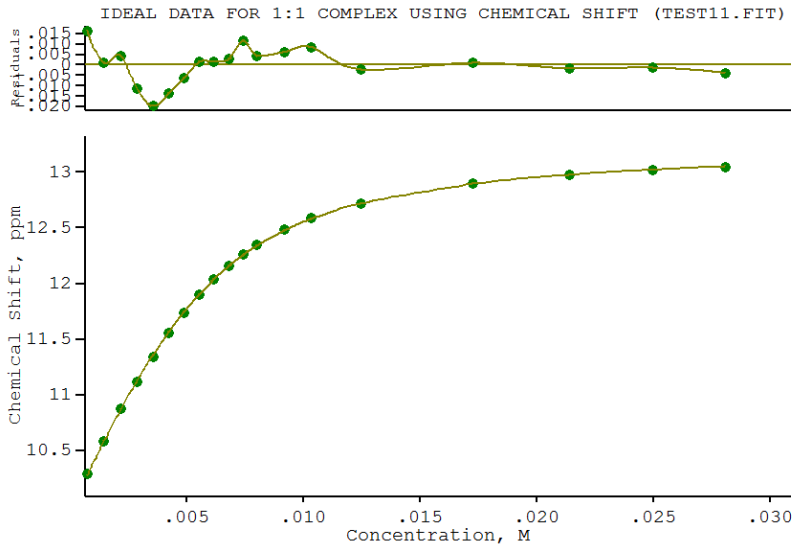

IDEAL DATA FOR 1:1 COMPLEX USING CHEMICAL SHIFT (TEST11.FIT)

Reaction: Sn + L = Sn(L)

FILE: TEST11.FIT (Measured shift is on 119Sn)

IDEAL DATA: K1 = 63.091; DELTA M = 20.0; DELTA ML = 120.0

File prepared by M. J. Hynes, October 22 2000

NO.	A	PARAMETER	DELTA	ERROR	CONDITION	DESCRIPTION
1	1	6.80594E+02	2.000E-01	1.089E+01	8.564E+00	K1
2	1	9.94371E+00	2.000E-01	6.785E-03	2.150E+00	SHIFT Sn
3	1	1.32520E+01	1.000E+00	7.901E-03	6.337E+00	SHIFT Sn(L)

0RMS ERROR = 9.15E-03 MAX ERROR = 1.97E-02 AT OBS.NO. 5

RESIDUALS SQUARED = 1.34E-03

RFACTOR = 0.0698 PERCENT

Figure 2.67 Titration of receptor **L_{12}** with TBA-BzO in DMSO-d_6/0.5% H_2O.

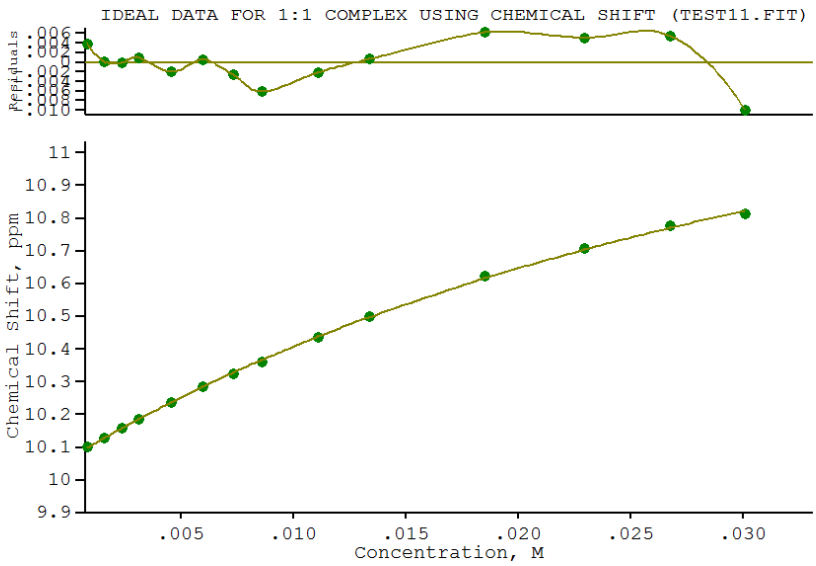

IDEAL DATA FOR 1:1 COMPLEX USING CHEMICAL SHIFT (TEST11.FIT)

Reaction: Sn + L = Sn(L)

FILE: TEST11.FIT (Measured shift is on 119Sn)

IDEAL DATA: K1 = 63.091; DELTA M = 20.0; DELTA ML = 120.0

File prepared by M. J. Hynes, October 22 2000

NO.	A	PARAMETER	DELTA	ERROR	CONDITION	DESCRIPTION
1	1	2.61989E+01	2.000E-01	1.630E+00	1.525E+02	K1
2	1	1.00659E+01	2.000E-01	3.411E-03	4.612E+00	SHIFT Sn
3	1	1.18570E+01	1.000E+00	6.355E-02	1.256E+02	SHIFT Sn(L)

0RMS ERROR = 4.89E-03 MAX ERROR = 9.93E-03 AT OBS.NO. 14

RESIDUALS SQUARED = 2.63E-04

RFACTOR = 0.0416 PERCENT

Figure 2.68 Titration of receptor **L_{12}** with TBA-Cl in DMSO-d_6/0.5% H_2O.

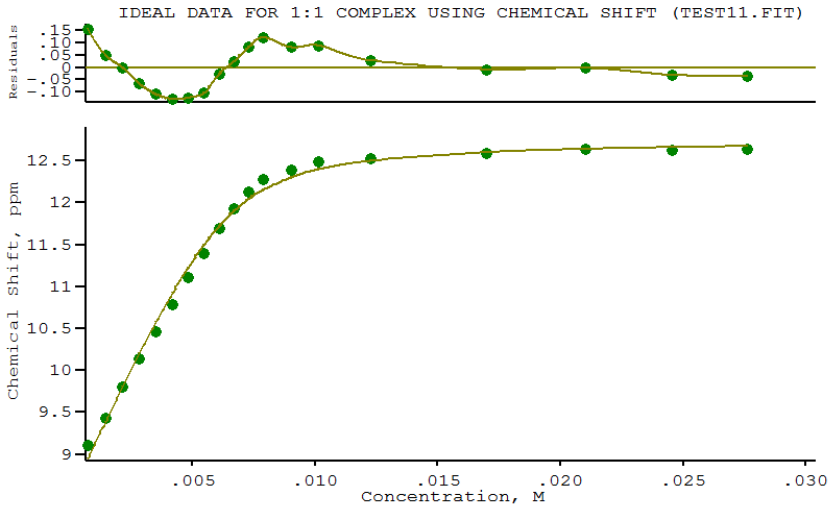

IDEAL DATA FOR 1:1 COMPLEX USING CHEMICAL SHIFT (TEST11.FIT)

Reaction: Sn + L = Sn(L)

FILE: TEST11.FIT (Measured shift is on 119Sn)

IDEAL DATA: K1 = 63.091; DELTA M = 20.0; DELTA ML = 120.0

File prepared by M. J. Hynes, October 22 2000

NO.	A	PARAMETER	DELTA	ERROR	CONDITION	DESCRIPTION
1	1	2.60819E+03	2.000E-01	4.436E+02	4.860E+00	K1
2	1	8.49457E+00	2.000E-01	5.914E-02	1.369E+00	SHIFT Sn
3	1	1.27468E+01	1.000E+00	5.700E-02	4.428E+00	SHIFT Sn(L)

0RMS ERROR = 8.89E-02 MAX ERROR = 1.55E-01 AT OBS.NO. 1

RESIDUALS SQUARED = 1.26E-01

RFACTOR = 0.7069 PERCENT

Figure 2.69 Titration of receptor **L_{13}** with TBA-AcO in DMSO-d_6/0.5% H_2O

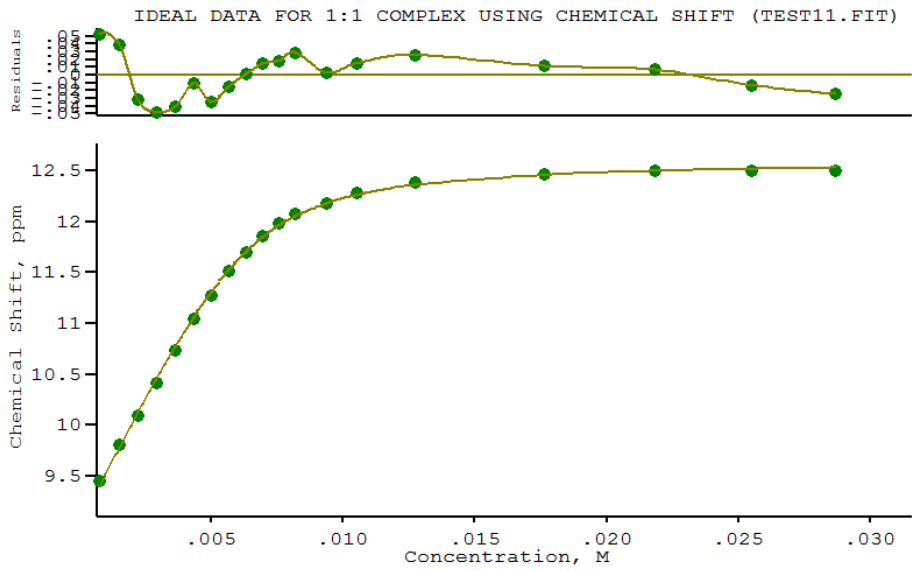

IDEAL DATA FOR 1:1 COMPLEX USING CHEMICAL SHIFT (TEST11.FIT)

Reaction: Sn + L = Sn(L)

FILE: TEST11.FIT (Measured shift is on 119Sn)

IDEAL DATA: K1 = 63.091; DELTA M = 20.0; DELTA ML = 120.0

File prepared by M. J. Hynes, October 22 2000

NO.	A	PARAMETER	DELTA	ERROR	CONDITION	DESCRIPTION
1	1	1.97969E+03	2.000E-01	1.216E+02	5.177E+00	K1
2	1	9.00986E+00	2.000E-01	2.029E-02	1.453E+00	SHIFT Sn
3	1	1.26067E+01	1.000E+00	1.950E-02	4.566E+00	SHIFT Sn(L)

0RMS ERROR = 2.97E-02 MAX ERROR = 5.28E-02 AT OBS.NO. 1

RESIDUALS SQUARED = 1.41E-02

RFACTOR = 0.2356 PERCENT

Figure 2.70 Titration of receptor **L_{13}** with TBA-BzO in DMSO-d_6/0.5% H_2O

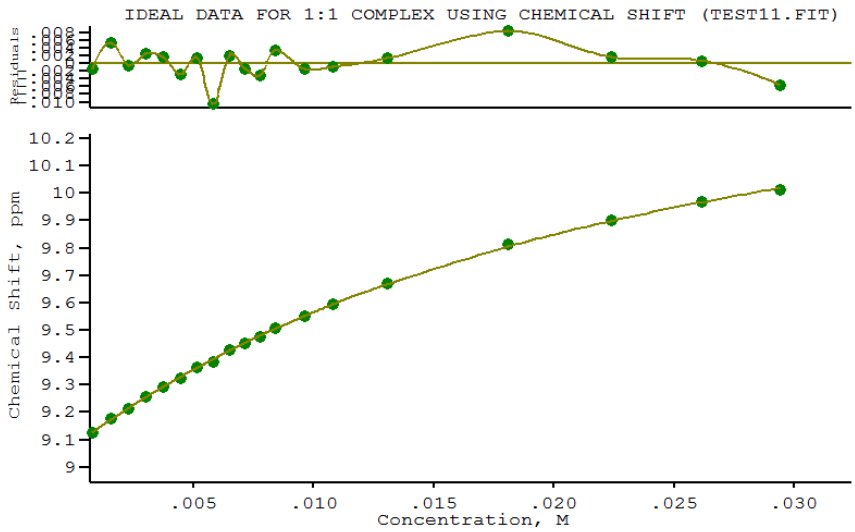

IDEAL DATA FOR 1:1 COMPLEX USING CHEMICAL SHIFT (TEST11.FIT)

Reaction: Sn + L = Sn(L)

FILE: TEST11.FIT (Measured shift is on 119Sn)

IDEAL DATA: K1 = 63.091; DELTA M = 20.0; DELTA ML = 120.0

NO.	A	PARAMETER	DELTA	ERROR	CONDITION	DESCRIPTION
1	1	5.21102E+01	2.000E-01	1.733E+00	7.496E+01	K1
2	1	9.07885E+00	2.000E-01	3.001E-03	5.349E+00	SHIFT Sn
3	1	1.07178E+01	1.000E+00	2.397E-02	5.402E+01	SHIFT Sn(L)

0RMS ERROR = 4.29E-03 MAX ERROR = 1.05E-02 AT OBS.NO. 8

RESIDUALS SQUARED = 2.95E-04

RFACTOR = 0.0415 PERCENT

Figure 2.71 Titration of receptor **L_{13}** with TBA-Cl in DMSO-d_6/0.5% H_2O

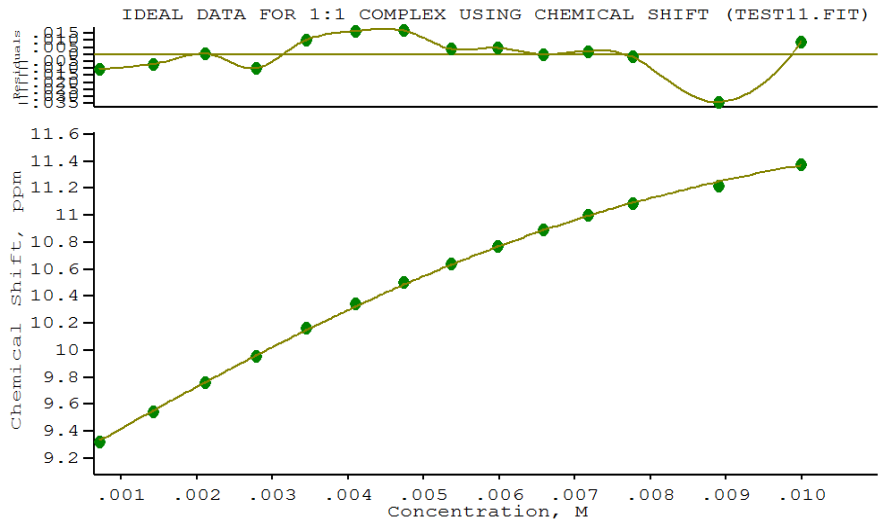

IDEAL DATA FOR 1:1 COMPLEX USING CHEMICAL SHIFT (TEST11.FIT)

Reaction: Sn + L = Sn(L)

FILE: TEST11.FIT (Measured shift is on 119Sn)

IDEAL DATA: K1 = 63.091; DELTA M = 20.0; DELTA ML = 120.0

NO.	A	PARAMETER	DELTA	ERROR	CONDITION	DESCRIPTION
1	1	8.71953E+02	2.000E-01	2.853E+02	5.432E+02	K1
2	1	9.10036E+00	2.000E-01	1.110E-02	2.799E+00	SHIFT Sn
3	1	1.20341E+01	1.000E+00	1.779E-01	5.742E+02	SHIFT Sn(L)

0RMS ERROR = 1.42E-02 MAX ERROR = 3.43E-02 AT OBS.NO. 13

RESIDUALS SQUARED = 2.23E-03

RFACTOR = 0.1203 PERCENT

Figure 2.72 Titration of receptor **L_{13}** with TBA-H_2PO_4 in DMSO-d_6/0.5% H_2O

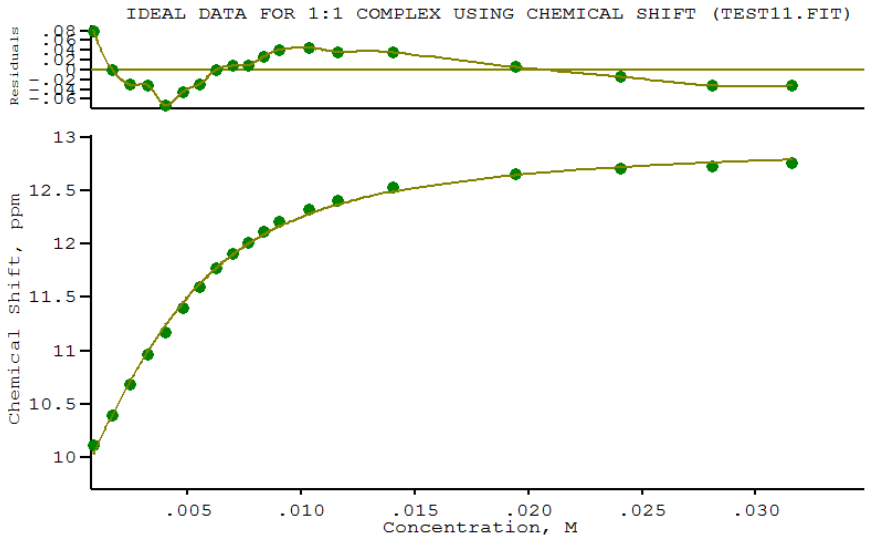

IDEAL DATA FOR 1:1 COMPLEX USING CHEMICAL SHIFT (TEST11.FIT)

Reaction: Sn + L = Sn(L)

FILE: TEST11.FIT (Measured shift is on 119Sn)

IDEAL DATA: K1 = 63.091; DELTA M = 20.0; DELTA ML = 120.0

NO.	A	PARAMETER	DELTA	ERROR	CONDITION	DESCRIPTION
1	1	5.99516E+02	2.000E-01	3.844E+01	8.639E+00	K1
2	1	9.64056E+00	2.000E-01	3.369E-02	2.412E+00	SHIFT Sn
3	1	1.29817E+01	1.000E+00	3.243E-02	5.930E+00	SHIFT Sn(L)

0RMS ERROR = 4.01E-02 MAX ERROR = 7.91E-02 AT OBS.NO. 1

RESIDUALS SQUARED = 2.58E-02

RFACTOR = 0.3111 PERCENT

Figure 2.73 Titration of receptor **L_{14}** with TBA-AcO in DMSO-d_6/0.5% H_2O

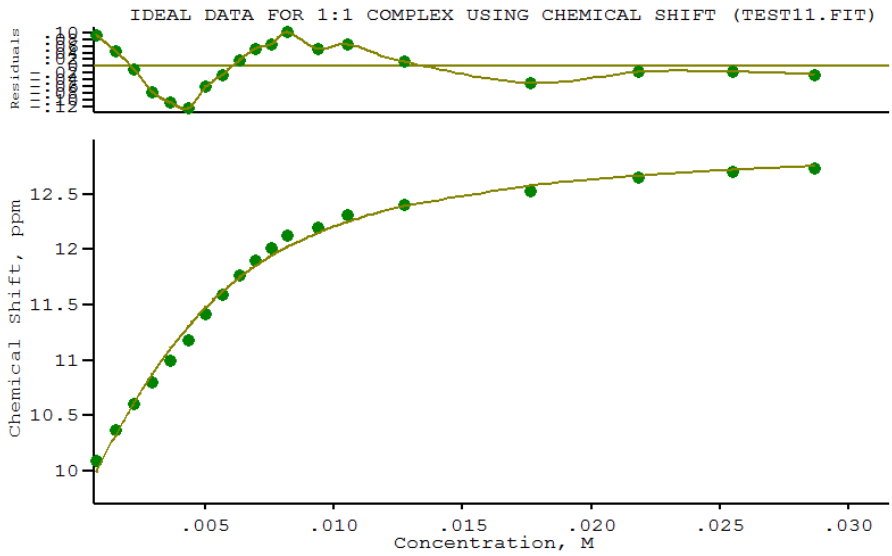

IDEAL DATA FOR 1:1 COMPLEX USING CHEMICAL SHIFT (TEST11.FIT)

Reaction: Sn + L = Sn(L)

FILE: TEST11.FIT (Measured shift is on 119Sn)

IDEAL DATA: K1 = 63.091; DELTA M = 20.0; DELTA ML = 120.0

NO.	A	PARAMETER	DELTA	ERROR	CONDITION	DESCRIPTION
1	1	5.14227E+02	2.000E-01	5.652E+01	9.947E+00	K1
2	1	9.63007E+00	2.000E-01	5.704E-02	2.639E+00	SHIFT Sn
3	1	1.30025E+01	1.000E+00	6.228E-02	6.649E+00	SHIFT Sn(L)

0RMS ERROR = 6.94E-02 MAX ERROR = 1.26E-01 AT OBS.NO. 6

RESIDUALS SQUARED = 7.70E-02

RFACTOR = 0.5426 PERCENT

Figure 2.74 Titration of receptor **L_{14}** with TBA-BzO in DMSO-d_6/0.5% H_2O

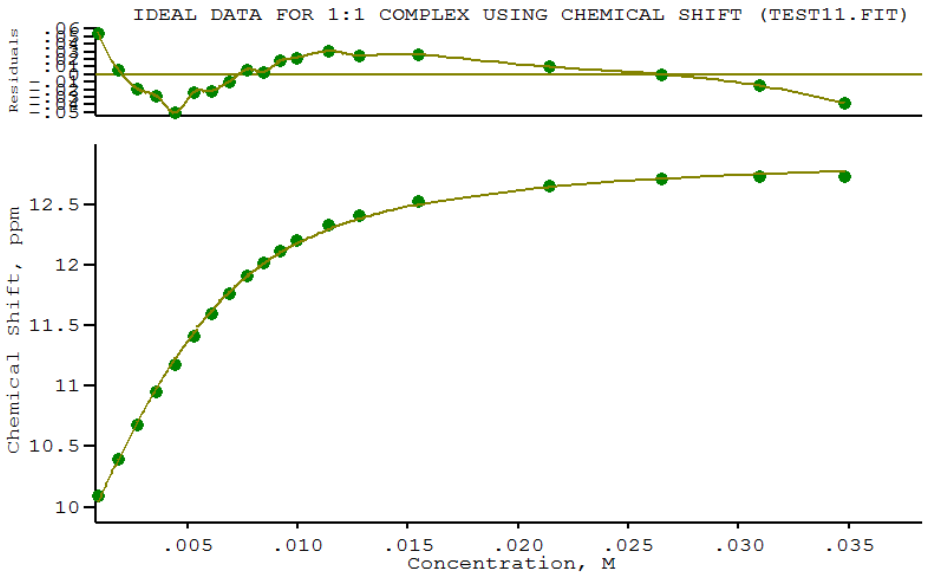

IDEAL DATA FOR 1:1 COMPLEX USING CHEMICAL SHIFT (TEST11.FIT)

Reaction: Sn + L = Sn(L)

FILE: TEST11.FIT (Measured shift is on 119Sn)

IDEAL DATA: K1 = 63.091; DELTA M = 20.0; DELTA ML = 120.0

NO.	A	PARAMETER	DELTA	ERROR	CONDITION	DESCRIPTION
1	1	3.30523E+01	2.000E-01	1.595E+00	9.657E+01	K1
2	1	9.78349E+00	2.000E-01	4.312E-03	5.670E+00	SHIFT Sn
3	1	1.16890E+01	1.000E+00	4.604E-02	7.138E+01	SHIFT Sn(L)

0RMS ERROR = 6.24E-03 MAX ERROR = 1.38E-02 AT OBS.NO. 19

RESIDUALS SQUARED = 6.24E-04

RFACTOR = 0.0561 PERCENT

Figure 2.75 Titration of receptor **L_{14}** with TBA-Cl in DMSO-d_6/0.5% H_2O

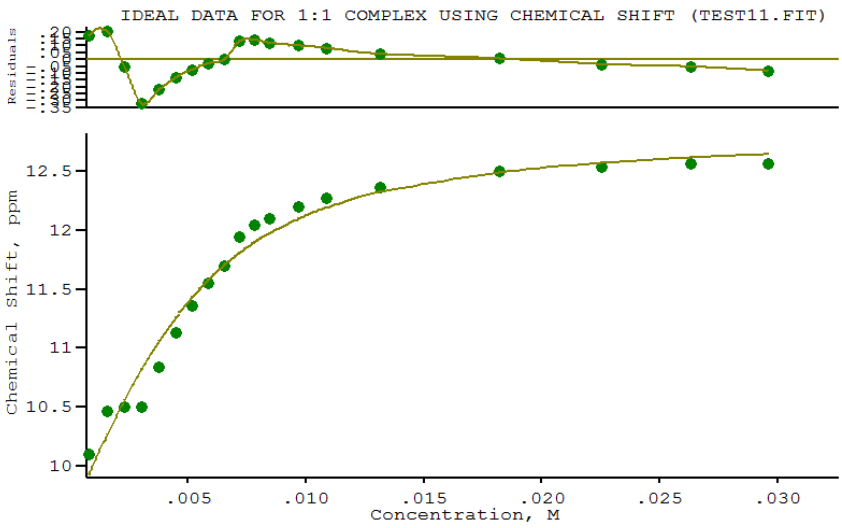

IDEAL DATA FOR 1:1 COMPLEX USING CHEMICAL SHIFT (TEST11.FIT)

Reaction: Sn + L = Sn(L)

FILE: TEST11.FIT (Measured shift is on 119Sn)

IDEAL DATA: K1 = 63.091; DELTA M = 20.0; DELTA ML = 120.0

NO.	A	PARAMETER	DELTA	ERROR	CONDITION	DESCRIPTION
1	1	5.83493E+02	2.000E-01	1.360E+02	9.072E+00	K1
2	1	9.56351E+00	2.000E-01	1.162E-01	2.437E+00	SHIFT Sn
3	1	1.28613E+01	1.000E+00	1.221E-01	6.260E+00	SHIFT Sn(L)

0RMS ERROR = 1.43E-01 MAX ERROR = 3.20E-01 AT OBS.NO. 4

RESIDUALS SQUARED = 3.29E-01

RFACTOR = 1.1271 PERCENT

Figure 2.76 Titration of receptor **L_{15}** with TBA-AcO in DMSO-d_6/0.5% H_2O

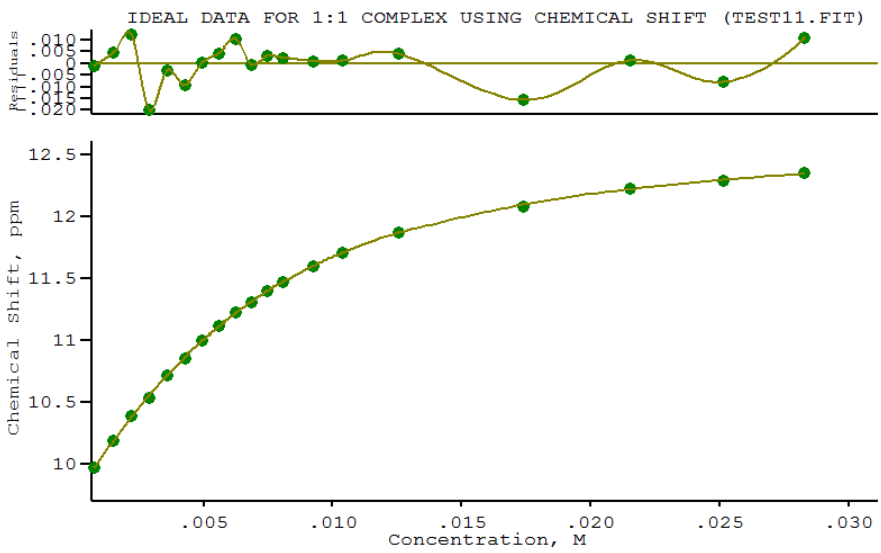

IDEAL DATA FOR 1:1 COMPLEX USING CHEMICAL SHIFT (TEST11.FIT)

Reaction: Sn + L = Sn(L)

FILE: TEST11.FIT (Measured shift is on 119Sn)

IDEAL DATA: K1 = 63.091; DELTA M = 20.0; DELTA ML = 120.0

NO.	A	PARAMETER	DELTA	ERROR	CONDITION	DESCRIPTION
1	1	3.01002E+02	2.000E-01	5.413E+00	1.482E+01	K1
2	1	9.73537E+00	2.000E-01	6.616E-03	3.027E+00	SHIFT Sn
3	1	1.27166E+01	1.000E+00	1.131E-02	9.942E+00	SHIFT Sn(L)

0RMS ERROR = 8.88E-03 MAX ERROR = 1.98E-02 AT OBS.NO. 4

RESIDUALS SQUARED = 1.26E-03

RFACTOR = 0.0721 PERCENT

Figure 2.77 Titration of receptor **L_{15}** with TBA-BzO in DMSO-d_6/0.5% H_2O

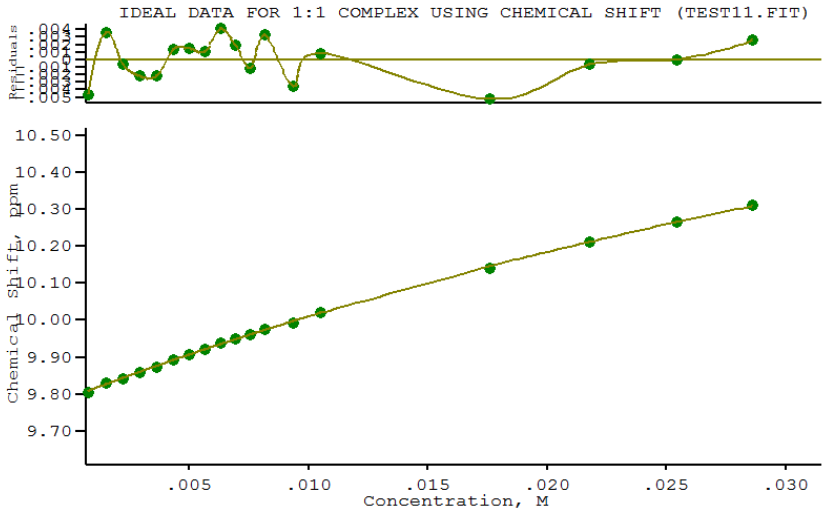

IDEAL DATA FOR 1:1 COMPLEX USING CHEMICAL SHIFT (TEST11.FIT)

Reaction: Sn + L = Sn(L)

FILE: TEST11.FIT (Measured shift is on 119Sn)

IDEAL DATA: K1 = 63.091; DELTA M = 20.0; DELTA ML = 120.0

NO.	A	PARAMETER	DELTA	ERROR	CONDITION	DESCRIPTION
1	1	1.40204E+01	2.000E-01	1.160E+00	4.829E+02	K1
2	1	9.79009E+00	2.000E-01	1.892E-03	6.047E+00	SHIFT Sn
3	1	1.16659E+01	1.000E+00	1.100E-01	4.209E+02	SHIFT Sn(L)

0RMS ERROR = 2.94E-03 MAX ERROR = 5.26E-03 AT OBS.NO. 15

RESIDUALS SQUARED = 1.30E-04

RFACTOR = 0.0269 PERCENT

Figure 2.78 Titration of receptor **L_{15}** with TBA-Cl in DMSO-d_6/0.5% H_2O

2.6.4 Crystallographic data

Table 2.3 Crystal data and structure refinement details of **L_1**

Empirical formula	$C_{13}H_{12}N_2O$
Formula weight	212.25
Crystal system	Orthorhombic
Space group	$Pca2_1$
Unit cell dimensions	a = 9.0641(3) Å α = 93.005(3)°
	b = 11.9420(5) Å β=92.645(3)°
	c = 11.7422(3) Å γ = 90°
Z	4
Crystal	Needles; Colourless
θ range for data collection	7.5240 – 77.9010°
Index ranges	$-11 \leq h \leq 10$, $-11 \leq k \leq 12$, $-14 \leq l \leq 14$
Reflections collected	2887
Independent reflections	1804 [R_{int} = 0.0187]
Completeness to θ = 67.13°	99.40%
Absorption correction	Multi-scan
Max. and min. transmission	1.00000 e 0.48845
Refinement method	Full-matrix least-squares on F^2
Data / restraints / parameters	1804/ 1/ 194
Goodness-of-fit on F^2	1.069
Final *R* indices [$F^2 > 2\sigma(F^2)$]	*R1* = 0.0350, *wR2* = 0.0903
***R* indices (all data)**	*R1* = 0.0352, *wR2* = 0.0907
Largest diff. peak and hole	0.182 and −0.170 e Å^{-3}

Equipment details: Single crystal X-ray diffractometer Rigaku Oxford Diffraction; XtaLAB Pro MM007 rotating anode source; PILATUS3 R 200K detector.

Table 2.4 Crystal data and structure refinement details of $\mathbf{L_{2\alpha}}$

Empirical formula	$C_{13}H_{10}Cl_2N_2O$
Formula weight	281.13
Crystal system	Triclinic
Space group	P_1
Unit cell dimensions	a = 4.6123(14) Å α = 93.005(3)°
	b = 11.9420(5) Å β = 92.645(3)°
	c = 22.8508(7) Å γ = 97.764(3)°
Z	4
Crystal	Prism; Colourless
Crystal size	0.7x0.01x0.01mm^3
θ range for data collection	1.6700 – 31.4990°
Index ranges	$-5 \leq h \leq 5$, $-15 \leq k \leq 15$, $-28 \leq l \leq 28$
Reflections collected	16939
Independent reflections	5202 [R_{int} = 0.0455]
Completeness to θ = 25.50°	98.94%
Absorption correction	Multi-scan
Max. and min. transmission	1.00000 and 0.54559
Refinement method	Full-matrix least-squares on F^2
Data / restraints / parameters	5202/ 0/ 325
Goodness-of-fit on F^2	1.162
Final *R* indices [$F^2 > 2\sigma(F^2)$]	*R1* = 0.0866, *wR2* = 0.2307
***R* indices (all data)**	*R1* = 0.0903, *wR2* = 0.2324
Largest diff. peak and hole	0.911 and -0.568 Å^{-3}

Equipment details: Single crystal X-ray diffractometer Diamond Light Source Beamline I19 EH1;synchrotron radiation λ = 0.6889 Å ;Crystal Logic 4-circle kappa goniometer; Rigaku Saturn 724+ CCD detector.

Table 2.5 Crystal data and structure refinement details of $L_{2\beta}$

Empirical formula	$C_{13}H_{10}Cl_2N_2O$
Formula weight	281.13
Crystal system	Triclinic
Space group	P_1
Unit cell dimensions	a = 4.5612(3) Å α = 103.972(7)°
	b = 11.5202(11) Å β = 94.249(5)°
	c = 12.1448(9) Å γ = 95.458(6)°
Z	4
Crystal	Discoid; Colourless
Crystal size	0.1684x0.1001x0.0113 mm^3
θ range for data collection	3.9540 – 73.5320°
Index ranges	$-5 \leq h \leq 5, -14 \leq k \leq 14, -15 \leq l \leq 10$
Reflections collected	4558
Independent reflections	2394 [R_{int} = 0.0412]
Completeness to θ = 66.97°	99.32%
Absorption correction	Gaussian
Max. and min. transmission	0.947 and 0.581
Refinement method	Full-matrix least-squares on F^2
Data / restraints / parameters	2394/ 0/ 163
Goodness-of-fit on F^2	1.141
Final *R* indices [$F^2 > 2\sigma(F^2)$]	*R1* = 0.0534, *wR2* = 0.1459
***R* indices (all data)**	*R1* = 0.0604, *wR2* = 0.1497
Largest diff. peak and hole	0.449 and -0.428 $Å^{-3}$

Equipment details: Single crystal X-ray diffractometer Rigaku Oxford Diffraction SuperNovaII diffractometer;Titan S2 CCD detector.

Table 2.6 Crystal data and structure refinement details of **L_5**

Empirical formula	$C_{13}H_9Cl_2N_3O_3$
Formula weight	326.13
Crystal system	Monoclinic
Space group	$P121/n_1$
Unit cell dimensions	a = 4.6027(7) Å α = 90°
	b = 48.5814(8) Å β = 95.7193(17)°
	c = 5.9207(14) Å γ = 90°
Z	4
Crystal	Prism; Colourless
Crystal size	0.186x0.096x0.023 mm^3
θ range for data collection	3.6660 – 79.4040°
Index ranges	$-5 \leq h \leq 5$, $-61 \leq k \leq 61$, $-7 \leq l \leq 6$
Reflections collected	53280
Independent reflections	2814 [R_{int} = 0.0497]
Completeness to θ = 66.97°	99.63%
Absorption correction	Analytical
Max. and min. transmission	0.901 and 0.505
Refinement method	Full-matrix least-squares on F^2
Data / restraints / parameters	2814/ 0/ 217
Goodness-of-fit on F^2	1.075
Final *R* indices [$F^2 > 2\sigma(F^2)$]	*R1* = 0.0690, *wR2* = 0.1522
***R* indices (all data)**	*R1* = 0.0702, *wR2* = 0.1525
Largest diff. peak and hole	1.113 and -0.539$Å^{-3}$

Equipment details: Single crystal X-ray diffractometer Rigaku Oxford Diffraction; XtaLAB Pro MM007 rotating anode source; PILATUS3 R 200K detector.

Table 2.7 Crystal data and structure refinement details of $\mathbf{L_{6\text{-}Bzo}}$

Empirical formula	C36 H51 I N4 O5
Formula weight	746.70
Crystal system	Monoclinic
Space group	P 121/n1
Unit cell dimensions	a = 8.87515(16)) Å α = 90°
	b = 22.2235(3) Å β = 92.2390(16)°
	c = 18.3822(3) Å γ = 90°
Z	4
Crystal	Block; yellow.
Crystal size	0.127x0.066x0.043 mm^3
θ range for data collection	3.9440 – 75.6100°
Index ranges	$-10 \leq h \leq 11$, $-17 \leq k \leq 27$, $-21 \leq l \leq 23$
Reflections collected	26957
Independent reflections	5574 [R_{int} = 0.0583]
Completeness to θ = 66.97°	99.94%
Absorption correction	Gaussian
Max. and min. transmission	0.766 and 0.542
Refinement method	Full-matrix least-squares on F^2
Data / restraints / parameters	5574/ 110/ 434
Goodness-of-fit on F^2	1.151
Final *R* indices [$F^2 > 2\sigma(F^2)$]	*R1* = 0.0405, *wR2* = 0.1088
***R* indices (all data)**	*R1* = 0.0420, *wR2* = 0.1107
Largest diff. peak and hole	0.798 and -1.271$Å^{-3}$

Equipment details: Single crystal X-ray diffractometer Rigaku Oxford Diffraction; XtaLAB Pro MM007 rotating anode source; PILATUS3 R 200K detector.

Table 2.8 Crystal data and structure refinement details of **L_8**

Empirical formula	$C_{13}H_9Cl_2N_3O_3$
Formula weight	326.13
Crystal system	Orthorombic
Space group	$Pna2_1$
Unit cell dimensions	a = 42.4563(6) Å α = 90°
	b = 6.5738(9) Å β = 90°
	c = 4.7887(11) Å γ = 90°
Z	4
Crystal	needles; pale yellow
θ range for data collection	4.1570 – 79.6120°
Index ranges	$-52 \leq h \leq 54$, $-8 \leq k \leq 8$, $-5 \leq l \leq 5$
Reflections collected	12318
Independent reflections	2458 [R_{int} = 0.0291]
Completeness to θ = 66.97°	99.80%
Absorption correction	Multi-scan
Max. and min. transmission	1.00000 and 0.74171
Refinement method	Full-matrix least-squares on F^2
Data / restraints / parameters	2458/ 1/ 191
Goodness-of-fit on F^2	1.064
Final *R* indices [$F^2 > 2\sigma(F^2)$]	*R1* = 0.0231, *wR2* = 0.0632
***R* indices (all data)**	*R1* = 0.0232, *wR2* = 0.0630
Largest diff. peak and hole	0.216 and -0.237 Å^{-3}

Equipment details: Single crystal X-ray diffractometer Rigaku Oxford Diffraction; XtaLAB Pro MM007 rotating anode source; PILATUS3 R 200K detector.

Table 2.9 Crystal data and structure refinement details of **$L_{8\text{-DMSO}}$**

Empirical formula	$C_{13}H_9Cl_2N_3O_3$
Formula weight	326.13
Crystal system	Triclinic
Space group	P_1
Unit cell dimensions	a = 12.0136(4) Å α = 65.778(3)°
	b = 12.6801(4) Å β = 72.336(3)°
	c = 13.8642(5) Å γ = 66.334(3)°
Z	2
Crystal	needles; pale yellow
θ range for data collection	4.0890 – 78.9190°
Index ranges	$-11 \leq h \leq 15$, $-16 \leq k \leq 16$, $-17 \leq l \leq 13$
Reflections collected	11444
Independent reflections	6031 [R_{int} = 0.0583]
Completeness to θ = 67.13°	85.42%
Absorption correction	Multi-scan
Max. and min. transmission	1.00000 and 0.74171
Refinement method	Full-matrix least-squares on F^2
Data / restraints / parameters	6031/ 0/ 456
Goodness-of-fit on F^2	1.114
Final *R* indices [$F^2 > 2\sigma(F^2)$]	*R1* = 0.0368, *wR2* = 0.1069
***R* indices (all data)**	*R1* = 0.0387, *wR2* = 0.1084
Largest diff. peak and hole	0.298 and -0.416 $Å^{-3}$

Equipment details: Single crystal X-ray diffractometer Rigaku Oxford Diffraction; XtaLAB Pro MM007 rotating anode source; PILATUS3 R 200K detector.

Table 2.10 Crystal data and structure refinement details of **$L_{11\text{-}DMF}$**

Empirical formula	$C_{15.68}\ H_{15.67}\ Cl_2\ N_{3.68}\ O_4\ S_{0.31}$
Formula weight	400.66
Crystal system	Monoclinic
Space group	$P12_{1/}n1$
Unit cell dimensions	a = 21.6216 (9) Å α = 90°
	b = 3.81142 (13) Å β = 115,885(5)°
	c = 22.9689(10) Å γ = 90°
Z	4
Crystal	needles; pale yellow
θ range for data collection	5.8120 – 75.3070°
Index ranges	$-26 \leq h \leq 23$, $-4 \leq k \leq 4$, $-28 \leq l \leq 23$
Reflections collected	34315
Independent reflections	7481[R_{int} = 0.0583]
Completeness to θ = 66.97°	99.58%
Absorption correction	Gaussian
Max. and min. transmission	0.838 and 0.388
Refinement method	Full-matrix least-squares on F^2
Data / restraints / parameters	3413/ 274/ 274
Goodness-of-fit on F^2	1.111
Final *R* indices [$F^2 > 2\sigma(F^2)$]	*R1* = 0.0498, *wR2* = 0.1445
***R* indices (all data)**	*R1* = 0.0523, *wR2* = 0.1476
Largest diff. peak and hole	0.410 and -0.518 $Å^{-3}$

Equipment details: Single crystal X-ray diffractometer Rigaku Oxford Diffraction SuperNovaII; Atlas S2 CCD detector.

Table 2.11 Crystal data and structure refinement details of **L_{14}**

Empirical formula	$C_{14}H_9Cl_2F_3N_2O$
Formula weight	349.13
Crystal system	Monoclinic
Space group	$P1c_1$
Unit cell dimensions	a = 11.4548(2) Å α = 90°
	b = 13.5410(2) Å β = 92.4156(16)°
	c = 9.02848(15) Å γ = 90°
Z	4
Crystal	needles; coluorness
Crystal size	0.444x0.0635x0.0262mm^3
θ range for data collection	3.862- 73.900°
Index ranges	$-14 \leq h \leq 14$, $-16 \leq k \leq 16$, $-11 \leq l \leq 11$
Reflections collected	27454
Independent reflections	5574 [R_{int} = 0.0583]
Completeness to θ = 66.97°	99.96%
Absorption correction	Gaussian
Max. and min. transmission	0.909 and 0.403
Refinement method	Full-matrix least-squares on F^2
Data / restraints / parameters	5574/ 74/ 425
Goodness-of-fit on F^2	1.027
Final *R* indices [$F^2 > 2\sigma(F^2)$]	*R1* = 0.0405, *wR2* = 0.1088
***R* indices (all data)**	*R1* = 0.0420, *wR2* = 0.1107
Largest diff. peak and hole	0.338 and -0.417 Å^{-3}

Equipment details: Single crystal X-ray diffractometer Rigaku Oxford Diffraction SuperNovaII; Atlas S2 CCD detector.

Table 2.12 Crystal data and structure refinement details of **L_{15}**

Empirical formula	$C_{14}H_{10}F_3IN_2O$
Formula weight	406.14
Crystal system	Orthorombic
Space group	P 2c -2ac
Unit cell dimensions	a = 29.971(5) Å α = 90°
	b = 4.5599(7) Å β = 90°
	c = 10.4038(14) Å γ = 90°
Z	4
Crystal	needles; coluorness
θ range for data collection	5.1770 - 72.4500°
Index ranges	$-36 \leq h \leq 36$, $-5 \leq k \leq 3$, $-12 \leq l \leq 11$
Reflections collected	5238
Independent reflections	2323 [R_{int} = 0.0719]
Completeness to θ = 66.97°	99.81%
Absorption correction	Gaussian
Max. and min. transmission	0.062 and 0.608
Refinement method	Full-matrix least-squares on F^2
Data / restraints / parameters	2323/ 229/ 219
Goodness-of-fit on F^2	1.102
Final *R* indices [$F^2 > 2\sigma(F^2)$]	*R1* = 0.0797, *wR2* = 0.2112
***R* indices (all data)**	*R1* = 0.0844, *wR2* = 0.2169
Largest diff. peak and hole	2.892 and -2.184 $Å^{-3}$

Equipment details: Single crystal X-ray diffractometer Rigaku Oxford Diffraction SuperNovaII;Titan S2 CCD detector.

References

1. Harris, K.; Atwood, J.; Steed, J., Encyclopedia of Supramolecular Chemistry. Atwood, JL, Steed, JW, Eds: 2004.

2. Jeffrey, G. A.; Jeffrey, G. A., *An introduction to hydrogen bonding*. Oxford university press New York: 1997; Vol. 12.

3. Atwood, J. L.; Steed, J. W., *Encyclopedia of supramolecular chemistry*. CRC Press: 2004; Vol. 1.

4. Chudzinski, M. G.; McClary, C. A.; Taylor, M. S., Anion receptors composed of hydrogen-and halogen-bond donor groups: modulating selectivity with combinations of distinct noncovalent interactions. *Journal of the American Chemical Society* **2011,** *133* (27), 10559-10567.

5. Clark, T.; Hennemann, M.; Murray, J. S.; Politzer, P., Halogen bonding: the σ-hole. *Journal of molecular modeling* **2007,** *13* (2), 291-296.

6. Erdelyi, M., Halogen bonding in solution. *Chemical Society Reviews* **2012,** *41* (9), 3547-3557.

7. Schulze, B.; Schubert, U. S., Beyond click chemistry–supramolecular interactions of 1, 2, 3-triazoles. *Chemical Society Reviews* **2014,** *43* (8), 2522-2571.

8. Chutia, R.; Das, G., Hydrogen and halogen bonding in a concerted act of anion recognition: F− induced atmospheric CO 2 uptake by an iodophenyl functionalized simple urea receptor. *Dalton Transactions* **2014,** *43* (41), 15628-15637.

9. Baggi, G.; Boiocchi, M.; Ciarrocchi, C.; Fabbrizzi, L., Enhancing the Anion Affinity of Urea-Based Receptors with a Ru (terpy) 22+ Chromophore. *Inorganic chemistry* **2013,** *52* (9), 5273-5283.

10. Etter, M. C.; Urbanczyk-Lipkowska, Z.; Zia-Ebrahimi, M.; Panunto, T. W., Hydrogen bond-directed cocrystallization and molecular recognition properties of diarylureas. *Journal of the American Chemical Society* **1990,** *112* (23), 8415-8426.

11. Kadam, S. A.; Martin, K.; Haav, K.; Toom, L.; Mayeux, C.; Pung, A.; Gale, P. A.; Hiscock, J. R.; Brooks, S. J.; Kirby, I. L., Towards the Discrimination of Carboxylates by Hydrogen-Bond Donor Anion Receptors. *Chemistry–A European Journal* **2015,** *21* (13), 5145-5160.

12. Kadam, S. A.; Haav, K.; Toom, L.; Haljasorg, T. i.; Leito, I., NMR Method for Simultaneous Host–Guest Binding Constant Measurement. *The Journal of organic chemistry* **2014,** *79* (6), 2501-2513.

13. Taouss, C.; Thomas, L.; Jones, P. G., Packing principles for urea and thiourea solvates: structures of urea: morpholine (1: 1), urea: 1, 4-dioxane (1: 1), thiourea: morpholine (4: 3) and thiourea: 1, 4-dioxane (4: 1). *CrystEngComm* **2013,** *15* (34), 6829-6836.

14. Olivari, M.; Montis, R.; Karagiannidis, L. E.; Horton, P. N.; Mapp, L. K.; Coles, S. J.; Light, M. E.; Gale, P. A.; Caltagirone, C., Anion complexation, transport and structural studies of a series of bis-methylurea compounds. *Dalton Transactions* **2015,** *44* (5), 2138-2149.

15. Hynes, M. J., EQNMR: a computer program for the calculation of stability constants from nuclear magnetic resonance chemical shift data. *Journal of the Chemical Society, Dalton Transactions* **1993,** (2), 311-312.

16. Ghosh, A.; Jose, D. A.; Das, A.; Ganguly, B., A density functional study towards substituent effects on anion sensing with urea receptors. *Journal of molecular modeling* **2010,** *16* (9), 1441-1448.

Chapter 3:

A new family of bis-urea receptors for the optical recognition of phosphates

3. A new family of bis-urea receptors or the optical recognition of phosphate

3.1 Introduction

Anion recognition is a fertile branch of Supramolecular Chemistry in constant development due the important key role of the anions species in lots of fields like biology, medicine and environment. [1,2,3,4,5]

In the anion recognition area, colorimetric and fluorescence sensor are widely involved because of their capacity to give a fast (naked eye for colorimetric sensor) response and their low cost, high performance in terms of sensitivity and good response time.

Among anions, phosphate species have received a remarkable attention due their involvement in biological system (central rule in DNA and RNA building, energy storage, gene regulations, muscle contraction, signal transduction and essential component of lipids membrane). [6,7]

Therefore, phosphates play a central rule also as constituents of medicinal drugs and fertilizers (high concentration of phosphate in water environment may cause the eutrophication of the aquatic system). [8]

For these reasons, a great effort has been put in the design of receptors for phosphate sensing. [9,10,11] Pyrophosphate, in particular, is a biological molecular target as the product of ATP hydrolysis under cellular conditions.[12] Pyrophosphate is particular important in different fields of biology and medicine. High concentration of pyrophosphate in synovial fluids is the cause of a rheumatologic disorder called CPDD (calcium pyrophosphate dehydrate disease). [13,14] Moreover, the concentration of pyrophosphate is connected with

the telomerase (a biomarker in cancer diagnosis) activity. [15] Because of its involvement in biological system and its importance, many different strategies

have been developed for designing chemosensors for Ppi including the use of charged receptors, [15,16] metal complexes, [17, 18, 19, 20, 21] or neutral receptors in particular urea or thiourea receptors. [22, 23, 24, 25, 26]

Recently, Caltagirone and co-workers have reported a new family of bis-ureas **74-79** able to recognize pyrophosphate anions with good response both through colorimetric and fluorescent evidences. [27]

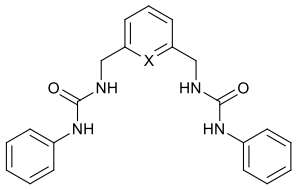

74 X= C
77 X= N

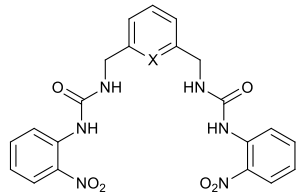

75 X= C
78 X= N

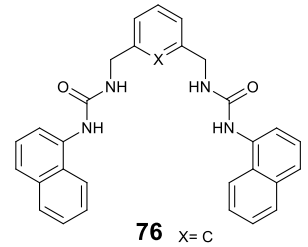

76 X= C
79 X= N

These receptors have the same central phenyl ring with different symmetrical arms decorated with napthyl, nitro and simple phenyl moieties.

The anion binding properties were performed by means of ^{1}H-NMR, UV-Visible and fluorescence spectroscopies. In particular, these receptors display a moderate-low affinity for all the anions studied (AcO^-, glutarate, malonate, BzO^-, $H_2PO_4^-$, $HPpi^{3-}$) except for **77** and **74-76** in respect of $H_2PO_4^-$ and $HPpi^{3-}$ respectively (Ka = 698 M^{-1} for the adduct **77**-$H_2PO_4^-$ and Ka = 5480 M^{-1} and Ka > 10^4 M^{-1} for the complex of $H_2PO_4^-$ with receptors **74** and **76** respectively).

The colorimetric sensors **75** and **78** contain two different nitrophenyl units that act as cromophore units. Receptor **75** shows in DMSO two absorption bands

centered at 277 and 380 nm respectively. Upon addition of increasing amount of hydrogen pyrophosphate the disappearance of the band at 277 nm and the decrease of the band at 380 nm with concomitant hypsochromic shift of 25 nm are observed (Figure 3.1 a). No significant change in the UV-Visible spectrum of receptor **75** were recorded with the other anions of the set studied. Sensor **78**, instead, shows a different behaviour. The free receptor has only one absorption band centered at 345 nm that involves in two different new bands at 284 and 490 nm upon the addition of the anion target (Figure 3.1b). This latter could be probably attributed with the deprotonation of the receptor.[28] For both the systems, the interaction with hydrogen pyrophosphate could be detected by naked eye with a colour change from yellow (free receptors in DMSO) to orange (receptors in presence of one equivalent of anion target).

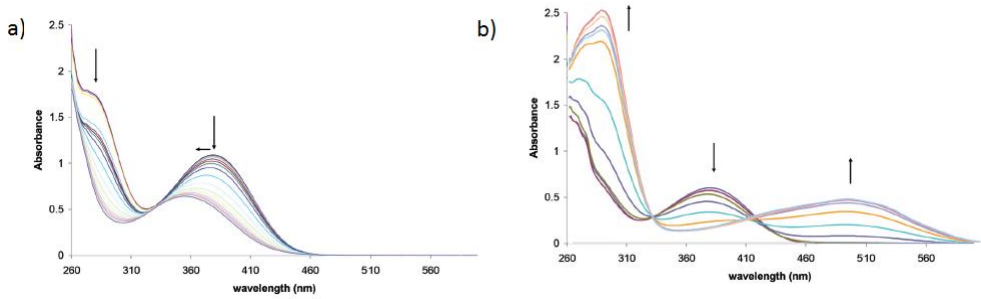

Figure 3.1 Changes in the UV-Visible spectra of **75** (a) (1.50 10^{-4} M) and **78** (b) (8.5 10^{-5} M) upon addition of increasing amounts of $(TBA)_3HPpi$ (2.5 10^{-2} M) in DMSO. All graphs are reported according to Ref.27.

Receptors **76** and **79** work as fluorescent sensor because of the presence of two naphtyl groups that act as fluorophore units. This time, the photophysical behaviour of both receptors in presence of the anion is very similar. The sensor **76** shows an emission band at 380 nm while sensor **79** at 375 nm (excitation at 345 nm for both receptors). Upon addition of $HPpi^{3-}$, a quenching of the free

receptor emission band following by the formation of a new band at 500 nm (band probably attributed to the intramolecular interaction in the excited state between the two aromatic moieties) is observed for both systems as showed in Figure 3.2.

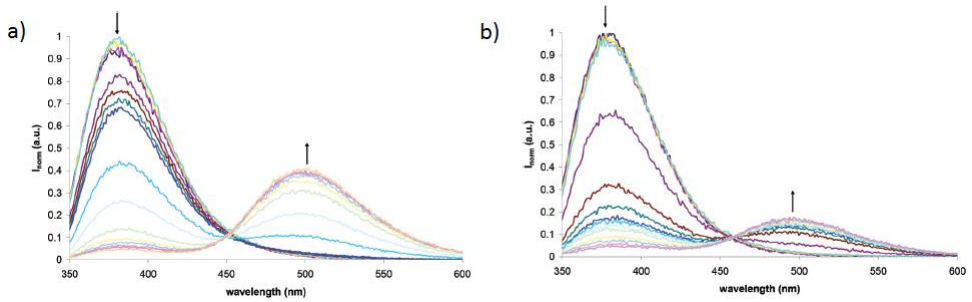

Figure 3.2 Changes in the fluorescence spectra of **74** (a) (1.50 10^{-4} M) and **77** (b) (8.5 10^{-5} M) upon addition of increasing amounts of $(TBA)_3HPpi$ (2.5 10^{-2} M) in DMSO. All graphs are reported according to Ref.27.

3.2 Fluorescent sensors

On the base of the anion sensors previously synthetized by our team reported in the introduction, we decided to design a similar family of indole based asymmetric bis-urea receptors **L_{16}-L_{18}** that can work as fluorescent sensors for hydrogen pyrophosphate anion due the presence of the naphtyl moiety as fluorophore unit. [29]

3.2.1. Synthesis

Receptors **L_{16}-L_{18}** were designed and successfully synthesized according to the Scheme 3.1. The synthesis is composed of two steps. The first is the formation of the indole urea starting from 7-aminoindole and 4-nitro-, 3-nitro-, or 2-nitro-phenyl isocyanate for **L_{16}**, **L_{17}**, and **L_{18}**, respectively. Then, upon reduction of the -NO_2 moiety into amine with Pd/C 10% in EtOH, the second urea function is

introduced on the phenyl ring by reaction with the 1-naphtyl isocyanate. The three receptors were obtained in yields over 80%.

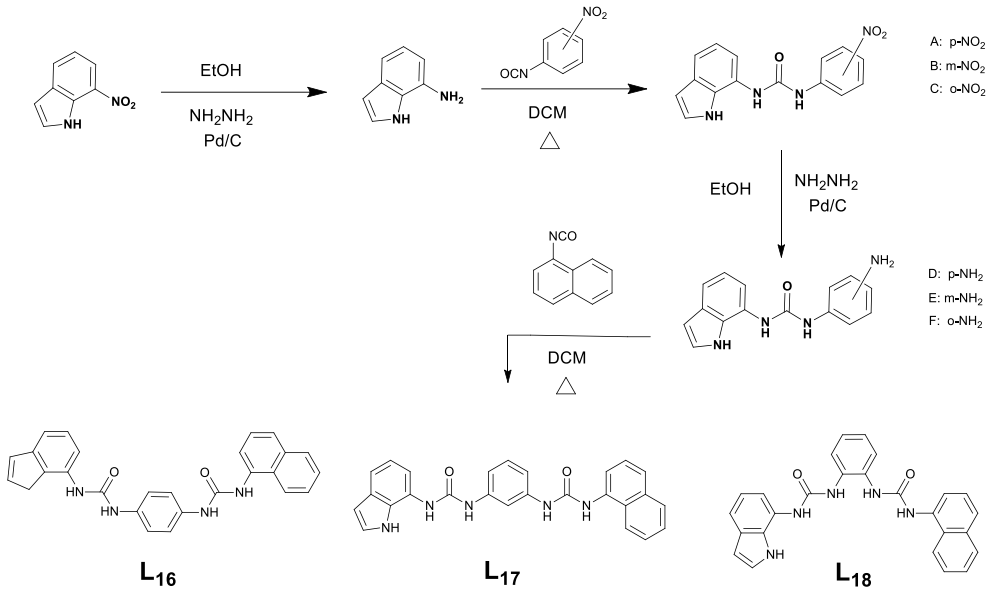

Scheme 3.1 Reaction scheme adopted for the synthesis of **L_{16}**, **L_{17}**, and **L_{18}**.

3.2.2. Solution studies

The anion binding properties of the receptors were investigated by means of ^{1}H-NMR, UV-Visible and fluorescence spectroscopies.

3.2.2.1 ^{1}H-NMR spectroscopy

In order to evaluate the anion binding capacity of the receptors, first ^{1}H-NMR titrations were carried out in DMSO-d_6. The EQNMR program [30] was used to calculate stability constants from the ^{1}H-NMR titration curves obtained fitting the data to a 1:1 binding model as shown in Table 3.1.

Table 3.1 Association constants (Ka/M^{-1}) for the equilibrium reactions of **L_{16}–L_{18}** with the tetrabutylammonium salts (tetraethyl in the case of hydrogencarbonate) of the anion considered in DMSO-d_6 at 300 K. The constants were calculated by following the shift of the indole NH. All errors estimated to be ≤15%

Receptor	F^-	AcO^-	HCO_3^-	$H_2PO_4^-$	$HPpi^{3-}$
L_{16}	Deprot. [a]	5830	3594	9190	n.d. [b]
L_{17}	Deprot. [a]	1252	1900	1911	n.d. [b]
L_{18}	Deprot. [a]	7430	n.d. [b]	$>10^4$	n.d. [b]

[a] The NH signals disappeared after the addition of one equivalent of anion. [b] No date but experimental evidence suggests strong interaction.

As shown in Table 3.1, fluoride causes deprotonation of the three receptors, while high and moderate high stability constants were observed in the case of acetate, dihydrogenphosphate, and hydrogencarbonate. It was impossible to calculate the association constant for the equilibrium of **L_{18}** with HCO_3^- because of the broadening of the signals attributed to the NHs. Also in the case of $HPpi^{3-}$ the broadening of the NHs proton signals was observed for all the three receptors but after the addition of 0.1 equivalents of the anion they disappeared. However, the peaks reappeared downfield shifted after the addition of an excess of anions (more than one equivalent), and this suggests strong interaction between this anion and the host molecules as showed in Figure 3.3. Due the broadening of the signals, any stability constant could be calculated.

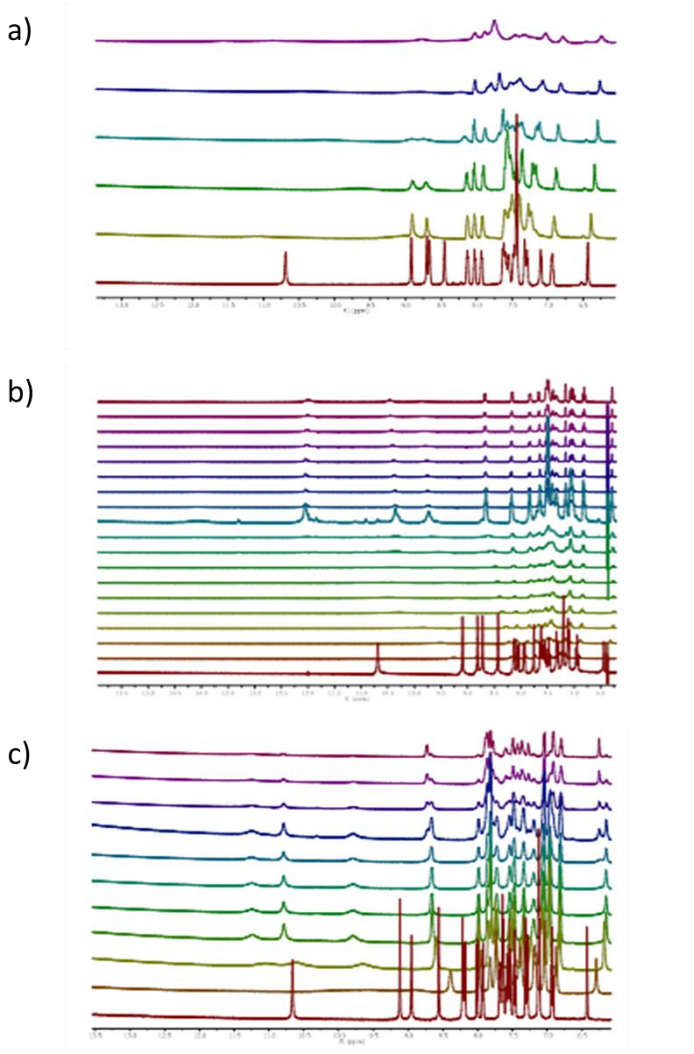

Figure 3.3 Stack plot of a DMSO-d_6 solution **L_{16}** (a), **L_{17}** (b) and **L_{18}** (c) (0.005 M) upon addition of $HPpi^{3-}$ (0.075 M).

Following the attribution of the proton signals of each receptors reported in Scheme 3.2 it is possible to speculate on different aspect of the coordination event.

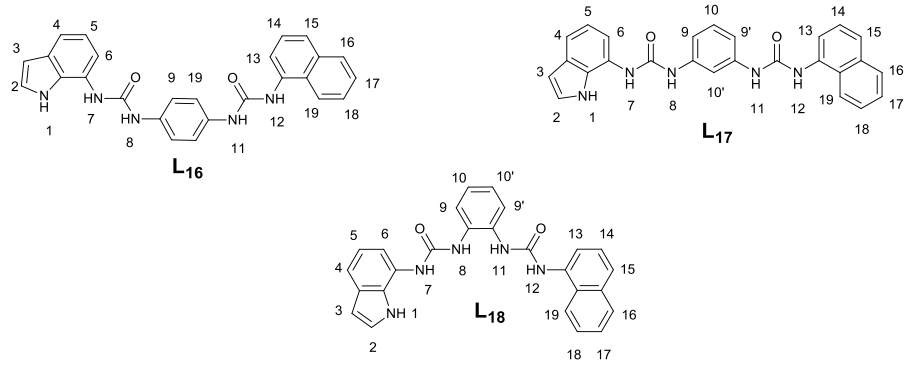

Scheme 3.2 Representation of receptors **L_{16}**, **L_{17}** and **L_{18}** with the numbering scheme adopted for discussion of the ^{1}H-NMR results.

First of all, as already previously observed for the receptors **c** and **f** (see above) , [27] also the doublet of the naphtalene fragment (CH19) adjacent to the urea NH12 is downfield shifted during the titration with this anion. This evidence can be explained assuming the active participation of this proton in the coordination event.

Analysing the changes in chemical shift of the NHs signals of each receptor with respect to the equivalents of the anion added, interesting trends can be pointed out.

As shown in Figure 3.4 in the case of $H_2PO_4^-$ (analogous observation can be made for the other anions) the three receptors show different behaviours. For **L_{16}** (Figure 3.4 a) and **L_{17}** (Figure 3.4 b) it is easy to recognize two different trends: the curves of three of the five NHs signals (attributed to NH1, NH7, and NH8) have the same neat inflection point, while for the other two (NH11 and NH12) the inflection point is less evident. [9]

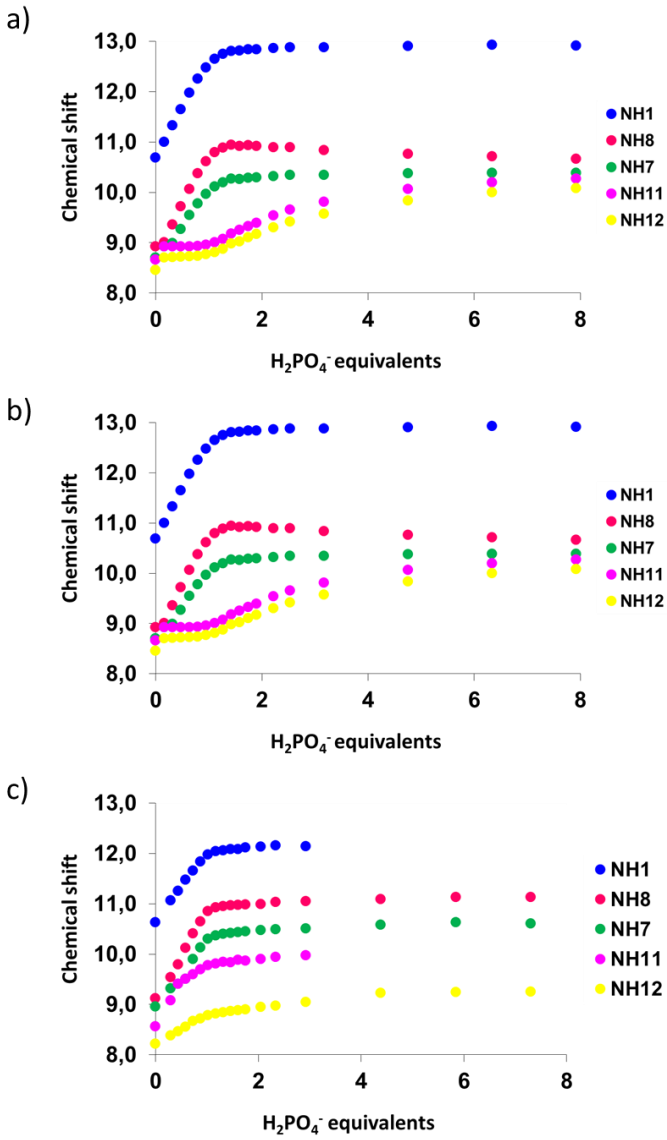

Figure 3.4 Changes of the ^{1}H-NMR shift for the NH protons upon addition of increasing amounts of $H_2PO_4^-$ to a DMSO-d_6 solution of **L$_{16}$** (a), **L$_{17}$** (b), and **L$_{18}$** (c).

The slope change of the curve for the protons NH1, NH7, and NH8 at 1:1 molar ratio anion/ligand is more evident for **L$_{16}$** than for **L$_{17}$**, while it is the opposite for

NH11 and NH12, probably because of the more open conformation of **L_{16}** with respect to **L_{17}** that eases the interaction with the indolic part of the molecule. On the other hand, in **L_{18}** the five NHs show a similar trend suggesting a cooperative behaviour towards anion binding. This evidence easily explains the higher stability constants calculated for **L_{18}** with respect to **L_{17}** and **L_{16}** at least for the CH_3COO^- and $H_2PO_4^-$. These results are in agreement with the designed pre-organization degree of the three receptors increasing in the order **L_{18}** > **L_{17}** > **L_{16}**.

3.2.2.2 UV-Visible and Fluorescence studies

The spectrophotometric and the spectrofluorimetric properties of **L_{16}-L_{18}** in DMSO were also investigated in order to evaluate the potential application of the three receptors as colorimetric and fluorescent sensor for anion recognition.

Receptor **L_{16}** shows two absorption bands at 270 nm (ε = 26000 M^{-1} cm^{-1}) and 304 nm (ε = 28600 M^{-1} cm^{-1}) and a shoulder at 330 nm (ε = 12400 M^{-1} cm^{-1}). Excitation at 330 nm leads to a weak emission centered at 483 nm ($\Phi = 8.7\ 10^{-3}$). Receptors **L_{17}** and **L_{18}** show an absorption band at 305 nm (27500 M^{-1} cm^{-1}) and 295 nm (ε = 29500 M^{-1} cm^{-1}) respectively, and a shoulder at 328 nm (ε =9900 M^{-1} cm^{-1} and 9500 M^{-1} cm^{-1} respectively). Upon excitation of a solution of **L_{17}** and **L_{18}** ($3.0\ 10^{-5}$ M) at 328 nm an emission band centered at 376 nm was observed for both the receptors ($\Phi = 9.1\ 10^{-2}$ and $2.6\ 10^{-2}$ respectively), attributed to the emission of the naphthalene fragment.

The absorption and emission spectra of the three ligands are reported in Figure 3.5.

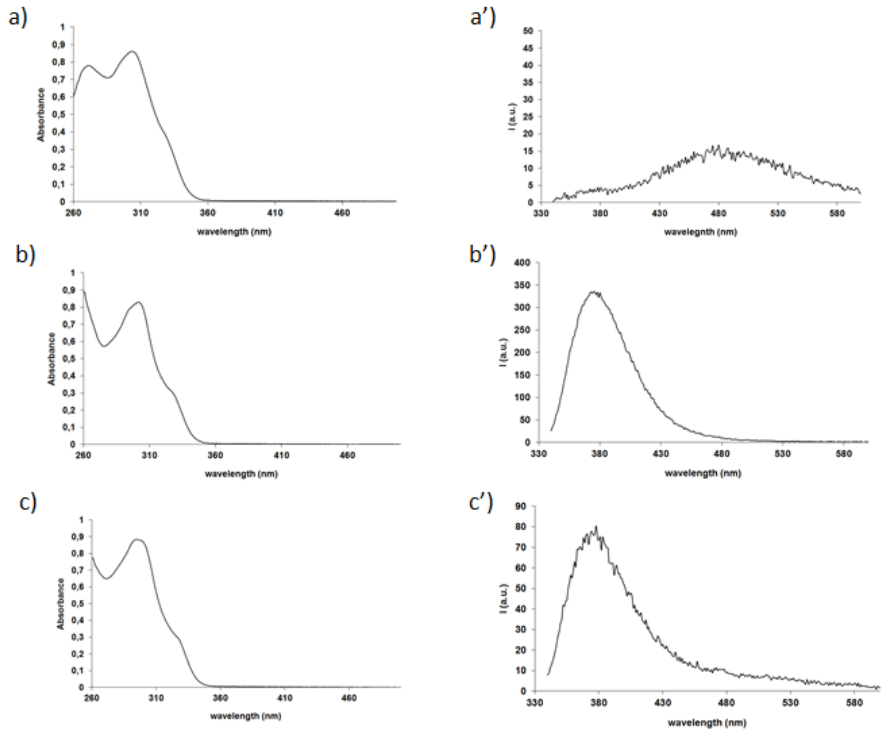

Figure 3.5 Absorption and Emission spectra of **L_{16}** (a and a'), **L_{17}** (b and b'), and **L_{18}** (c and c') in DMSO (3.0 10^{-5} M).

Addition of increasing amounts of the anions studied to a DMSO solution of every receptor did not cause any significant changes in the UV-Vis spectra of **L_{16}**, **L_{17}** and **L_{18}**, while differences in the emission behaviours were found for all the three receptors with the anions studied, in particular with hydrogenpyrophosphate.

The increase of the anions concentration in a solution of **L_{16}** caused a negligible change in the emission intensity of the free receptor except from the case of $HPpi^{3}$. Upon addition of increasing amount of this anion (up to 10 equivalents) we did not observed any changes in the fluorescence properties of the free ligand. Only when a large excess of anion was added, the interaction between

L_{16} and $HPpi^{3-}$ led to an interesting increasing in the intensity of the emission band centered at 483 nm as shown in Figure 3.6. The receptor was able to recognize $HPpi^{3-}$ in DMSO with a LOD = 2 10^{-5} M.

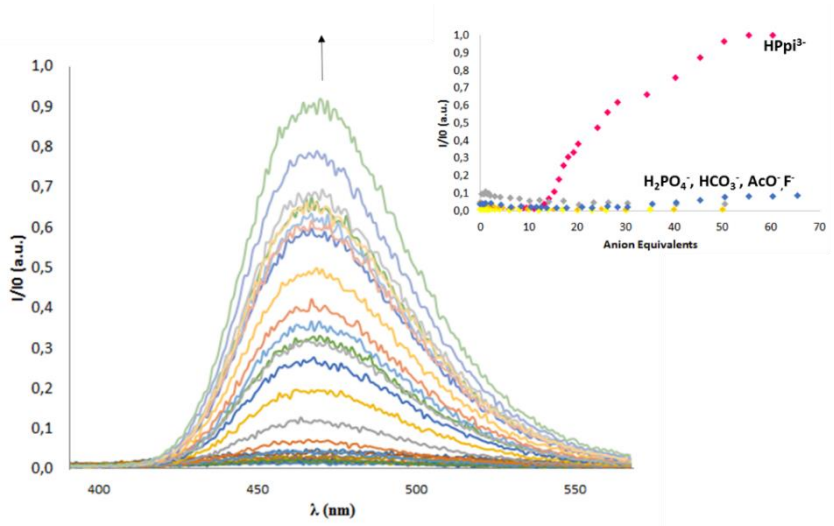

Figure 3.6 Changes in the fluorescence spectra of **L_{16}** (3.0 10^{-5} M) upon addition of increasing amounts of $HPpi^{3-}$ (2.5 10^{-2} M) in DMSO. Inset: Plot of I/I0 vs. anion equivalents at 476 nm.

The same selectivity to $HPpi^{3-}$ with respect to the other species investigated was also observed for receptors **L_{17}** and **L_{18}**. The quenching of the band at 376 nm was displayed for all the anion set studied but upon addition of hydrogenpyrophosphate the formation of a new emission band centered at 476 nm was observed for both receptors as reported in Figure 3.7. LOD concentration for $HPpi^{3-}$ in DMSO of 1.0 10^{-5}M and 2.0 10^{-5}M were calculated for **L_{17}** and **L_{18}** respectively.

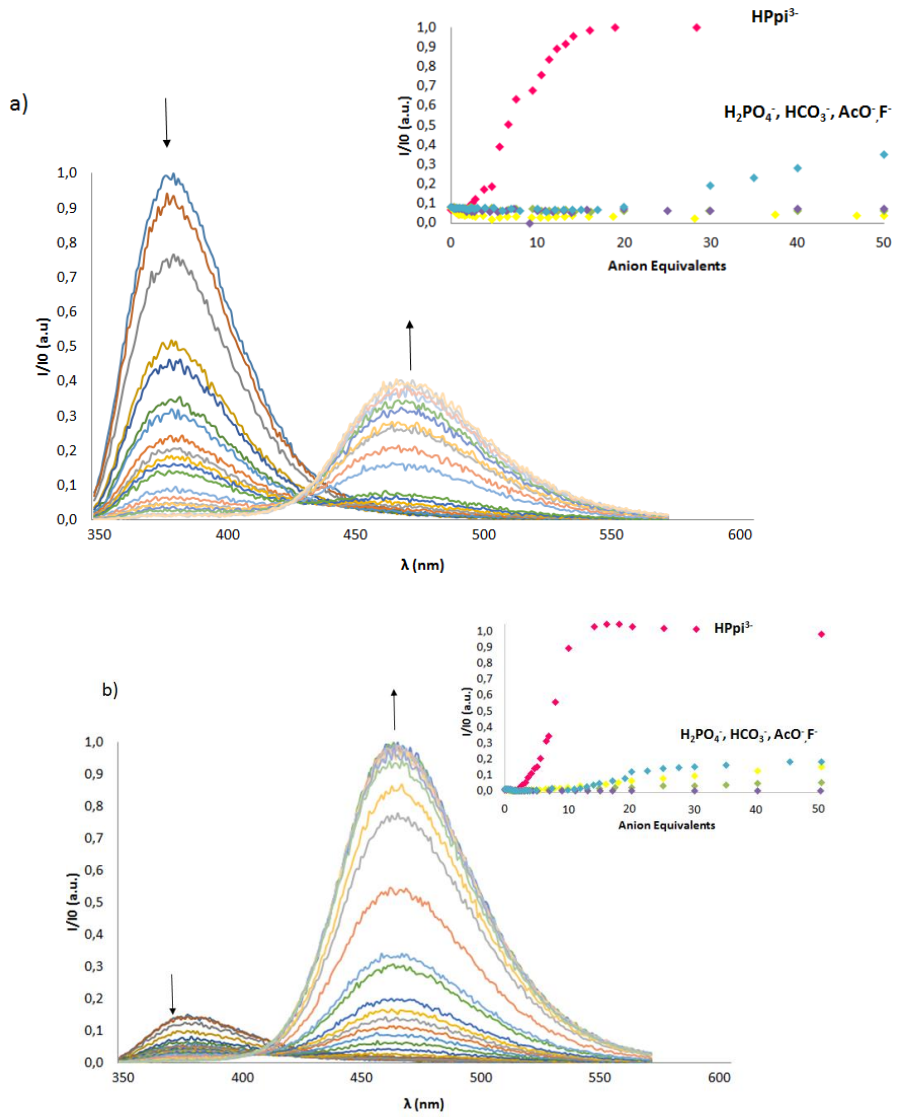

Figure 3.7 Changes in the fluorescence spectra of **L_{17}** (a) and **L_{18}** (b) ($3.0\ 10^{-5}$ M) upon addition of increasing amounts of $HPpi^{3-}$ ($2.5\ 10^{-2}$ M) in DMSO. Inset: Plot of I/I0 vs. anion equivalents at 476 nm for **L_{17}** (a) and **L_{18}** (b).

As it is possible to note also $H_2PO_4^-$ and F^- caused the formation of the new band at 476 nm (only F^-, in the case of **L_{17}**), but its intensity is negligible compared to that observed in the case of $HPpi^{3-}$ (Figure 3.8).

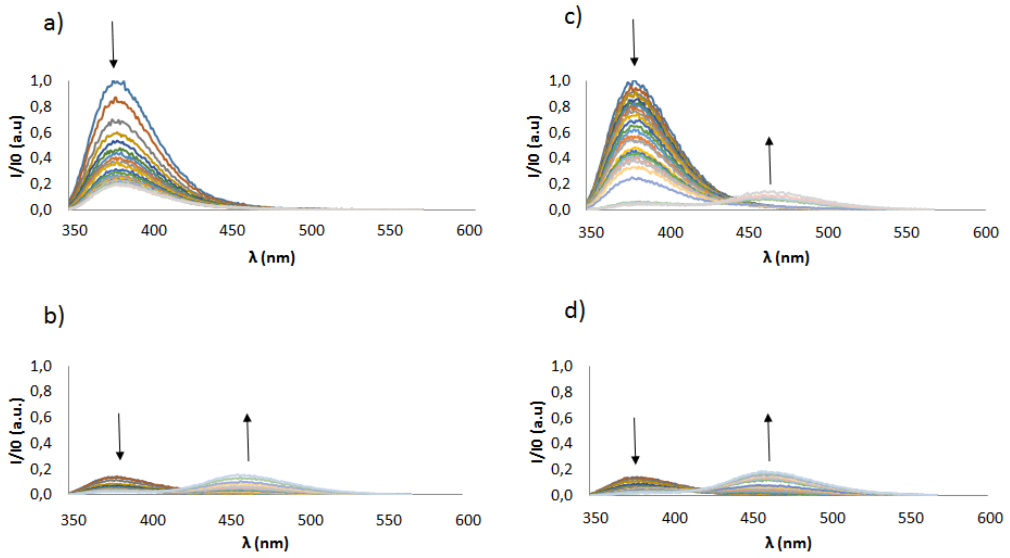

Figure 3.8 Changes in the fluorescence spectra of **L_{17}** and **L_{18}** ($3.0\ 10^{-5}$ M) upon addition of increasing amounts of $H_2PO_4^-$ (a and c respectively for **L_{17}** and **L_{18}**), and F^- (b and d respectively for **L_{17}** and **L_{18}**) in DMSO.

In order to evaluate the selectivity degree of the three receptor to $HPpi^{3-}$, competitivity studies were carried out in DMSO by adding to a solution of each receptor 20 equivalents of the anion target and 50 equivalents of all the other anions. As shown in Figure 3.9, the best response in terms of selectivity was achieved with receptor **L_{18}**.

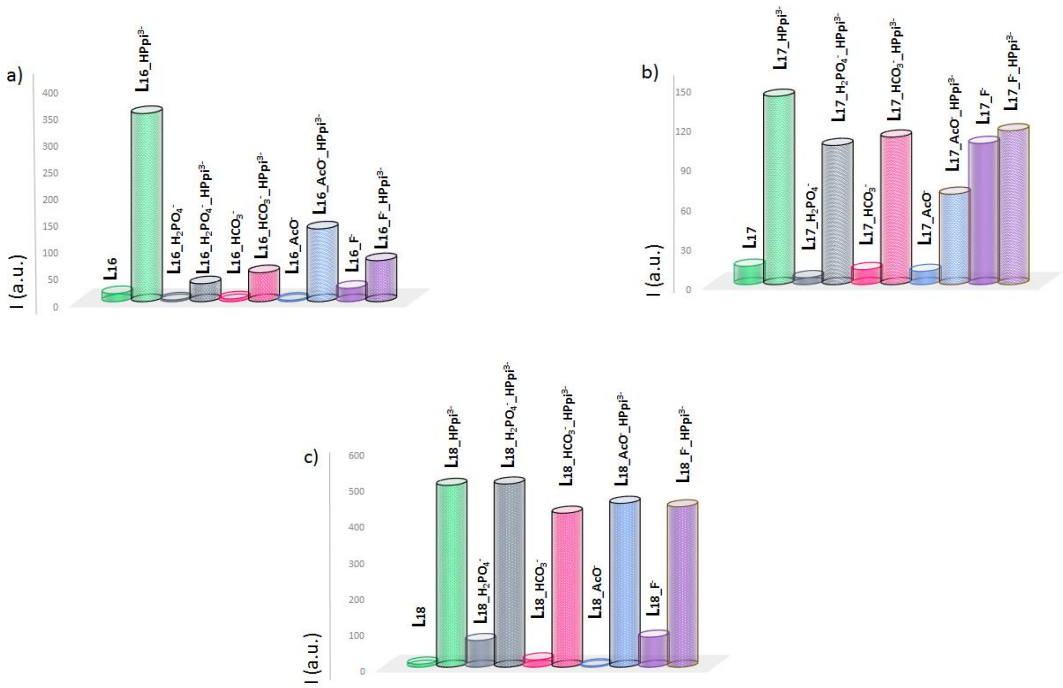

Figure 3.9 Anion competition study for **L16** (λ_{em} = 483 nm, λ_{exc} = 330 nm) (a), **L17** (λ_{em} = 476 nm, λ_{exc} = 330 nm) (b) and **L18** (λ_{em} = 483 nm, λ_{exc} = 330 nm) (c), [3.0 10^{-5} M] in the presence of 20 equivalents of $HPpi^{3-}$ and 50 equivalents of the other anions in DMSO.

Due the remarkable affinity of receptor **L18** for $HPpi^{3-}$, we decided to test its ability to sense the presence of this anionic target in pure water. As already reported by other authors chemosensors can be embedded in micellar or vesicular systems for the chromo- and fluorogenic sensing of chemical species in water. [31,32,33,34]

Although the receptor **L18** is highly insoluble in water, in the presence of a micellar solution of the cationic surfactant cetyltrimethylammonium bromide (CTAB) after ultrasonication (2 hours) we observed a complete solubilisation of **L18**, suggesting that the micelles act as carrier for the receptor molecules. Inside

the micelles **L_{18}** showed an absorption band at 292 nm (ε = 15000 $M^{-1}cm^{-1}$) with a shoulder at 326 nm (ε = 5000 $M^{-1}cm^{-1}$). When excited at 326 nm two emission bands were observed: one at 364 nm and another at 419 nm as shown in Figure 3.10.

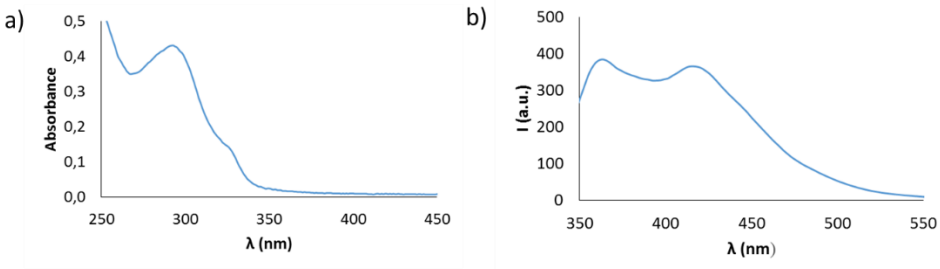

Figure 3.10 Absorption (a) and emission (b) spectra of **L_{18}** in CTAB micelles.

This latter emission band could be possibly ascribed to the formation of an intermolecular excimer as suggested by dilution studies. Decreasing the concentration of receptor **L_{18}** from 2.4 10^{-5} M to 1.2 10^{-6} M in water at pH 7 with 0.01 M CTAB in fact, the emission intensity of the band at 419 nm decreasing simultaneously as shown in Figure 3.11.

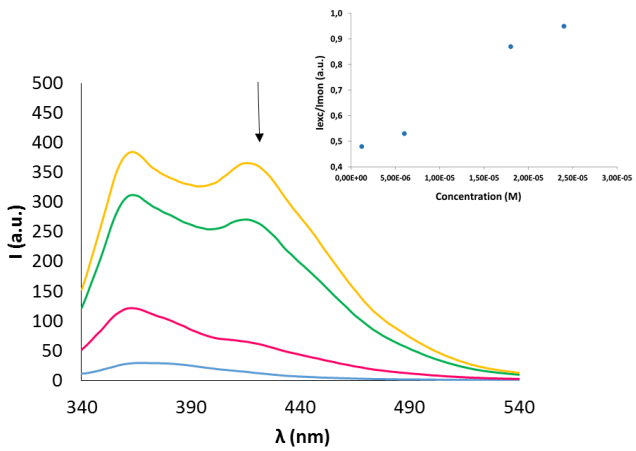

Figure 3.11 Emission spectra of **L_{18}** in water at pH 7 with 0.01 M CTAB at different concentrations. Inset: Plot of the Iexcimer/Imonomer vs concentration**.** The graph is reported according to Ref. 29.

Upon addition of increasing amounts of $HPpi^{3-}$ a partial quenching of the fluorescence was observed (Figure 3.12). This response was obtained only in presence of this anion with respect to the other anions tested (Figure 3.13).

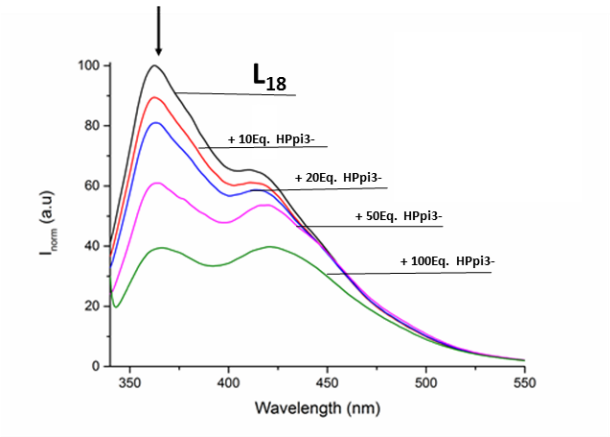

Figure 3.12 Changes in the emission spectra of **L_{18}** in water at pH 7 with 0.01 M CTAB upon addition of increasing amounts of $HPpi^{3-}$.

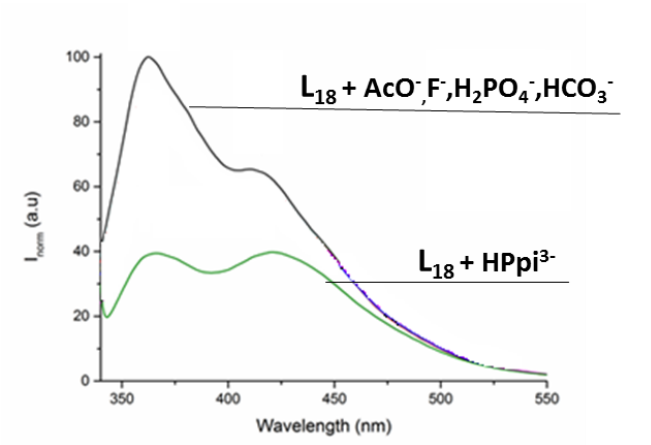

Figure 3.13 Changes in the fluorescence spectrum of **L_{18}** ($3.0\ 10^{-5}$ M) in water at pH 7 with 0.01 M CTAB in the presence of 50 equivalents of AcO^-, F^-, $H_2PO_4^-$, HCO_3^-, and $HPpi^{3-}$.

This result confirmed that the selectivity in terms of luminescence was maintained even in the micelles (LOD= $1.5\ 10^{-4}$ M), although in this case the response signal is surprisingly only a quenching of the fluorescence without the formation of a new emission band, as observed in DMSO. These experiments suggest that receptor **L_{18}** could be used to sense $HPpi^{3-}$ in a pure water environment.

3.2.2.3 Theoretical calculations

In order to confirm and better understand the interaction between the three receptors and $HPpi^{3-}$, theoretical calculation have been performed by means of an empirical forcefield method (AMBER3).[35] The molecular modeling investigations were performed in a 1 : 1 ligand-to-anion molar ratio evaluating the atomic partial charges at the PM3 semi-empirical level of theory [36, 37] and using an implicit simulation of the solvent environment (ε = 4R). The potential

energy surface of all the systems has been explored by means of simulated annealing (T = 600 K, equilibration time = 10 ps, run time = 10 ps and cooling time = 10 ps, time step = 1.0 fs). For each studied system, 80 conformations have been sampled.

The molecular modelling reported in Figure 3.14 show that for the systems with receptors **L_{20}** and **L_{21}**, the anion interacts via H-bonds with both arms of the ligands. This fact confirm the ^{1}H-NMR results previously discussed about the synergic action of the NHs protons for receptor **L_{21}** and the less marked difference in the two NMR trends for receptor **L_{20}** in respect of receptor **L_{19}** (see Figure 3.4). The indole and naphthalene fragments are brought in close proximity due the presence of the anion so they give π-stacking.

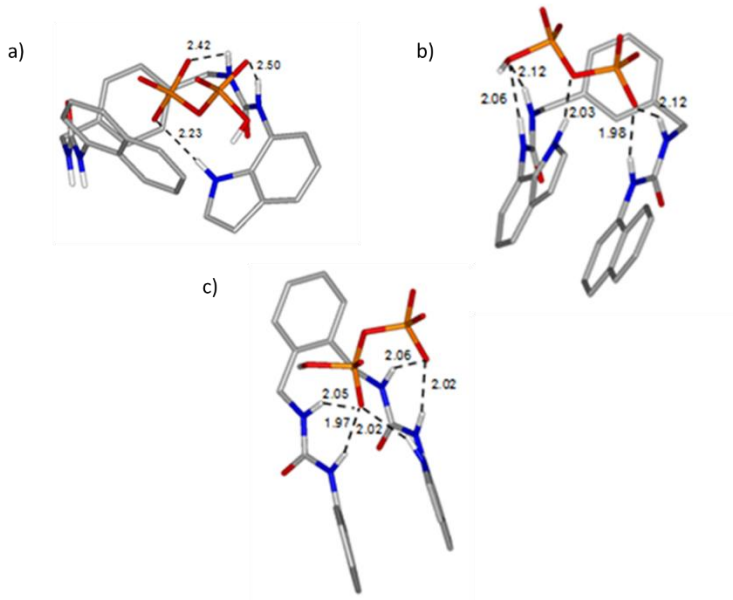

Figure 3.14 Calculated lowest energy conformers for **L_{19}** (a), **L_{20}** (b), and **L_{21}** (c) in their 1:1 adducts with $HPpi^{3-}$. The images are reported according to Ref. 29.

Due the open conformation of receptor **L_{19}**, theoretical calculation display that the anion interacts with only one of the two ureidic fragment (Fig) . The NHs protons involved in the coordination event are the NHs of the indole arm while no interaction are observed with the naphthalene moiety, thus preventing the formation of π-stacking interactions. Also in this case, the result is consistent with the two well different ^{1}H-NMR trends discussed in the previously section (see Figure 3.4 c).

Despite the absence of a more accurate simulation of the excited states for the three adducts, the results can be used to give some hints about the different spectrofluorimetric properties of our ligands. In particular, the results show that anion assisted intermolecular π-π interaction involving the naphtalene groups is more easily achieved by **L_{20}** and **L_{21}** than by **L_{19}**, and this would explain the observation of the new red-shifted fluorescence band only for the formers.

Most likely, the remarkably different binding mode found for **L_{20}** - **L_{21}** and receptor **L_{19}** could be connected to the different reciprocal position of the urea functions around the central phenyl ring.

3.2.3. Solid state studies

Despite many attempts to crystallize the adducts of the three receptors with phosphate anion guests, only in the case of **L_{17}** with $H_2PO_4^-$ and $HPpi^{3-}$ we were able to isolate samples suitable for single crystal X-ray diffraction (for more details see ESI). Crystals for both the adducts were obtained by slow diffusion of diethyl ether vapour into a $MeCN/MeNO_2$ (1:1 v/v) solution of **L_{17}** containing an excess of the TBA^+ salt of the appropriate anion.

(**L$_{17}$**)($H_2PO_4^-$)$_2$)(TBA)$_2$ crystallizes in the orthorhombic crystal system (space group: P*ca*2$_1$). The asymmetric unit of the adduct (Figure 3.15 a) contains two independent **L$_{17}$** receptor units and four independent $H_2PO_4^-$ anions balanced by four TBA^+ cations (Z' = 2) and one water molecule. The two independent receptor units adopt a planar conformation with the naphtalene and indole planes slightly tilted with respect the plane of the phenyl spacer (Figure 3.15 b).

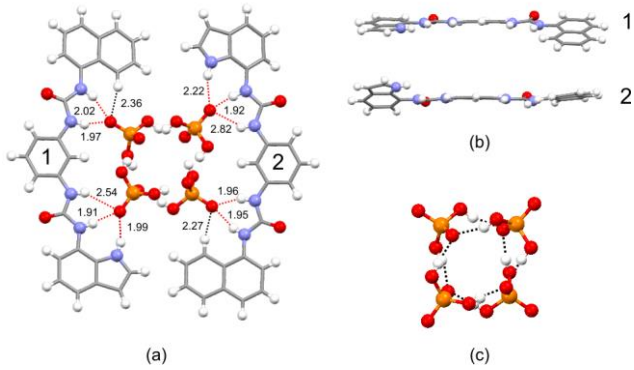

Figure 3.15 Asymmetric unit of (**L$_{17}$**)($H_2PO_4^-$)$_2$)(TBA)$_2$, tetrabuthylammonium (TBA^+) cations and disorder are omitted for clarity. (a) Main intermolecular interactions involved in the receptor-anion complex; (b) view of the conformations of the symmetrically independent receptor units; (c) tetrameric cluster of hydrogen bonded $H_2PO_4^-$ anions. N-H...O hydrogen bonds are indicated as red dashed lines, C-H...O interactions as black dashed lines. The two independent receptor units are indicated as 1 and 2 respectively. The D-H...A distances are all expressed in Å. The images are reported according to Ref. 29**.**

The structure shows a cyclic tetrameric molecular arrangement of $H_2PO_4^-$ anions (Figure 3.15 c), connected via a set of (P)O-H...O(P) hydrogen bonds (O...O distances lie in the range 2.60-2.64 Å). Although oligomeric $H_2PO_4^-$ anions aggregates are typically formed in solution at high concentrations, these are relatively rare in solid state, where infinite chains or more extended networks are very common. [38] [39] In particular, to the best of our knowledge, only four

hydrogen bonded $H_2PO_4^-$ tetrameric clusters with a similar geometry as in the adduct here described have been isolated so far. [40 41 42 43]

The cluster interacts with a H_2O molecule via two O-H...O hydrogen bonds (O...O distances lie in the range 2.80-3.00 Å) and is then surrounded by two symmetrically independent molecules of **L_{17}**, resulting in an overall 1:2 receptor/anion molar ratio in the adduct in the solid state (Figure 3.15). Only one of the two receptors exhibits a whole molecule disorder resulting in indole and naphthalene sides overlapping (55:45). It is interesting that the second unit has no significant disorder thus resulting in an overall preference for the indole sides to be opposite to each other rather than adjacent. It could also be that the partial water molecule influences which orientation of ligand exists. For each independent receptors the two anions are bonded on the two different sides of the molecule, the indole side and the naphtalene side.

On the indole side, the anion interacts via three N-H...O hydrogen bonds, one involving the indole NH (N...O distances are 2.832(5) Å for the independent molecule 1 and 3.034(13) Å for the independent molecule 2) and two involving the urea NHs (N...O distances are 2.787(4) Å and 3.305(5) Å for the independent molecule 1 and 2.758(4) Å and 3.075(6) Å for the independent molecule 2). On the naphtalene side the anion can only interact with the urea NHs via two N-H...O hydrogen bonds (N...O distances are 2.779(4) Å and 2.833(4) Å for the independent molecule 1 and 2.795(4) Å and 2.771(4) Å for the independent molecule 2), supported by a third C-H...O weak hydrogen bond (C...O distances are 3.285(5) Å for the independent molecule 1 and 3.265(8) Å for the independent molecule 2).

(**L_{17}**)(HPpi)$(TBA)_2$ crystallizes in the orthorombic crystal system (space group: P*ban*). The asymmetric unit contains just half of both **L_{17}** receptor units and,

surprisingly, an H_2Ppi^{2-} anion (Z' = 1/2). Both the **L_{17}** receptor unit and H_2Ppi^{2} anion show whole molecule disorder such that to suitably model them requires two complete independent moieties of both the **L_{17}** receptor unit and H_2Ppi^{2-} anion with all atoms are ¼ occupancy. Also in this adduct the two independent receptor units adopt a planar conformation. However, in this case, the naphtalene and indole planes show a major tilting with respect the plane of the phenyl spacer (Figure 3.16 b).

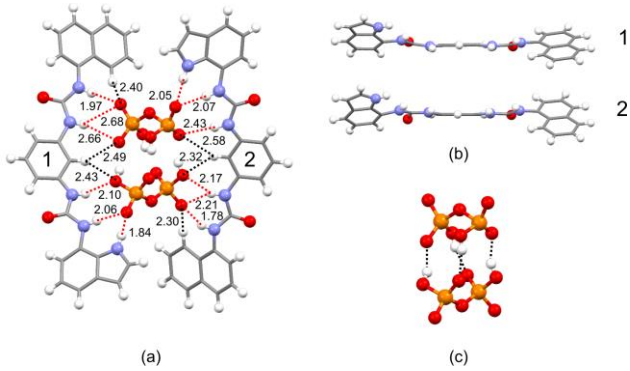

Figure 3.16 Asymmetric unit of (**L_{17}**)(H_2Ppi)$(TBA)_2$, tetrabuthylammonium (TBA^+) cations and disorder are omitted for clarity. (a) Main intermolecular interactions involved in the receptor-anion complex; (b) view of the conformations of the symetrically independent receptor units; (c) dimeric cluster of hydrogen bonded $HPpi^{3-}$ anions. N-H...O hydrogen bonds are indicated as red dashed lines, C-H...O interactions as black dashed lines. The two independent receptor units are indicated as 1 and 2 respectively. The D-H...A distances are all expressed in Å. The images are reported according to Ref. 29.

The two independent H_2Ppi^{2-} anions are connected with each other via four O-H...O hydrogen bonds with distances lying in the range 1.77-1.80 Å. This dimeric arrangement then interacts with the two independent receptors via a set of N-H...O and C-H...O interactions respectively involving both the ureidic and indolic

NHs and the phenyl and the naphthalene aromatic CHs, resulting in a 1:1 receptor/anion molar ratio in the adduct in the solid state (Figure 3.16 a).

Similarly to the previous structure, the anion interacts on the indole side via three N-H...O hydrogen bonds, two involving the urea NHs (N...O distances are 2.90(4) Å and 2.92(4) Å for the independent molecule 1 and 2.94(4) Å and 3.26(5) Å for the independent molecule 2) and one involving the indole NH (N...O distances are 2.66(3) Å for the independent molecule 1 and 2.89(4) Å for the independent molecule 2). On the other side of the molecule, due to the absence of any strong hydrogen bond donor in the naphtalene group, the anion only interacts with the two urea NHs (N...O distances are 3.42(4) Å and 3.42(3) Å for the independent molecule 1 and 2.53(4) Å and 2.99(5) Å for the independent molecule 2). This is also supported by a C-H...O weak hydrogen bond (C...O distances are 3.16(3) Å for the independent molecule 1 and 3.17(4) Å for the independent molecule 2) involving a naphtalene CH. Differently to the previous structure the central part of the molecule also contributes to the interaction with the anion (Figure 3.16 a), with the phenyl CH interacting with the two anions via short C-H...O interactions (C-H...O distances are in the range 2.30 - 2.60 Å).

The results obtained in the solid state are consistent with the conditions chosen for the crystallization experiments, in which the strong excess of anions used might favour stochiometries higher than 1:1 [44] and/or clusters formation. For the same reason the results are not completely in agreement with the observations made in solution studies (see above). These differences are particularly evident for $((\mathbf{L_{17}})(H_2PO_4^-)_2)(TBA)_2$ which is characterized by a 1:2 receptor/anion molar ratio. In this regard, it must be emphasized that generally the results obtained by solution studies might not always be consistent with those obtained in the solid state for many different reasons. The simplest explanation can be given considering that a molecule in solid state must satisfy a primary requirement

which consist of forming a periodic 3-D assembly and this might also involve changes at molecular level (e.g. adoption of a different conformation) [45] to ensure the development of the crystal packing along the three dimensions. From this point of view, the case of host-guest complexes (a multicomponent system) might even more complicate the matter, giving clusters formation or stoichiometry ratios different to those observed in solution. A different case is what observed for (**L_{17}**)(HPpi)$(TBA)_2$, in which a proton transfer on the $HPpi^{3-}$ moiety resulted in a structure containing H_2Ppi^{2-} anions. This might be due to presence of water in the solvent of crystallization .

3.3 Colorimetric sensors

Starting from the encouraging results obtained with receptor **L_{18}** in terms of affinity for hydrogenpyrophosphate and its selective recognition in pure water, we decided to synthetize the receptors **L_{19}-L_{21}**.

These bis-urea receptors have the same base skeleton of **L_{18}** but they have a nitro phenyl moiety instead of the naphthyl fragment in order to introduce in the system a cromophoric unit to obtain receptors that can be used as colorimetric sensors for $HPpi^{3-}$ species. The only structural difference between receptors **L_{19}-L_{21}** is the position of the NO_2^- group on the phenyl ring arm (*ortho* for **L_{19}**, *meta* for **L_{20}** and *para* for **L_{21}**) with the purpose to evaluate the role of the substitution position in the anion binding ability of the systems. Then, because of the good performance observed for **L_{21}**, we synthesized the analogue receptor **L_{22}** that presents an amino group in place of the nitro one with the aim of comparing the effects of an electron donor and an electron withdrawing group with respect to the anion binding ability of the receptor.

3.3.1 Synthesis

Receptors **L_{19}-L_{21}** were synthesized following the **Scheme 3.3**. The synthesis is very similar to that adopted for receptors **L_{16}-L_{18}** previously described. The base structure is obtained from reaction of 7-aminoindole and 2-nitro-phenyl isocyanate. Then, upon reduction of the -NO_2 moiety into amine with Pd/C 10% in EtOH, the second urea function is introduced on the phenyl ring by reaction with the 2-nitro-, 3-nitro-, or 4-nitro-phenyl isocyanate for **L_{19}**, **L_{20}**, and **L_{21}**, respectively. **L_{22}** is obtained, instead, for simple reduction of receptor **L_{21}** with Pd/C 10% in EtOH. Also in this case, all receptors are obtained in yields over 80%.

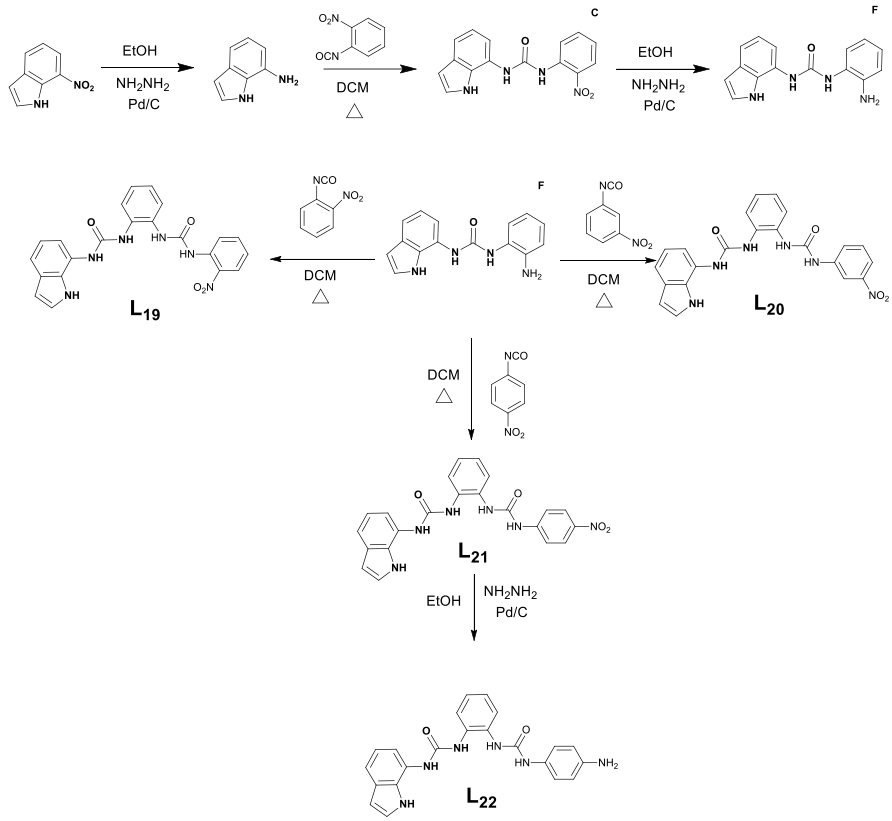

Scheme 3.3 Reaction scheme adopted for the synthesis of **L_{19}**, **L_{20}, L_{21}**, and **L_{22}**.

3.3.2 Solution studies

3.3.2.1 ^{1}H-NMR spectroscopy

In order to evaluate the anion binding capacity of the receptors, also in this case ^{1}H-NMR titrations were carried out in DMSO-*d*$_6$. Unfortunately, any stability constants could be calculated for the nitro-functionalised receptors **L_{19}-L_{21}** because of the broadening of the NHs proton signals upon the addition of the anion guests. Figure 3.17 shows the ^{1}H-NMR titrations for the nitro-receptors

with dihydrogenphosphate but the same trend can be found for the other anions.

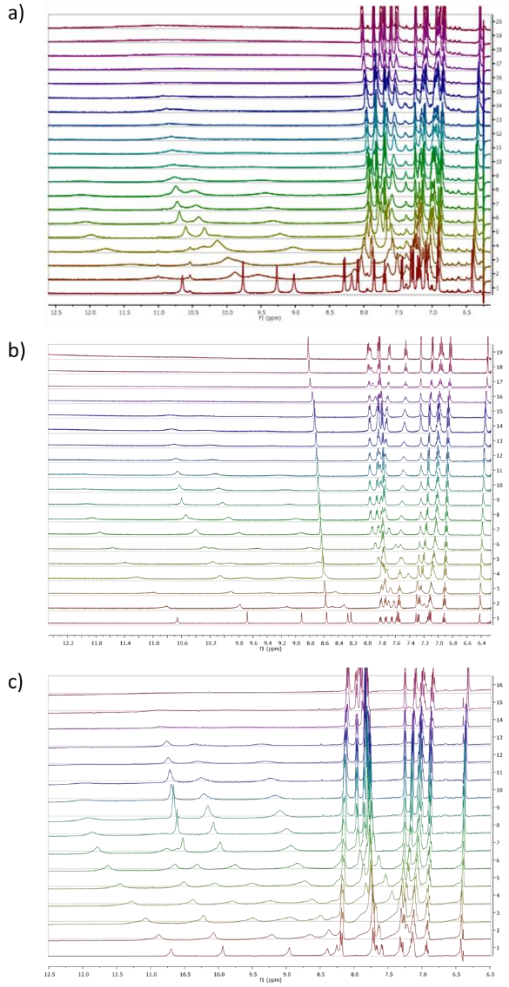

Figure 3.17 Stack plots of a DMSO-d_6 solutions of **L_{19}** (a), **L_{20}** (b) and **L_{21}** (c) (0.005 M) upon addition of $H_2PO_4^-$ (0.075 M).

However, the EQNMR program[30] was used to calculate stability constants from the ^{1}H-NMR titration curves obtained fitting the data to a 1:1 binding model for receptor **L_{22}**. The values are reported in Table 3.2.

Table 3.2 Association constants (K_a/M^{-1}) for the equilibrium reactions of **L_{22}** with the tetrabutylammonium salts (tetraethyl in the case of hydrogencarbonate) of the anion considered in DMSO-d_6 at 300 K. All errors estimated to be ≤18%.

Receptor	F^-	HCO_3^-	$H_2PO_4^-$	$HPpi^{3-}$
L_{22}	Deprot. [a]	$>10^4$	8544	n.d. [b]

[a] The NH signals disappeared after the addition of 1,5 equivalents of anion.
[b] Experimental evidence suggests strong interaction.

As it is possible to note in Figure 3.18 fluoride causes deprotonation of the receptor after 1,5 equivalents of the anion added (Figure 3.18a) while all the NHs protons signals remain visible until the titration end in the case of HCO_3^- guest (Figure 3.18b). The equilibrium of **L_{22}** with $H_2PO_4^-$, instead, shows a moderate high stability while, as reported in previous sections for receptors **L_{16}-L_{18}** , in the case of **L_{22}** with $HPpi^{3-}$ it was impossible determinate the stability constant due the broadening of the NHs protons signals even if this evidence, shown in Figure 3.18d , suggests a strong interaction with the receptor.

a)

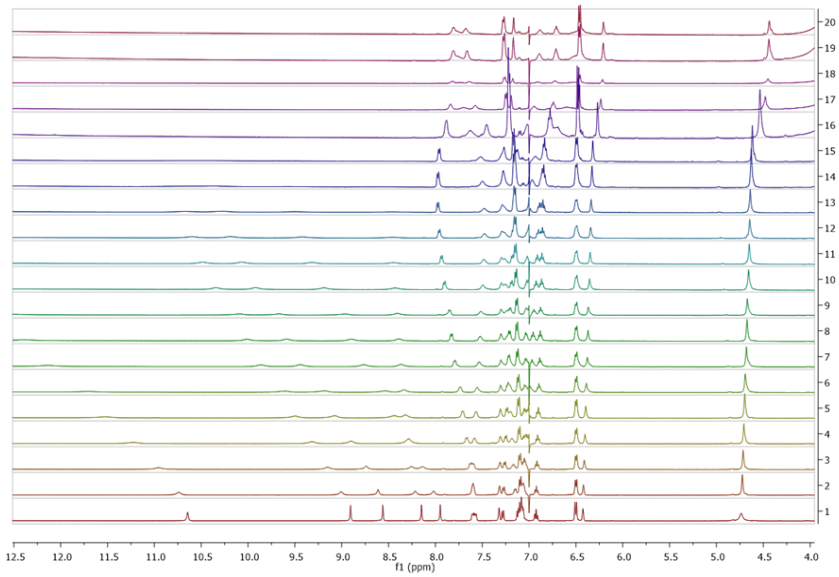
20
19
18
17
16
15
14
13
12
11
10
9
8
7
6
5
4
3
2
1
12.5 12.0 11.5 11.0 10.5 10.0 9.5 9.0 8.5 8.0 7.5 7.0 6.5 6.0 5.5 5.0 4.5 4.0
f1 (ppm)

b)

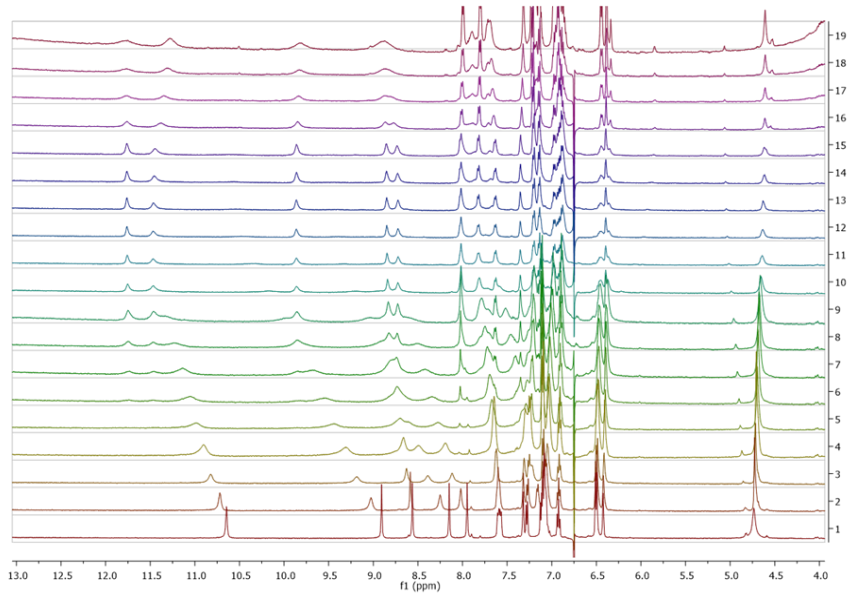
19
18
17
16
15
14
13
12
11
10
9
8
7
6
5
4
3
2
1
13.0 12.5 12.0 11.5 11.0 10.5 10.0 9.5 9.0 8.5 8.0 7.5 7.0 6.5 6.0 5.5 5.0 4.5 4.0
f1 (ppm)

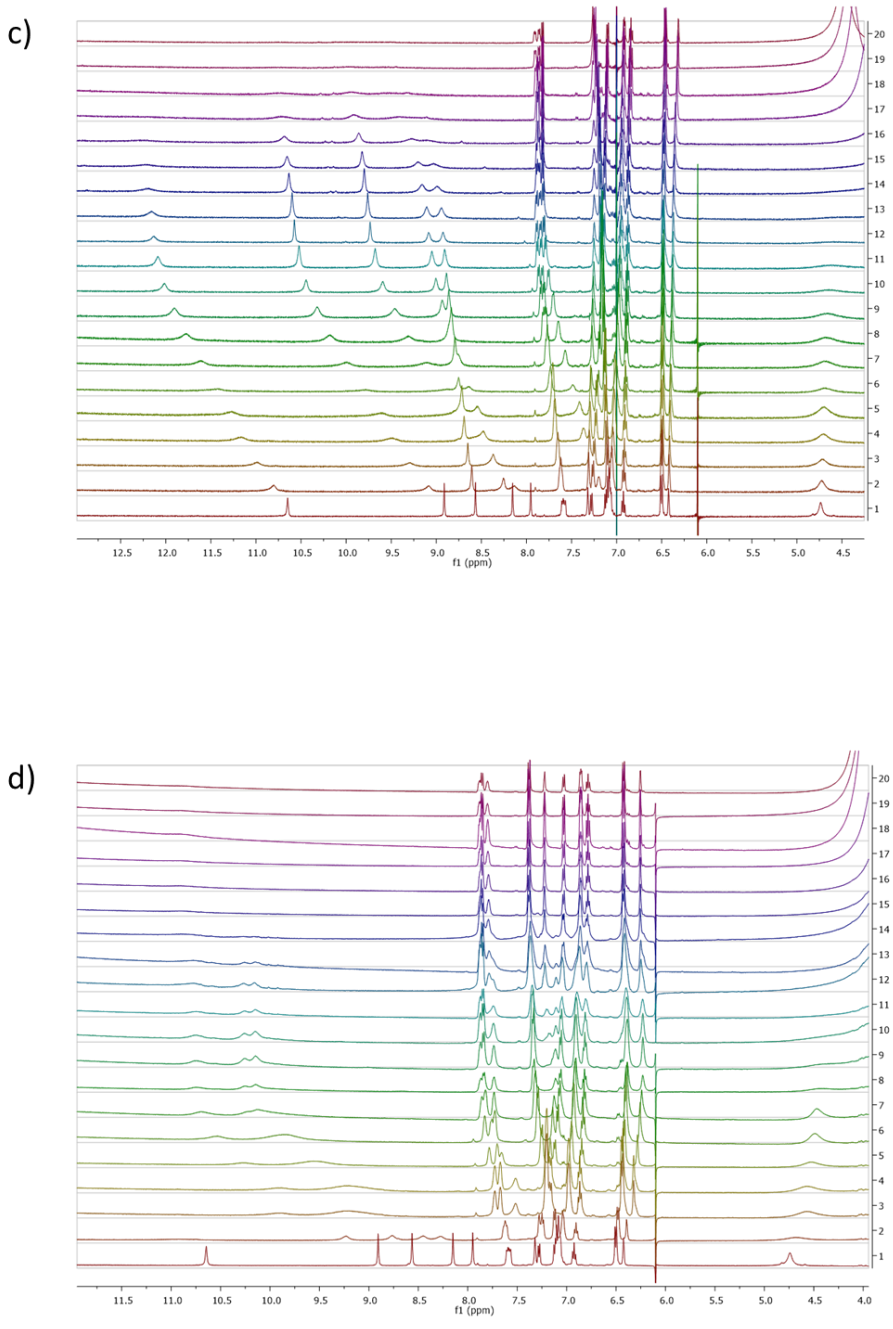

Figure 3.18 Stack plots of a DMSO-d_6 solution of **L_{22}** (0.005 M) upon addition of F^- (a), HCO_3^- (b), $H_2PO_4^-$ (c) and $HPpi^{3-}$(d) (0.075 M).

3.3.2.2 UV-Visible spectroscopy

The spectrophotometric properties of the receptors **L_{19}-L_{21}** were investigated in DMSO in order to verify whether the different nitro group dispositions on the phenyl ring could influence the photophysical properties of the receptors and their behaviour as colorimetric sensors.

Receptors **L_{19}**, **L_{20}** and **L_{21}** show an absorption band at 375 nm (ε = 3740 M^{-1} cm^{-1}), 350 nm (ε = 1330 M^{-1} cm^{-1}) and 354 nm (ε = 17433 M^{-1} cm^{-1}) respectively. Figure 3.19 shows the absorption spectra for each receptor.

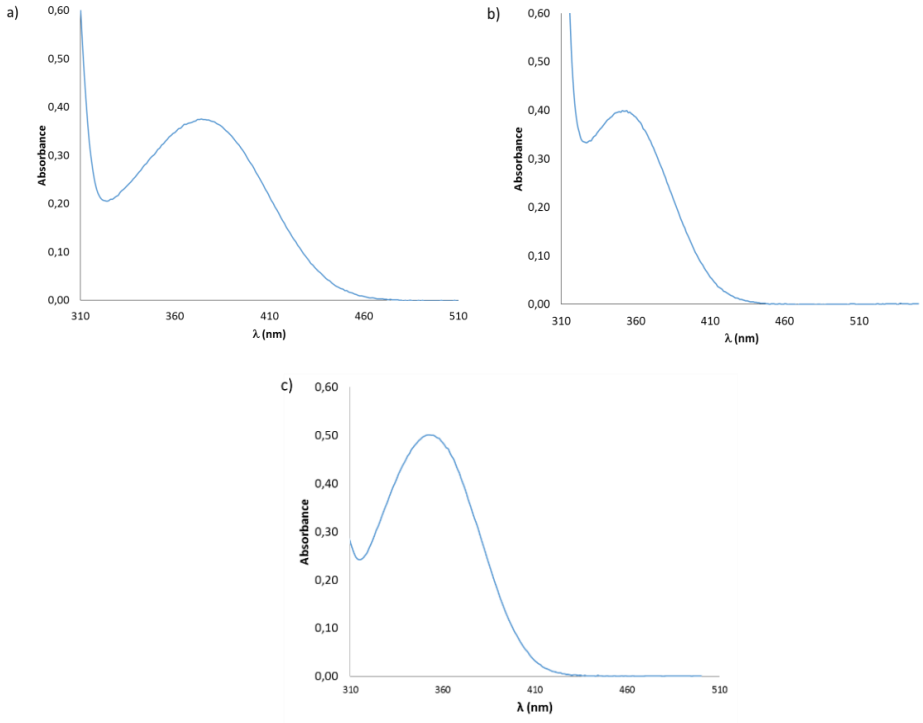

Figure 3.19 Absorption spectra of **L_{19}** (a), **L_{20}** (b) and **L_{21}** (c) in DMSO (1.0 10^{-4} M , 3.0 10^{-4} M and 3.0 10^{-5} M, respectively for **L_{19}**, **L_{20}** and **L_{21}**).

The anion binding ability of these ligands were studied by means of UV-Visible titrations with an anion set including $H_2PO_4^-$, HPp_i^{3-}, F^-, HCO_3^-, Mal^-, Glu^-, NO_3^-, CN^-, ClO_4^-, Cl^-, BzO^-, AMP, ADP and ATP. The result of this study suggested a good affinity of all the receptors for phosphate species (in particular for $HPpi^{3-}$) among the other anions under investigation and the best results were obtained for **L_{21}**.

Addition of increasing amounts of the anions studied for a DMSO solution of every receptor did not cause any significant changes in the UV-Vis spectra of **L_{19}**, **L_{20}** and **L_{21}** except in the cases of $H_2PO_4^-$, HPp_i^{3-}, F^-, HCO_3^- and ADP.

Increasing the concentration of dihydrogenphosphate and hydrogenpyrophosphate in a solution of **L_{19}** and to **L_{20}** in DMSO, a decrease in the absorption intensity of both receptors was observed (Figure 3.20).

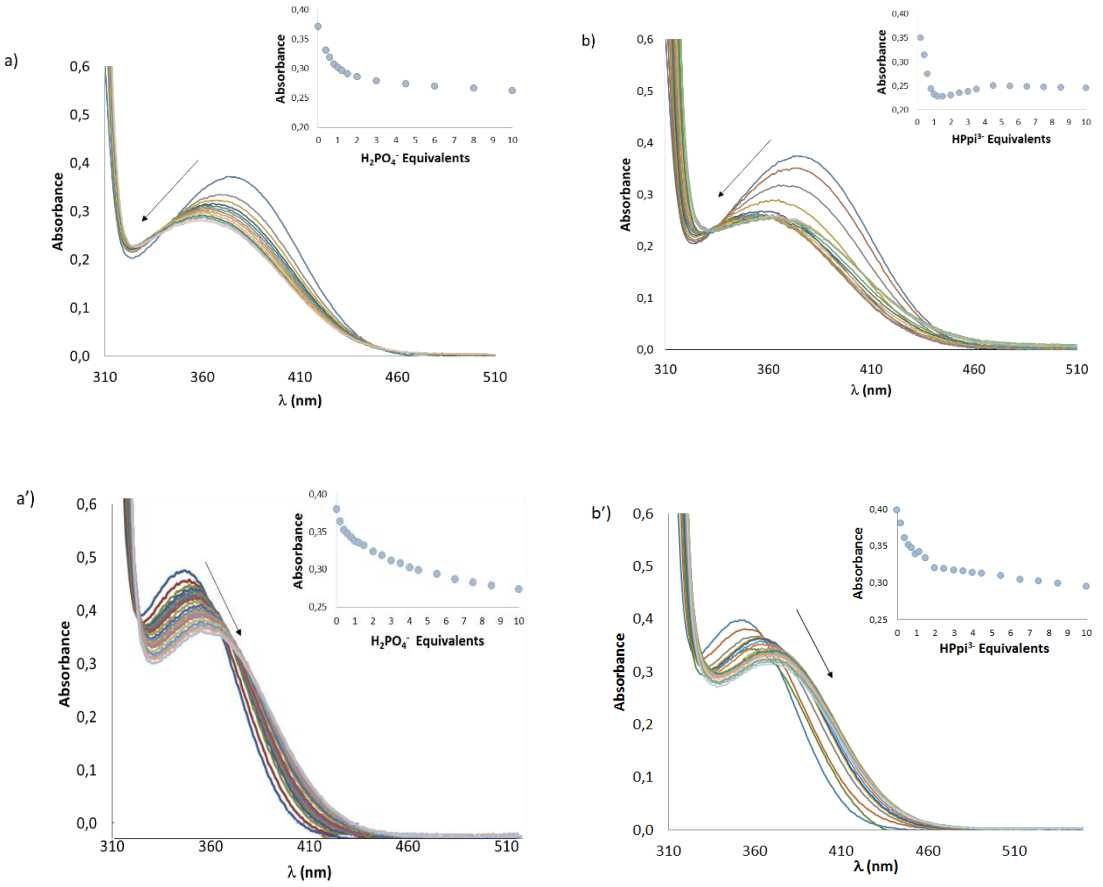

Figure 3.20 Changes in the UV-Visible spectra of **L_{19}** (a and b) and **L_{20}** (a' and b') ($1.0\ 10^{-4}$ M, $3.0\ 10^{-4}$ M for **L_{19}** and **L_{20}**, respectively) upon addition of increasing amounts of $H_2PO_4^-$ and $HPpi^{3-}$ ($2.5\ 10^{-2}$ M) in DMSO. Inset: Plot of Abs vs. anion equivalents at 375 nm and 350 nm for **L_{19}** and **L_{20}**, respectively.

These absorbance decreases are accompanied by a blue shift for **L_{19}** and a redshift for **L_{20}**. The same trend was observed also adding ADP species even if the reduction of the intensity of the free ligands absorption band was less remarkable with respect to the effect found for $H_2PO_4^-$ and HPp_i^{3-} as displayed in Figure 3.21.

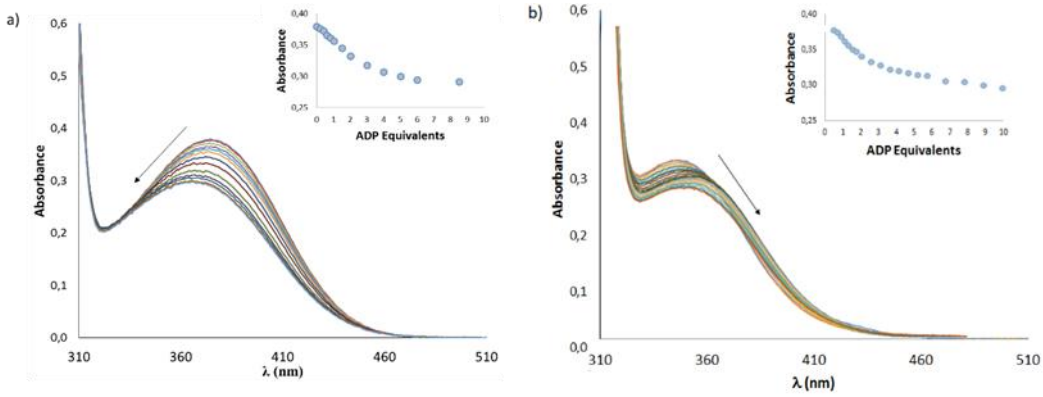

Figure 3.21 Changes in the UV-Visible spectra of **L_{19}** (a) and **L_{20}** (b) ($1.0\ 10^{-4}$ M, $3.0\ 10^{-4}$ M) upon addition of increasing amounts of ADP ($2.5\ 10^{-2}$ M) in DMSO. Inset: Plot of Abs vs. anion equivalents at 375 nm and 350 nm for **L_{19}** and **L_{20},** respectively.

Addition of hydrogencarbonate and fluoride to a **L_{19}** and **L_{20}** DMSO solution caused the decrease of the absorption intensity of the free receptors and the formation of a new band at 418 nm (ε = 4950 and 5270 $M^{-1}\ cm^{-1}$ for HCO_3^- and F^-, respectively) for receptor **L_{19}** and a shoulder at 500 nm (ε = 53 and 320 $M^{-1}\ cm^{-1}$ for HCO_3^- and F^-, respectively) for receptor **L_{20}** (Figure 3.22) that could probably be attributed to the formation of deprotonated species as confirmed by comparison with fluoride species.

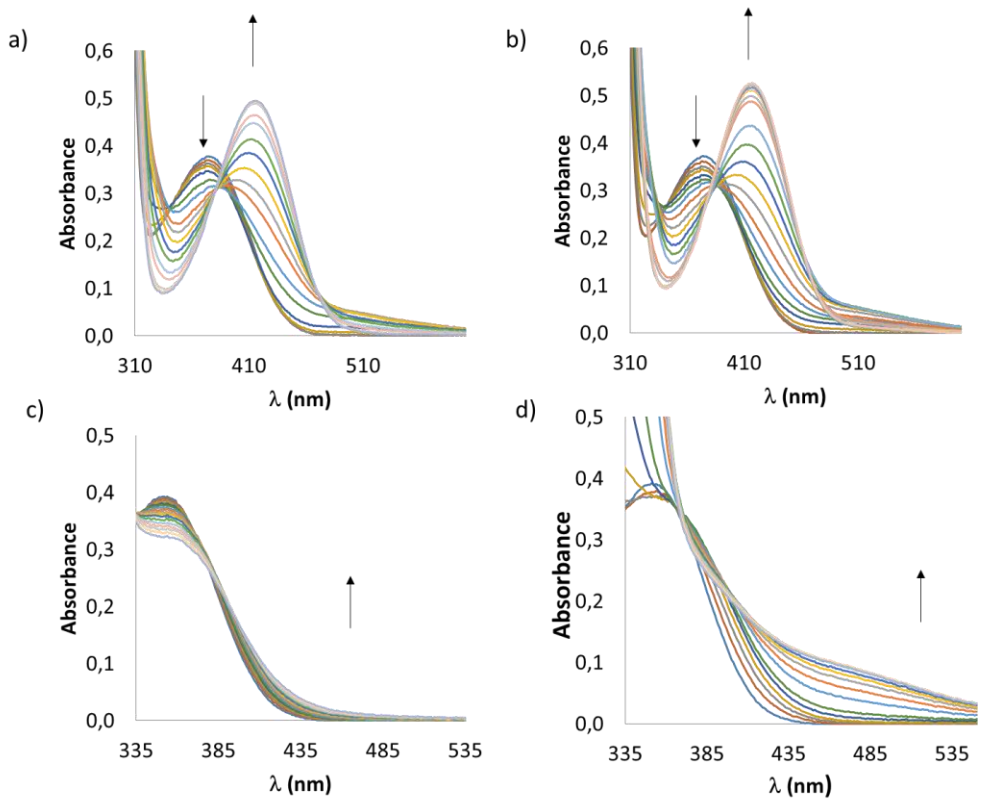

Figure 3.22 Changes in the UV-Visible spectra of **L_{19}** and **L_{20}** ($1.0\ 10^{-4}$ M and $3.0\ 10^{-4}$ M respectively) upon addition of increasing amounts of HCO_3^- (figures a and c for **L_{19}** and **L_{20}** respectively) and F^- (Figures b and d for **L_{19}** and **L_{20}**, respectively) ($2.5\ 10^{-2}$ M) in DMSO.

The interaction of **L_{19}** and **L_{20}** in DMSO with $H_2PO_4^-$, HPp_i^{3-}, $F^-$and HCO_3^- leads to a naked-eye chromatic change from yellow and light yellow solutions (for **L_{19}** and **L_{20}** respectively) to orange or intense yellow as indicated in Figure 3.23.

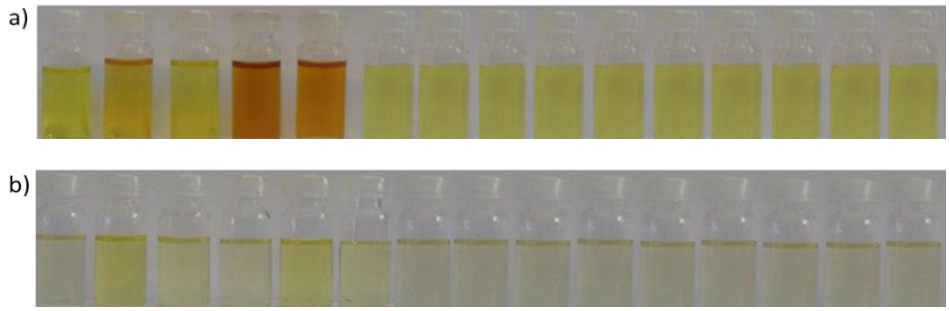

Figure 3.23 Colour change of **L_{19}** (a) and **L_{20}** (b) (both 0.01M) in DMSO upon addition of 1 equivalent of the correspondent tetrabutylammonium anion salt (tetraethyl in the case of HCO_3^-) (2.5 10^{-2}M). From left to right: receptor, $HPpi^{3-}$, $H_2PO_4^-$, F^-, HCO_3^-, ADP, AMP, ATP, Mal^-, Glu^-, NO_3^-, CN^-, ClO_4^-, Cl^- and BzO^-.

In the case of **L_{21}**, the interaction with dihydrogenphosphate led to a weak increase in the absorption intensity of the receptor and a redshift up to 1 equivalent of anion, but the increase of the concentration of this species resulted in a absorbance reduction as shown in Figure 3.24

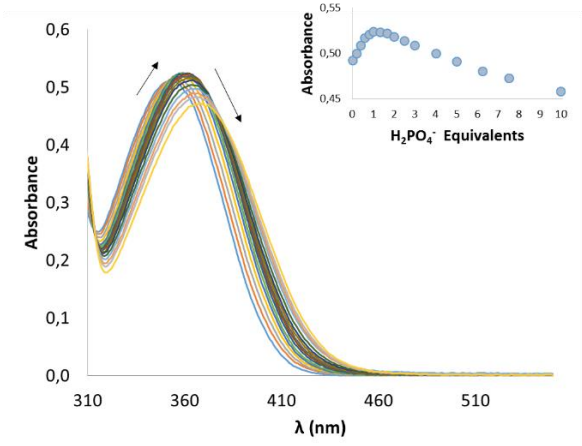

Figure 3.24 Changes in the UV-Visible spectra of **L_{21}** (3.0 10^{-5} M) upon addition of increasing amounts of $H_2PO_4^-$ (2.5 10^{-3} M) in DMSO. Inset: Plot of Abs vs. anion equivalents obtained following the absorption maximum.

Adding hydrogenpyrophosphate to the same receptor, the absorption spectra shows a new band red-shifted of 18 nm with respect to the free ligand absorption with an isosbestic point at 358 nm that remains stable up to 5 equivalents of anion added as reported in Figure 3.25.

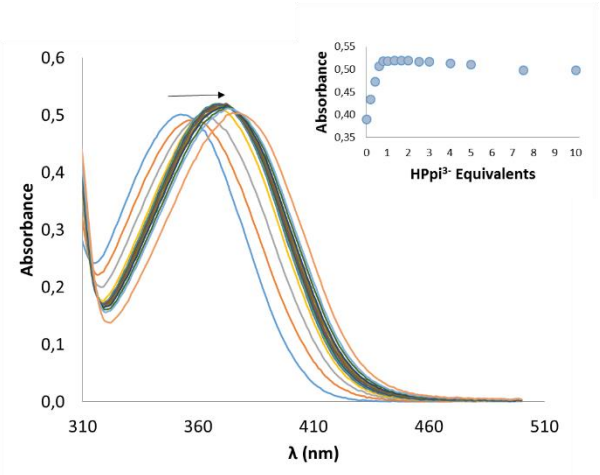

Figure 3.25 Changes in the UV-Visible spectra of $\mathbf{L_{21}}$ ($3.0\ 10^{-5}$ M) upon addition of increasing amounts of $HPpi^{3-}$ ($2.5\ 10^{-3}$ M) in DMSO. Inset: Plot of Abs vs. anion equivalents obtained following the absorption maximum.

Also in the case of ADP species, the interaction with $\mathbf{L_{21}}$ involved to the presence of a new band at 367 nm, 13 nm red-shifted with respect to the absorption of the free $\mathbf{L_{21}}$ (Figure 3.26).

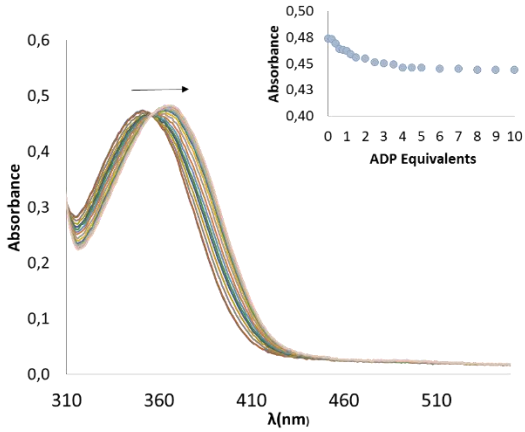

Figure 3.26 Changes in the UV-Visible spectra of **L_{21}** ($3.0\ 10^{-5}$ M) upon addition of increasing amounts of ADP ($2.5\ 10^{-3}$ M) in DMSO. Inset: Plot of Abs vs. anion equivalents obtained following the absorption maximum.

The interaction with hydrogencarbonate and fluoride to **L_{21}** led to the formation of a new band at 468 nm ($\varepsilon = 4200\ M^{-1}\ cm^{-1}$ and $\varepsilon = 1933\ M^{-1}\ cm^{-1}$ for HCO_3^- and F^- respectively) that can be attributed to the deprotonated species absorption (Figure 3.27).

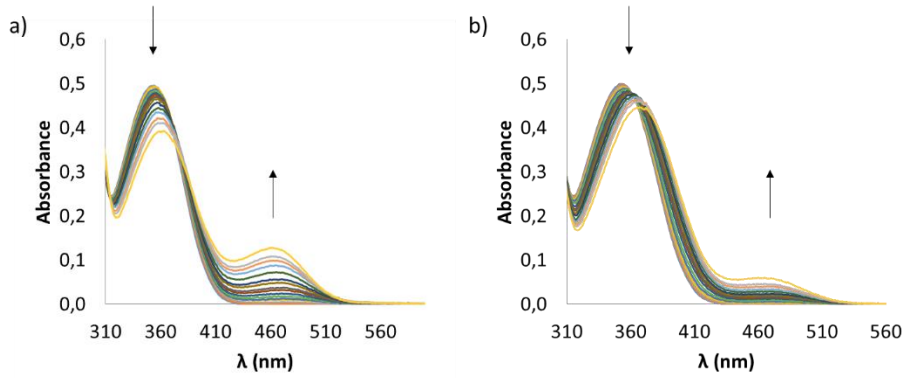

Figure 3.27 Changes in the UV-Visible spectra of **L_{21}** ($3.0\ 10^{-5}$ M) upon addition of increasing amounts of HCO_3^- (a) and F^- (b) ($2.5\ 10^{-2}$ M) in DMSO.

Also in this case, the complexation event involves to a naked-eye chromatic change of the receptor in presence of the anions as shown in Figure 3.28.

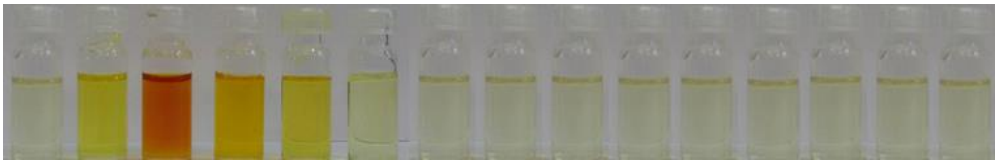

Figure 3.28 Colour change of **L_{21}** (0.01M) in DMSO upon addition of 1 equivalent of the correspondent tetrabutylammonium anion salt (tetraethyl in the case of HCO_3^-) ($2.5\ 10^{-2}$ M). From left to right: receptor, $H_2PO_4^-$, F^-, $HPpi^{3-}$, HCO_3^-, ADP, AMP, ATP, Mal^-, Glu^-, NO_3^-, CN^-, ClO_4^-, Cl^-, BzO^-.

In Table 3.3 all the LOD (Limit of detection) calculated for the recognition of $H_2PO_4^-$, HPp_i^{3-} and ADP in DMSO are reported.

Table 3.3 Limit of detection concentration (LOD) of receptors **L_{19}**, **L_{20}** and **L_{21}** for $H_2PO_4^-$, $HPpi^{3-}$ and ADP in DMSO.

Receptor	$H_2PO_4^-$	$HPpi^{3-}$	ADP
L_{19}	$2.0\ 10^{-4}$ M	$2.0\ 10^{-4}$ M	$4.1\ 10^{-5}$ M
L_{20}	$6.0\ 10^{-5}$ M	$6.0\ 10^{-5}$ M	$2.2\ 10^{-5}$ M
L_{21}	$6.0\ 10^{-6}$ M	$6.0\ 10^{-6}$ M	$6.0\ 10^{-6}$ M

The best selectivity towards the phosphate species observed for **L_{21}** with respect to receptors **L_{19}** and **L_{20}** can be probably explained focusing on the position of the nitro group in the phenyl ring.

Receptors **L_{19}** and **L_{21}** present the nitro group in *ortho* and *para* positions respectively. Considering the presence of an electron withdrawing group in these positions, we can hypothesize a higher acidity of the NH ureidic protons

compared to the corresponding ones in receptor **L_{20}** and, as a consequence, a higher capacity to interact with the anion species by hydrogen bond. Instead, among receptors **L_{19}** and **L_{21}** steric impediment considerations can be taken into account to explain the best response of **L_{21}**. The presence of the nitro group in the *ortho* position of the phenyl ring may obstruct the access of the anion in the pseudo-coordination cavity of the receptor while the open conformation of receptor **L_{21}**, may facilitate the coordination event.

Due the interesting results obtained, we decided to evaluate the capacity of **L_{21}** to recognize in a selective way phosphate species also in more competitive media. Following the experiment previously described for receptor **L_{18}**,[29] also **L_{21}** was embedded into CTAB micelles and UV-Visible titrations were carried out in pure water. The receptor inside the micelles shows an absorption band at 345 nm in pure water at pH 7 as reported in Figure 3.29.

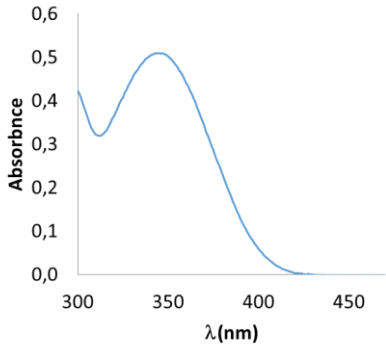

Figure 3.29 Absorption spectra of **L_{21}** in CTAB micelles ($3.0\ 10^{-5}$ M).

Upon addition of increasing amount of $HPpi^{3-}$ and ADP, a decrease of the absorption (with a weak redshift in the case of hydrogenpyrophosphate) of the band was observed (Figure 3.30) while the presence of $H_2PO_4^-$ in the system did not cause any variations in the absorption properties of the receptor.

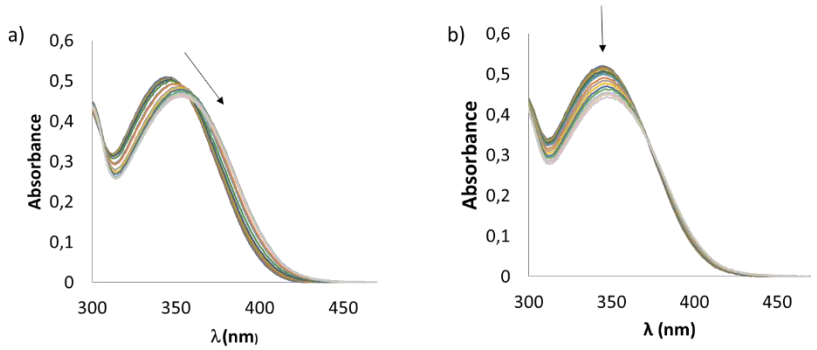

Figure 3.30 Changes in the UV-Visible spectra of **L_{21}** ($3.0\ 10^{-5}$ M) upon addition of increasing amounts of $HPpi^{3-}$ (a) and ADP (b) ($2.5\ 10^{-2}$ M) in CTAB micelles.

These results indicate that the selectivity for phosphate species ($HPpi^{3-}$ and ADP with a LOD of $8.7\ 10^{-4}$ M and $4.4\ 10^{-4}$ M respectively) in terms of absorption was maintained even in the micelles, suggesting a possible use of **L_{21}** to sense these species also in a pure water environment.

3.4 Conclusion

In conclusion we synthesized a new family of asymmetrical bis-urea anion receptors containing an indole pendant moiety as well as with a naphthalene (receptors **L_{16}**-**L_{18}**) , nitro-phenyl (receptors **L_{19}**-**L_{21}**) or amino-phenyl (receptor **L_{22}**) fragment. We have demonstrated that by simply chancing the substituents and their reciprocal position with respect to the central phenyl ring (in the case of ligands **L_{16}**-**L_{18}**) or to the phenyl fragment (in the case of ligands **L_{19}**-**L_{21}**) in the pendant urea moieties, we can influence the colorimetric and fluorimetric properties and the pre-organization of the receptors and we can increase the anion binding affinity. The best results have been achieved for the fluorimetric sensor **L_{18}** and the colorimetric sensor **L_{21}** both able to recognize $HPpi^{3}$ in DMSO and in pure water environment when they embedded in CTAB micelles.

3.5 Experimental methods

All reactions were performed in oven-dried glassware under a slight positive pressure of nitrogen. ^{1}H-NMR (400 MHz, 500MHz) and ^{13}C NMR (100 MHz, 125MHz) spectra were determined on a Varian INOVA-400 spectrometer, and Varian INOVA-500 spectrometer. Chemical shifts for ^{1}H NMR are reported in parts per million (ppm), calibrated to the residual solvent peak set, with coupling constants reported in Hertz (Hz). The following abbreviations are used for spin multiplicity: s = singlet, d = doublet, t = triplet, m = multiplet . Chemical shifts for ^{13}C NMR are reported in ppm, relative to the central line of a septet at δ = 39.52 ppm for deuteriodimethylsulfoxide. Infrared (IR) spectra were recorded on a NICOLET 5700 FT-IR spectrophotometer and reported in wavenumbers (cm^{-1}). Microanalytical data were obtained using a Fisons EA CHNS-O instrument (T = 1000 °C). Fluorescence spectra were recorded on a Cary Eclypse spectrofluorimeter. All solvents and starting materials were purchased from commercial sources where available. Proton NMR titrations were performed by adding aliquots of the putative anionic guest (as the TBA salt, 0.075 M) in a solution of the receptor (0.005M) in DMSO-d_6/0.5% water to a solution of the receptor (0.005M). 7-aminoindole [46] was synthesised following a literature procedure. Mass spectra in positive-ion mode were recorded on a triple quadruple QqQ Varian 310-MS mass spectrometer using the atmospheric-pressure ESI technique. The 20 μl of sample of binder in DMSO solutions were introduced into the ESI source by a Varian HPLC pump without column, at a flow rate of 250μL/min using a 1:1 /CH_3OH:H_2O mixture . A dwell time of 4 s was used, needle voltage of 4000 V, shield voltage of 600 V, housing temperature of 60 °C, drying gas temperature of 400 °C, nebuliser gas pressure of 46 PSI, drying gas pressure of 35 PSI and a detector voltage of 1490 V were used. Mass spectra were acquired in the 250-500amu range.

3.5.1 Synthetic procedure

Synthesis of 1-(1H-indol-7-yl)-3-(4-nitrophenyl) urea (A)

A solution of 1-isocyanate-4-nitrobenzene (0.4300g, 2.618 mmol) in dichloromethane (20ml) was added dropwise to a solution of 7-amino1-indole (0.3707 g, 2.80 mmol) in dichlomethane (10ml). The mixture was refluxed for 12h and then it was filtred to give the desired compound as a red solid. Yield 76% (0.6294 g, 8.028 mmol); M.p.:220°C; ^{1}H-NMR (400 MHz,DMSO-d_6, 298K): δH: 10.7 (s, 1H); 9.69(s, 1H); 9.09 (s, 1H); 8.2 (d, J= 9.2 Hz, 2H); 7.74 (d, J=9.2, 2H); 7.36 (s, 1H); 7.34- 7,32 (m, 1H); 7.13 (d, J=7.4, 1H); 6.96 (t, J=7.7, 1H); 6.45-6.43 (m, 1H). IR: (KBr, cm-1): v CO: 1302.05 (CO stretching); v NH: 3353.83 (NH urea stretching).

Synthesis of 1-(1H-indol-7-yl)-3-(3-nitrophenyl) urea (B)

A solution of 1-isocyanate-3-nitrobenzene (0.303g, 1.846 mmol) in dichloromethane (20ml) was added dropwise to a solution of 7-aminoindole (0.2445g, 1.85 mmol) in dichlomethane (10ml). The mixture was refluxed for 12h and then it was filtred to give the desired compound as a yellow solid. Yield 92% (0.503g, 1.7 mmol); M.p.: 114°C; ; ^{1}H-NMR (400 MHz,DMSO-d_6, 298K): δH: 10.73 (s, 1H); 9.3 (s, 1H); 8.63 (s, 1H); 8.6(t, J= 2.0 Hz, 1H); 7.84-7.81 (m, 1H); 8.19-8.16 (m, 1H); 7.58 (t, J= 7.58, 1H); 7.36-7.33 (m, 2H); 7.10 (d, J=7.39, 1H); 6.96 (t, J= 7.7 Hz, 1H); 6.46-6.43 (m, 1H). IR: (KBr, cm-1): v CO: 1540.45 (CO stretching); v NH: 3321.60 (NH urea stretching).

Synthesis of 1-(1H-indol-7-yl)-3-(2-nitrophenyl) urea (C)

A solution of 1-isocyanate-2-nitrobenzene (0.3060 g, 1.864 mmol) in dichloromethane (20ml) was added dropwise to a solution of 7-aminoindole (0.2445g, 1.85 mmol) in dichlomethane (10ml). The mixture was refluxed for 12h and then it was filtred to give the desired compound as a yellow solid. Yield 92% (0.5029g, 1.7 mmol); M.p.: 114°C; ^{1}H-NMR (400 MHz,DMSO-d_6, 298K): δH: 10.68 (s, 1H); 9,71 (s, 1H); 9.56 (s, 1H); 8.42 (d, J= 8.3 Hz, 1H); 8.12 (d, J= 8.2 Hz, 1H); 7.71 (t, J= 7.5 Hz, 1H); 7.37-7.34(m, 2H); 7.22-7.17 (m, 2H); 6.97 (t, J= 7.6 Hz, 1H); 6.46 (s, 1H);IR: (KBr, cm-1): v CO: 1540.45 (CO stretching); v NH: 3321.60 (NH urea stretching).

Synthesis of 1-(4-aminophenyl)-3-(1H-indol-7-yl) urea (D)

Palladium on activate carbon 10% (0.095 g) was added to a solution of A (0.6294 g, 2.124 mmol) in ethanol (100ml) and then the mixture was stirred for a few minutes under inert atmosphere. Hydrazine (1,7 ml) was then added and the resulting mixture was refluxed for 30 minutes. The solution was filtred with CELITE to remove palladium and the filtrate was concentrated in vacuum to give a beige solid, which was washed in dichloromethane to give the desired compound as a white solid. Yield 55% (0.2138g, 1.303 mmol); M.p.: >250°C; 1H-NMR (500 MHz,DMSO-d_6, 298K), δH: 10.74 (s, 1H, NH2 urea); 8.46 (s, 1H, NH2 urea); 8.36 (s, 1H, NH2 urea); 7.26-7.30 (m,1H); 7.26 (d, J= 7.6 Hz, 1H); 7.12 (d, J= 8.3 Hz, 2H); 7.06 (d, J= 7.5 Hz, 1H); 6.90 (t, J= 7.5 Hz, 1H); 6.53 (d, J= 8 Hz, 2H); 4.75 (s, 2H).IR: (KBr, cm-1): v CO: 1551.57 (CO stretching); v NH: 3292.99 (NH urea stretching).

Synthesis of 1-(3-aminophenyl)-3-(1H-indol-7-yl)urea (E)

Palladium on activate carbon 10% (0.01028g) was added to a solution of B (0.487g, 1.644 mmol) in ethanol (150ml) and then the mixture was stirred for a

few minutes under inert atmosphere. Hydrazine (2,9ml) was then added and the resulting mixture was refluxed for 30 minutes. The solution was filtered with CELITE to remove palladium and the filtrate was concentrated in vacuum to give a beige solid, which was washed in dichloromethane to give the desired compound as a white solid. Yield 79% (0.3471g, 1.303 mmol); M.p.: >250°C; ^{1}H-NMR (500 MHz,DMSO-d_6, 298K), δH: 10.64 (s, 1H); 8.44 (s, 1H); 8.39 (s, 1H); 7.32 (t, J= 2.7 Hz, 1H); 7.29 (d, J= 7.8 Hz, 1H); 7.09 (d, J= 7.4 Hz, 1H); 6.95-6.89 (m, 2H); 6.81 (s, 1H); 6.63 (d, J= 8.7 Hz, 1H); 6.44 (t, J= 2.6 Hz, 1H); 6.22 (d, J= 9.0 Hz, 1H); 4.94 (s, 2H).IR: (KBr, cm-1): v CO: 1566.69 (CO stretching); v NH: 3286.21 (NH urea stretching).

Synthesis of 1-(2-aminophenyl)-3-(1H-indol-7-yl)urea (F)

Palladium on activate carbon 10% (0.01028g) was added to a solution of C (0.487g, 1.644 mmol) in ethanol (150ml) and then the mixture was stirred for a few minutes under inert atmosphere. Hydrazine (2,9ml) was then added and the resulting mixture was refluxed for 30 minutes. The solution was filtered with CELITE to remove palladium and the filtrate was concentrated in vacuum to give a beige solid, which was washed in dichloromethane to give the desired compound as a white solid. Yield 79% (0.3471g, 1.303 mmol); M.p.: >250°C; ^{1}H-NMR (500 MHz,DMSO-d_6, 298K), δH: 10.64 (s, 1H); 8.44 (s, 1H); 8.39 (s, 1H); 7.32 (t, J= 2.7 Hz, 1H); 7.29 (d, J= 7.8 Hz, 1H); 7.09 (d, J= 7.4 Hz, 1H); 6.95-6.89 (m, 2H); 6.81 (s, 1H); 6.63 (d, J= 8.7 Hz, 1H); 6.44 (t, J= 2.6 Hz, 1H); 6.22 (d, J= 9.0 Hz, 1H); 4.94 (s, 2H).IR: (KBr, cm-1): v CO: 1566.69 (CO stretching); v NH: 3286.21 (NH urea stretching).

Synthesis of L_{16}

A solution of naphtyl-isocyanate (0.2204 g, 1.303 mmol) in acetonitrile (10 ml) was added dropwise to a solution of D (0.3470 g, 1.303 mmol), in acetonitrile

(20ml). The mixture was refluxed for 12h and then it was filtred to give the desired compound as a beige solid. Yield 80% (0.2126 g, 4.882 mmol); M.p.: > 250°C; ^{1}H-NMR (500 MHz, DMSO-d_6, 298 K δH: 10.67 (s, 1H); 8.92 (s, 1H); 8.70 (s, 1H); 8.64 (s, 1H); 8.43 (s, 1H); 8.14 (d, J= 8.3 Hz, 1H); 8.03 (d, J= 7.4 Hz, 1H); 7.94 (d, J= 8.0 Hz, 1H); 7.64-7.58 (m, 2H); 7.55 (t, J= 7.4 Hz, 1H); 7.49-7.42 (m, 5H); 7.33 (t, J= 2.5 Hz, 1H); 7.30 (d, J=7 .9 Hz, 1H); 7.09 (d, J= 7.3 Hz, 1H); 6.94 (t, J= 7.7 Hz, 1H); 6.43 (t, J= 2.3 Hz, 1H). ^{13}C-NMR (100 MHz, DMSO- d_6, 298 K), δC: 212.10; 153.17; 153.00; 134.46; 134.34; 134.12; 133.73; 129.25; 128.89; 128.44; 125.89; 125.67; 125.17; 123.94; 122.74; 121.28; 119.24; 119.04; 118.87; 117.16; 115.64; 113.50; 101. LRMS (ES+): m/z: 458.2 $[M\text{-}Na]^{+}$

Synthesis of L_{17}

A solution of naphtyl-isocyanate (0.2204g, 1.303mmol) in acetonitrile (10ml) was added dropwise to a solution of E (0.3470g, 1.303mmol), in acetonitrile (20ml). The mixture was refluxed for 12h and then it was filtred to give the desired compound as a beige solid. Yield 84% (0.2756g, 2,034 mmol); M.p.: > 250°C; ^{1}H-NMR (400 MHz,DMSO- d_6, 298K): δH: 10.71 (s, 1H); 9.10 (s, 1H); 8.84 (s, 1H); 8.72 (s, 1H); 8.46 (s, 1H); 8.14 (d, J= 8.3 Hz, 1H); 8.06 (d, J= 7.5 Hz, 1H); 7.93 (d, J= 8.1 Hz, 1H); 7.76 (s, 1H); 7.62 (t, J= 8.3 Hz, 2H); 7.58-7.53 (m, 2H); 7.48 (t, J= 7.8 Hz, 1H); 7.33- 7.29 (m, 2H); 7.21 (d, J= 4.6 Hz, 2H); 7.1 (d, J= 7.2 Hz, 2H); 6.94 (t, J= 7.7 Hz, 1H). ^{13}C-NMR (126 MHz, DMSO- d_6, 298 K), δC: 152.74; 134.32; 133.69; 129.23; 129.11; 128.97; 128.43; 125.86; 125.74; 125.67; 125.15; 123.72; 122.78; 121.18; 119.00; 117.02; 115.77; 113.64; 111.88; 111.54; 107.88; 101.49.IR: (KBr, cm-1): v CO: 1557.48 (CO stretching); v NH: 3275.42 (NH urea stretching). LRMS (ES+): m/z: 458.2 $[M\text{-}Na]^{+}$.

Synthesis of L_{18}

A solution of naphtyl-isocyanate (0.0973g, 0.575mmol) in acetonitrile (10ml) was added dropwise to a solution of F (0.1531g, 0.575mmol), in acetonitrile (20ml). The mixture was refluxed for 12h and then it was filtred to give the desired compound as a beige solid. Yield 85% (0.2119g, 4,865 mmol); M.p.: > 211°C; ^{1}H-NMR (500 MHz, DMSO-d_6, 298 K), δH: 10.66 (s, 1H); 9.12 (s, 1H); 8.96 (s, 1H); 8.56 (s, 1H); 8.22 (s, 1H); 8.20 (d, J= 8.3 Hz, 1H); 8.02 (d, J= 7.6 Hz, 1H); 7.93 (d, J= 7.8 Hz, 1H); 7.69-7.63 (m, 3H); 7.59-7.52 (m, 2H); 7.47 (t, J= 7.8 Hz, 1H); 7.32-7.28 (m, 2H); 7.12 (t, J= 4.7 Hz, 4H); 6.93 (t, J= 7.7 Hz, 1H). ^{13}C- NMR (100 MHz, DMSO-d_6, 298 K), δC: 131.51; 129.29; 128.62; 126.03; 125.85; 125.59; 125.05; 124.44; 124.00; 122.98; 119.03; 117.77; 115.65; 113.16; 104.72; 101.47. IR: (KBr, cm-1): v CO: 1565.82 (CO stretching); v NH: 3310.42 (NH urea stretching). LRMS (ES+): m/z: 458.2 $[M-Na]^{+}$.

Synthesis of L_{19}

A solution of 1-isocyanate-2-nitrobenzene (0.0944g, 0,575mmol) in acetonitrile (5ml) was added dropwise to a solution of F (0.1525g, 0,573mmol), in acetonitrile (20ml). The mixture was refluxed for 12h and then it was filtred to give the desired compound as an orange solid. Yield 86% (0.21256g, 0,494mmol); M.p.: > 205°C; ^{1}H-NMR (400 MHz,DMSO- d_6, 298K): δH: 10.61 (s, 1H); 9.75 (s, 1H); 9.24 (s, 1H); 8.95 (s, 1H); 8.28 (d, J= 8.4 Hz, 1H); 8.12 (s, 1H); 8.09 (d, J= 7.7 Hz, 1H); 7.85 (d, J= 8.0 Hz, 1H); 7.69 (t, J= 7.5 Hz, 1H); 7.43 (d, J= 7.7 Hz, 1H); 7.35-7.25 (m, 2H); 7.23-7.17 (m, 2H); 7.08 (t, J= 7.8 Hz, 2H); 6.02 (t, J= 7.7 Hz, 1H). ^{13}C-NMR (126 MHz, DMSO- d_6, 298 K), δC: 152.74; 134.32; 133.69; 129.23; 129.11; 128.97;

Synthesis of L_{20}

A solution of 1-isocyanate-3-nitrobenzene (0.0972g, 0,592mmol) in acetonitrile (5ml) was added dropwise to a solution of F (0,1540g, 0,578mmol), in acetonitrile

(20ml). The mixture was refluxed for 12h and then it was filtred to give the desired compound as a light yellow solid. Yield 68% (0.2489g, 0,578mmol); M.p.: > 200°C; ^{1}H-NMR (400 MHz,DMSO- d_6, 298K): δH: 10.64 (s, 1H); 9.66 (s, 1H); 8.89 (s, 1H); 8.57 (s, 1H); 8.24 (s, 1H); 8.20 (s, 1H); 7.81 (d, J= 8.0 Hz, 1H); 7.73 (d, J= 8.0 Hz, 1H); 7.65 (d, J= 7.5 Hz, 1H); 7.60-7.52 (m, 2H); 7.34-7.27 (m, 2H); 7.16-7.09 (m, 3H); 6.92 (t, J= 7.6 Hz, 1H); 6.39 (s, 1H). ^{13}C-NMR (126 MHz, DMSO- d_6, 298 K), δC: 153.77; 153.18; 148.14; 141.26; 132.02; 130.77; 130.05; 129.30; 128.79; 125.14; 124.60; 124.17; 124.05; 123.79; 119.01; 116.18; 115.83; 113.50; 112.09; 101.48.

Synthesis of L_{21}

A solution of 1-isocyanate-4-nitrobenzene (0.0974g, 0,593mmol) in acetonitrile (5ml) was added dropwise to a solution of F (0,1537g, 0,577mmol), in acetonitrile (20ml). The mixture was refluxed for 12h and then it was filtred to give the desired compound as a white solid. Yield 98% (0.2434g, 0,565mmol); M.p.: > 205°C; ^{1}H-NMR (400 MHz,DMSO- d_6, 298K): δH: 10.64 (s, 1H); 9.88 (s, 1H); 8.88 (s, 1H); 8.33 (s, 1H); 8.19 (s, 1H); 8.19 (d, J= 8.2 Hz, 2H); 7.71 (d, J= 8.2 Hz, 2H); 7.66 (d, J= 7.5 Hz, 1H); 7.58 (d, J= 7.7, 1H); 7.36-7.26 (m, 2H); 7.20-7.05 (m, 3H); 6.39 (t, J= 7.2 Hz, 1H); 6.43 (s, 1H).^{13}C-NMR (126 MHz, DMSO-d_6, 298 K), δC: 153.74; 152.75; 146.56; 140.95; 132.07; 130.55; 129.32; 125.15; 124.79; 124.26; 124.06; 123.74; 119.01; 117.03; 115.88; 113.54; 101.48.

Synthesis of L_{22}

Palladium on activate carbon 10% (0.100g) was added to a solution of **L_{21}** (0.221g, 0.513 mmol) in ethanol (100ml) and then the mixture was stirred for a few minutes under inert atmosphere. Hydrazine (1,7 ml) was then added and the resulting mixture was refluxed for 30 minutes. The solution was filtered with CELITE to remove palladium and the filtrate was concentrated in vacuum to give

the desired compound as a white solid. Yield 89% (0.183g, 0.457mmol); ^{1}H-NMR (500 MHz,DMSO-d_6, 298K), δH: 10.64 (s, 1H); 8.44 (s, 1H); 8.39 (s, 1H); 7.32 (t, J= 2.7 Hz, 1H); 7.29 (d, J= 7.8 Hz, 1H); 7.09 (d, J= 7.4 Hz, 1H); 6.95-6.89 (m, 2H); 6.81 (s, 1H); 6.63 (d, J= 8.7 Hz, 1H); 6.44 (t, J= 2.6 Hz, 1H); 6.22 (d, J= 9.0 Hz, 1H); 4.94 (s, 2H). ^{13}C-NMR (125 MHz, DMSO-d_6, 298 K), δC: 153.70; 153.57; 143.96; 131.97; 131.05; 129.23; 128.56; 125.05; 124.44; 124.02; 123.60; 123.43; 120.65; 120.42; 119.03; 115.97; 114.12; 113.09; 101.47.

3.5.2 UV-Visible Titration Spectra

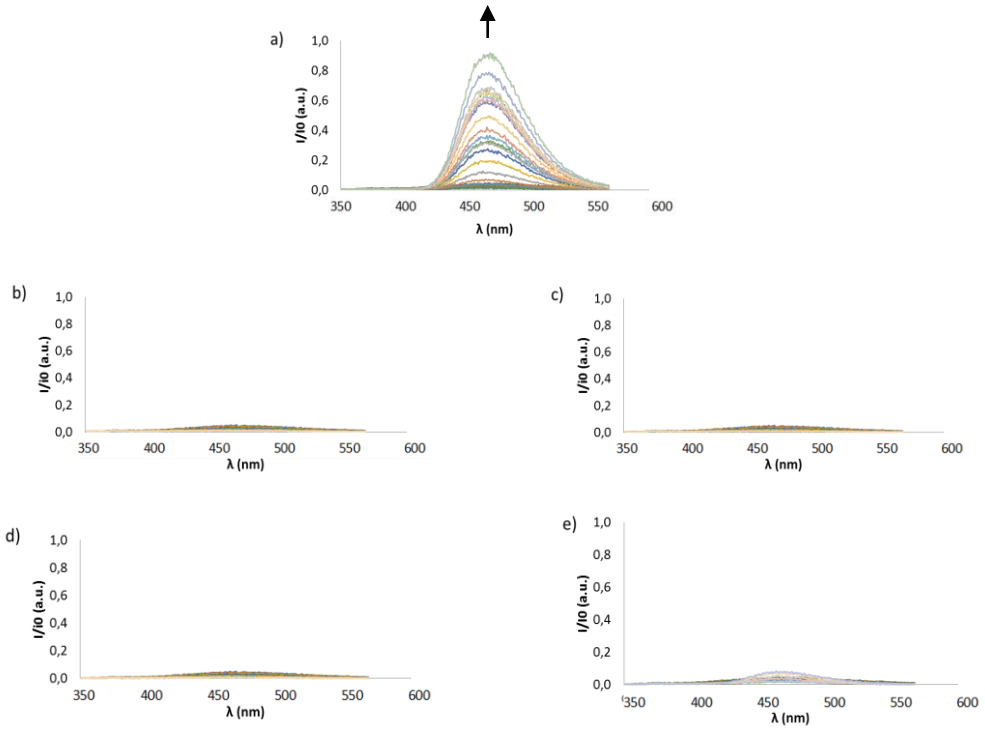

Figure 3.31 Changes in the fluorescence spectra of **L_{16}** ($3.0\cdot10^{-5}$ M) upon addition of increasing amounts of $HPpi^{3-}$ (a), $H_2PO_4^-$ (b), AcO^- (c), HCO_3^- (d) and F^- (e) in DMSO.

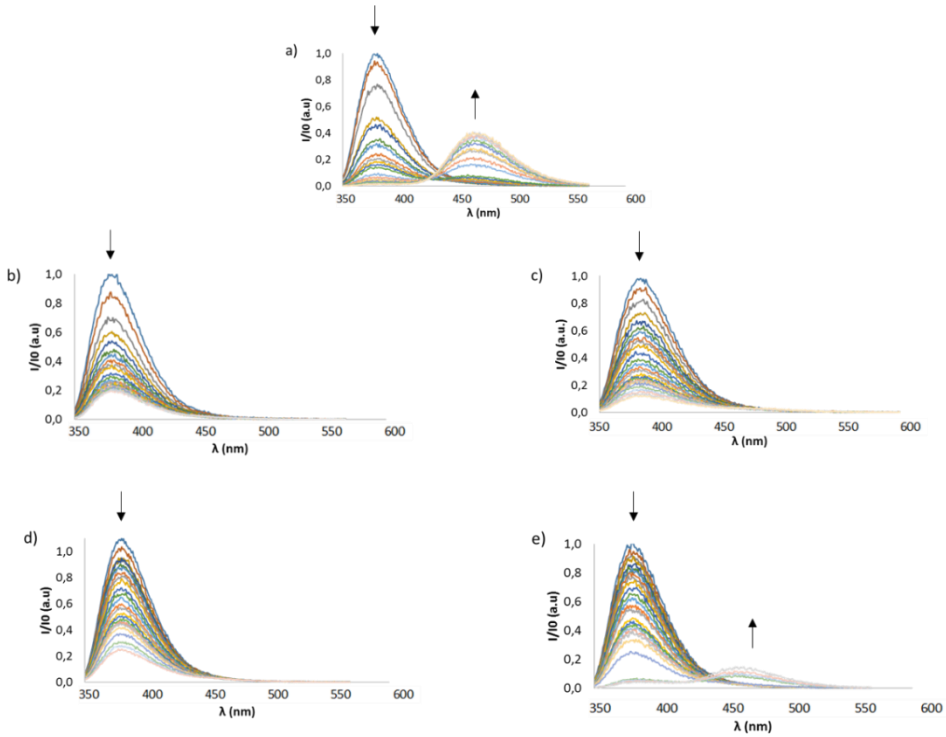

Figure 3.32 Changes in the fluorescence spectra of **L_{17}** ($3.0 \cdot 10^{-5}$ M) upon addition of increasing amounts of $HPpi^{3-}$ (a), $H_2PO_4^-$ (b), AcO^- (c), HCO_3^- (d) and F^- (e) in DMSO.

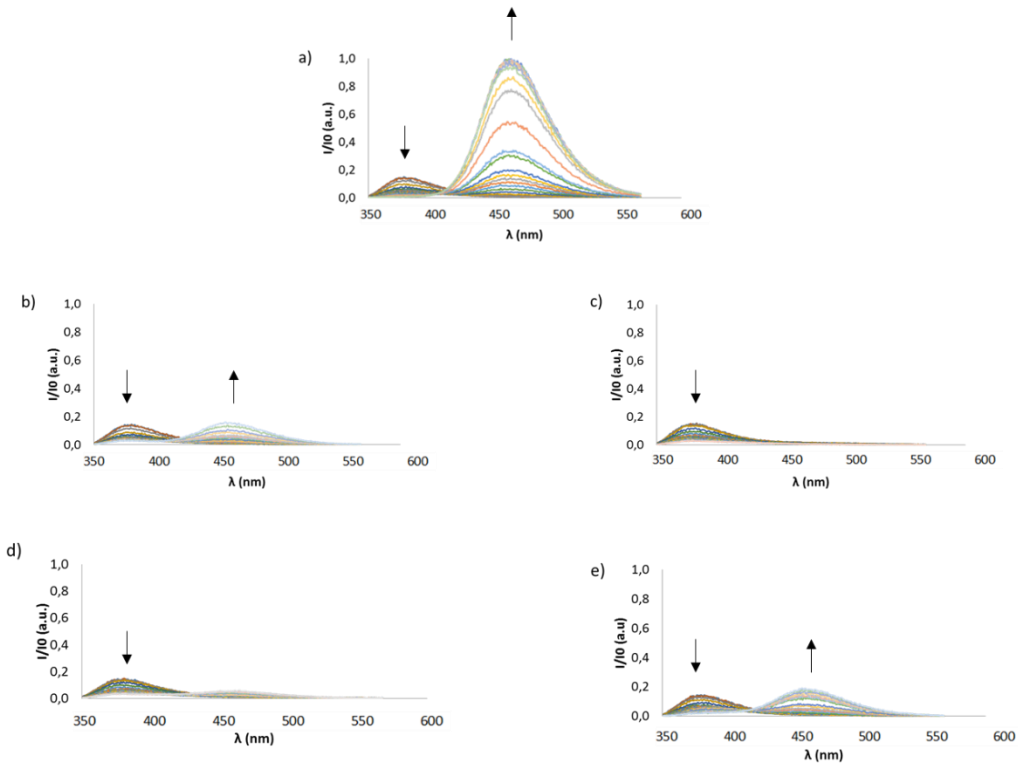

Figure 3.33 Changes in the fluorescence spectra of **L_{18}** ($3.0 \cdot 10^{-5}$ M) upon addition of increasing amounts of $HPpi^{3-}$ (a), $H_2PO_4^-$ (b), AcO^- (c), HCO_3^- (d) and F^- (e) in DMSO.

3.5.3 Crystallographic Data

Table 3.4 Crystal data and structure refinement details of (**L17**)($H_2PO_4^-$)$_2$)(TBA)$_2$ and **L17**)(H_2Ppi)(TBA)$_2$.

CCDC dep. number	1435845	1435846
Empirical formula	$C_{116}H_{195}N_{14}O_{20.50}P_4$	$C_{58}H_{95}N_7O_9P_2$
Formula weight	2237.73	1096.34
Temperature	100(2) K	100.15 K
Wavelength	0.71075 Å	0.71075 Å
Crystal system	Orthorhombic	Orthorhombic
Space group	$Pca2_1$	Pban
Unit cell dimensions	a = 16.1474(7) Å α = 90°	a = 22.394(12) Å α = 90°
	b = 28.4487(12) Å β = 90°	b = 16.369(8) Å β = 90°
	c = 26.5040(9) Å γ = 90°	c = 17.539(10) Å γ = 90°
Z	4	4
Crystal	Prism; Colourless	Plate; colourless
Crystal size	0.24 × 0.22 × 0.22 mm^3	0.08 × 0.08 × 0.01 mm^3
θ range for data collection	2.113 – 27.503°	2.158 – 25.027°
Index ranges	$-20 \le h \le 20$, $-35 \le k \le 36$, $-31 \le l \le 34$	$0 \le h \le 26$, $0 \le k \le 19$, $0 \le l \le 20$
Reflections collected	106562	5686
Independent reflections	27595 [R_{int} = 0.0402]	5685 [R_{int} = 0.0000]
Completeness to θ = 25.242°	99.8 %	99.9 %
Absorption correction	Semi–empirical from equivalents	Semi–empirical from equivalents
Max. and min. transmission	1.000 and 0.688	1.000 and 0.534
Refinement method	Full-matrix least-squares on F^2	Full-matrix least-squares on F^2
Data / restraints / parameters	27595 / 1341 / 1712	5685 / 1691 / 878
Goodness-of-fit on F^2	1.039	1.043
Final *R* indices [$F^2 > 2\sigma(F^2)$]	*R1* = 0.0511, *wR2* = 0.1288	*R1* = 0.0839, *wR2* = 0.2651
***R* indices (all data)**	*R1* = 0.0602, *wR2* = 0.1355	*R1* = 0.1566, *wR2* = 0.3026
Largest diff. peak and hole	0.733 and –0.324 e Å^{-3}	0.360 and –0.347 e Å^{-3}

Diffractometer: *Rigaku AFC12* goniometer equipped with an enhanced sensitivity (HG) *Saturn724+* detector mounted at the window of an *FR-E+ SuperBright* molybdenum rotating anode generator with HF *Varimax* optics (100µm focus). **Cell determination and data collection**: *CrystalClear-SM Expert 3.1 b27* (Rigaku, 2013). **Data reduction, cell refinement and absorption correction**: *CrystalClear-SM Expert 3.1 b27 (Rigaku, 2013).* **Structure solution**: *SHELXS-2013* (Sheldrick, G.M. (2008). Acta Cryst. A64, 112-122). **Structure refinement**: *SHELXL-2014* (Sheldrick, G.M. (2008). Acta Cryst. A64, 112-122). **Graphics:** *OLEX2* (Dolomanov, O. V., Bourhis, L. J., Gildea, R. J., Howard, J. A. K. & Puschmann, H. (2009). J. Appl. Cryst. 42, 339-341).

Table 3.5 Hydrogen bonds [Å and °] for (**L$_{17}$**)($H_2PO_4^-$)$_2$)(TBA)$_2$

D*–H···*A	***d*(*D*–H)**	***d*(H···*A*)**	***d*(*D*···*A*)**	**∠(*DHA*)**
N32–H32A···O42^{i}	0.88	1.92	2.758(4)	159.4
N33–H33···O42^{i}	0.88	2.31	3.070(6)	145.3
N34–H34···O55	0.88	1.97	2.795(4)	155.7
N35–H35A···O55	0.88	1.93	2.771(4)	158.2
N31–H31···O42^{i}	0.88	2.23	3.034(13)	152.3
N31A–H31A···O55	0.88	2.24	3.07(2)	157.3
N1–H1···O52	0.88	1.99	2.832(5)	161.1
N2–H2···O52	0.88	1.91	2.787(4)	175.5
N3–H3···O52	0.88	2.54	3.305(5)	145.2
N4–H4···O45	0.88	1.97	2.779(4)	152.1
N5–H5···O45	0.88	2.01	2.833(4)	154.6
O47–H47···O51	0.84	1.85	2.624(4)	152.2
O43–H43A···O56^{ii}	0.84	1.80	2.605(4)	160.3
O44–H44···O46	0.84	1.82	2.643(4)	165.7
O53–H53B···O46	0.84	1.80	2.636(4)	171.2
O54–H54B···O56^{ii}	0.84	1.77	2.602(4)	171.4
O57–H57···O51^{i}	0.84	1.79	2.615(4)	168.7
O58–H58···O41^{i}	0.84	1.81	2.620(4)	162.8
O201–H20J···O42	0.87	2.52	3.316(10)	153.4
O201–H20J···O44	0.87	2.11	2.840(10)	141.5
O201–H20K···O48	0.87	2.40	2.974(9)	123.8

Symmetry transformations used to generate equivalent atoms:
(i) –x+1,–y+1,z–1/2 (ii) –x+1,–y+1,z+1/2

Table 3.6 Hydrogen bonds [Å and °] for (**L_{17}**)(HPpi)$(TBA)_2$.

D–H···*A*	***d*(*D*–H)**	***d*(H···*A*)**	***d*(*D*···*A*)**	**∠(*DHA*)**
N1–H1···O12	0.88	2.10	2.90(4)	150.7
N2–H2···O11	0.88	2.06	2.92(4)	163.7
N3–H3···O22	0.88	2.67	3.42(4)	145.0
N4–H4···O21	0.88	1.98	2.85(4)	172.2
N5–H5···O11	0.88	1.84	2.66(3)	153.6
O12–H12···O22	0.84	1.78	2.535(16)	149.3
O16–H16···O26	0.84	1.77	2.567(16)	158.5
O23–H23A···O17	0.84	1.80	2.592(15)	155.5
O27–H27···O13	0.84	1.79	2.604(16)	162.5
N51–H51···O26	0.88	2.43	3.26(6)	157.3
N52–H52···O25	0.88	2.06	2.94(4)	175.6
N53–H53···O16	0.88	2.17	2.99(5)	153.8
N54–H54···O15	0.88	1.78	2.53(4)	141.0
N55–H55···O25	0.88	2.05	2.89(3)	159.8

3.5.4 Proton NMR titration fitting

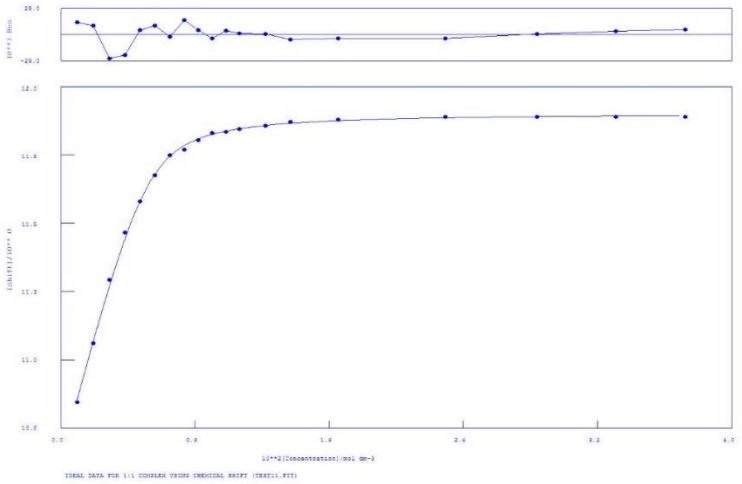

```
Calculations by WinEQNMR Version 1.20 by Michael J. Hynes
Program run at 13:47:18   on 07/18/2014

 IDEAL DATA FOR 1:1 COMPLEX USING CHEMICAL SHIFT (TEST11.FIT)
  Reaction:   M + L = ML
 FILE: TEST11.FIT
 IDEAL DATA: K1 = 63.091; DELTA M = 20.0; DELTA ML = 120.0
 File prepared by M. J. Hynes, October 22 2000

NO.  A   PARAMETER   DELTA    ERROR   CONDITION   DESCRIPTION
   1  1  3.59363E+03 2.000E-01 2.364E+02 3.495E+00    K1
   2  1  1.06851E+01 2.000E-01 8.936E-03 1.342E+00    SHIFT
M
   3  1  1.19077E+01 1.000E+00 4.589E-03 3.031E+00    SHIFT
ML

0RMS ERROR = 9.82E-03  MAX ERROR = 2.29E-02 AT OBS.NO.  3
 RESIDUALS SQUARED = 1.54E-03
 RFACTOR =     0.0771 PERCENT
```

Figure 3.34 ^{1}H-NMR titration of $\mathbf{L_{16}}$ with $TEAHCO_3$ in DMSO-d_6.

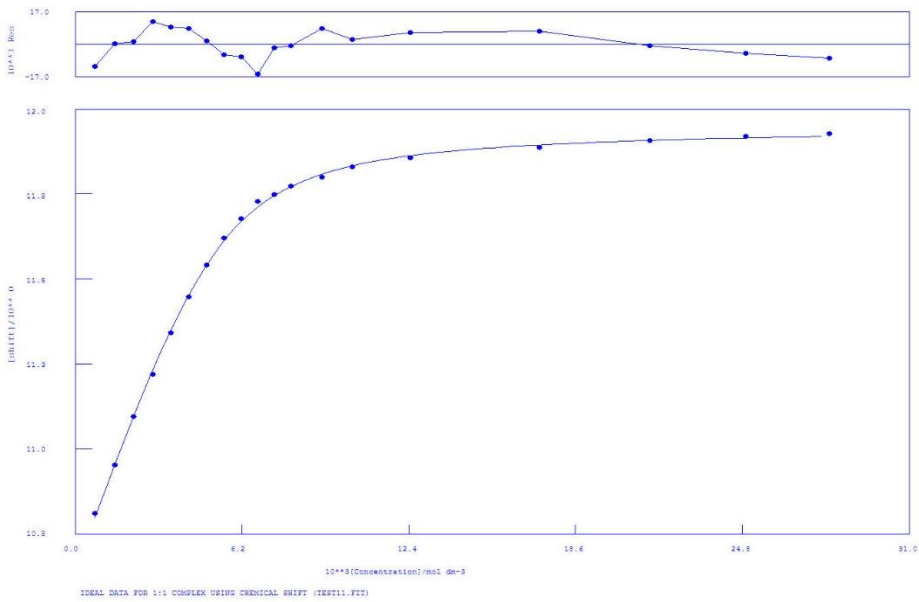


```
Calculations by WinEQNMR Version 1.20 by Michael J. Hynes
Program run at 14:19:37   on 07/18/2014

 IDEAL DATA FOR 1:1 COMPLEX USING CHEMICAL SHIFT (TEST11.FIT)
  Reaction:    M + L = ML
 FILE: TEST11.FIT
 IDEAL DATA: K1 = 63.091; DELTA M = 20.0; DELTA ML = 120.0
 File prepared by M. J. Hynes, October 22 2000

NO.  A   PARAMETER    DELTA     ERROR    CONDITION   DESCRIPTION
   1   1  1.90062E+03 2.000E-01 7.965E+01 5.211E+00     K1
   2   1   1.06892E+01 2.000E-01 5.872E-03 1.523E+00    SHIFT
M
   3   1  1.19499E+01 1.000E+00 4.938E-03 4.431E+00     SHIFT
ML

0RMS ERROR = 7.83E-03  MAX ERROR = 1.56E-02 AT OBS.NO. 10
 RESIDUALS SQUARED = 9.82E-04
 RFACTOR =      0.0619 PERCENT
```

Figure 3.35 ^{1}H-NMR titration of **L_{17}** with $TEAHCO_3$ in DMSO-d_6.

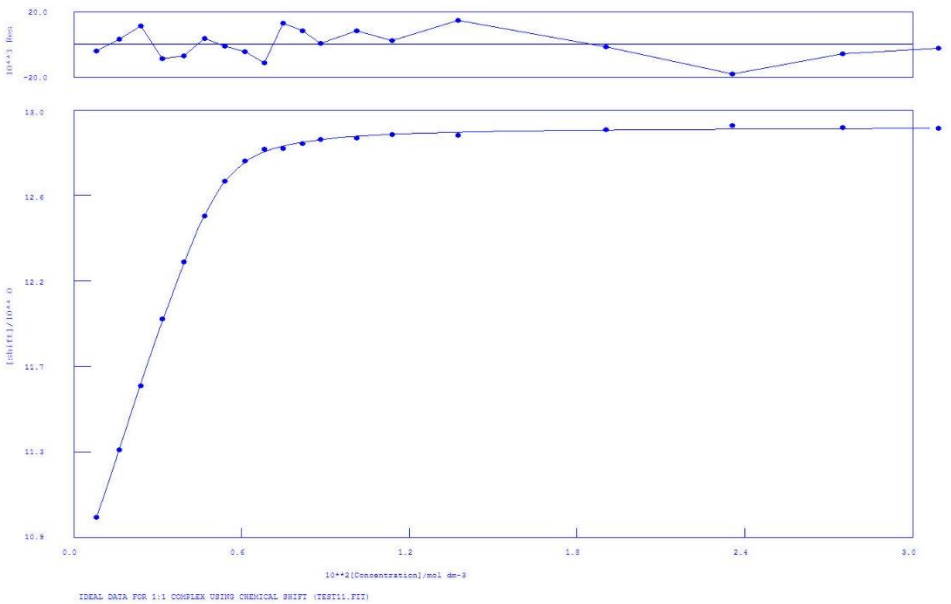

Calculations by WinEQNMR Version 1.20 by Michael J. Hynes

Program run at 09:16:03 on 07/18/2014

```
 IDEAL DATA FOR 1:1 COMPLEX USING CHEMICAL SHIFT (TEST11.FIT)
  Reaction:   M + L = ML
 FILE: TEST11.FIT
 IDEAL DATA: K1 = 63.091; DELTA M = 20.0; DELTA ML = 120.0
 File prepared by M. J. Hynes, October 22 2000

NO.  A  PARAMETER   DELTA    ERROR   CONDITION  DESCRIPTION
   1  1  9.19353E+03 2.000E-01 4.203E+02 2.342E+00    K1
   2  1  1.06469E+01 2.000E-01 7.317E-03 1.173E+00    SHIFT
M
   3  1  1.29169E+01 1.000E+00 3.655E-03 2.222E+00    SHIFT
ML

0RMS ERROR = 9.17E-03  MAX ERROR = 1.83E-02 AT OBS.NO. 17
 RESIDUALS SQUARED = 1.34E-03
 RFACTOR =     0.0672 PERCENT
```

Figure 3.36 ^{1}H-NMR titration of **L_{16}** with $TBAH_2PO_4$ in DMSO-d_6.

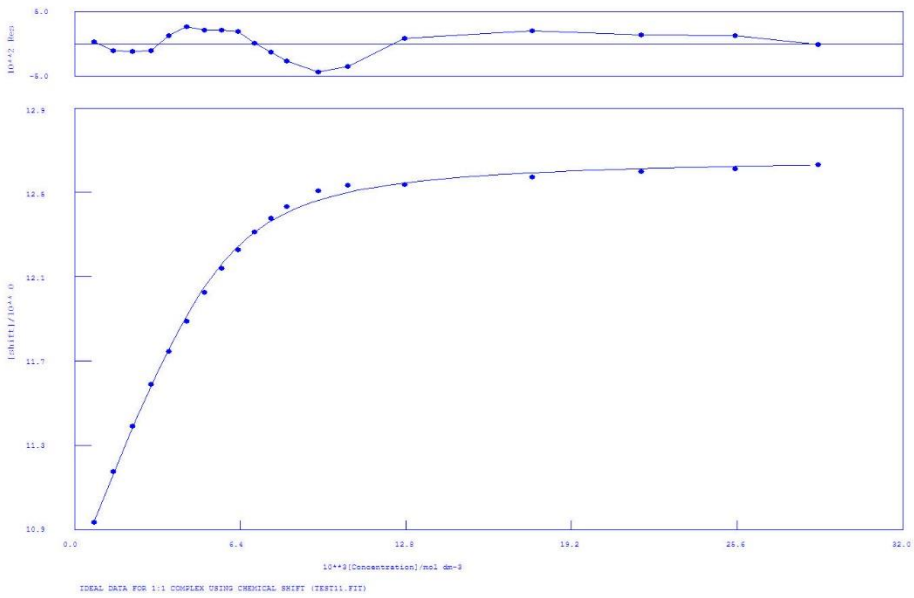


```
Calculations by WinEQNMR Version 1.20 by Michael J. Hynes
Program run at 14:13:16   on 07/18/2014

 IDEAL DATA FOR 1:1 COMPLEX USING CHEMICAL SHIFT (TEST11.FIT)
  Reaction:   M + L = ML
 FILE: TEST11.FIT
 IDEAL DATA: K1 = 63.091; DELTA M = 20.0; DELTA ML = 120.0
 File prepared by M. J. Hynes, October 22 2000

NO.  A   PARAMETER   DELTA    ERROR   CONDITION  DESCRIPTION
   1  1  1.91221E+03 2.000E-01 1.428E+02 5.100E+00    K1
   2  1   1.06971E+01 2.000E-01 1.578E-02 1.485E+00   SHIFT
M
   3  1  1.26723E+01 1.000E+00 1.361E-02 4.412E+00    SHIFT
ML

0RMS ERROR = 2.16E-02  MAX ERROR = 4.46E-02 AT OBS.NO. 13
 RESIDUALS SQUARED = 7.43E-03
 RFACTOR =     0.1631 PERCENT
```

Figure 3.37 ^{1}H-NMR titration of **L_{17}** with $TBAH_2PO_4$ in DMSO-d_6.

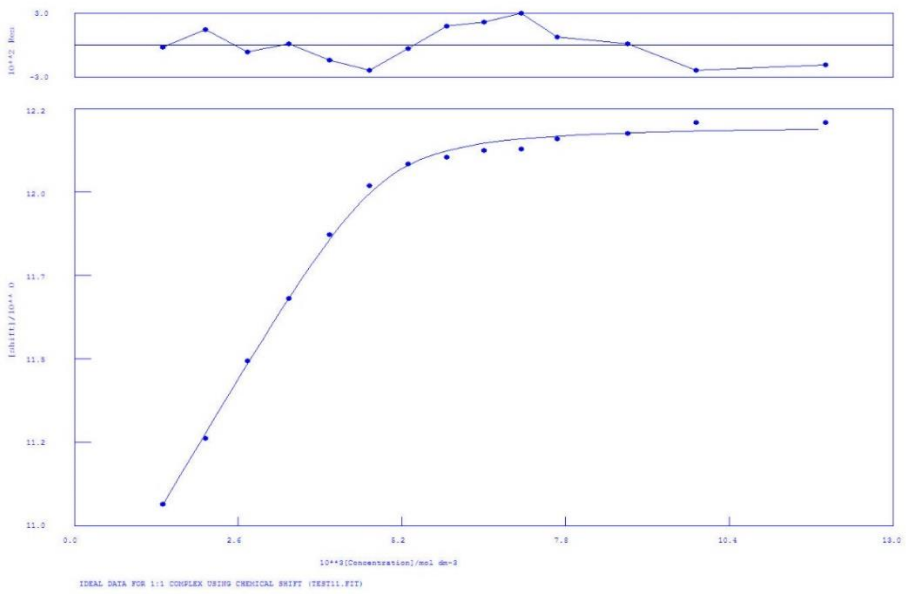


```
Calculations by WinEQNMR Version 1.20 by Michael J. Hynes
Program run at 13:04:38   on 05/22/2014

 IDEAL DATA FOR 1:1 COMPLEX USING CHEMICAL SHIFT (TEST11.FIT)
  Reaction:   M + L = ML
 FILE: TEST11.FIT
 IDEAL DATA: K1 = 63.091; DELTA M = 20.0; DELTA ML = 120.0
 File prepared by M. J. Hynes, October 22 2000

NO.  A   PARAMETER   DELTA    ERROR   CONDITION  DESCRIPTION
   1  1  1.44560E+04 2.000E-01 2.735E+03 4.069E+00    K1
   2  1   1.06252E+01 2.000E-01 1.821E-02 1.225E+00    SHIFT
M
   3  1  1.21546E+01 1.000E+00 1.174E-02 4.070E+00    SHIFT
ML

0RMS ERROR = 1.83E-02  MAX ERROR = 2.96E-02 AT OBS.NO. 10
 RESIDUALS SQUARED = 3.68E-03
 RFACTOR =     0.1366 PERCENT
```

Figure 3.38 ^{1}H-NMR titration of **L_{18}** with $TBAH_2PO_4$ in DMSO-d_6.

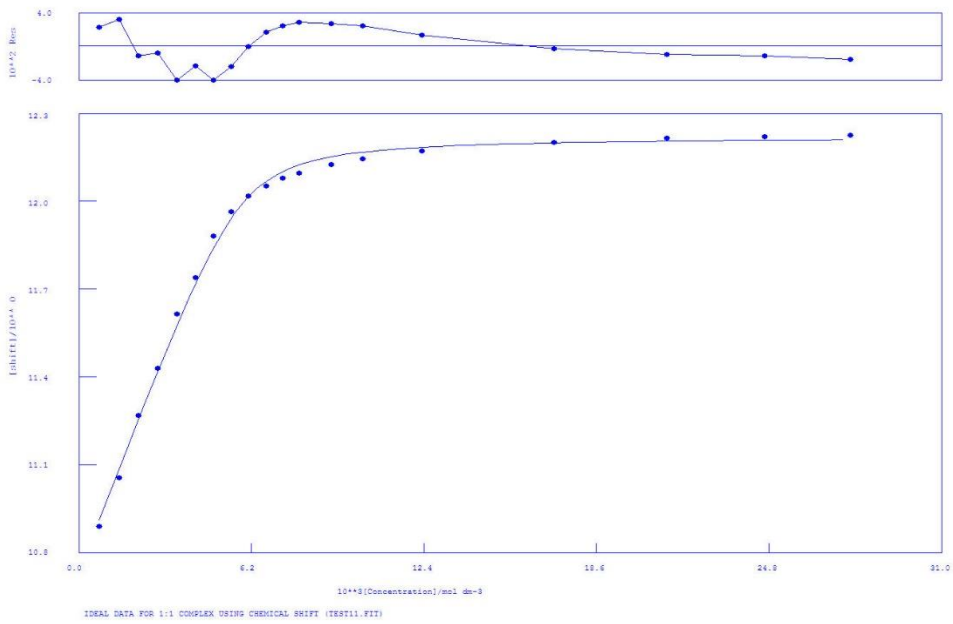


```
Calculations by WinEQNMR Version 1.20 by Michael J. Hynes
Program run at 13:30:12   on 07/18/2014

 IDEAL DATA FOR 1:1 COMPLEX USING CHEMICAL SHIFT (TEST11.FIT)
  Reaction:   M + L = ML
 FILE: TEST11.FIT
 IDEAL DATA: K1 = 63.091; DELTA M = 20.0; DELTA ML = 120.0
 File prepared by M. J. Hynes, October 22 2000

NO.  A   PARAMETER   DELTA    ERROR   CONDITION  DESCRIPTION
   1  1  5.82968E+03 2.000E-01 8.591E+02 3.190E+00    K1
   2  1   1.07293E+01 2.000E-01 1.716E-02 1.217E+00    SHIFT
M
   3  1  1.22204E+01 1.000E+00 1.223E-02 3.053E+00    SHIFT
ML

0RMS ERROR = 2.46E-02  MAX ERROR = 4.02E-02 AT OBS.NO.  5
 RESIDUALS SQUARED = 9.68E-03
 RFACTOR =     0.1902 PERCENT
```

Figure 3.39 ^{1}H-NMR titration of L_{16} with TBAAcO in DMSO-d_6.

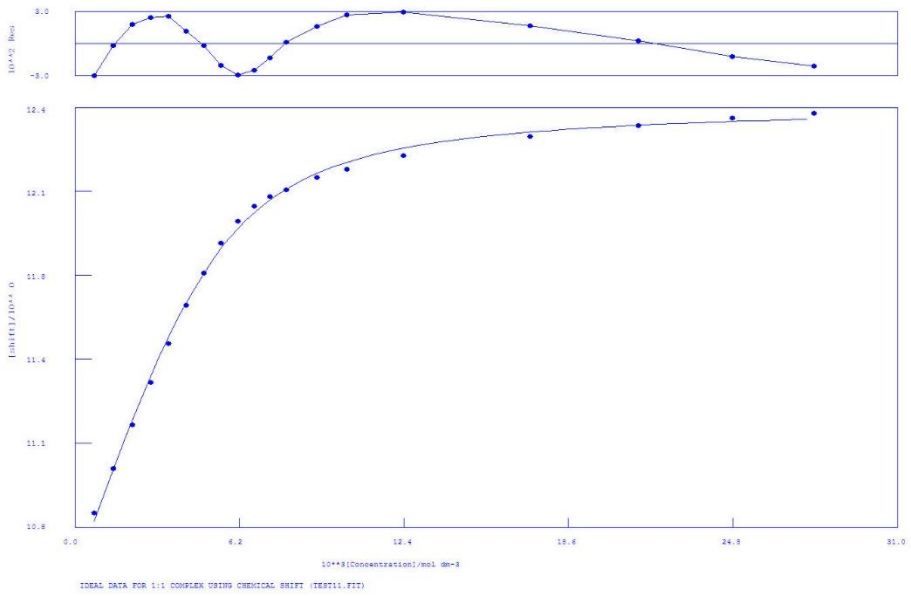


```
Calculations by WinEQNMR Version 1.20 by Michael J. Hynes
Program run at 14:00:08   on 07/18/2014

 IDEAL DATA FOR 1:1 COMPLEX USING CHEMICAL SHIFT (TEST11.FIT)
  Reaction:   M + L = ML
 FILE: TEST11.FIT
 IDEAL DATA: K1 = 63.091; DELTA M = 20.0; DELTA ML = 120.0
 File prepared by M. J. Hynes, October 22 2000

NO.  A   PARAMETER   DELTA    ERROR   CONDITION  DESCRIPTION
   1  1  1.25223E+03 2.000E-01 3.870E+01 1.622E+00    K1
   2  1   1.06110E+01 2.000E-01 1.518E-02 1.521E+00    SHIFT
M
   3  1  1.24161E+01 1.000E+00 8.525E-03 1.606E+00    SHIFT
ML

0RMS ERROR = 2.15E-02  MAX ERROR = 3.04E-02 AT OBS.NO.  1
 RESIDUALS SQUARED = 7.40E-03
 RFACTOR =     0.1664 PERCENT
```

Figure 3.40 ^{1}H-NMR titration of $\mathbf{L_{17}}$ with TBAAcO in DMSO-d_6.

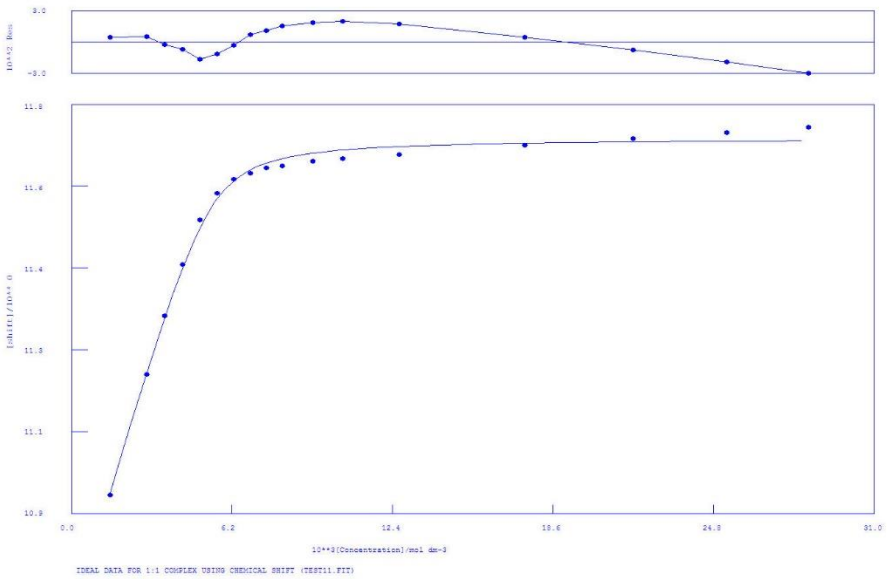


```
Calculations by WinEQNMR Version 1.20 by Michael J. Hynes
Program run at 15:20:17   on 05/21/2014

 IDEAL DATA FOR 1:1 COMPLEX USING CHEMICAL SHIFT (TEST11.FIT)
  Reaction:   M + L = ML
 FILE: TEST11.FIT
 IDEAL DATA: K1 = 63.091; DELTA M = 20.0; DELTA ML = 120.0
 File prepared by M. J. Hynes, October 22 2000

NO.  A   PARAMETER   DELTA    ERROR   CONDITION  DESCRIPTION
   1  1  7.43233E+03 2.000E-01 1.010E+03 2.593E+00    K1
   2  1   1.06595E+01 2.000E-01 1.664E-02 1.230E+00    SHIFT
M
   3  1  1.17248E+01 1.000E+00 6.791E-03 2.557E+00    SHIFT
ML

0RMS ERROR = 1.53E-02  MAX ERROR = 3.03E-02 AT OBS.NO. 17
 RESIDUALS SQUARED = 3.29E-03
 RFACTOR =     0.1202 PERCENT
```

Figure 3.41 ^{1}H-NMR titration of $\mathbf{L_{18}}$ with TBAAcO in DMSO-d_6.

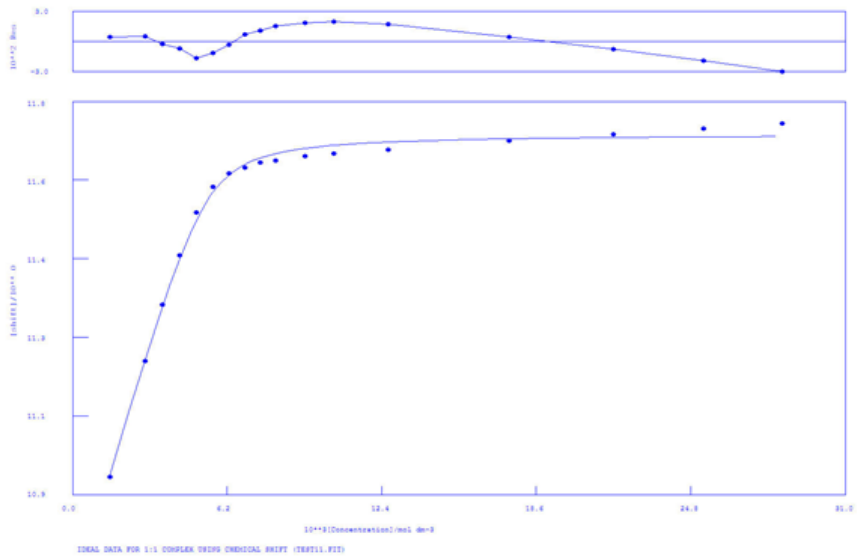

```
Calculations by WinEQNMR Version 1.20 by Michael J. Hynes
Program run at 15:20:17   on 05/21/2014

 IDEAL DATA FOR 1:1 COMPLEX USING CHEMICAL SHIFT (TEST11.FIT)
  Reaction:   M + L = ML
 FILE: TEST11.FIT
 IDEAL DATA: K1 = 63.091; DELTA M = 20.0; DELTA ML = 120.0
 File prepared by M. J. Hynes, October 22 2000

NO.  A   PARAMETER   DELTA    ERROR   CONDITION  DESCRIPTION
   1  1  7.43233E+03 2.000E-01 1.010E+03 2.593E+00    K1
   2  1   1.06595E+01 2.000E-01 1.664E-02 1.230E+00    SHIFT
M
   3  1  1.17248E+01 1.000E+00 6.791E-03 2.557E+00    SHIFT
ML

0RMS ERROR = 1.53E-02  MAX ERROR = 3.03E-02 AT OBS.NO. 17
 RESIDUALS SQUARED = 3.29E-03
 RFACTOR =     0.1202 PERCENT
```

Figure 3.42 ^{1}H-NMR titration of $\mathbf{L_{18}}$ with $TBAH_2PO_4$ in DMSO-d_6.

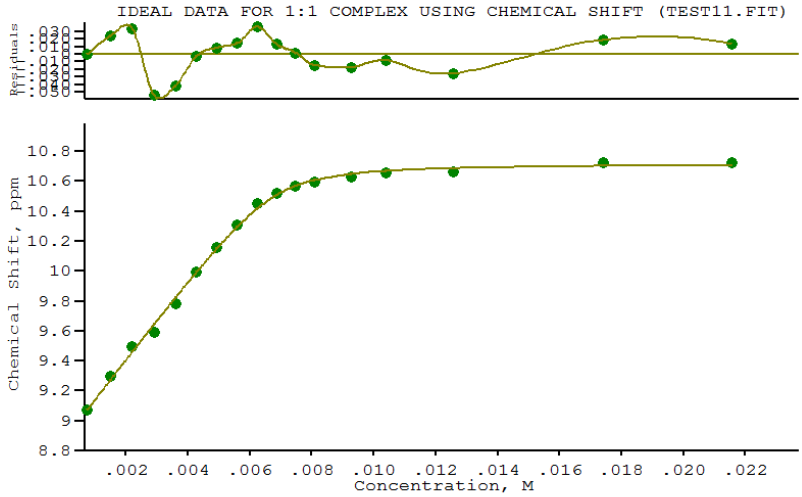


```
Calculations by WinEQNMR2 Version 2.00 by Michael J. Hynes
Program run at 16:53:18   on 11/04/2016

 IDEAL DATA FOR 1:1 COMPLEX USING CHEMICAL SHIFT (TEST11.FIT)
  Reaction:   Sn + L = Sn(L)
IDEAL DATA: K1 = 63.091; DELTA M = 20.0; DELTA ML = 120.0
 File prepared by M. J. Hynes, October 22 2000

  Equilibrium constants are floating point numbers

NO.  A   PARAMETER   DELTA    ERROR   CONDITION  DESCRIPTION
1 1  8.54369E+03 2.000E-01 1.551E+03 3.868E+00    K1
2 1  8.87530E+00 2.000E-01 1.723E-02 1.186E+00   SHIFT Sn
3 1  1.07216E+01 1.000E+00 1.671E-02 3.974E+00   SHIFT Sn(L)

0RMS ERROR = 2.65E-02  MAX ERROR = 5.41E-02 AT OBS.NO.  4
 RESIDUALS SQUARED = 9.85E-03
 RFACTOR =     0.2358 PERCENT
```

Figure 3.43 ^{1}H-NMR titration of **L_{22}** with $TBAH_2PO_4$ in DMSO-d_6.

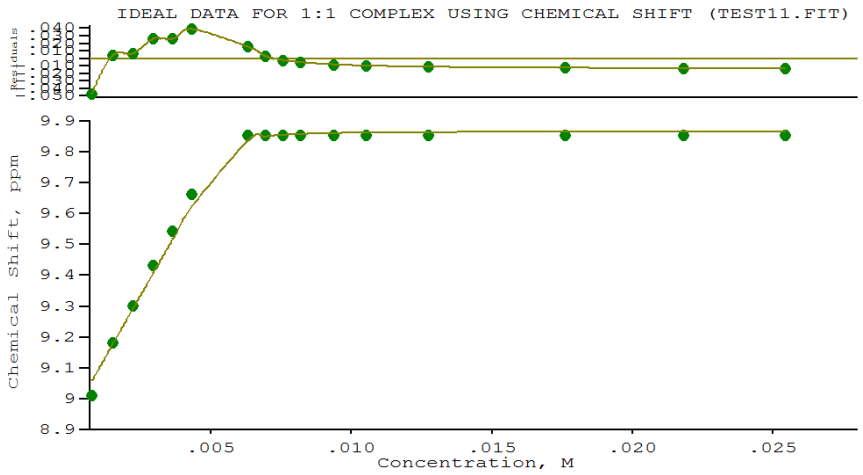


```
Calculations by WinEQNMR2 Version 2.00 by Michael J. Hynes
Program run at 17:45:05   on 11/04/2016

 IDEAL DATA FOR 1:1 COMPLEX USING CHEMICAL SHIFT (TEST11.FIT)
  Reaction:   Sn + L = Sn(L)
IDEAL DATA: K1 = 63.091; DELTA M = 20.0; DELTA ML = 120.0
 File prepared by M. J. Hynes, October 22 2000

  Equilibrium constants are floating point numbers

NO.  A   PARAMETER   DELTA    ERROR   CONDITION  DESCRIPTION
   1  1  3.94997E+04 2.000E-01 4.203E+03 1.045E+00    K1
   2  1   8.93777E+00 2.000E-01 1.569E-02 1.095E+00    SHIFT
Sn
   3  1  9.86648E+00 1.000E+00 6.918E-03 1.120E+00    SHIFT
Sn(L)

0RMS ERROR = 2.19E-02  MAX ERROR = 4.71E-02 AT OBS.NO.  1
 RESIDUALS SQUARED = 6.24E-03
 RFACTOR =     0.2042 PERCENT
```

Figure 3.44 ^{1}H-NMR titration of **L_{22}** with $TBEHCO_3$ in DMSO-d_6.

References

1. Sessler, J. L.; Gale, P. A.; Cho, W.-S., *Anion receptor chemistry*. Royal Society of Chemistry: 2006.

2. Gale, P. A.; Gunnlaugsson, T., Preface: supramolecular chemistry of anionic species themed issue. *Chemical Society Reviews* **2010,** *39* (10), 3595-3596.

3. Martinez-Manez, R.; Sancenón, F., Fluorogenic and chromogenic chemosensors and reagents for anions. *Chemical Reviews* **2003,** *103* (11), 4419-4476.

4. Wenzel, M.; Hiscock, J. R.; Gale, P. A., Anion receptor chemistry: highlights from 2010. *Chemical Society Reviews* **2012,** *41* (1), 480-520.

5. Wiskur, S. L.; Ait-Haddou, H.; Lavigne, J. J.; Anslyn, E. V., Teaching old indicators new tricks. *Accounts of chemical research* **2001,** *34* (12), 963-972.

6. Adams, R. L., *The biochemistry of the nucleic acids*. Springer Science & Business Media: 2012.

7. Egli, M.; Saenger, W., *Principles of nucleic acid structure*. Springer Science & Business Media: 2013.

8. Tiessen, H., Phosphorus in the global environment: Transfers, cycles and management. **1995**.

9. Bazzicalupi, C.; Bencini, A.; Lippolis, V., Tailoring cyclic polyamines for inorganic/organic phosphate binding. *Chemical Society Reviews* **2010,** *39* (10), 3709-3728.

10. Bencini, A.; Bartoli, F.; Caltagirone, C.; Lippolis, V., Zinc (II)-based fluorescent dyes: Luminescence modulation by phosphate anion binding. *Dyes and Pigments* **2014,** *110*, 169-192.

11. Hargrove, A. E.; Nieto, S.; Zhang, T.; Sessler, J. L.; Anslyn, E. V., Artificial receptors for the recognition of phosphorylated molecules. *Chemical reviews* **2011,** *111* (11), 6603-6782.

12. M. C.P. and v. H. K.E., B., The Benjamin/Cummings; Publishing Co., R. C., CA, 1990.

13. Doherty, M.; Belcher, C.; Regan, M.; Jones, A.; Ledingham, J., Association between synovial fluid levels of inorganic pyrophosphate and short term radiographic outcome of knee osteoarthritis. *Annals of the rheumatic diseases* **1996,** *55* (7), 432-436.

14. Timms, A.; Zhang, Y.; Russell, R.; Brown, M., Genetic studies of disorders of calcium crystal deposition. *Rheumatology* **2002,** *41* (7), 725-729.

15. Xu, S.; He, M.; Yu, H.; Cai, X.; Tan, X.; Lu, B.; Shu, B., A quantitative method to measure telomerase activity by bioluminescence connected with telomeric repeat amplification protocol. *Analytical biochemistry* **2001,** *299* (2), 188-193.

16. Sokkalingam, P.; Kim, D. S.; Hwang, H.; Sessler, J. L.; Lee, C.-H., A dicationic calix [4] pyrrole derivative and its use for the selective recognition and displacement-based sensing of pyrophosphate. *Chemical Science* **2012,** *3* (6), 1819-1824.

17. Francesconi, O.; Gentili, M.; Bartoli, F.; Bencini, A.; Conti, L.; Giorgi, C.; Roelens, S., Phosphate binding by a novel Zn (II) complex featuring a trans-1, 2-diaminocyclohexane ligand. Effective anion recognition in water. *Organic & biomolecular chemistry* **2015,** *13* (6), 1860-1868.

18. Jiao, S.-Y.; Li, K.; Zhang, W.; Liu, Y.-H.; Huang, Z.; Yu, X.-Q., Cd (II)-terpyridine-based complex as a ratiometric fluorescent probe for pyrophosphate detection in solution and as an imaging agent in living cells. *Dalton Transactions* **2015,** *44* (3), 1358-1365.

19. Lee, D. H.; Kim, S. Y.; Hong, J. I., A fluorescent pyrophosphate sensor with high selectivity over ATP in water. *Angewandte Chemie International Edition* **2004,** *43* (36), 4777-4780.

20. Liu, X.; Ngo, H. T.; Ge, Z.; Butler, S. J.; Jolliffe, K. A., Tuning colourimetric indicator displacement assays for naked-eye sensing of pyrophosphate in aqueous media. *Chemical Science* **2013,** *4* (4), 1680-1686.

21. S. I. Kondo, Y. N. a. M. U., RSC Adv., 2014, 4,; 27140–27145.

22. Gunnlaugsson, T.; Davis, A. P.; O'Brien, J. E.; Glynn, M., Fluorescent sensing of pyrophosphate and bis-carboxylates with charge neutral PET chemosensors. *Organic letters* **2002,** *4* (15), 2449-2452.

23. Kim, S. K.; Singh, N. J.; Kim, S. J.; Swamy, K.; Kim, S. H.; Lee, K.-H.; Kim, K. S.; Yoon, J., Anthracene derivatives bearing two urea groups as fluorescent receptors for anions. *Tetrahedron* **2005,** *61* (19), 4545-4550.

24. Kwon, J. Y.; Jang, Y. J.; Kim, S. K.; Lee, K.-H.; Kim, J. S.; Yoon, J., Unique hydrogen bonds between 9-anthracenyl hydrogen and anions. *The Journal of organic chemistry* **2004,** *69* (15), 5155-5157.

25. Lowe, A. J.; Long, B. M.; Pfeffer, F. M., Examples of Regioselective Anion Recognition among a Family of Two-, Three-, and Four-"Armed" Bis-, Tris-, and Tetrakis (thioureido)[n] Polynorbornane hosts. *The Journal of organic chemistry* **2012,** *77* (19), 8507-8517.

26. Quinlan, E.; Matthews, S. E.; Gunnlaugsson, T., Colorimetric recognition of anions using preorganized tetra-amidourea derived calix [4] arene sensors. *The Journal of organic chemistry* **2007,** *72* (20), 7497-7503.

27. Caltagirone, C.; Bazzicalupi, C.; Isaia, F.; Light, M. E.; Lippolis, V.; Montis, R.; Murgia, S.; Olivari, M.; Picci, G., A new family of bis-ureidic receptors for pyrophosphate optical sensing. *Organic & biomolecular chemistry* **2013,** *11* (15), 2445-2451.

28. Boiocchi, M.; Del Boca, L.; Esteban-Gómez, D.; Fabbrizzi, L.; Licchelli, M.; Monzani, E., Anion-Induced Urea Deprotonation. *Chemistry–A European Journal* **2005,** *11* (10), 3097-3104.

29. Casula, A.; Bazzicalupi, C.; Bettoschi, A.; Cadoni, E.; Coles, S. J.; Horton, P. N.; Isaia, F.; Lippolis, V.; Mapp, L. K.; Marini, G. M.; Montis, R.; Scorciapino, M. A.; Caltagirone, C., Fluorescent asymmetric bis-ureas for pyrophosphate recognition in pure water. *Dalton Transactions* **2016,** *45* (7), 3078-3085.

30. Hynes, M. J., EQNMR: a computer program for the calculation of stability constants from nuclear magnetic resonance chemical shift data. *Journal of the Chemical Society, Dalton Transactions* **1993,** (2), 311-312.

31. Ábalos, T.; Royo, S.; Martínez-Máñez, R.; Sancenón, F.; Soto, J.; Costero, A. M.; Gil, S.; Parra, M., Surfactant-assisted chromogenic sensing of cyanide in water. *New Journal of Chemistry* **2009,** *33* (8), 1641-1645.

32. Jose, D. A.; Stadlbauer, S.; König, B., Polydiacetylene-Based Colorimetric Self-Assembled Vesicular Receptors for Biological Phosphate Ion Recognition. *Chemistry–A European Journal* **2009,** *15* (30), 7404-7412.

33. Banerjee, S.; Bhuyan, M.; König, B., Tb (III) functionalized vesicles for phosphate sensing: membrane fluidity controls the sensitivity. *Chemical Communications* **2013,** *49* (50), 5681-5683.

34. Cametti, M.; Dalla Cort, A.; Bartik, K., Fluoride Binding in Water: A New Environment for a Known Receptor. *ChemPhysChem* **2008,** *9* (15), 2168-2171.

35. Release, H., 7.5 for windows, molecular modeling system, Hypercube. *Inc. http://www. hyper. com* **2002**.

36. Stewart, J. J., Optimization of parameters for semiempirical methods I. Method. *Journal of Computational Chemistry* **1989,** *10* (2), 209-220.

37. Stewart, J. J., Optimization of parameters for semiempirical methods II. Applications. *Journal of Computational Chemistry* **1989,** *10* (2), 221-264.

38. Rajbanshi, A.; Wan, S.; Custelcean, R., Dihydrogen phosphate clusters: trapping H2PO4–tetramers and hexamers in urea-functionalized molecular crystals. *Crystal Growth & Design* **2013,** *13* (5), 2233-2237.

39. Hursthouse, M. B.; Montis, R.; Niitsoo, L.; Sarson, J.; Threlfall, T. L.; Asiri, A. M.; Khan, S. A.; Obaid, A. Y.; Al-Harbi, L. M., Anhydrates and/or hydrates in nitrate, sulphate and phosphate salts of 4-aminopyridine,(4-AP) and 3, 4-diaminopyridine (3, 4-DAP): the role of the water molecules in the hydrates. *CrystEngComm* **2014,** *16* (11), 2205-2219.

40. Blažek, V.; Molčanov, K.; Mlinarić-Majerski, K.; Kojić-Prodić, B.; Basarić, N., Adamantane bisurea derivatives: anion binding in the solution and in the solid state. *Tetrahedron* **2013,** *69* (2), 517-526.

41. Karle, J. M.; Karle, I. L., Crystal and molecular structure of the antimalarial agent 4-(tert-butyl)-2-(tert-butylaminomethyl)-6-(4-chlorophenyl) phenol dihydrogen

phosphate (WR 194,965 phosphate). *Antimicrobial agents and chemotherapy* **1988,** *32* (4), 540-546.

42. Koralegedara, M. B.; Aw, H. W.; Burns, D. H., Initial structural studies of charged receptors that bind to inorganic phosphate anion and to an anionic phospholipid found in bacterial membranes. *The Journal of organic chemistry* **2011,** *76* (6), 1930-1933.

43. Yin, Z.; Zhang, Y.; He, J.; Cheng, J.-P., A new tripodal anion receptor with selective binding for H 2 PO 4− and F− ions. *Tetrahedron* **2006,** *62* (4), 765-770.

44. Olivari, M.; Montis, R.; Karagiannidis, L. E.; Horton, P. N.; Mapp, L. K.; Coles, S. J.; Light, M. E.; Gale, P. A.; Caltagirone, C., Anion complexation, transport and structural studies of a series of bis-methylurea compounds. *Dalton Transactions* **2015,** *44* (5), 2138-2149.

45. Mori, M.; Chuman, T.; Fujimori, T.; Kato, K.; Ohkubo, A.; Toda, S., Conformational difference in the solid state and in solution of methyl 2, 3, 4-trideoxy-2, 4-di-C-methyl-6-O-trityl-α-d-lyxo-hexopyranoside. *Carbohydrate research* **1984,** *127* (2), 171-179.

46. Zieliński, T.; Dydio, P.; Jurczak, J., Synthesis, structure and the binding properties of the amide-based anion receptors derived from 1H-indole-7-amine. *Tetrahedron* **2008,** *64* (3), 568-574.

Chapter 4:

Selenourea-based receptors for anion recognition: an NMR study

4. Selenourea-based receptors for anion recognition: an NMR study

4.1 Introduction

Selenium is a controversial element. In the past, it was described as a highly toxic element for the biological system causing poisoning. However, in the last years it has been discovered that Selenium is an essential nutrient for the correct physiological processes in the human organism. [1] At this purpose, a very important role in the self-defence mechanism against oxidative stress is played by some selenoproteins such as glutathione peroxidase. [2,3] The work of these proteins is based on the presence of Selenium as an active centre where important redox reactions with ROS species (Reactive Oxygen Species) take place. [4] Alterations in the equilibrium between the oxidative stress and the Selenium levels lead to a large number of diseases such as rheumatoid arthritis,[5] pancreatitis, diabetes[6] and cardiovascular complications. Recent medicine studies have suggested the interesting anticancer ability of many Selenium derivatives to induce apoptosis of tumor cells and reduce cancerous metastasis in animals.[7,8,9,10] Moreover, a wide range of Selenium compound show anti-inflammatory, antihypertensive, antiviral, antibacterial, and antifungal properties. [11,12,13] Due these significant properties, the interest towards Selenium compounds has quickly developed. OrganoSelenium derivatives have been extensively used as key synthetic intermediates [14,15,16,17] and ligands in asymmetric synthesis. [18,19,20] Also Selenium-containing derivatives such as isoselenocyanates, [21,22,23,] selenocarbamates, [24,25] selenoheterocycles [26,27,28] and selenoureas [29] are quite popular.

4.1.1 Selenoureas: an overview

Currently, the most common use of selenourea compounds is in the antioxidant activity field.[30,31,32] Reactive Oxygen Species (ROS) and Reactive Nitrogen Species (RNS), such as free radicals, superoxide anion, hydroperoxides, organic peroxides, nitric oxide (NO), are involved in very important biological process such as intra- and inter-cellular redox signalling,[33] gene transcription,[34] neurotransmitter activity and immune response.[34] However when the equilibrium between ROS/RNS species and natural antioxidant defences is disrupted, there is an evidence of oxidative stress.[35] This phenomenon has been associated with different diseases like cancer,[36] or neurodegenerative disorder.[37]

Fernández-Bolaños *et al.* reported the synthesis and a biological study of different families of lipophilic organoselenium compounds including selenoureas, with *in vitro* antioxidant activity.[30] These compounds were evaluated as ROS scavengers against free radicals and hydrogen peroxide, in particular.

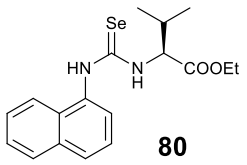

80

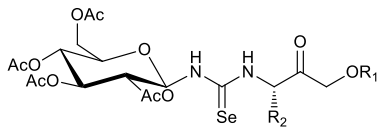

81 R_1=Et; R_2= H
82 R_1=Et; R_2=CH_2Ph
83 R_1=Et; R_2= CH_2OH
84 R_1=Et; R_2= iPr
85 R_1=Me; R_2=

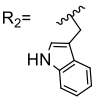

Among the selenocompounds studied, the remarkable results in terms of anti-radical capacity (reported in EC_{50}, effective concentration for scavenging 50% of the initial DPPH, stable free radical commonly used for the anti-radical activity

studies [38] were found for the naphthyl and sugar-based selenoureas. Compound **80** acted as the best free radical scavenger with an EC_{50} of 19.3± 3 μM (the well-known anti-oxidant ascorbic acid presents a scavenging activity of 13.3± 3 μM). Interesting, the anti-hydrogen peroxide activity of these selenourea is very low compared with the other seleno-based compound like selenocarbamate and selenohydantois that instead, can be considered as a good candidate as H_2O_2 scavengers.

Lopez and colleagues reported another application of selenourea species as antioxidant agents.[39] They designed and synthesised compound **86** that can be defined as a concrete example of dual multitarget drugs for the cure of the Gaucher disease and its side effects. The Gaucher pathology is a recessively inherited disease caused by a mutation of the GBA1 gene (glucocerebrosidase) that leads to the misfolding of the β-glucosidase. In addition, the loss of the cognitive function associated to the neurological complications of Gaucher disease involves the levels of acetylcholinesterase (AChE) that, in turn, is involved in some of the physiological manifestations of dementia-type diseases. Furthermore, an oxidative cellular stress condition, commonly associated with neurological pathologies, is observed in these conditions.[40,41] Structure **86** has been designed for inhibiting simultaneously β-glucosidase, responsible for the Gaucher disease, and acetylcholinesterease, connected with its effects, with an antioxidant activity at the same time due the presence of three specific moieties able to act selectively for each aspect above mentioned.

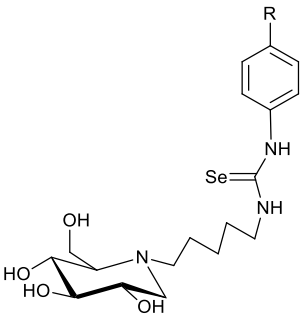

86a R=Br
86b R=OMe
86c R=Me

The presence of polyhydroxilate piperidines guarantees a glycosidase inhibitor site [42,43, 44] and the incorporation of an arylalkyl fragment on the nitrogen increases the selectivity for this process. The presence of Selenium in C=Se bond leads to an increase in the antioxidant activity with respect to the ROS species while the deoxynojirimycin residue of **86**, partially protonated at physiological pH values, can mimic the iminium cation of acetylcoline. All the synthesized compounds, in particular compound **86a**, were found to be strong competitive β-glucosidase (Ki in 1.6-5.5 μM range) and AChE inhibitors. The antiproliferative properties of compounds **86a-c** were tested on six solid human tumor cell lines with good results in the case of 6a with respect to A549,HBL-100 and T47D cell lines (GI_{50} 7.0-12.0 μM).

We report here the synthesis of a new family of functionalized selenourea compounds. On the base of the interesting acidic nature of the NHs protons of the selenourea site previously mentioned (see Chapter one), we decided to study these molecules for anion recognition. The anion sensing and binding ability of these systems were evaluated by means of NMR studies in order to verify the possibility to use these molecules as receptor for specific anionic targets.

4.2 Synthesis

Receptors **L_{25-31}**, were designed and successfully synthesized according to Scheme 4.1. The synthesis consists in a reaction between a suitable phenyl isoselenocyanate (phenyl,[45] naphthyl[45] and 4-chlorophenyl synthesized in agreement with Scheme 4.2) and an appropriate amine (aniline, 1-naphtylamine, 2,4-dichloroaniline, 2,4-dibromoaniline and 2-iodoaniline) in a mixture of dry DCM and EtOH. The receptors were obtained in a wide range of yields 21-84%. Bis-phenylurea and bis-phenylthiourea **L_{23}** and **L_{24}** were synthetized as controlreceptors. [46,47,48,49]

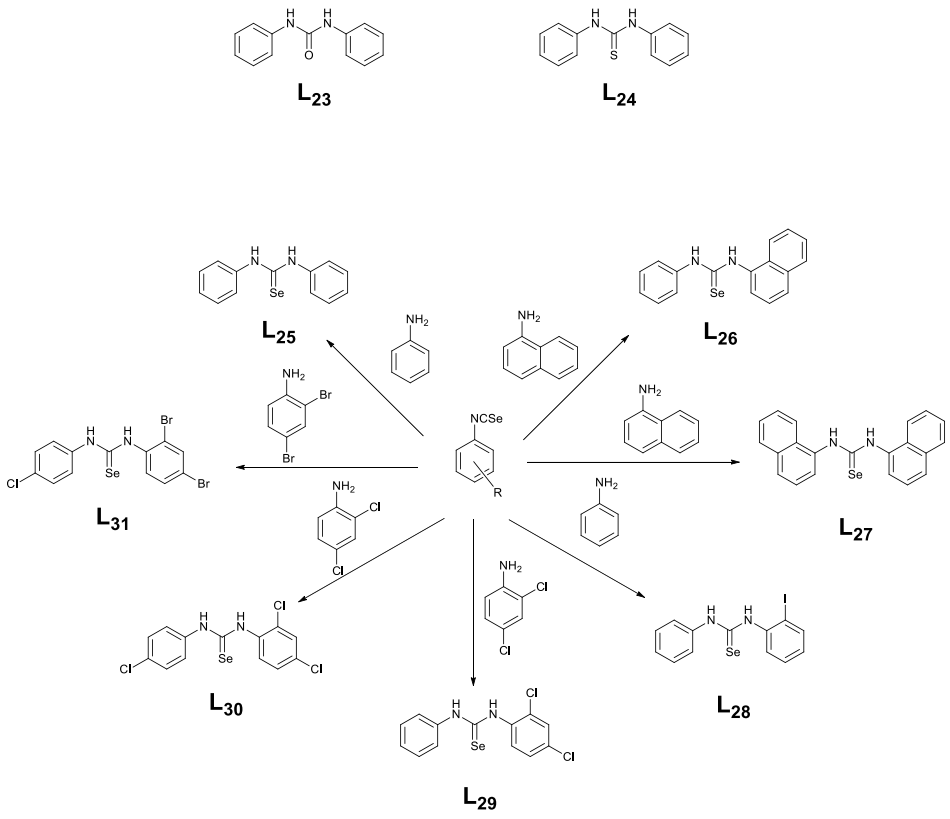

Scheme 4.1 Reaction scheme adopted for the synthesis of receptors **L_{25}-L_{31}**.

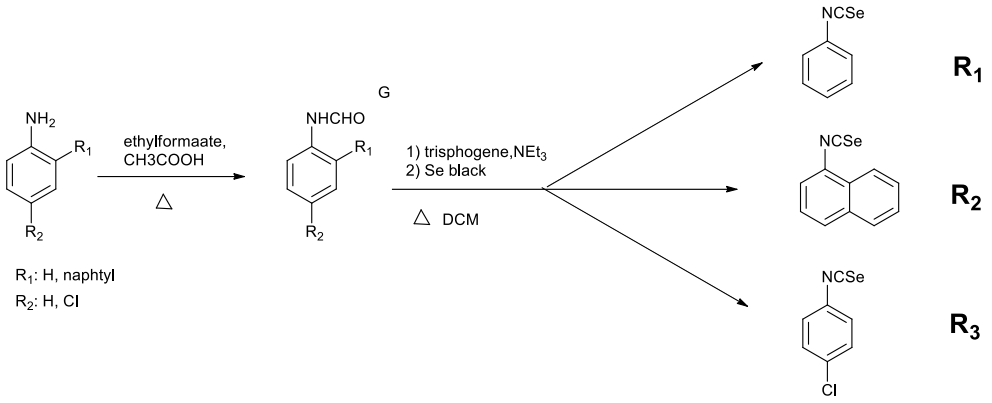

Scheme 4.2 Reaction scheme adopted for the synthesis of the isoselenocyanates $\mathbf{R_1}$-$\mathbf{R_3}$.

4.3 NMR spectroscopy studies

In order to evaluate the properties of the receptors during the complexation event with the anions, a detailed NMR study was carried out by means of titrations in DMSO-d_6 as competitive media and 2D-NMR techniques. First, a preliminary investigation of $\mathbf{L_{26}}$ (chosen as a reference receptor because of its simple and asymmetric structure) in the presence of acetate, used as control anion species, was performed, with the aim to better understand the behaviour of the selenourea-based receptor. Then, ^{1}H-NMR titrations with a specific anion set was carried out for all the synthesized receptors. The studied set involved anionic species with different geometry and space steric hindrance including AcO^-, $H_2PO_4^-$, Cl^- and BzO^-.

4.3.1 Preliminary investigations

The first part of the NMR analysis focussed on the titration, reported in Figure 4.1, of **L_{26}** with acetate. In theory, due to the asymmetric structure of the receptor we should predict the presence of only two NHs selenourea signals: one on the phenyl ring side and one on the naphthyl ring side. However, as it is possible to observe in the stack plot of the titration, six different singlet signals, suggesting the presence of more than one species in the system. These six signals were classified on the basis of their relative frequency as two signals at high (> 10 ppm), two at intermediate (around 10 ppm) and two at low frequencies (< 6 ppm) respectively.

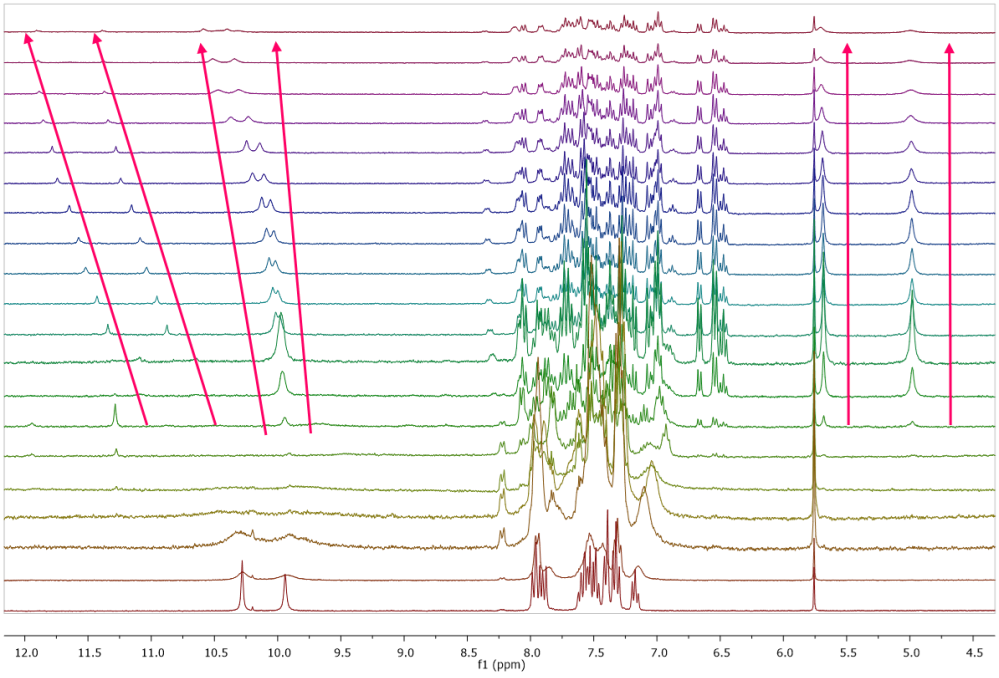

Figure 4.1 Stack plot of the titration of **L_{26}** (0.005M) with acetate as TBA salt (0.075M) in DMSO-d_6.

In order to better understand the presence of multiple species in solution and the nature of the new signals observed after the addition of the anion, a series of bidimensional NMR experiments like g-COSY, TOCSY and ROESY were carried out on a sample of $\mathbf{L_{26}}$ in DMSO-d_6 with 2.5 equivalents of acetate. This specific host:guest ratio was chosen because all of the six singlets were present and well resolved in the spectrum (see Figure 4.2).

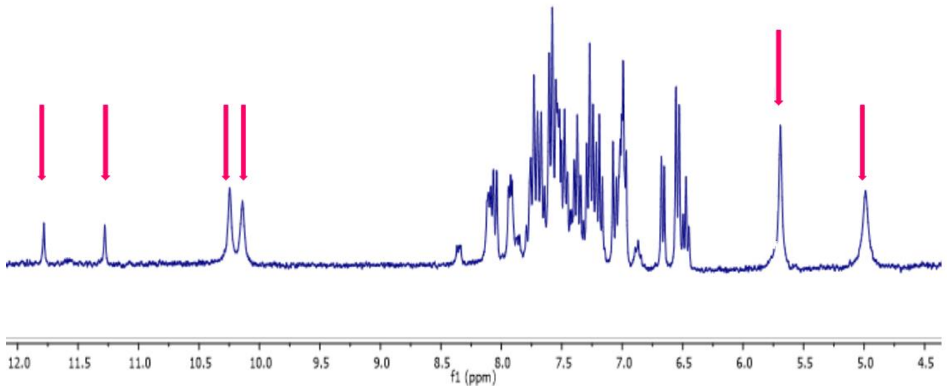

Figure 4.2 Spectrum in DMSO-d_6 of $\mathbf{L_{26}}$ (0.005M) with 2.5 equivalents of acetate as TBA salt (0.075M).

A series of considerations can be done on the basis of the results of the 2D-NMR experiments. First of all, by means of the g-COSY experiment no correlation *via* scalar coupling was found for these six peaks confirming the multiplicity observed. Then, an accurate analysis of the correlations found in the g-COSY spectrum, a total of 8 distinct spin were identified in the aromatic protons region.

Each of the identified spin-systems comprised three resonances and were divided into three groups, on the basis of frequency pattern and spectral range. It is worth noting that a total of three spin-systems are expected for the $\mathbf{L_{26}}$, one for the phenyl and two for the naphthyl moiety. Thus, the collected evidence

suggested the existence of at least three different species in the system. TOCSY and ROESY NMR experiments confirmed the connection between the proton signals previously attributed via g-COSY.

In addition, each of the above mentioned six singlets was found to correlate via dipolar through-space interaction with either one or two aromatic spin-systems, with biunivocal correspondence. Among the six singlets, a dipolar interaction (ROE) was found for the two downfield signals at 11.65 and 11.15 ppm indicating that the correspondent two protons belonged to the same species.

Finally, on the basis of all the collected evidence, theoretical spectra simulation and the well-known usual downfield shift of the protons involved in the coordination event, [50,51,52,53] we were able to attribute the observed resonances and identified spin-systems in a consistent and comprehensive scheme for all the species in the system.

These species and their NH protons were in agreement with the presence of one bi-coordinated and two different mono-coordinated adduct of receptor $\mathbf{L_{26}}$ with acetate as summarized in Figure 4.3 .

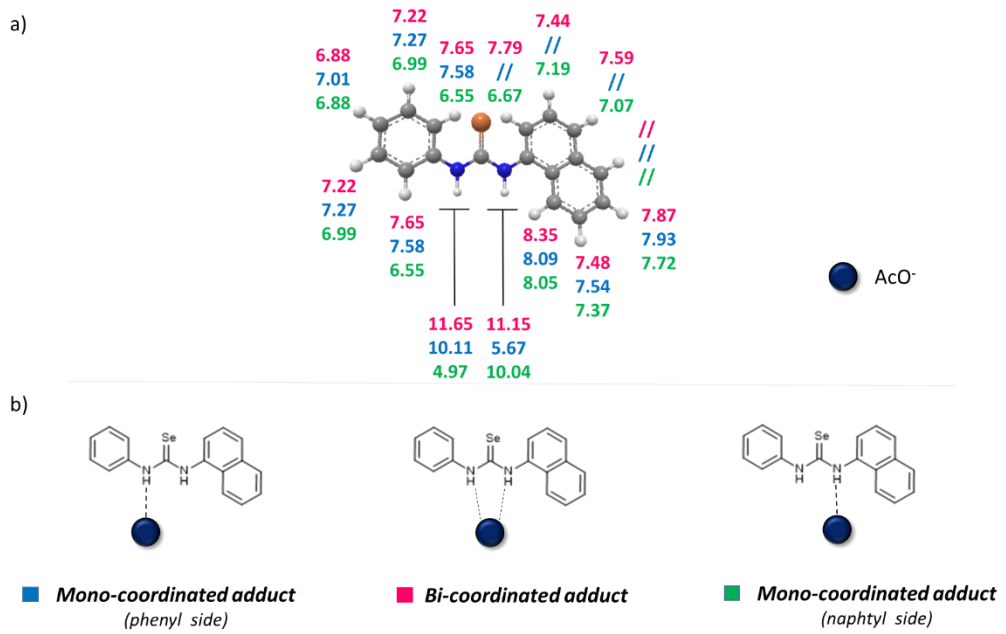

Figure 4.3 ^{1}H-NMR frequencies attribution of receptor **L$_{26}$** and the structures of the hypothesised mono and bi-coordinated adducts with acetate.

4.3.2 Anion binding: a qualitative ^{1}H-NMR study

With the aim to evaluate the anion binding ability of receptors **L$_{25\text{-}31}$**, ^{1}H-NMR titrations with an anionic set (AcO^-, $H_2PO_4^-$, Cl^- and BzO^-) were carried out on DMSO-*d$_6$* solution of the receptors. We decided to point the attention on three different aspects that could influence the complexation event: the variation of the heteroatom (O, S, and Se) in the C=X site, the type of anion target involved, and the steric hindrance of the receptors. To simplify the discussion of the results obtained we will focus, during the discussion, on the data of **L$_{25}$**, **L$_{26}$** and **L$_{27}$** chosen as control receptors. However, a similar behaviour was found for all the receptors studied (for the complete series of titrations of all receptors with the anion set investigated see paragraph 4.5.3).

4.3.2.1. Variation of the heteroatoms in the C=X site

As already mentioned in the Introduction chapter, moving from ureas, to thioureas and selenoureas, the NHs protons should be expected to be more acidic and at the same time, in theory, the hydrogen bond should be stronger.

In Figure 4.4 the titrations of the ligands **L_{23}**, **L_{24}** and **L_{25}** with acetate as a guest are reported. These receptors show the same symmetric bis-phenyl structure and the only variation is the presence of an Oxygen, Sulfur and Selenium atoms respectively in the C=X group.

a)

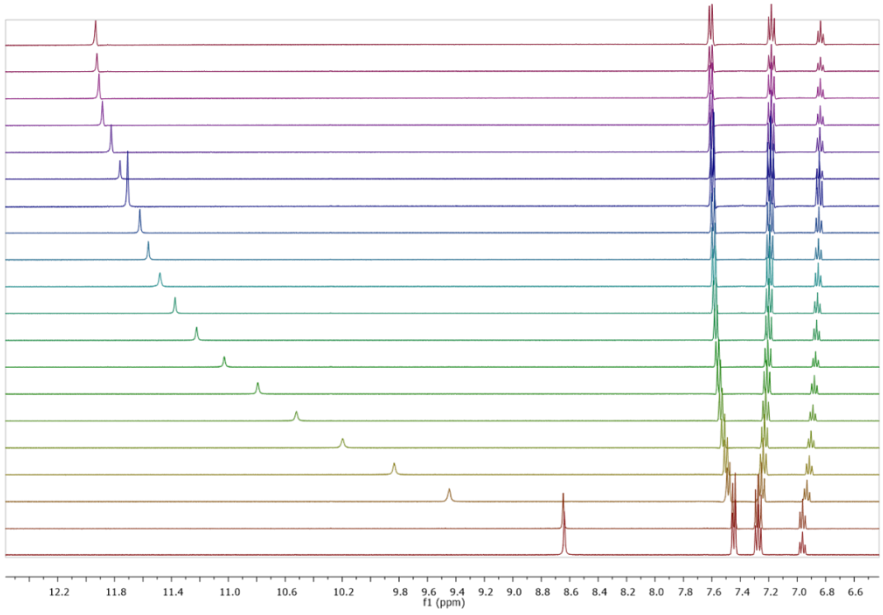

b)

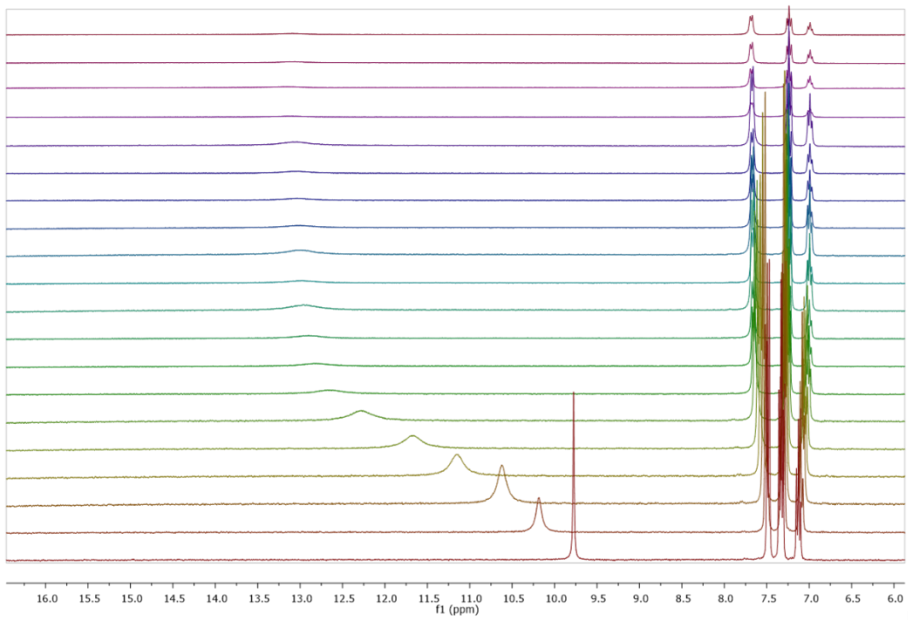

c)

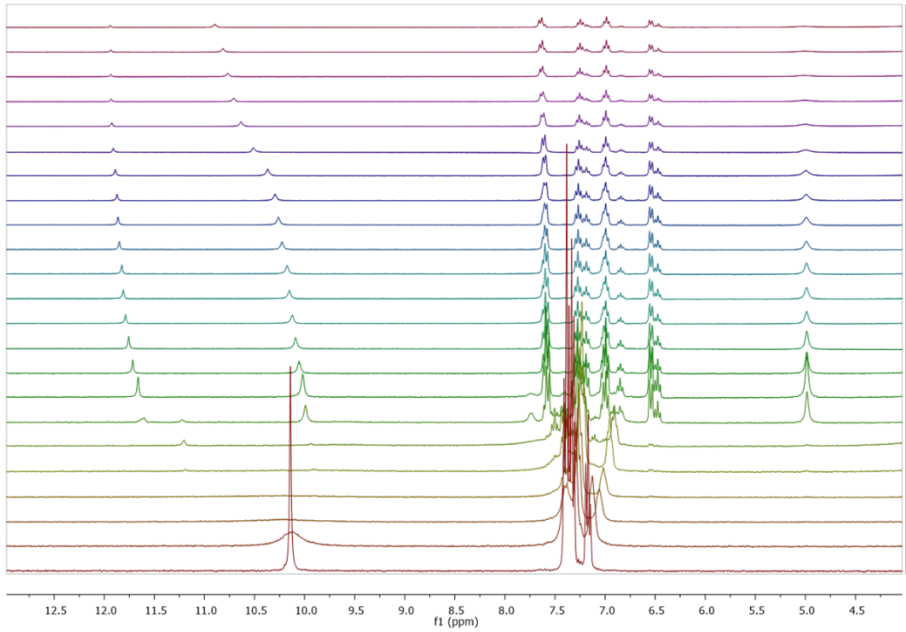

Figure 4.4 Stack plots of the titrations of **L_{23}**, **L_{24}** and **L_{25}** (0.005M) with acetate (0.075M) (a, b and c for the titration of **L_{23}**, **L_{24}** and **L_{25}**, respectively) in DMSO-d_6.

For receptors **L_{23}**, **L_{24}** an usual coordination behaviour was found. Upon addition of increasing amount of acetate, the well-known downfield shift of the NHs signals was observed for both ligands (Figure 4.4 a and b). As expected, because of the more acidic nature of the NHs, in the case of **L_{24}**, the addition of more than one equivalent of the guest caused the deprotonation of the receptor. In contrast, in the case of **L_{25}**, the host-guest interaction caused the disappearance of the NHs protons of the free receptor and the formation of three new peaks at 11.85, 10.29 and 4.99 ppm (Figure 4.4c). This evidence was consistent with the formation of the bi and mono-coordinated adduct as explained in the previously paragraph for receptor **L_{26}** with the same anion. The different behaviour found for the selenourea receptor with respect to the urea and the thiourea ligands under the same experimental conditions and in the presence of the same anion, has to be attributed to the presence of Selenium as heteroatom.

Roberts and co-workers reported a ^{1}H-NMR investigation of the effect of the hydrogen bond on the rotation rates around the C-N bonds in simple and methylated urea and thiourea molecules.[54] They demonstrated that the influence of the temperature and the interaction of urea and thiourea with acetate via hydrogen bond affects the rate of the rotation around the C-N bonds of these compounds. In absence of guest in both cases, the free receptor is able to rotate relatively fast (with respect to the NMR time scale) so that a single, time averaged NH peak is observed. By decreasing the temperature, the rotation becomes slower and slower, until two separate peaks of resonance appears, one for the *cis* and one for the *trans* protons with respect to the Oxygen/Sulfur atom, as shown in Figure 4.5a in the case of thiourea. Also the presence of hydrogen bond interaction influences the rotation. Stronger hydrogen bond leads to a change in the rotation energy barrier and the difference in the chemical shift between the two kinds of protons (*cis* and *trans*) becomes more evident (Figure

4.5 b for the urea system). Indeed, this effect was amplified for the thiourea with respect to the urea.

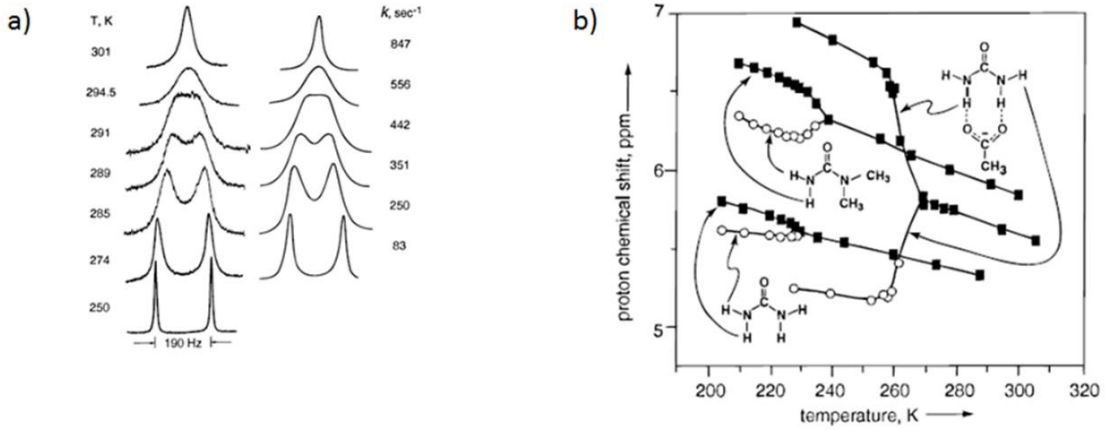

Figure 4.5 a) Temperature dependence of the ^{1}H resonances of 100 mM thiourea in DMF/DMSO-d_6. Experimental spectra on the left and calculated on the right. b) Temperature dependences of N-H chemical shift for urea, urea-acetate and 1,1-dimethylurea. All shifts measured relative to the dimethylformamide formyl resonance at 8.03 ppm. The points are (▪) and (◦) correspond to *trans*- and *cis*-urea protons. All graph and images are reported according to Ref. 54.

In the hypothesis that the hydrogen bond in the selenourea is even more strong than in the analogue urea and thiourea, we can suppose that the effect described above should be much more evident for the selenourea receptors and this theory could justify the presence of multiple species at the same time as observed only for the titration of **L$_{25}$** with acetate with respect to **L$_{23}$** and **L$_{24}$** (Figure 4.4c). A variable temperature ^{1}H-NMR experiment was carried out in order to prove this theory. By forcing the rotation with an increase of temperature, we should have been able to overcome the energy barrier and finally obtain only the bi-coordinated adduct. Unfortunately, increasing the temperature (up to 60°C, the maximum permitted by our NMR equipment) we were not able to reach the coalescence probably because the presence of Selenium strongly amplifies the range of the above discussed phenomenon and because of the higher steric

hindrance of the side-chains of the present receptors when compared to the molecules investigated by Roberts and co-workers. Nevertheless, the data obtained are consistent with the studies already reported in the literature.

4.3.2.2. Variation of the typology of the anion

Using receptor $\mathbf{L_{26}}$ as fixed reference receptor, titrations with acetate, benzoate, dihydrogen phosphate and chloride were carried out in DMSO-d_6 in order to evaluate the attitude of the receptor to coordinate anion of different size and geometries. Considering all the concepts explained in the previously paragraphs about the possibility to have one bi-coordinated and two mono-coordinated adducts (coordinated by the NH proton on either the phenyl or naphthyl side) we can summarised the results obtained from the titrations in Figure 4.6 where the species presented in each coordination system are clearly identified.

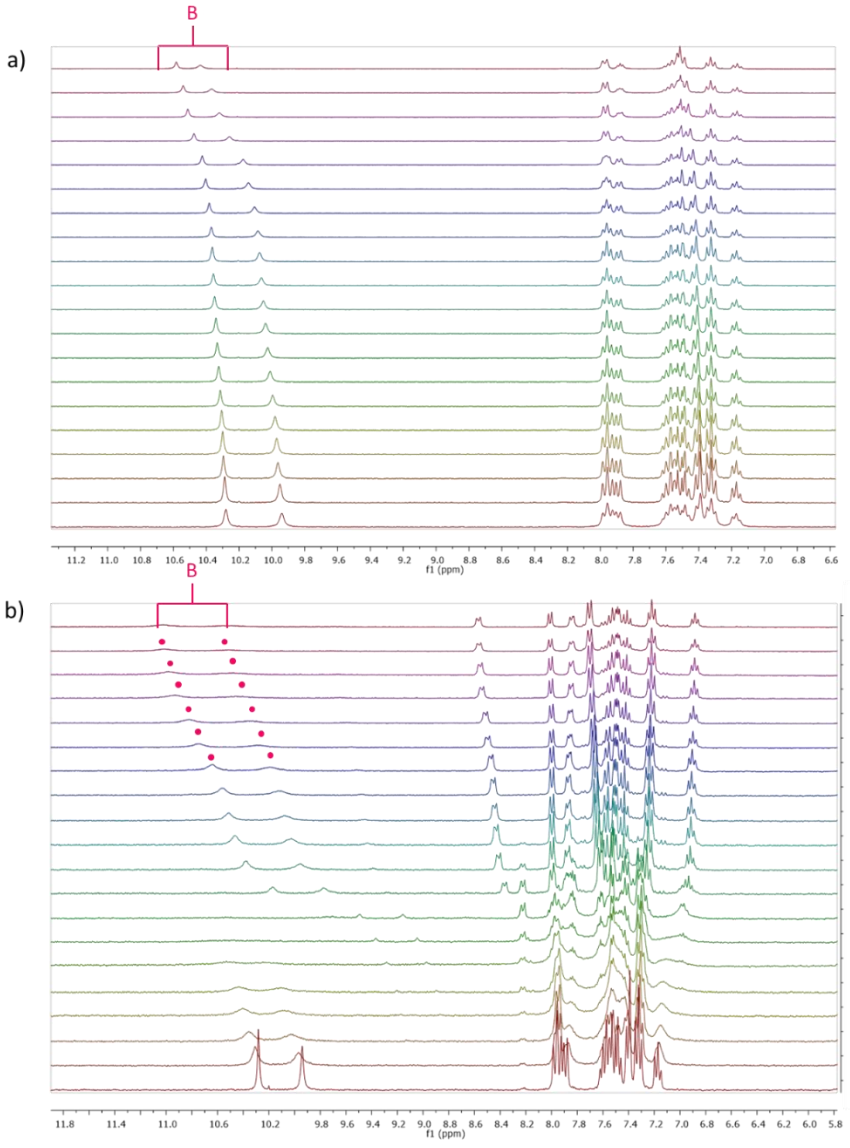
a)
B
11.2 11.0 10.8 10.6 10.4 10.2 10.0 9.8 9.6 9.4 9.2 9.0 8.8 8.6 8.4 8.2 8.0 7.8 7.6 7.4 7.2 7.0 6.8 6.6
f1 (ppm)
b)
B
11.8 11.4 11.0 10.6 10.2 9.8 9.6 9.4 9.2 9.0 8.8 8.6 8.4 8.2 8.0 7.8 7.6 7.4 7.2 7.0 6.8 6.6 6.4 6.2 6.0 5.8
f1 (ppm)

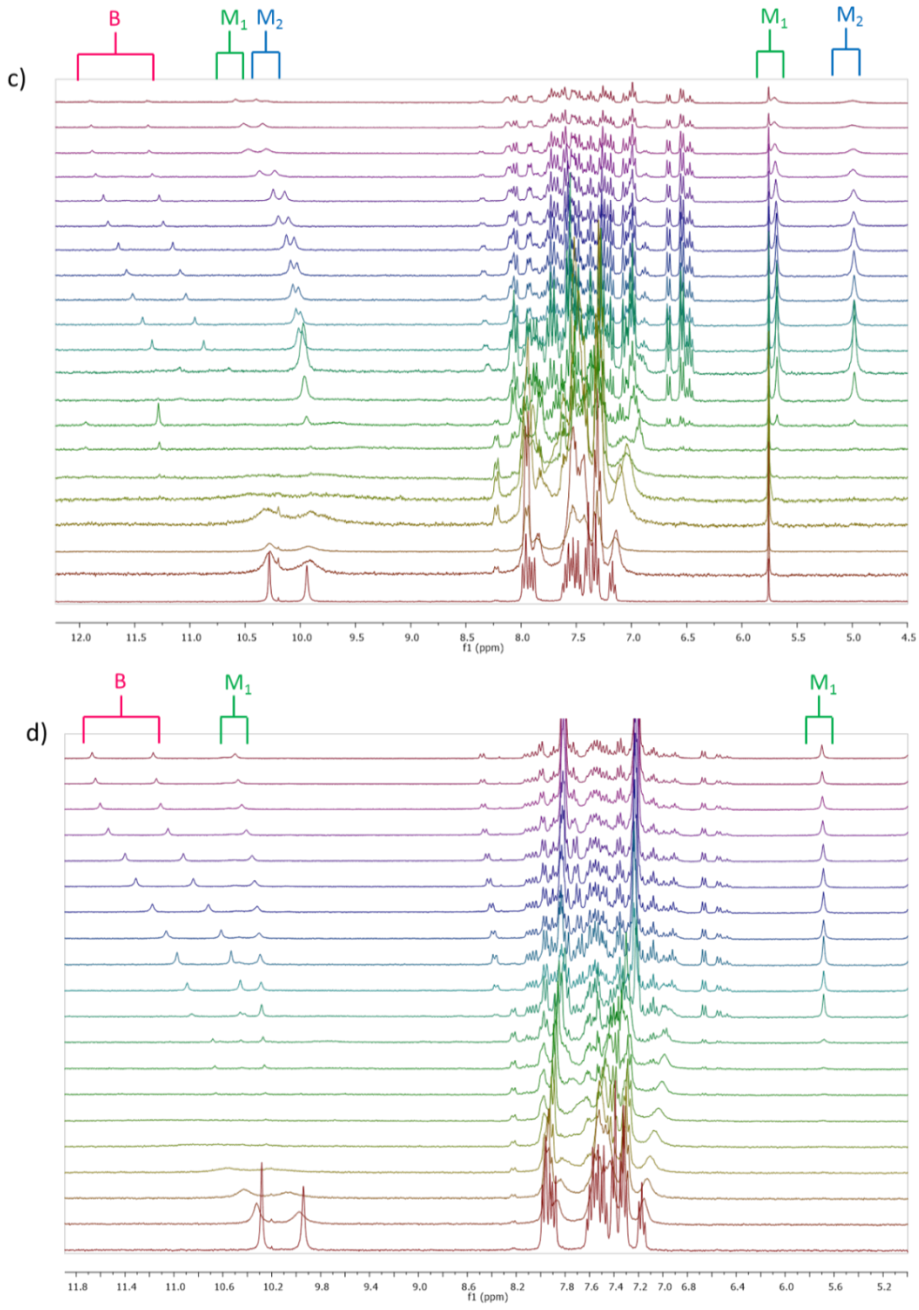

Figure 4.6 Stack plots of the titrations in DMSO-d_6 of **L_{26}** (0.005M) with Cl^-, $H_2PO_4^-$, AcO^- and BzO^- (figure a, b, c and d respectively) as TBA salt (0.075M). The label B, M1 and M2 indicate the bi-coordinated adduct and the two mono-coordinated forms, respectively. *In Figure b the presence of poorly visible peaks is indicated by red dots.

Summarising, in the case of chloride only a weak interaction with the receptor was found when an excess of anion was added (Figure 4.6a). The stack plot of the titration with dihydrogen phosphate shows only the presence of a bi-coordinated form while either acetate and benzoate present both bi-coordinated and mono-coordinated adduct forms (two mono-coordinated forms for acetate, only one for benzoate) (see Figure 4.6 c and d).

These behaviours can be explained considering the shape and the relative size of the different anions under investigation. Y-shape anion, as acetate and benzoate, are commonly coordinated by urea and thiourea receptors via two hydrogen bond interactions because of the high complementary of shape between them and the ureidic NH that point at the same direction. [46,55] However, we can postulate (see the structure simulations in Figure 4.7) that the presence of a large Selenium atom in the receptor influences the space disposition of the aromatic arms and consequently the directionality of the hydrogen bonds from the NHs protons (see Figure 4.7d).

We can suppose that Y-shape anions can also interact via one hydrogen bond at time without the proper shape complementarity between host and guest.

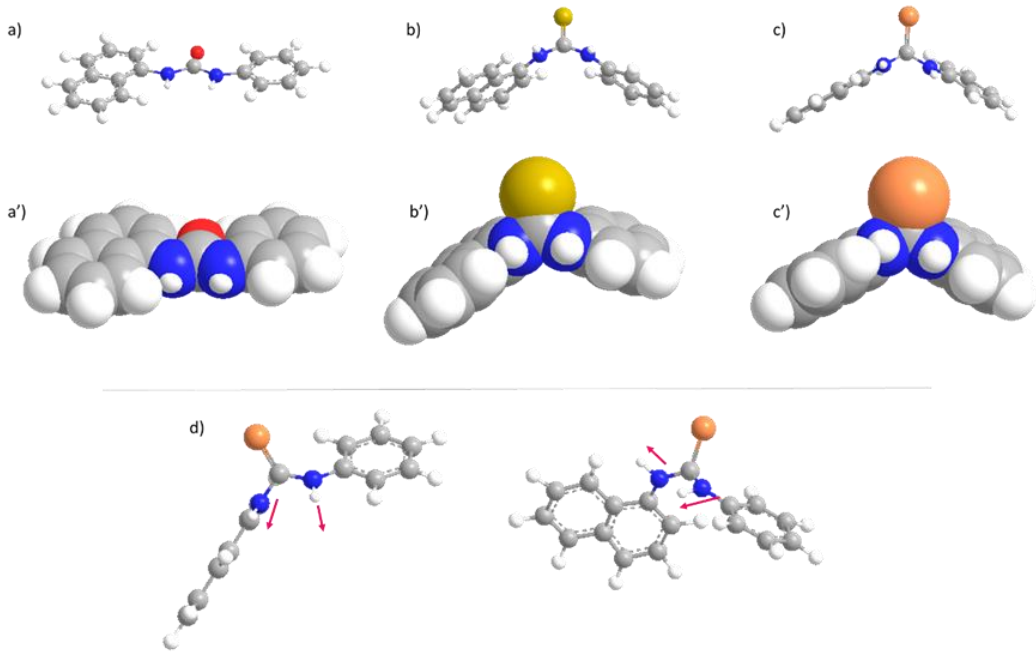

Figure 4.7 Ball and sticks and space fill representations of the 1-naphtyl-3phenyl urea (a and a'), thiourea (b and b') and selenourea (c and c') and NH hydrogen bonding directionality in the case of 1-naphtyl-3phenyl selenourea obtained using ChemBio3D (12.0 Version) software.

Indeed, the behaviour of both acetate and benzoate with receptor $\mathbf{L_{26}}$ is in agreement with this theory. Benzoate showed only one mono-coordinated adduct presumably due its higher steric hindrance when compared to acetate, which implied the formation of a preferential coordination direction (probably on the less cluttered phenyl side). However, depending on the rotation about C-N bond, also the bi-coordinated species appears (see Figure 4.6d).

In the titration of $\mathbf{L_{26}}$ with dihydrogen phosphate, only the formation of the bi-coordinated species was observed (see Figure 4.6b). The absence of mono-coordinated adduct can be explained by considering the tetrahedrical geometry

of the dihydrogen phosphate anion. The presence of four oxygen atoms that point to different directions should, in theory, facilitate the coordination event for receptors with a "distorted" conformation as **L_{26}** so that probavility to be coordinated by two hydrogen bonds from the NHs protons at the same time should increase (see Figure 4.6b).

4.3.2.3. Variation of the steric hindrance of the receptor

With the aim to evaluate the effect of the steric hindrance of the aromatic substituents of the receptors on the anion binding ability, ^{1}H-NMR titrations in DMSO-d_6 were carried out on receptors **L_{25}**, **L_{26}** and **L_{27}** solutions with acetate. The stack plots of the spectra collected for each titration are reported in Figure 4.8.

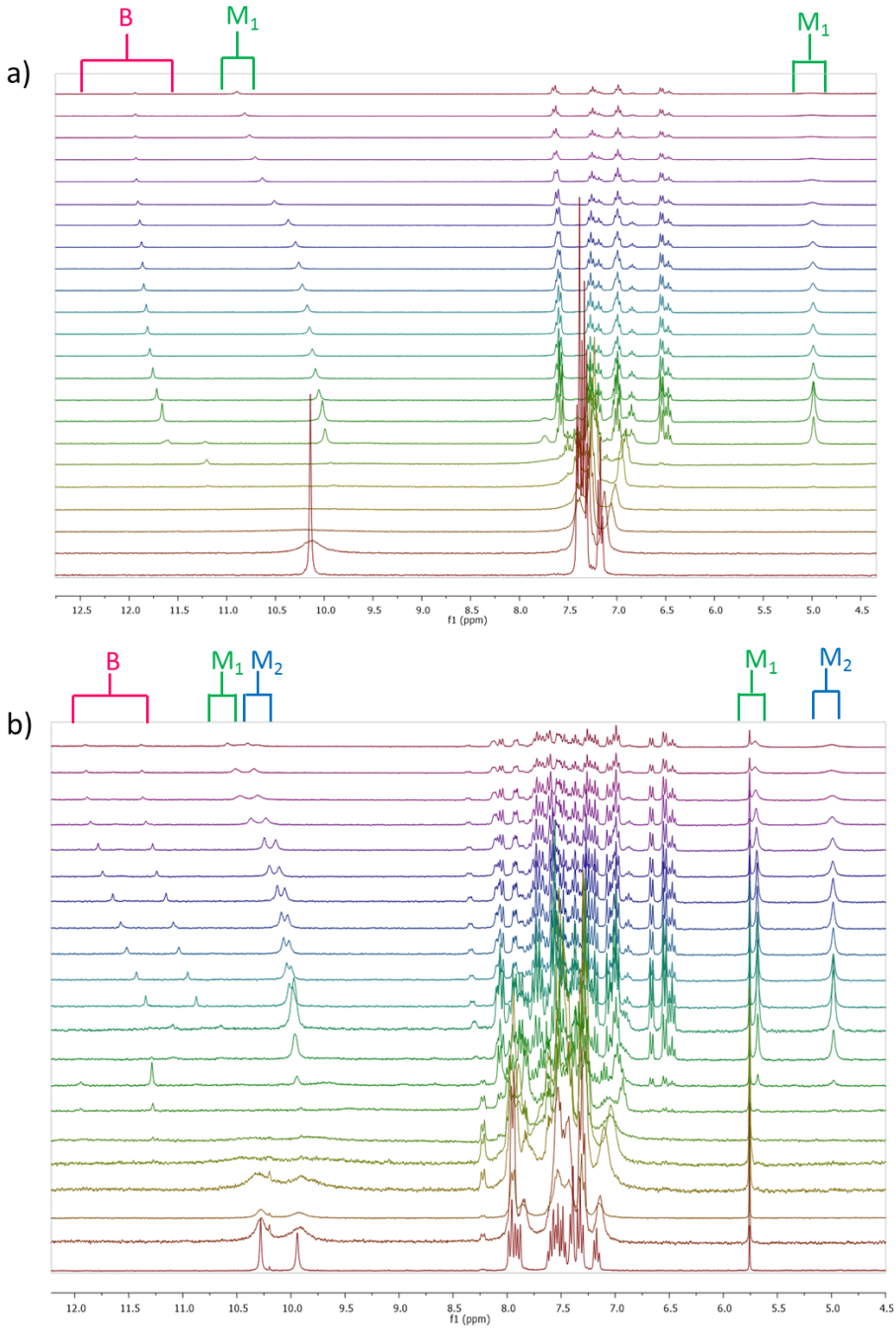
a)
B
M1
M1
12.5 12.0 11.5 11.0 10.5 10.0 9.5 9.0 8.5 8.0 7.5 7.0 6.5 6.0 5.5 5.0 4.5
f1 (ppm)
b)
B
M1
M2
M1
M2
12.0 11.5 11.0 10.5 10.0 9.5 9.0 8.5 8.0 7.5 7.0 6.5 6.0 5.5 5.0 4.5
f1 (ppm)

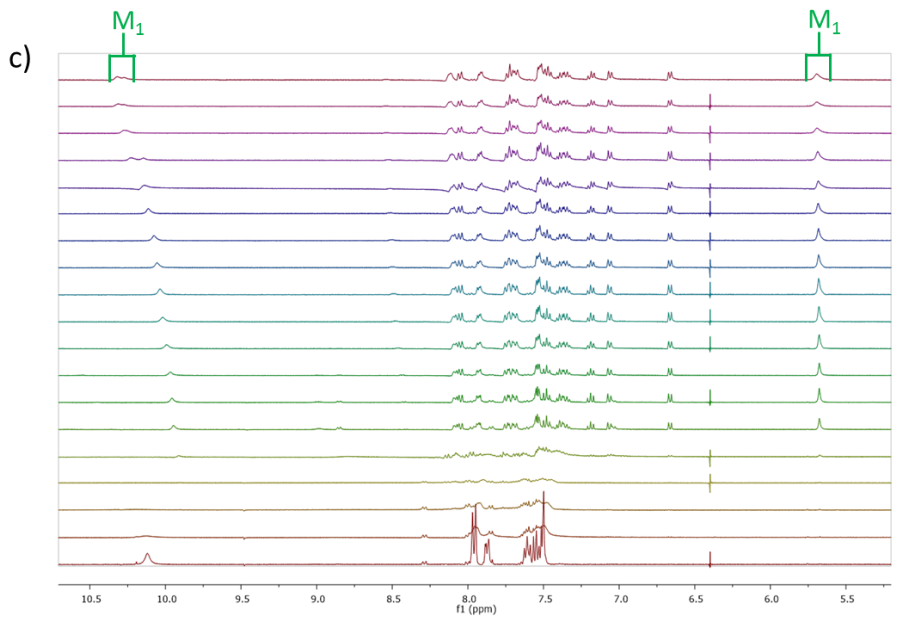

Figure 4.8 Stack plots of the titrations of **L25**, **L26** and **L27** (0.005M) (figure a, b and c, respectively) with acetate as TBA salt (0.075M) in DMSO-d_6

Both the titrations involving receptors **L25** and **L26** show the presence of the bi-coordinated adduct and the correspondent mono-coordinated form (one and two for **L25** and **L26**, Figure 4.8a and b respectively) while in the case of **L27** only the mono-coordinated specie appears. This evidence can easily find justification considering the different steric hindrance of **L27** with respect to the other two receptors. The presence of two naphthyl arms in the structure should probably slow down the rotation about the two C-N bonds and, in turn, the anion possibility to be coordinated via two hydrogen bonds should decrease considerably. The only adduct formed is the mono-coordinated as displayed in the stack plot reported in Figure 4.8 c.

4.4 Conclusion

We have successfully designed and synthesized receptor **$L_{25\text{-}31}$** with the aim to investigate the possibility to use these selenourea-based receptors for the anion recognition *via* hydrogen bond. This is the first study of this kind on selenourea molecules to the best of our knowledge. Using receptors **L_{25}**, **L_{26}** and **L_{27}** as control molecules, we were able to identify different trends in the coordinating behaviours of these systems depending on the kind of anion used and the steric hindrance of the receptor structure. We demonstrated that the presence of Selenium strictly influence the anion binding leading to the formation of different kinds of adducts, bi-coordinated or mono-coordinated: tetrahedrical anions encourage the formation of the former, while Y-shape guests favour the latter. These results could be used as the base for a future work on the possibility to tune the structure and the properties of selenourea-based compounds increasing their anion binding attitude.

4.5 Experimental methods

^{1}H (300 MHz) titrations and ^{13}C (75.5 MHz) NMR spectra were recorded on Bruker Avance-300 and Avance-500 spectrometers.Additional experiments (at 300K) for resonance assignments were acquired with a Unity Inova 500NB high-resolution spectrometer (Agilent Technologies, CA, USA) operating at a ^{1}H frequency of 500 MHz, equipped with a high-field indirect detection probe. The ^{1}H spectrum was acquired using a 6.6 µs pulse (90°), 1 s delay time, 1.5 s acquisition time and a spectral width of 8.0 kHz. ^{1}H-^{1}H correlation gCOSY experiment was recorded over the same spectral window using 2048 complex points and sampling each of the 256 increments with 64 scans. The same acquisition parameters have been applied, together with a mixing time of 80 ms (mixing scheme mlev17), for the

acquisition of the TOCSY. Also ROESY was acquired with the same parameters, with a mixing time of 200 ms (mixing scheme troesy). Chemical shifts for ^{1}H-NMR are reported in parts per million (ppm), calibrated to the residual solvent peak set, with coupling constants reported in Hertz (Hz). The following abbreviations are used for spin multiplicity: s = singlet, d = doublet, t = triplet, m = multiplet. Chemical shifts for ^{13}C NMR are reported in ppm, relative to the central line of a septet at δ = 39.52 ppm for deuteriodimethylsulfoxide. All solvents and starting materials were purchased from commercial sources where available. Proton NMR titrations were performed by adding aliquots of the putative anionic guest (as the TBA salt, 0.075 M) in a solution of the receptor (0.005M) in DMSO-d_6 to a solution of the receptor (0.005M). Mass spectra (CI, EI, FAB and LSI) were recorded on Kratos MS-80-RFA and Micromass AutoSpec-Q mass spectrometers with a resolution of 1000 or 10,000 (10% valley definition). For the FAB and LSI spectra, ions were produced by a beam of xenon atoms and Cs^{+} ions, respectively, using 1-thioglycerol as matrix and NaI as additive. TLC was performed on aluminum pre-coated sheets (E. Merck Silica Gel 60 F_{254}); spots were visualized by UV light, by charring with 10% H_2SO_4 in EtOH. Column chromatography was performed using E. Merck Silica Gel 60 (40–63 mm). All the reactions and purifications involving organoSelenium derivatives were carried out in the darkness by using aluminum foil.

4.5.1 Synthetic procedure

Synthesis of R_3

A solution of *para*-chloroaniline in ethylformiate (10mL) and 550 μL of acetic acid was stirred and refluxed for one day. By solvent evaporation a white solid was obtained and purified by column chromatography in Hexane:AcOEt in a ratio 1:1 (v/v) to obtain the correspondent formamide. Than, to a refluxing mixture of formamides (0.257 g, 1.65 mmol), Et_3N (7.19 mmol), and 4 Å molecular sieves in dry dichloromethane (5mL) was dropwise added a solution of triphosgene (0.260 g, 0.876 mmol) in dry dichloromethane (2 mL), under Ar, over a period of 1 h. After the addition, the resulting mixture was refluxed for 2.5 h and then black Selenium powder (0.260g, 3.29 mmol) was added and refluxed overnight. After a column chromatography in Hexane:AcOEt in a ratio 1:1 (v/v), the desired compound was obtained as white solid. Yield 50 % (0,179g, 0,827 mmol). ^{1}H-NMR (300 MHz,DMSO-*d_6*, 298K): δH: 7.58-7.51 (m, 4H). ^{13}C-NMR (75.5 MHz, DMSO-d_6, 298 K), δC: 132.97, 129.92, 128.39, 128.16, 127.74.

Synthesis of L_{25}

A solution of **R_1** (0.200 g, 1.098 mmol) in dry DCM (2mL) was added dropwise to a solution of aniline (0.102 g, 1,098 mmol) in ethanol absolute (2mL) in the darkness under Ar. The mixture was stirred for 4h at room temperature and then it was filtered to give the desired compound as white solid. Yield 84 %(0,255 g, 0,927 mmol). ^{1}H-NMR (300 MHz,DMSO-*d_6*, 298K): δH: 10.14 (s, 1H); 7.41-7.31 (m, 8H); 7.15 (t, 7.1, Hz, 2H). ^{13}C-NMR (75.5 MHz, DMSO-d_6, 298 K), δC: 179.40, 140.06, 128.92, 125.54, 125.22. ESI m/z 299.0051 $[M+Na]^+$.

Synthesis of L_{26}

A solution of **R_2** (0.200 g, 0,862 mmol) in dry DCM (2mL) was added dropwise to a solution of aniline (0.102 g, 0,862 mmol) in ethanol absolute (2mL) in the darkness under Ar. The mixture was stirred for 4h at room temperature and then it was filtered to give the desired compound as white solid. Yield 79 % (0,220 g, 0,676 mmol).^{1}H-NMR (300 MHz,DMSO-d_6, 298K): δH: 10.28 (s, 1H); 9.94 (s, 1H); 7.99-7.88 (m, 3H); 7.63-7.46 (m, 4H); 7.38 (d, J= 7.2 Hz, 2H); 7.30 (t, J= 7.8 Hz, 2H); 7.15 (t, J= 7.2 Hz, 1H). ^{13}C-NMR (75.5 MHz, DMSO-d_6, 298 K), δC: 180.30, 140.28, 136.07, 134.46, 130.35, 128.88, 128.58, 127.74, 126.75, 126.63, 126.22, 126.18, 125.95, 123.76. ESI m/z 349.0210 $[M+Na]^+$.

Synthesis of L_{27}

A solution of **R_2** (0.200 g, 0,862 mmol) in dry DCM (2mL) was added dropwise to a solution of naphthalenamine (0.123 g, 0,862 mmol) in ethanol absolute (2mL) in the darkness under Ar. The mixture was stirred for 4h at room temperature and then it was filtered to give the desired compound as white solid. Yield 55 % (0.178 g, 0,474mmol).^{1}H-NMR (300 MHz,DMSO-d_6, 298K): δH: 10.14 (s, 1H); 7.95 (d, J= 7.9, Hz, 2H); 7.91-7.87 (m, 1H); 7.64-7.51 (m, 4H); 7.42-7.33 (m, 4H); 7.21 (t, 7.2 Hz, 1H). ^{13}C-NMR (75.5 MHz, DMSO-d_6, 298 K), δC: 181.30, 136.28, 134.40, 130.66, 128.53, 127.83, 126.77, 126.68, 126.62, 126.17, 123.78. ESI m/z 399.0367 $[M+Na]^+$.

Synthesis of L_{28}

A solution of **R_1** (0.100 g, 0,549 mmol) in dry DCM (2mL) was added dropwise to a solution of 2-iodoaniline (0.120 g, 0,862 mmol) in ethanol absolute (2mL) in the darkness under Ar. The mixture was stirred for 4h at room temperature and then it was filtered to give the desired compound as white solid. Yield 21 % (0,046

g, 0,015 mmol).^{1}H-NMR (300 MHz,DMSO-*d*$_6$, 298K): δH: 10.19 (s, 1H); 9.79 (s, 1H); 7.86 (d, J= 7.8 Hz, 2H); 7.48 (d, J= Hz, 2H); 7.42-7.33 (m, 4H); 7.21 (t, 7.2 Hz, 1H). ^{13}C-NMR (75.5 MHz, DMSO-d$_6$, 298 K), δC: 179.62, 142.56, 139.56, 139.23, 130.74, 129.2, 129.16, 129.12, 126.04, 125.58, 100.69. ESI m/z 424.9013 $[M+Na]^+$.

Synthesis of L_{29}

A solution of **R_1** (0.200 g, 1.101 mmol) in dry DCM (2mL) was added dropwise to a solution of 2,4-dichloroaniline (0.178 g, 1.101 mmol) in ethanol absolute (2mL) in the darkness under Ar. The mixture was stirred for 4h at room temperature and then it was filtered and washed with hexane to give the desired compound as white solid. Yield 33% (0,113g, 0,328 mmol). ^{1}H-NMR (300 MHz,DMSO-*d*$_6$, 298K): δH: 10.33 (s, 1H); 9.84 (s, 1H); 7.68 (d, J= 1.7 Hz, 1H); 7.49-7.35 (m, 6H); 7.19 (t, 7.22 Hz, 1H). ^{13}C-NMR (75.5 MHz, DMSO-d$_6$, 298 K), δC: 180.03, 139.49, 137.04, 132.82, 132.36, 132.20, 129.47, 129.26, 127.99, 126.16, 125.42. ESI m/z 366.9268 $[M+Na]^+$.

Synthesis of L_{30}

A solution of **R_3** (0.331 g, 1.530 mmol) in dry DCM (2mL) was added dropwise to a solution of 2,4-dichloroaniline (0.248 g, 1.531 mmol) in ethanol absolute (2mL) in the darkness under Ar. The mixture was stirred for over night at room temperature and then it was filtered to give the desired compound as pale pink solid. Yield 62% (0.356 g, 0,940 mmol). ^{1}H-NMR (300 MHz,DMSO-*d*$_6$, 298K): δH: 10.32 (s, 1H); 9.98 (s, 1H); 7.69 (d, J= 1.7 Hz, 1H); 7.48-7.40 (m, 6H); ^{13}C-NMR (75.5 MHz, DMSO-d$_6$, 298 K), δC: 180.45, 138.67, 136.78, 132.81, 132.37, 132.28, 130.20, 129.58, 129.08, 128.11, 127.30. ESI m/z 378.9056 $[M+Na]^+$.

Synthesis of L_{31}

A solution of **R_3** (0.236 g, 1.087 mmol) in dry DCM (2mL) was added dropwise to a solution of 2,4-dibromoaniline (0.273 g, 1.088 mmol) in ethanol absolute (2mL) in the darkness under Ar. The mixture was stirred for over night at room temperature and then it was filtered to give the desired compound as white solid. Yield 59% (0.598 g, 1.279 mmol). ^{1}H-NMR (300 MHz,DMSO-*d_6*, 298K): δH: 10.29 (s, 1H); 9.94 (s, 1H); 7.94 (d, J= 1.7 Hz, 1H); 7.56 (t, J= 7,58 Hz, 1H); 7.48-7.36 (m, 5H); ^{13}C-NMR (75.5 MHz, DMSO-d_6, 298 K), δC: 180.18, 138.68, 138.64, 135.09, 132.80, 131.55, 130.20, 129.07, 127.35, 123.91, 120.72. ESI m/z 468.8027 $[M+Na]^+$.

4.5.2 ^{1}H-NMR titrations

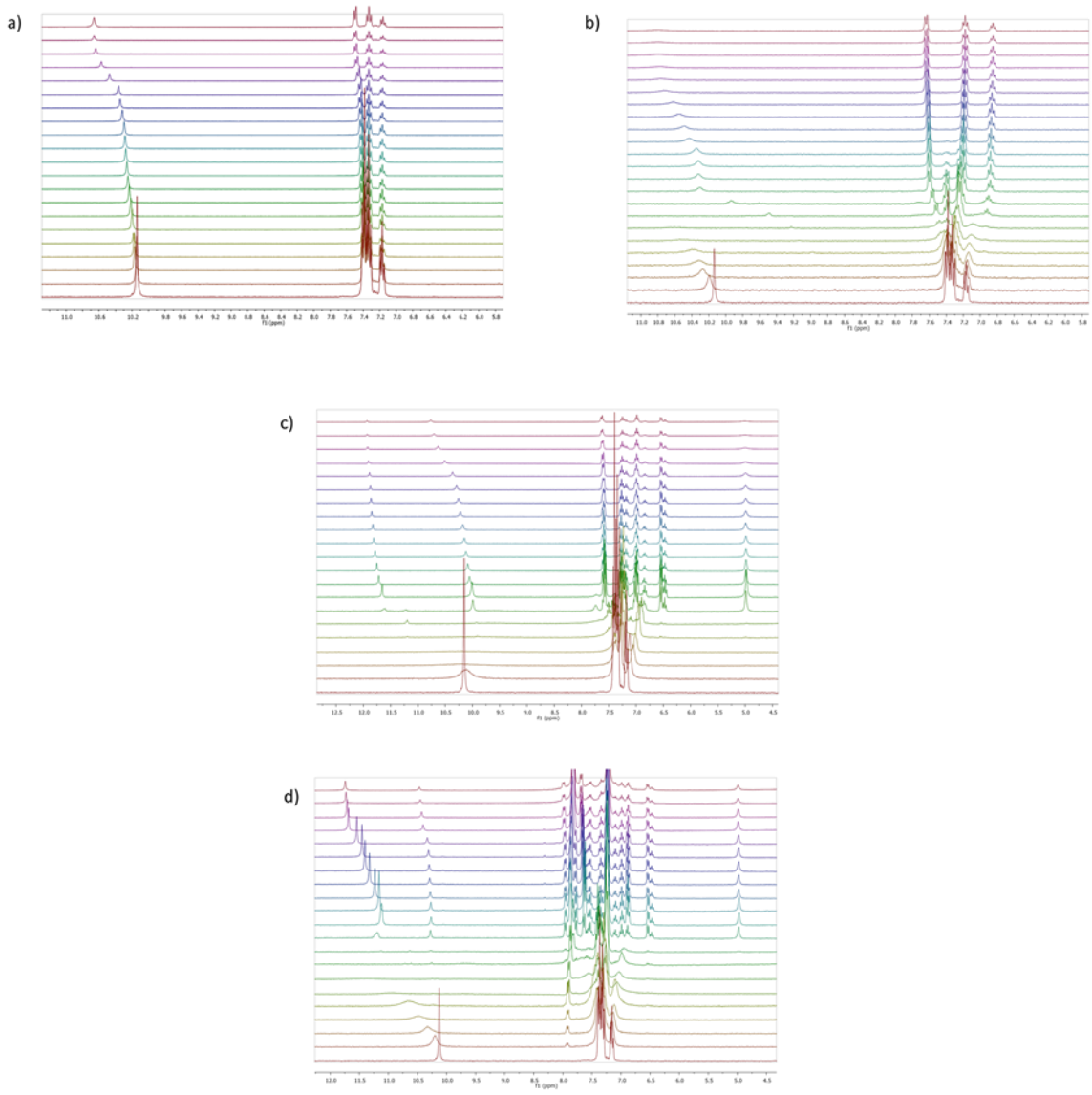

Figure 4.9 Stack plots of the ^{1}H-NMR titrations of **L_{25}** (0.005M) upon addition of increasing amounts of Cl^- (a), $H_2PO_4^-$ (b), AcO^- (c) and BzO^- (d) (0.075M) in DMSO-d_6.

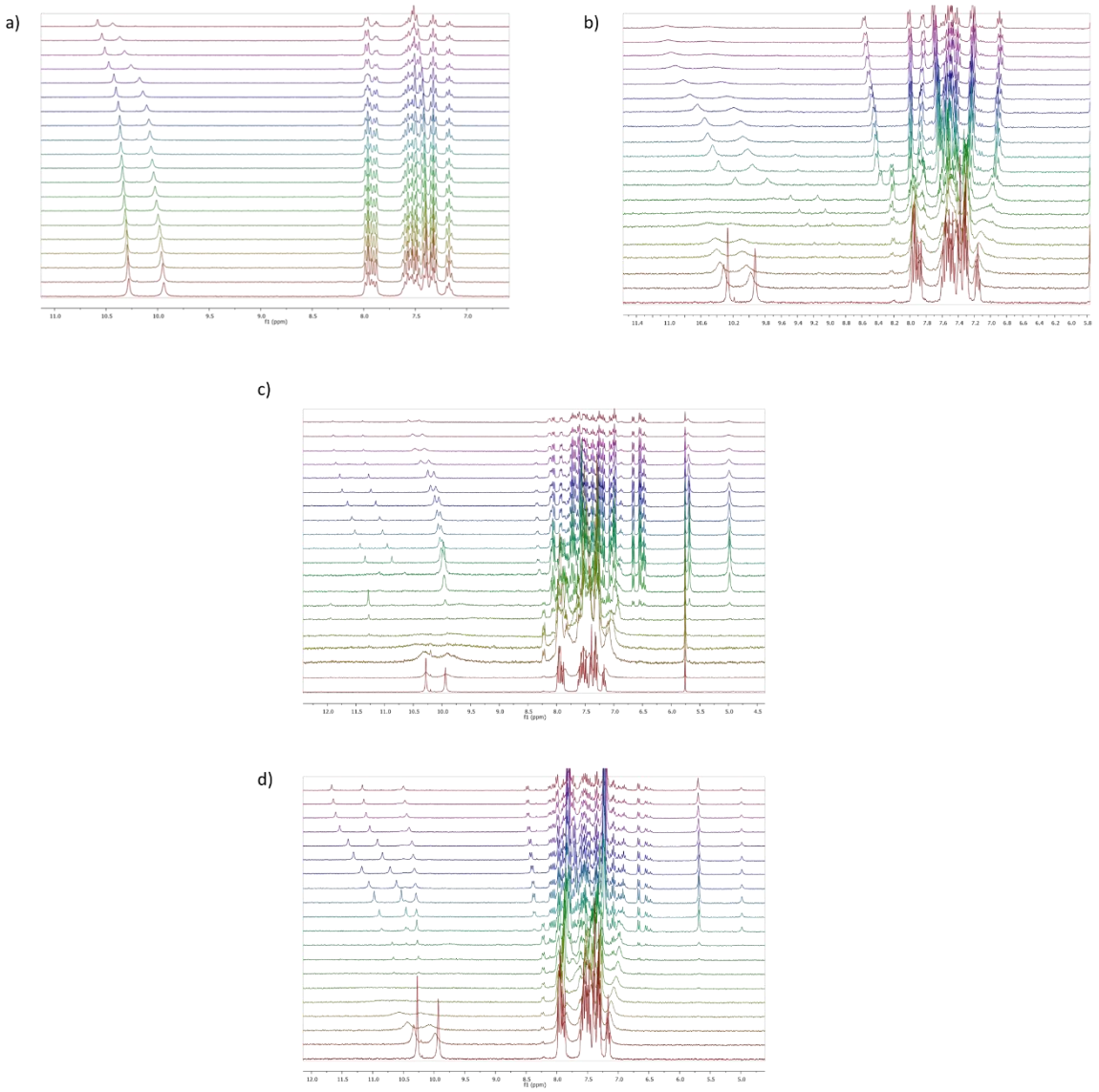

Figure 4.10 Stack plots of the ^{1}H-NMR titrations of **L_{26}** (0.005M) upon addition of increasing amounts of Cl^- (a), $H_2PO_4^-$ (b), AcO^- (c) and BzO^- (d) (0.075M) in DMSO-d_6.

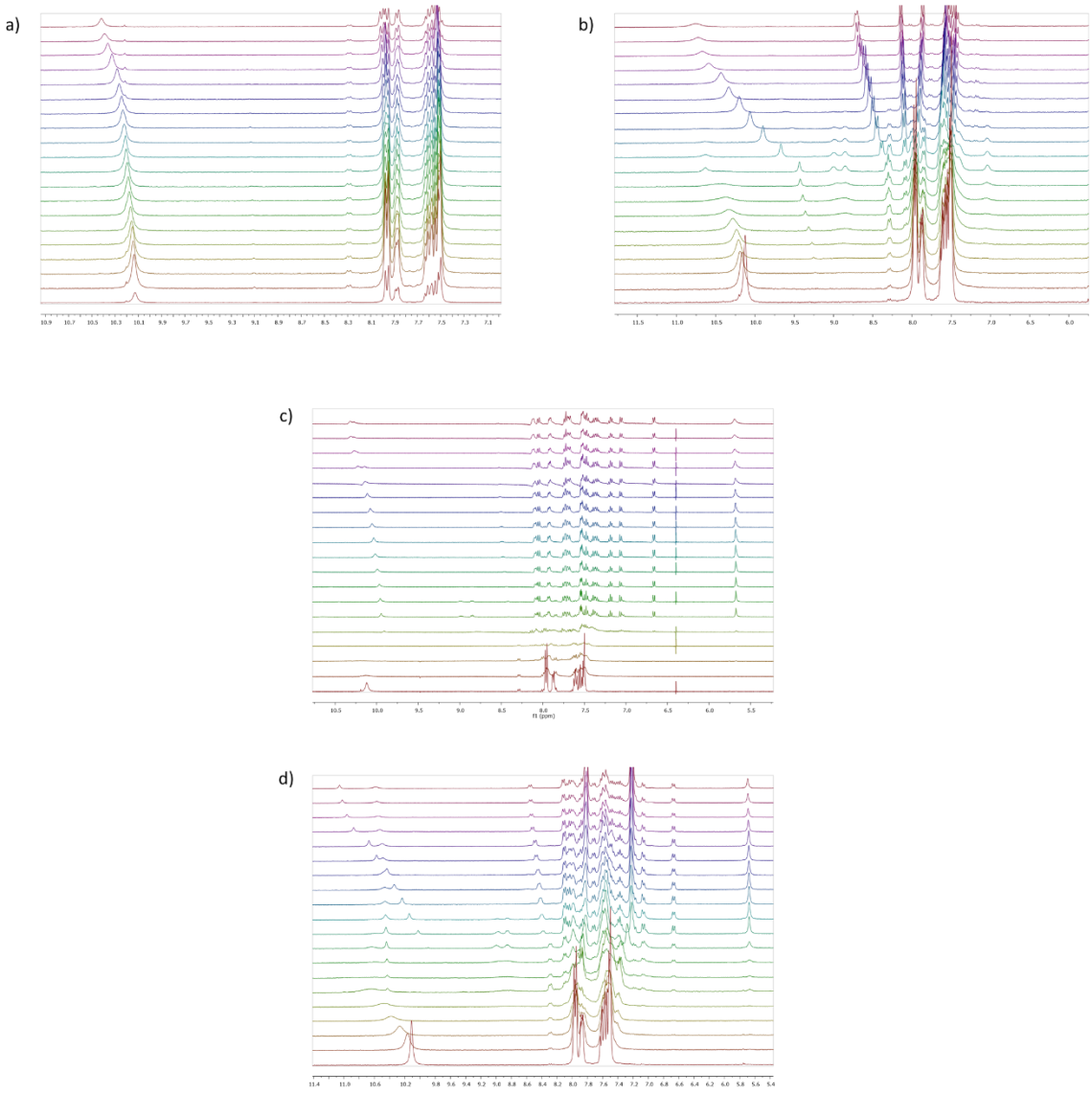

Figure 4.11 Stack plots of the ^{1}H-NMR titrations of **L_{27}** (0.005M) upon addition of increasing amounts of Cl^- (a), $H_2PO_4^-$ (b), AcO^- (c) and BzO^- (d) (0.075M) in DMSO-d_6.

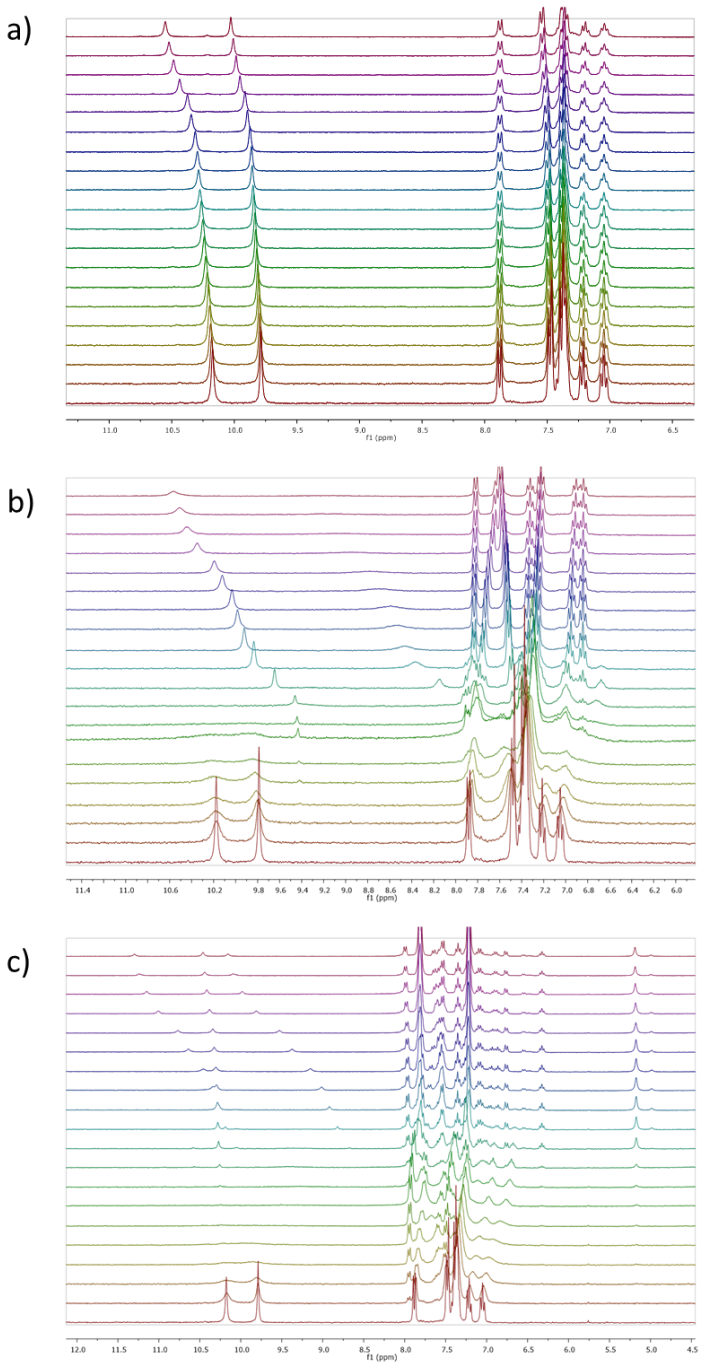

Figure 4.12 Stack plots of the ^{1}H-NMR titrations of **L_{28}** (0.005M) upon addition of increasing amounts of Cl^- (a), $H_2PO_4^-$ (b) and BzO^- (c) (0.075M) in DMSO-d_6.

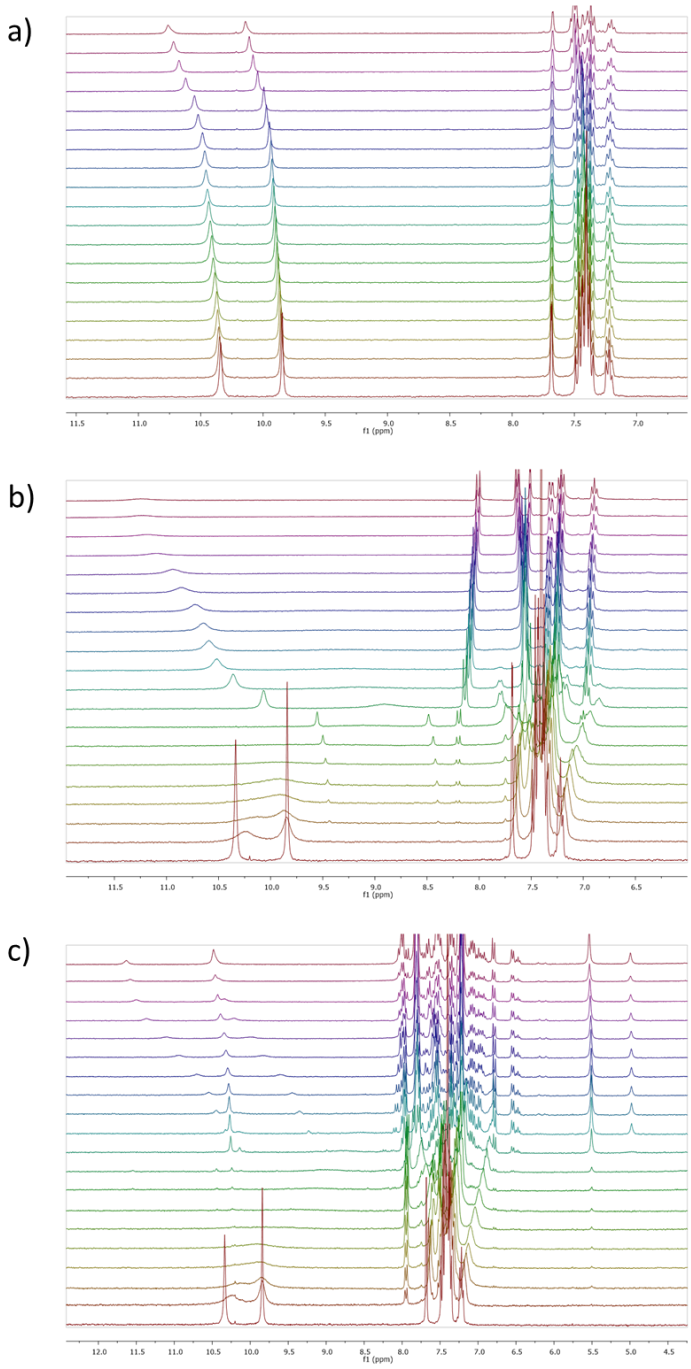

Figure 4.13 Stack plots of the ^{1}H-NMR titrations of **L_{29}** (0.005M) upon addition of increasing amounts of Cl^- (a), $H_2PO_4^-$ (b) and BzO^- (c) (0.075M) in DMSO-d_6.

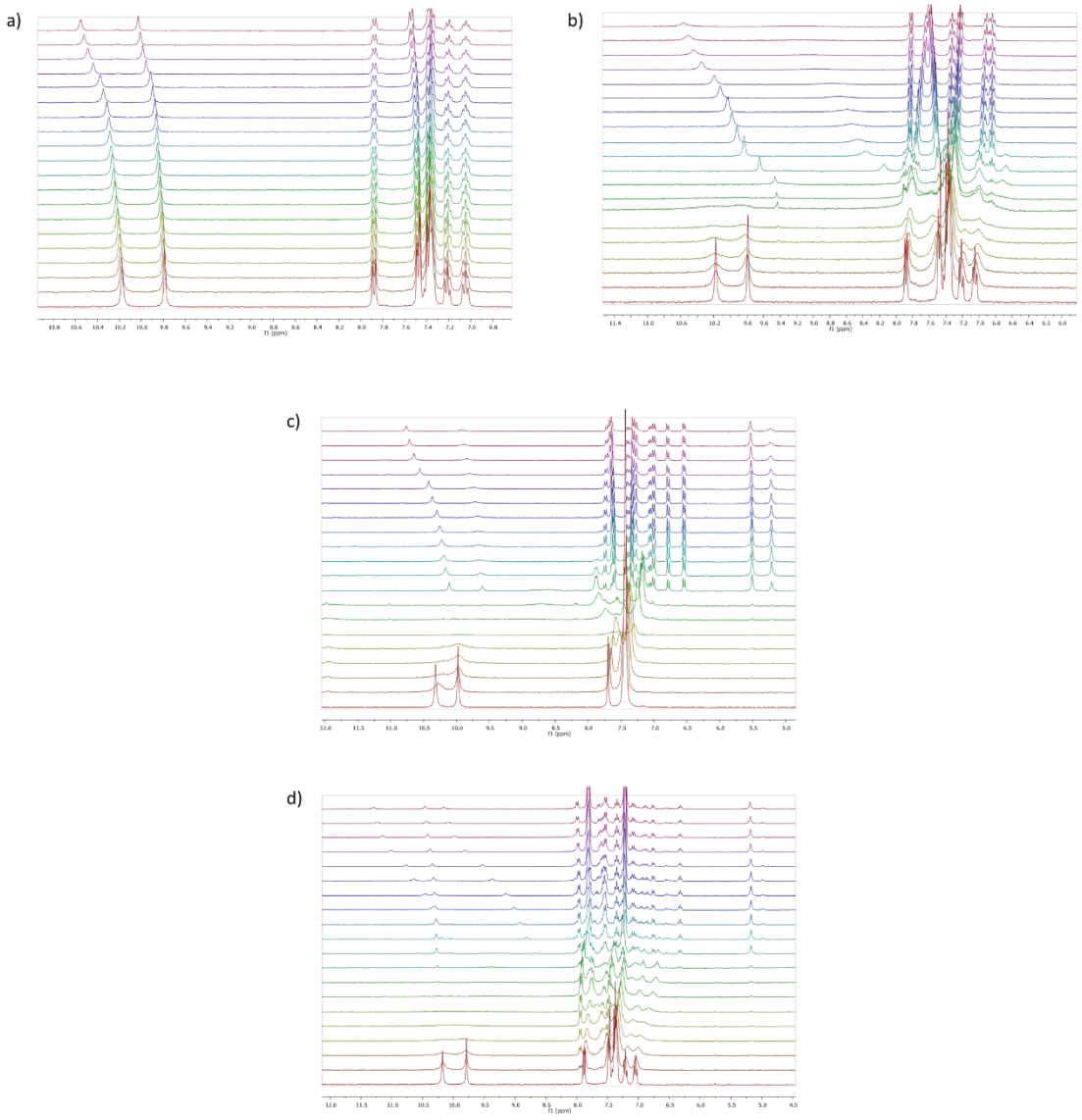

Figure 4.14 Stack plots of the ^{1}H-NMR titrations of **L_{30}** (0.005M) upon addition of increasing amounts of Cl^- (a), $H_2PO_4^-$ (b), AcO^- (c) and BzO^- (d) (0.075M) in DMSO-d_6.

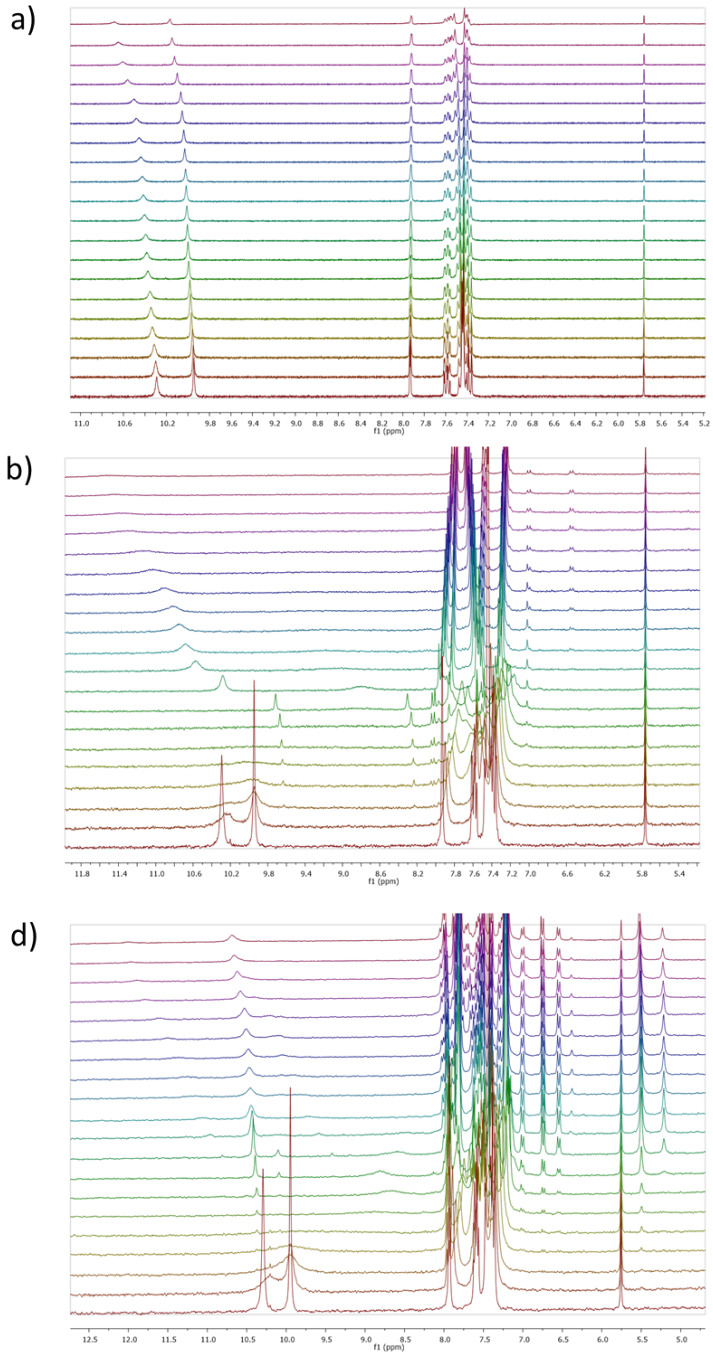

Figure 4.15 Stack plots of the ^{1}H-NMR titrations of **L_{31}** (0.005M) upon addition of increasing amounts of Cl^- (a), $H_2PO_4^-$ (b) and BzO^- (c) (0.075M) in DMSO-*d_6*.

References

1. Naithani, R., Organoselenium compounds in cancer chemoprevention. *Mini reviews in medicinal chemistry* **2008,** *8* (7), 657-668.

2. Wessjohann, L. A.; Schneider, A.; Abbas, M.; Brandt, W., Selenium in chemistry and biochemistry in comparison to sulfur. *Biological chemistry* **2007,** *388* (10), 997-1006.

3. Pire, L.; Deby-Dupont, G.; Lemineur, T.; Preiser, J.-C., How to keep oxidative stress under control? *Current Nutrition & Food Science* **2007,** *3* (3), 222-235.

4. Battin, E. E.; Brumaghim, J. L., Antioxidant activity of sulfur and selenium: a review of reactive oxygen species scavenging, glutathione peroxidase, and metal-binding antioxidant mechanisms. *Cell biochemistry and biophysics* **2009,** *55* (1), 1-23.

5. H Gandhi, U.; P Nagaraja, T.; Sandeep Prabhu, K., Selenoproteins and their role in oxidative stress and inflammation. *Current Chemical Biology* **2013,** *7* (1), 65-73.

6. Xu, T.; Liu, Y.; Meng, J.; Zeng, J.; Xu, X.; Mi, M., [The combined effects of insulin and selenium in improving insulin signal transduction in skeletal muscles of diabetic rats]. *Xi bao yu fen zi mian yi xue za zhi= Chinese journal of cellular and molecular immunology* **2013,** *29* (12), 1245-1250.

7. Madhunapantula, S. V.; Desai, D.; Sharma, A.; Huh, S. J.; Amin, S.; Robertson, G. P., PBISe, a novel selenium-containing drug for the treatment of malignant melanoma. *Molecular Cancer Therapeutics* **2008,** *7* (5), 1297-1308.

8. Lee, J.-H.; Shin, S. H.; Kang, S.; Lee, Y.-S.; Bae, S., A novel activation-induced suicidal degradation mechanism for Akt by selenium. *International journal of molecular medicine* **2008,** *21* (1), 91.

9. Rooprai, H. K.; Kyriazis, I.; Nuttall, R. K.; Edwards, D. R.; Zicha, D.; Aubyn, D.; Davies, D.; Gullan, R.; Pilkington, G. J., Inhibition of invasion and induction of apoptosis by selenium in human malignant brain tumour cells in vitro. *International journal of oncology* **2007,** *30* (5), 1263-1272.

10. Li, D.; Graef, G. L.; Yee, J. A.; Yan, L., Dietary supplementation with high-selenium soy protein reduces pulmonary metastasis of melanoma cells in mice. *The Journal of nutrition* **2004,** *134* (6), 1536-1540.

11. Akbaraly, N. T.; Arnaud, J.; Hininger-Favier, I.; Gourlet, V.; Roussel, A.-M.; Berr, C., Selenium and mortality in the elderly: results from the EVA study. *Clinical chemistry* **2005,** *51* (11), 2117-2123.

12. Balasankar, T.; Gopalakrishnan, M.; Nagarajan, S., Synthesis and antibacterial activity of some 5-(4-biphenylyl)-7-Aryl [3, 4-d]-1, 2, 3-benzoselenadiazoles. *Journal of enzyme inhibition and medicinal chemistry* **2007,** *22* (2), 171-175.

13. Soriano-Garcia, M., Organoselenium compounds as potential therapeutic and chemopreventive agents: a review. *Current medicinal chemistry* **2004,** *11* (12), 1657-1669.

14. Santi, C.; Santoro, S.; Testaferri, L.; Tiecco, M., A simple zinc-mediated preparation of selenols. *Synlett* **2008,** *2008* (10), 1471-1474.

15. Tiecco, M.; Testaferri, L.; Bagnoli, L.; Scarponi, C.; Temperini, A.; Marini, F.; Santi, C., Selenium promoted synthesis of enantiopure pyrrolidines starting from chiral aminoalcohols. *Tetrahedron: Asymmetry* **2007,** *18* (23), 2758-2767.

16. Valerio, S.; Iadonisi, A.; Adinolfi, M.; Ravidà, A., Novel approaches for the synthesis and activation of thio-and selenoglycoside donors. *The Journal of organic chemistry* **2007,** *72* (16), 6097-6106.

17. Witczak, Z. J.; Czernecki, S., Synthetic applications of selenium-containing sugars. *Advances in carbohydrate chemistry and biochemistry* **1998,** *53*, 143-199.

18. McGarrigle, E. M.; Myers, E. L.; Illa, O.; Shaw, M. A.; Riches, S. L.; Aggarwal, V. K., Chalcogenides as organocatalysts. *Chemical reviews* **2007,** *107* (12), 5841-5883.

19. Braga, A. L.; Ludtke, D. S.; Vargas, F., Enantioselective synthesis mediated by catalytic chiral organoselenium compounds. *Current Organic Chemistry* **2006,** *10* (15), 1921-1938.

20. Tiecco, M.; Testaferri, L.; Bagnoli, L.; Scarponi, C.; Temperini, A.; Marini, F.; Santi, C., Organoselenium mediated asymmetric cyclizations. Synthesis of enantiomerically pure 1, 6-dioxaspiro [4.4] nonanes. *Tetrahedron: Asymmetry* **2006,** *17* (19), 2768-2774.

21. Braverman, S.; Cherkinsky, M.; Birsa, M.; Ley, S.; Noyori, R.; Knight, J., Science of Synthesis. Thieme: Stuttgart: 2005.

22. Petrov, M.; Zmitrovich, N., Organic isoselenocyanates. *Russian journal of general chemistry* **1999,** *69* (2), 245-256.

23. Back, T. G., *Organoselenium chemistry: a practical approach*. OUP Oxford: 1999.

24. Garud, D. R.; Makimura, M.; Ando, H.; Ishihara, H.; Koketsu, M., First regioselective iodocyclization of O-allylselenocarbamates. *Tetrahedron Letters* **2007,** *48* (44), 7764-7768.

25. Barton, D. H.; Parekh, S. I.; Tajbakhsh, M.; Theodorakis, E. A.; Chi-Lam, T., A convenient and high yielding procedure for the preparation of isoselenocyanates. Synthesis and reactivity of O-alkylselenocarbamates. *Tetrahedron* **1994,** *50* (3), 639-654.

26. Heimgartner, H.; Zhou, Y.; Atanassov, P. K.; Sommen, G. L., Isoselenocyanates as Building Blocks for Selenium-Containing Heterocycles. *Phosphorus, Sulfur, and Silicon* **2008,** *183* (4), 840-855.

27. Sommen, G. L.; Linden, A.; Heimgartner, H., Selenium-Containing Heterocycles from Isoselenocyanates: 4-Methylselenazole Derivatives from the Reaction with Malononitrile and Propargyl Chloride. *Helvetica Chimica Acta* **2008,** *91* (2), 209-219.

28. Garud, D. R.; Koketsu, M.; Ishihara, H., Isoselenocyanates: a powerful tool for the synthesis of selenium-containing heterocycles. *Molecules* **2007,** *12* (3), 504-535.

29. Koketsu, M.; Ishihara, H., Thiourea and selenourea and their applications. *Current Organic Synthesis* **2006,** *3* (4), 439-455.

30. Merino-Montiel, P.; Maza, S.; Martos, S.; López, Ó.; Maya, I.; Fernández-Bolaños, J. G., Synthesis and antioxidant activity of O-alkyl selenocarbamates, selenoureas and selenohydantoins. *European Journal of Pharmaceutical Sciences* **2013,** *48* (3), 582-592.

31. Mishra, B.; Hassan, P.; Priyadarsini, K.; Mohan, H., Reactions of biological oxidants with selenourea: formation of redox active nanoselenium. *The Journal of Physical Chemistry B* **2005,** *109* (26), 12718-12723.

32. (a) Bhaskara Reddy, M. V.; Srinivasulu, D.; Peddanna, K.; Apparao, C.; Ramesh, P., Synthesis and Antioxidant Activity of New Thiazole Analogues Possessing Urea, Thiourea, and Selenourea Functionality. *Synthetic Communications* **2015,** *45* (22), 2592-2600; (b) Fernandes, A. P.; Gandin, V., Selenium compounds as therapeutic agents in cancer. *Biochimica et Biophysica Acta (BBA)-General Subjects* **2015,** *1850* (8), 1642-1660.

33. Thannickal, V. J.; Fanburg, B. L., Reactive oxygen species in cell signaling. *American Journal of Physiology-Lung Cellular and Molecular Physiology* **2000,** *279* (6), L1005-L1028.

34. Fang, Y.-Z.; Yang, S.; Wu, G., Free radicals, antioxidants, and nutrition. *Nutrition* **2002,** *18* (10), 872-879.

35. Kohen, R.; Nyska, A., Invited review: Oxidation of biological systems: oxidative stress phenomena, antioxidants, redox reactions, and methods for their quantification. *Toxicologic pathology* **2002,** *30* (6), 620-650.

36. Grek, C. L.; Tew, K. D., Redox metabolism and malignancy. *Current opinion in pharmacology* **2010,** *10* (4), 362-368.

37. Butterfield, D. A.; Perluigi, M.; Sultana, R., Oxidative stress in Alzheimer's disease brain: new insights from redox proteomics. *European journal of pharmacology* **2006,** *545* (1), 39-50.

38. Sharma, O. P.; Bhat, T. K., DPPH antioxidant assay revisited. *Food chemistry* **2009,** *113* (4), 1202-1205.

39. Olsen, J. I.; Plata, G. B.; Padrón, J. M.; López, Ó.; Bols, M.; Fernández-Bolaños, J. G., Selenoureido-iminosugars: A new family of multitarget drugs. *European Journal of Medicinal Chemistry* **2016,** *123*, 155-160.

40. Niedzielska, E.; Smaga, I.; Gawlik, M.; Moniczewski, A.; Stankowicz, P.; Pera, J.; Filip, M., Oxidative stress in neurodegenerative diseases. *Molecular neurobiology* **2015**, 1-32.

41. Lee, Y.-J.; Kim, S.-J.; Heo, T.-H., Protective effect of catechin in type I Gaucher disease cells by reducing endoplasmic reticulum stress. *Biochemical and biophysical research communications* **2011,** *413* (2), 254-258.

42. Yagi, M.; Kouno, T.; Aoyagi, Y.; Murai, H., The structure of moranoline, a piperidine alkaloid from Morus species. *Journal of the Agricultural Chemical Society of Japan* **1976**.

43. Butters, T.; Van den Broek, L.; Fleet, G.; Krulle, T.; Wormald, M.; Dwek, R.; Platt, F., Molecular requirements of imino sugars for the selective control of N-linked glycosylation and glycosphingolipid biosynthesis. *Tetrahedron: Asymmetry* **2000,** *11* (1), 113-124.

44. Lachmann, R. H., Miglustat: substrate reduction therapy for glycosphingolipid storage disorders. **2005**.

45. López, Ó.; Maza, S.; Ulgar, V.; Maya, I.; Fernández-Bolaños, J. G., Synthesis of sugar-derived isoselenocyanates, selenoureas, and selenazoles. *Tetrahedron* **2009,** *65* (12), 2556-2566.

46. Kadam, S. A.; Martin, K.; Haav, K.; Toom, L.; Mayeux, C.; Pung, A.; Gale, P. A.; Hiscock, J. R.; Brooks, S. J.; Kirby, I. L., Towards the Discrimination of Carboxylates by Hydrogen-Bond Donor Anion Receptors. *Chemistry–A European Journal* **2015,** *21* (13), 5145-5160.

47. Kadam, S. A.; Haav, K.; Toom, L.; Haljasorg, T. i.; Leito, I., NMR Method for Simultaneous Host–Guest Binding Constant Measurement. *The Journal of organic chemistry* **2014,** *79* (6), 2501-2513.

48. Etter, M. C.; Urbanczyk-Lipkowska, Z.; Zia-Ebrahimi, M.; Panunto, T. W., Hydrogen bond-directed cocrystallization and molecular recognition properties of diarylureas. *Journal of the American Chemical Society* **1990,** *112* (23), 8415-8426.

49. Lu, A.; Wang, Z.; Zhou, Z.; Chen, J.; Wang, Q., Application of “hydrogen bonding interaction” in new drug development: Design, synthesis, antiviral activity, and SARs of thiourea derivatives. *Journal of agricultural and food chemistry* **2015,** *63* (5), 1378-1384.

50. Casula, A.; Bazzicalupi, C.; Bettoschi, A.; Cadoni, E.; Coles, S. J.; Horton, P. N.; Isaia, F.; Lippolis, V.; Mapp, L. K.; Marini, G. M., Fluorescent asymmetric bis-ureas for pyrophosphate recognition in pure water. *Dalton Transactions* **2016,** *45* (7), 3078-3085.

51. Gale, P. A.; Busschaert, N.; Haynes, C. J.; Karagiannidis, L. E.; Kirby, I. L., Anion receptor chemistry: highlights from 2011 and 2012. *Chemical Society Reviews* **2014,** *43* (1), 205-241.

52. Amendola, V.; Fabbrizzi, L.; Mosca, L., Anion recognition by hydrogen bonding: urea-based receptors. *Chemical Society Reviews* **2010,** *39* (10), 3889-3915.

53. Gómez, D. E.; Fabbrizzi, L.; Licchelli, M.; Monzani, E., Urea vs. thiourea in anion recognition. *Organic & biomolecular chemistry* **2005,** *3* (8), 1495-1500.

54. Haushalter, K. A.; Lau, J.; Roberts, J. D., An NMR Investigation of the Effect of Hydrogen Bonding on the Rates of Rotation about the CN Bonds in Urea and Thiourea. *Journal of the American Chemical Society* **1996,** *118* (37), 8891-8896.

55. Brooks, S. J.; Gale, P. A.; Light, M. E., Carboxylate complexation by 1, 1'-(1, 2-phenylene) bis (3-phenylurea) in solution and the solid state. *Chemical communications* **2005,** (37), 4696-4698.

Chapter 5:

Selenoureas:

a new class of chemosensors for anion recognition

5. Selenoureas: a new class of chemosensors for anion recognition

5.1 Introduction

Moving down along the chalcogen group, in the Periodic Table, interesting trends in binding properties can be put in evidence. In compounds containing chalcolgen atoms, the absorption and emission maxima shift to longer wavelengths changing the atom from Oxygen to Sulfur to Selenium and also their softness increases. On this purpose, Selenium shows a borderline hard/soft nature that can be tuned as required to recognize specific analyte targets. Due to the low oxidation potential of Selenium and its capacity to change its valance state, organoselenium derivatives are very sensitive in oxidizing species such as thiols and ROS.[1,2] Moreover, the high reactivity of selenoderivatives, in particular Se-P, Se-N and Se-O bonds, makes these compounds very attractive for fluorescence detection via chemical reactions.

For these reasons, nowadays, selenoderivatives sensing probes able to recognize neutral and ionic species through economic techniques such as fluorescence and UV-Visible spectroscopies are developing in the supramolecular chemistry.[3]

5.1.1 Selenoderivative probes for neutral molecules

Tang and coworkers have reported the synthesis and the recognition properties of the organoSelenium based probe **87** able to recognize thiols, in particular GSH, also in live cells by means of fluorescence spectroscopy with high signal to noise ratio. [4] Receptor **87** was synthetized by reaction between selenenyl chloride and the well known fluorescence dye rhodamine 110. This receptor does not show fluorescence emission in the free form but the interaction with thiols results in a Se-N bond cleavage with the consequent increase of the emission intensity of the system.

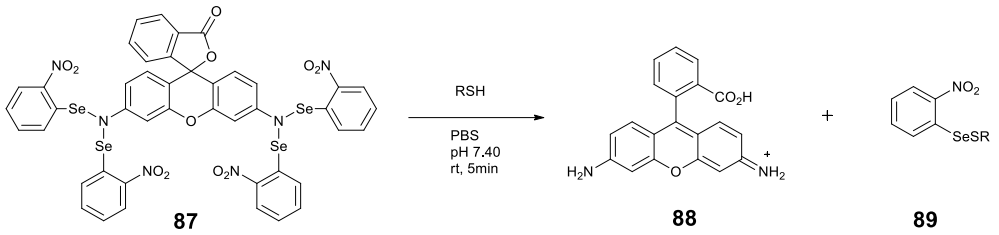

The study focused on GSH species as representative thiol because of its higher abundance in cells. The binding capacity of 8 was performed at 25°C in aqueous solution (PBS, pH 7.40) and upon addition of GSH a pronounced fluorescence increase was observed instantly up to 5 min (Figure 5.1 a) indicating a good selectivity of receptor **87** to GSH species. Moreover, the change in the emission properties of the receptor after the interaction with the target causes also a chromatic variation of the system from light yellow (free receptor) to yellow-green (receptor upon addition of GSH) as reported in (Figure 5.1 b) .

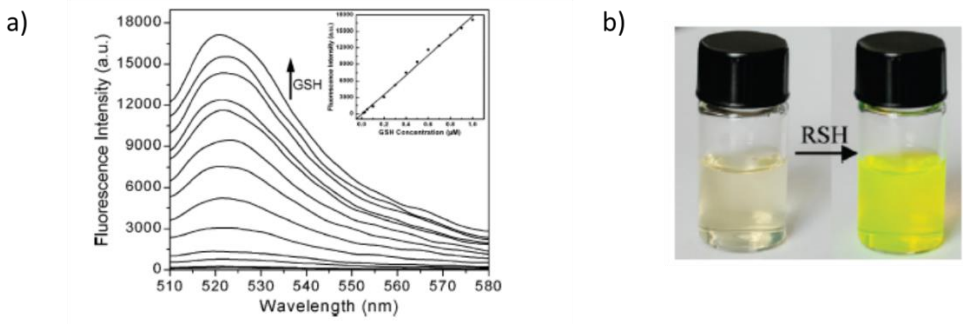

Figure 5.1 a) Fluorescence responses of Receptor **87** (0.50 mM) after the addition of GSH after incubation at 25 °C for 5 min in PBS (pH 7.40, 15 mM). b) The colour change of Receptor **87** (15 mM) upon addition of a thiol (60 mM). All graph and images are reported according to Ref.4.

Then, the selectivity of receptor **87** was evaluated also within living cells. In particular, cell lines HL-7702 cells and HepG2 were chosen. Normal hepatocytes (HL-7702) display high levels of thiols while cells affected by oxidative stress (HepG2) commonly show a decline in thiol concentration.[4] The receptor was incubated in cells for 5min at 37 °C (1 : 100 DMSO–PBS v/v, pH 7.40 environment) and as expected a strong fluorescence intensity was found through confocal microscopy in the case of HL-7702 line cells while only a weak emission intensity was observed for HepG2 line. This result suggests the interesting and concrete applicability of **87** as fluorescence imaging probe for thiols in cells.

Han and coworkers reported the Selenium derivative probe **90** that can recognize in a selective way hypochloric acid. [5,6] The spectroscopy properties of this receptor were studied under physiological conditions (20 mM PBS, pH 7.40) where it was found that **90** is able to binding HOCl with a good selectivity. Upon addition of increasing amount of NaOCl as a HOCl source, an increase in the emission intensity was observed and on the base of these data a detection limit of 10.86 10^{-7} M was determined for NaClO (Figure 5.2).

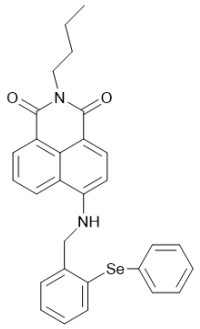

90

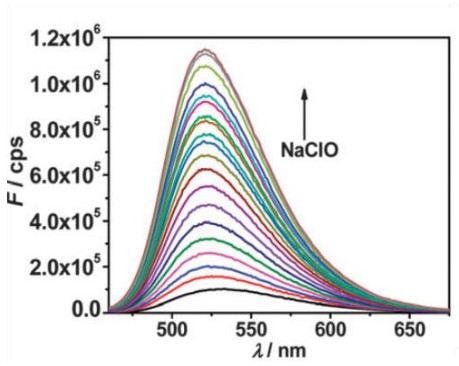

Figure 5.2 Changes in the fluorescence spectra of Receptor **90** with different concentrations of NaOCl. The graph is reported according to Ref.5-6.

The proposal mechanism of probe **90** is reported in Scheme 5.1 . Basically, the key point of the mechanism of this system is the fluorescence modulation between selenide and selenoxide. Viscosity and temperature-dependent experiments demonstrated that the increase of the fluorescence intensity of **90** after interaction with NaOCl can be associated to an excited state configuration twist process. The nonbonding interaction between the Se and N atoms results in the weak fluorescence of **90**. The system shows no interferences by reducing agents except for H_2S and thiols.

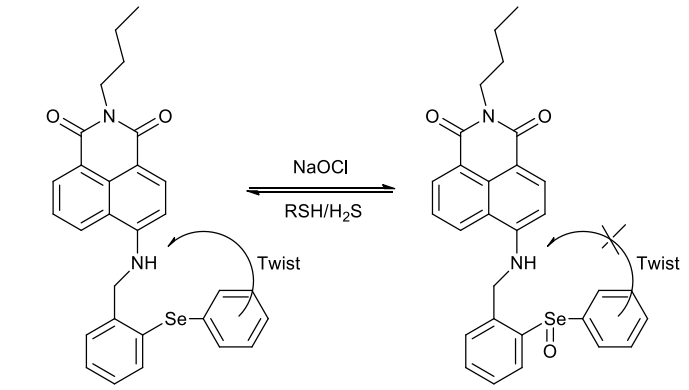

Scheme 5.1 Proposed mechanism of fluorescence response to HOCl reversibly of Receptor **90**.

Due the importance of hypochloric acid among ROS species and the remarkable data results, Han et al. decided to evaluate the attitude of **90** as fluorescence probe for the imaging in living cells. For these experiments the mouse macrophage cell line RAW264.7 was used with good response because the cells

remained viable throughout the whole experiment and the probe was demonstrated to have a very low toxicity.

5.1.2 Selenoderivative probes for ionic species

Zeng and colleagues have designed a new hemicyanine based chemosensor **92** for the selective recognition of Hg^{2+}. [7]

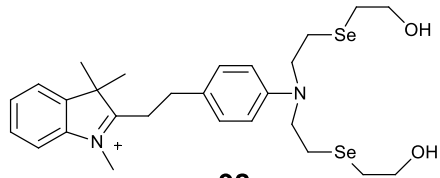

92

This receptor is able to bind Hg^{2+} in a mixed EtOH-H_2O (1:1, v/v) and pure water environment through the two Selenium binding sites and the host-guest interaction causes a change of the colorimetric and fluorescence properties of the free receptor. **92** shows an absorption band centred at 529 nm in aqueous media that does not change upon addition of a wide range of cations. The presence of Hg^{2+}, instead, causes a decrease of the absorption intensity of the band at 529 nm following by the formation of a new band centred at 404 nm with an isosbestic point at 457 nm. This variation is also visible by naked eye (Figure 5.3 b).

The selective recognition of Hg^{2+} leads also to a change of the fluorescence properties. Receptor **92** displays an emission band centred at 587 nm in water that decreases in intensity upon addition of the target cation with a blue shift to 575 nm (Figure 5.3c) following an “on-off” mechanism.

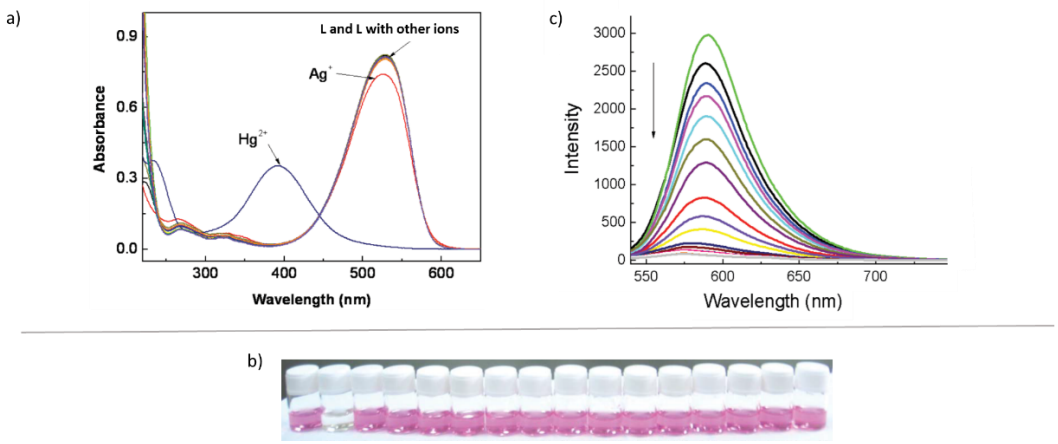

Figure 5.3 a) UV-vis responses of Receptor **92** (11.5 mM) upon the addition of the nitrate salts (10 Eq.) in H_2O. b) Naked-eye chromatic change of **92** (10 mM) in the presence of 10 Eq. of different nitrate salts of, from left to right, Na^+, K^+, NH_4^+, Mg^{2+}, Ca^{2+}, Pb^{2+}, Hg^{2+}, Co^{2+}, Cd^{2+}, Zn^{2+}, Ni^{2+}, Cu^{2+}, Cr^{3+}, Fe^{3+} and Ag^+ in H_2O. c) Fluorescent titration spectra of **92** (1 mM) in the presence of increasing amount of Hg^{2+} water λ_{exc} = 540 nm. All graph and images are reported according to Ref. 7.

Huang and coworkes developed the fluorescence sensor **93** based on the coumarin moiety. [8] This receptor is able to bind in a selective way Ag^+ over relevant competing metals through a synergic interaction from both Selenium atoms (Ag^+ presents a high selenophilicity) and the coumarin fragment that guarantees a high photostability. The binding properties of the receptor **93** were evaluated in ethanol/water (1:1, v/v) environment where a detection limit of 52 nM for Ag^+ was found.

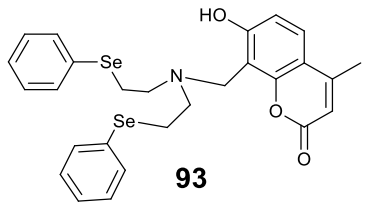

93

Sensor **93** exhibits an absorption band at 320 nm and the addition of increasing amounts of silver ions causes a decrease in the intensity of this band while a new band centred at 375 nm increases gradually. The same selectivity was found also in the emissive behaviour. The receptor exhibits an emission band centred at 445 nm that shows a linear enhancement with the increase of silver ions concentration as reported in Figure 5.4a. Moreover, probe **93** is able to discriminate Ag^{+} over similar ions such as Cu^{2+} and Hg^{2+} that instead respond with a reduction of the emission intensity as shown in Figure 5.4b.

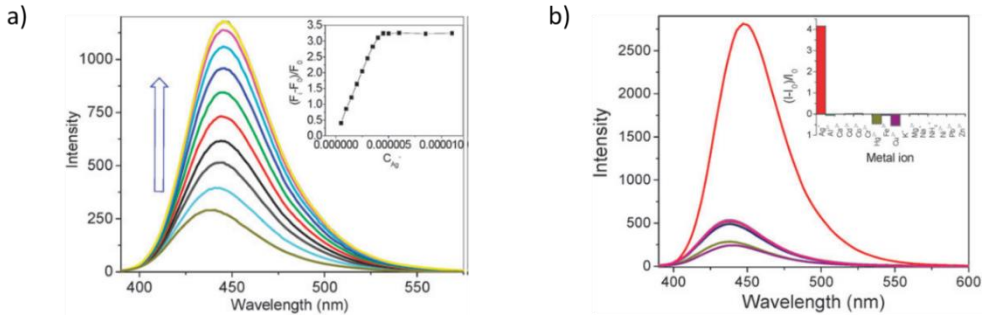

Figure 5.4 a) Fluorescent titration spectra of Receptor **93** (4 mM) in presence of different concentrations of Ag^{+} in ethanol/water (1 : 1, v/v); Inset: Fluorescence at 445 nm (4 mM) as a function of the Ag+ concentration. λ_{exc} = 360 nm. b) Fluorescence spectra of Receptor **93** (5.0 mM) upon the addition of the nitrate salts (2.0 equiv.) in ethanol/H_2O (1 : 1, v/v). Inset: histogram representing the fluorescence enhancement and quenching of **93** in the presence of metal ions. All graph and images are reported according to Ref. 8.

Han and colleagues reported the synthesis of the BODIPY based receptor **94**. [9] This receptor can discriminate the presence of $ONOO^{-}$ species among other peroxides and oxides in PBS solution (pH 7.4, 5% acetonitrile). The key point in the recognition process , reported in Scheme 5.2, is the spirocyclization reaction in compound **95** inducted by $ONOO^{-}$ that generates the compound **96** , which is

less fluorescent than **94** due to an ICT process. This probe finds application for the detection of different intracellular peroxynitrite levels in the RAW264.7 cell line.

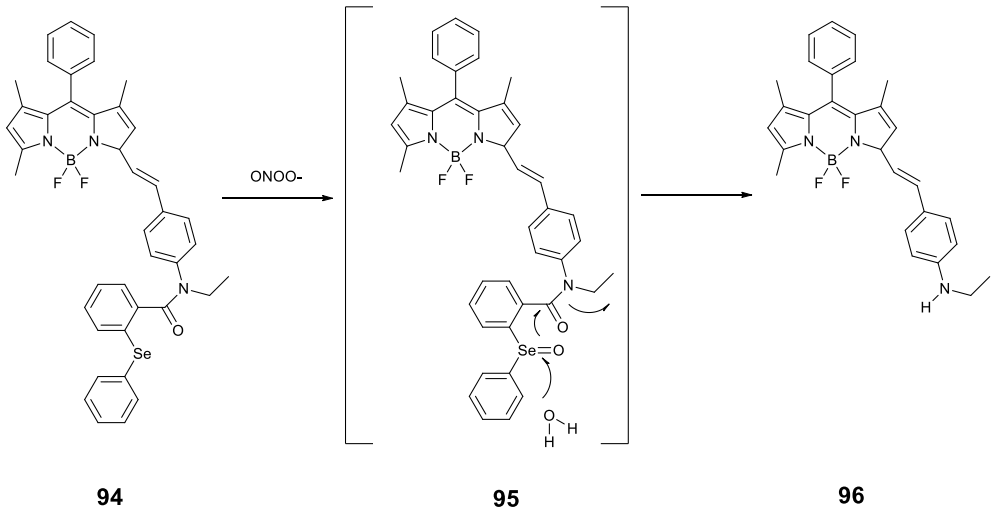

Scheme 5.2 Mechanism proposal for the interaction of $ONOO^-$ with receptor **94.**

Churchill and colleagues reported the synthesis and the anion sensing studies of a novel bis(BODIPY)diselenide receptor **97**. [10] This compound showed a remarkable affinity for the selective detection of superoxide among other ROS species (HOCl, OH•, H2O2, O2•−, tBuOOH and tBuO•) in an MeCN/H_2O (70:30 v/v) mixture with a detection limit of 12.9 μM. The selective recognition of superoxide happened via oxidation of the Selenium centre of **97** to form diselonoxide **98** according to Scheme 5.3. The interaction between receptor **97** and this target caused a strong green fluorescence due the remove of the photoinducedelectron transfer (PET) from the diphenyldiselenide group to the BODIPY moiety that led to the BODIPY-based fluorescence emission.

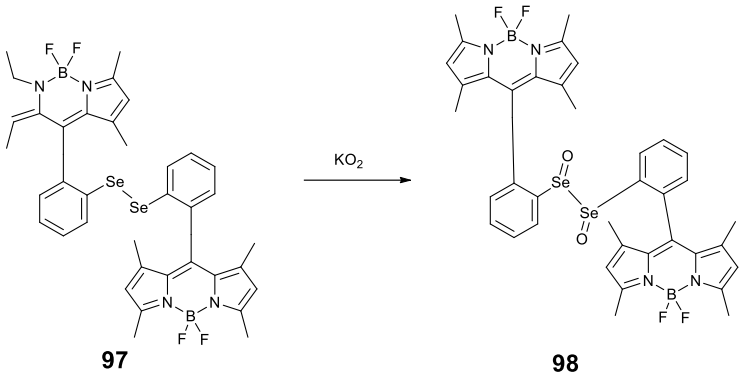

Scheme 5.3 Mechanism proposal for the interaction of superoxide with receptor **97.**

Goswami at all. designed the selenodiazole-based receptor **99** that shows a pivaloyl group as a binding unit and a benzoselenoimidazole that acts as a signal transducing entity. [11] This compound was found to be a fluorescent sensor for the selective recognition of carboxylate ions. The increase of the fluorescence emission intensity of the free receptor with a bathocromic shift was observed upon addition of a carboxylate ion (adamantine-1-carboxylate, pivalate, acetate and phenyl acetate) into a solution of **99** in $CHCl_3$. The complexation event was observed in agreement with the mechanism proposed in Scheme 5.4. A preferential affinity for hindered carboxylate anions with respect to other small anions such as F^-, Cl^-, Br^{--}, I^-, and carboxylic acids was demonstrated by means of NMR, UV-Visible and fluorescence spectroscopies.

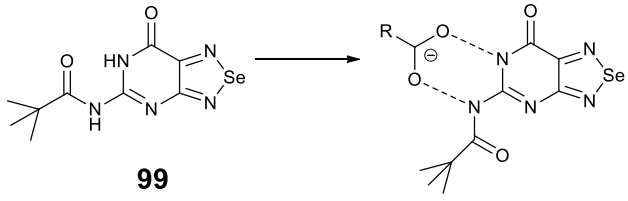

Scheme 5.4 Mechanism for the interaction of carboxylate anion with receptor **99.**

Due the interesting behaviours of the selenourea-based receptors discussed in the previous chapter, we decided to study two of them, **L_{26}** and **L_{27}**, and synthetize another receptor **L_{32}** with the aim to evaluate the possibility to use these molecules as optical sensors for anion recognition. **L_{26}** and **L_{32}** are asymmetric selenoureas bearing a phenyl ring and a naphthalene or a coumarin moiety, respectively. **L_{27}** is a symmetric naphthalene substituted selenourea. Due the particular behaviour of the selenourea based receptors in terms of anion coordination via hydrogen bond displayed in chapter four of this thesis, we included anions with nucleophilic nature (CN^- and S^{2-}) in the set studied in order to verify the possibility to recognize anions via a chemical reaction involving the selenourea site.

5.2 Synthesis

Receptors **L_{26}, L_{27}** and **L_{32}** were designed and successfully synthesized according to Scheme 5.5. The synthesis is a simple reaction between the phenyl isoselenocyanate [12] dissolved in dry DCM and the suitable amine (aniline, 1-naphtylamine and 7-amino-4,methylamine for **L_{26}, L_{27}** and **L_{32}**, respectively) dissolved in EtOH. The three receptors were obtained in moderate yields in the range of 37-79%.

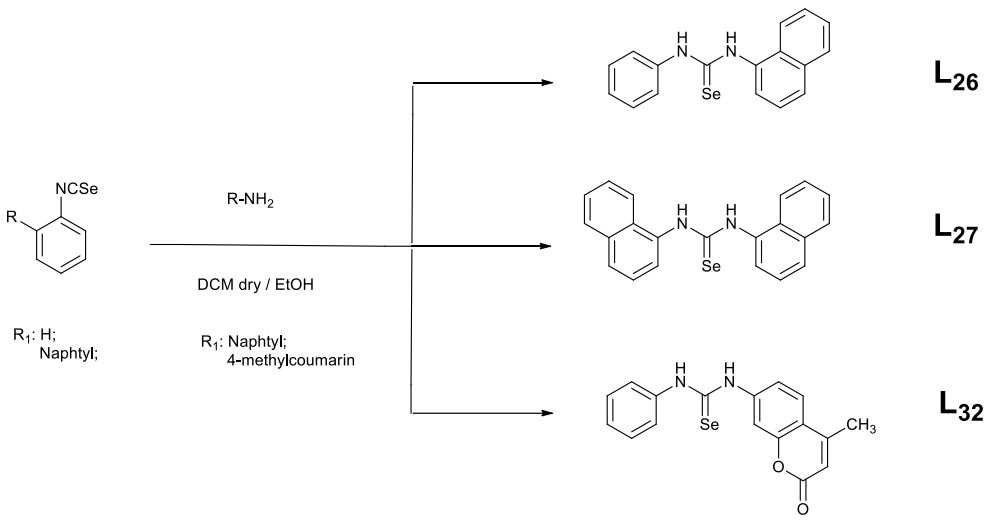

Scheme 5.5 Reaction scheme adopted for the synthesis of **L_{26}**, **L_{27}** and **L_{32}**.

5.3 From Oxygen, to Sulfur, to Selenium: a preview

In order to verify the possibility to observe a chemical reaction of the three receptors with TBACN, ^{1}H-NMR experiments with receptor **L_{25}** and this salt were carried out in DMSO-*d_6* solution. This preventive step was conducted using **L_{25}** due its simple structure with no substituents in order to avoid interference during the host-guest interaction event. Bis-phenyl urea **L_{23}** [13,14,15] and bis-phenyl thiourea **L_{24}** [16] were used as control molecules because of their well know property to coordinate anions via hydrogen bond [17,18,19,20] to demonstrate the increasing reactivity of the urea site moving from Oxygen to Sulfur to Selenium.

Figure 5.5 shows the titration of **L_{23}**, **L_{24}** and **L_{25}** with TBACN in DMSO-*d_6* where two different trends were found. In the case of **L_{23}** an usual downfield shift of the urea NHs signal was observed upon addition of increasing amounts of CN^- (Figure 5.5a and b). In the case of **L_{24}**, we observed an upfield shift of the thiourea NHs

signal (probably because of the higher acidity of the NH protons with respect to receptor **L_{23}**), and, after the addition of 1Eq. of cyanide, the receptor deprotonation was observed. In contrast, a completely different behaviour was observed for receptor **L_{32}**, i.e. the disappearance of the selenourea NHs signal at 10.2 ppm and the formation of a new signal at 4.3 ppm were observed (Figure 5.5 c). This result was a preliminary confirmation of the different interaction with cyanide and the selenourea-based receptor **L_{32}** with respect to the ordinary coordination behaviour of **L_{23}** and **L_{24}**. For this reason, we decided to better investigate the selenourea-based receptors **L_{26}**, **L_{27}** and **L_{32}**, by means of UV-Visible, fluorescence and NMR spectroscopies.

a)

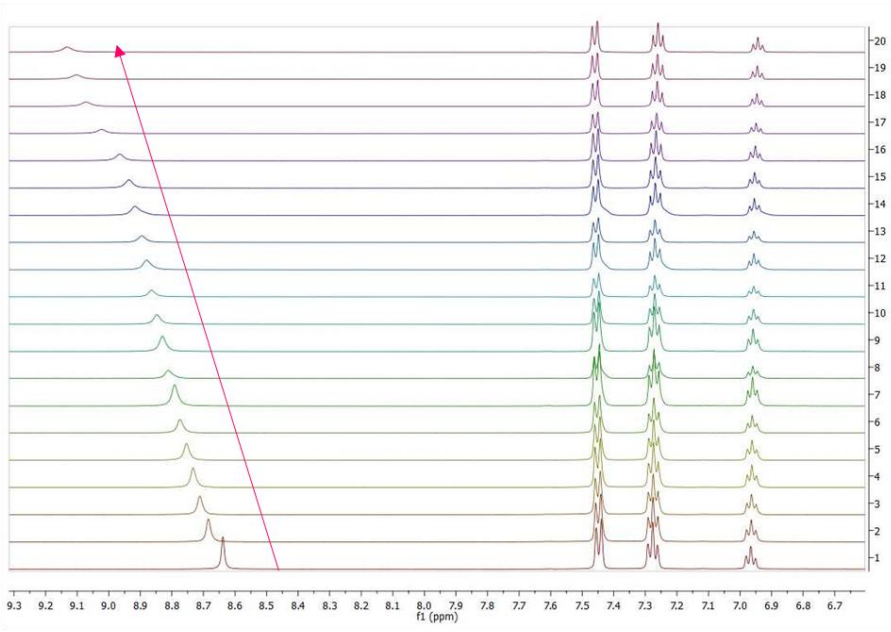
9.3 9.2 9.1 9.0 8.9 8.8 8.7 8.6 8.5 8.4 8.3 8.2 8.1 8.0 7.9 7.8 7.7 7.6 7.5 7.4 7.3 7.2 7.1 7.0 6.9 6.8 6.7
f1 (ppm)

b)

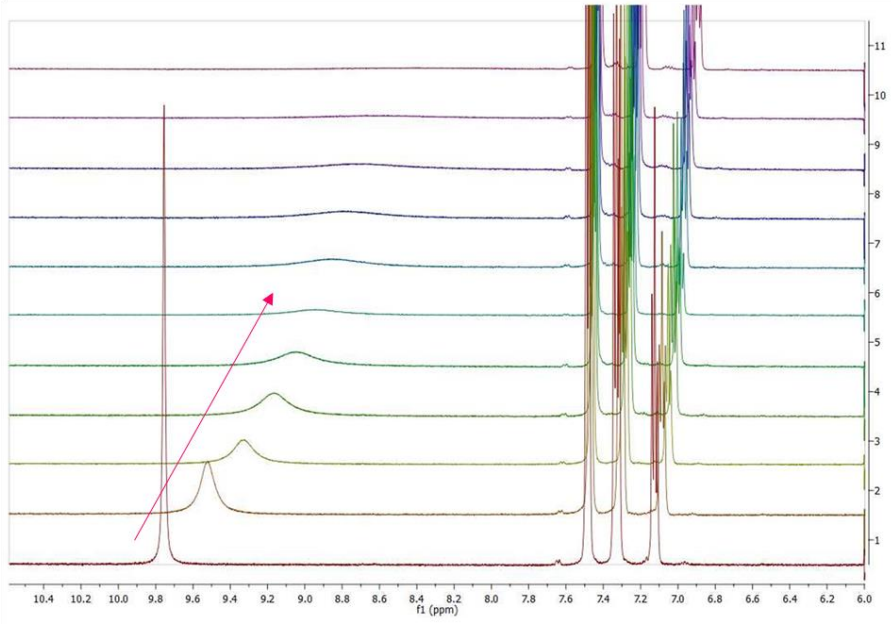
10.4 10.2 10.0 9.8 9.6 9.4 9.2 9.0 8.8 8.6 8.4 8.2 8.0 7.8 7.6 7.4 7.2 7.0 6.8 6.6 6.4 6.2 6.0
f1 (ppm)

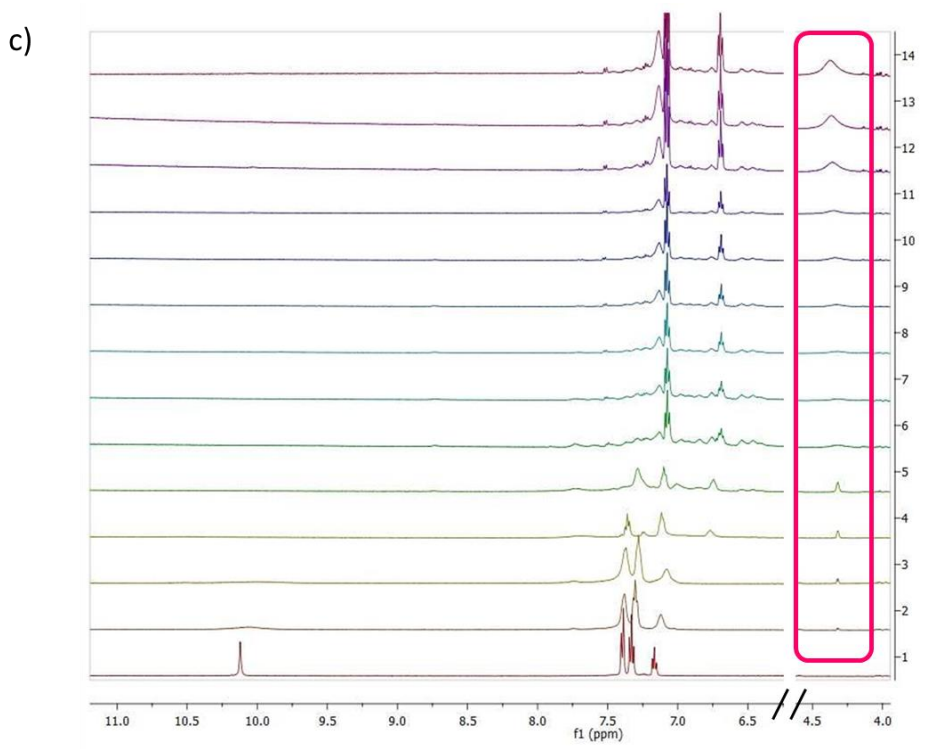

Figure 5.5 Stack plots of the ^{1}H-NMR titrations with TBACN (0.075M) in DMSO-d_6 of: a) **L_{23}**, b) **L_{24}** and c) **L_{25}** (0.005M).

5.4 UV-Visible and fluorescence spectroscopies

The sensing properties of **L_{26}**, **L_{27}** and **L_{32}** towards different anions (S^{2-}, CN^-, AcO^-, SO_3^{2-}, F^-, HCO_3^-, HSO_4^-, $H_2PO_4^-$, NO_3^-, Br^-, I^-,ClO_4^-, BzO^-, OH^-, SCN^-, and Cit^{3-}) were firstly investigated in MeCN.

Receptor **L_{26}** shows an absorption band centred at 290 nm (ε = 11366 M^{-1} cm^{-1}). Upon addition of one equivalent of S^{2-},CN^-, AcO, F^-, $H_2PO_4^-$ and BzO^- only a weak absorption decrease of the free receptor was observed (Figure 5.6) for all these anions except for CN^- that caused, in addition, the formation of a shoulder in the range of 350-400 nm (Figure 5.6 a).

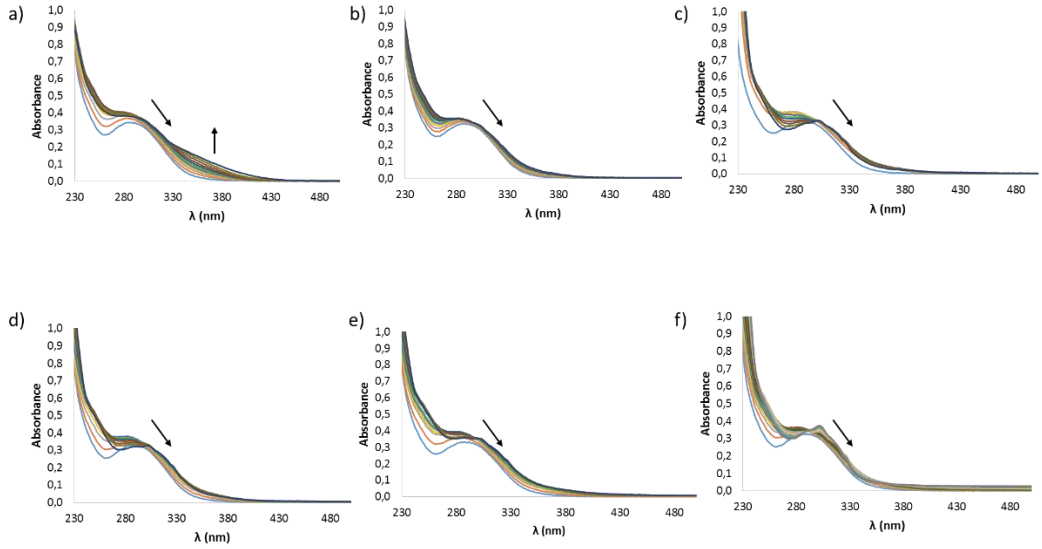

Figure 5.6 Changes in the absorption spectra of **L_{26}** ($3.0 \cdot 10^{-5}$M) in MeCN upon addition of increasing amounts (up to 1 equivalent) of anion ($2.5 \cdot 10^{-3}$ M): a) CN^-, b) S^{2-}, c) $H_2PO_4^-$, d) AcO^-, e) F^- and f) BzO^-. Anions were added as TBA salts (AcO^-, F^-, BzO^-, $H_2PO_4^-$, CN^-) and Na (S^{2-}).

As shown in Figure 5.7b, addition of an excess of this species (up to 5 equivalents) confirmed the presence of a new band at 391 nm (ε =8400 M^{-1} cm^{-1}) that remained stable also after addition of many equivalents of guest added (up to 50 equivalents as shown in Figure 5.7c). This interaction caused a visible naked eye chromatic change from the colourless receptor solution to yellow after the addition of cyanide (see Figure 5.7d).

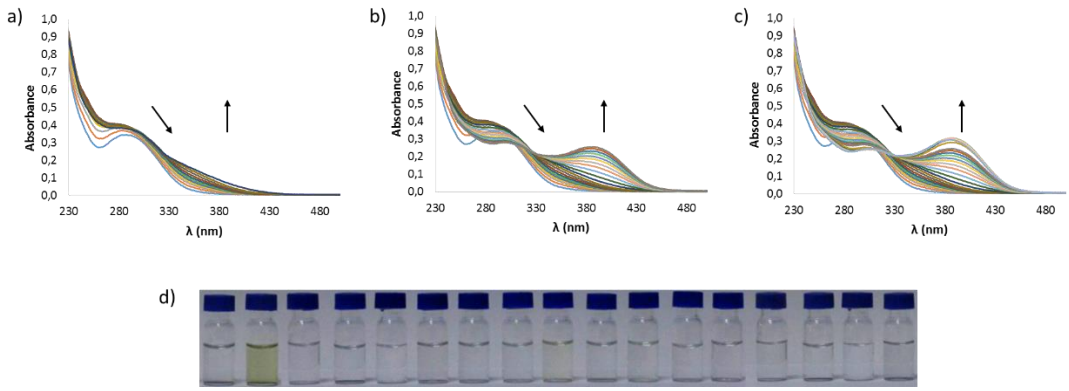

Figure 5.7 Changes in the absorption spectra of $\mathbf{L_{26}}$ ($3.0 \cdot 10^{-5}$M) in MeCN upon addition of increasing amounts of CN^- ($2.5 \cdot 10^{-3}$ M): a) up to 1 equivalent, b) up to 5 equivalents and c) up to 50 equivalents. d) Naked-eye colour change of $\mathbf{L_{26}}$ in MeCN; from left to right: receptor, + 1Eq. CN^-,+ 1Eq. S^{2-},+ 1Eq. AcO^-, + 1Eq. SO_3^{2-}, + 1Eq. F^-, + 1Eq. HCO_3^-,+ 1Eq. HSO_4^-,+ 1Eq. $H_2PO_4^-$, + 1Eq. NO_3^-, + 1Eq. Br^-,+ 1Eq. I^-, + 1Eq. ClO_4^-, + 1Eq. BzO^-, + 1Eq. OH^-, + 1Eq. SCN^-, and + 1Eq. Cit^{3-}.

Receptor $\mathbf{L_{27}}$ was designed with two symmetric napthyl arms with the purpose to increase the photosensibility properties of the system adding one more naphthyl group in place of the phenyl ring of $\mathbf{L_{26}}$. This host molecule shows an absorption band centred at 284 nm (ε = 16167 M^{-1} cm^{-1}). In this case, after addition of one equivalent of AcO, Bzo^-, HCO_3^-, F^-, $H_2PO_4^-$,S^{2-} and CN^- , the formation of a new band at 316-318 nm was observed with an isosbestic point at 294 nm for AcO^-, BzO^-, HCO_3^-, F^- and at 298 nm for S^{2-},CN^- (Figure 5.8).

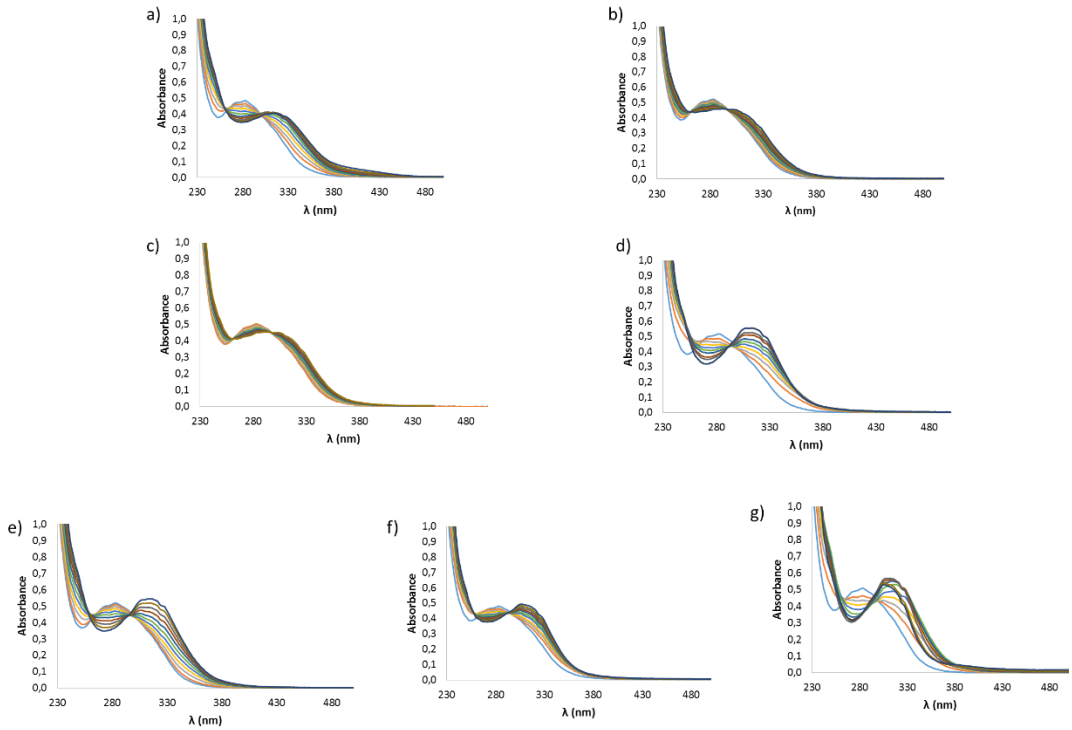

Figure 5.8 Changes in the absorption spectra of **L_{27}** ($3.0 \cdot 10^{-5}$M) in MeCN upon addition of increasing amounts (up to 1 equivalent) of anion ($2.5 \cdot 10^{-3}$ M): a) CN^-, b) S^{2-}, c) $H_2PO_4^-$ d) AcO^-, e) F^-, f) BzO^- and g) HCO_3^-. Anions were added as TBA salts (AcO^-, F^-, BzO^-, $H_2PO_4^-$, CN^-), TEA (HCO_3^-) and Na (S^{2-}).

Also for receptor **L_{27}**, addition of an excess of cyanide led to the formation of a well define band at 410 nm that remains stable also in strong guest excess condition (see Figure 5.9).

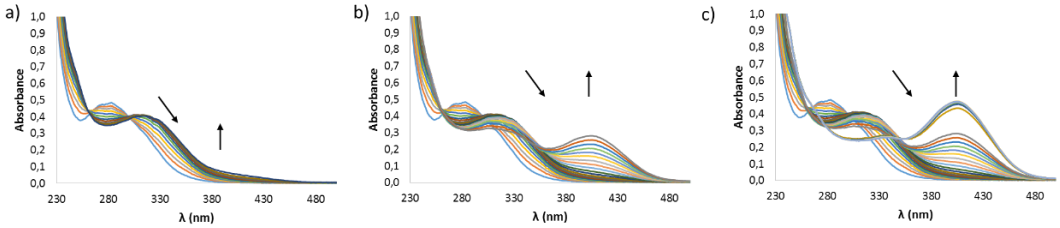

Figure 5.9 Changes in the absorption spectra of **L_{27}** ($3.0 \cdot 10^{-5}$M) in MeCN upon addition of increasing amounts of CN^- ($2.5 \cdot 10^{-3}$ M): a) up to 1 equivalent, b) up to 5 equivalents and c) up to 50 equivalents.

However, for both receptors **L_{26}** and **L_{27}**, upon addition of the above-mentioned anions any specific response in terms of fluorescence changes was not observed.

In order to try to improve the selectivity of the receptors above described, we decided to test them in a more competitive media, H_2O/MeCN 75:25 (v/v). Unfortunately, we did not observed significant change in the UV-Visible spectra for receptor **L_{26}** while it was impossible to carry out these experiments for **L_{27}** due its low solubility in the solvent mixture.

Regarding **L_{32}**, the formation of a new absorption band at around 360 nm with the presence of an isosbestic point at 333 nm was observed when one equivalent of S^{2-}, CN^-, AcO^-, F^-, HCO_3^-, and BzO^- was added (Figure 5.10).

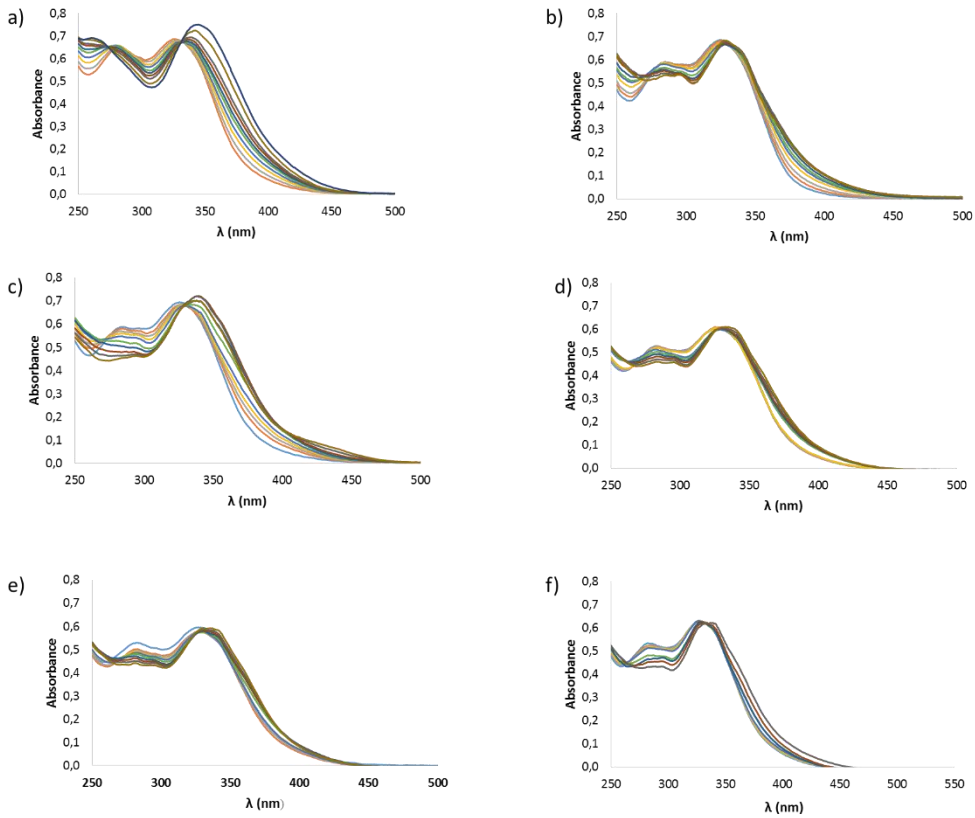

Figure 5.10 Changes in the absorption spectra of $\mathbf{L_{32}}$ ($3.0 \cdot 10^{-5}$M) in MeCN upon addition of increasing amounts (up to 1 equivalent) of anion ($2.5 \cdot 10^{-3}$ M): a) CN^-, b) S^{2-}, c) AcO^-, d) F^-, e) BzO^- and f) HCO_3^-. Anions were added as TBA salts (AcO^-, F^-, BzO^-, CN^-), TEA (HCO_3^-) and Na (S^{2-}).

In this case, addition of an excess of anion (up to 50 equivalents) causes severe changes in the absorption spectrum of the free receptor, suggesting the presence of multiple equilibria in solution. Upon excitation of $\mathbf{L_{32}}$ at 333 nm an emission band at 414 nm was observed. However, also in this case, in presence of the anions we did not observed any specific response in terms of fluorescence changes.

Also in the case of **L_{32}**, we decided to repeat the measurements in a more competitive solvent mixture (H_2O/MeCN 75:25 (v/v)).

Interestingly, in these conditions, we observed changes in the absorption spectrum of **L_{32}** only in the presence of S^{2-} and CN^- (Figure 5.11).

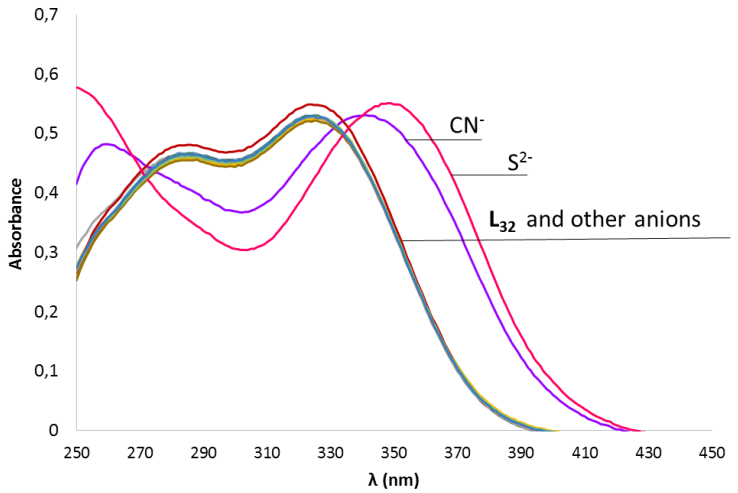

Figure 5.11 Changes in the absorption spectrum of **L_{32}** ($3.0 \cdot 10^{-5}$M) in H_2O/ MeCN (75:25 v/v) upon addition one equivalent of anions.

In this solvent mixture **L_{32}** shows two absorption bands at 281 nm (ε = 16052 $M^{-1}cm^{-1}$) and 324 nm (ε = 18329 $M^{-1}cm^{-1}$). Upon addition of a small aliquot of S^{2-} and CN^- a dramatic change was observed (also visible at naked eye, Figure 5.12 c) with the loss of the band of the free receptor and the formation of a new absorption band at 353 nm (ε = 25145 $M^{-1}cm^{-1}$).

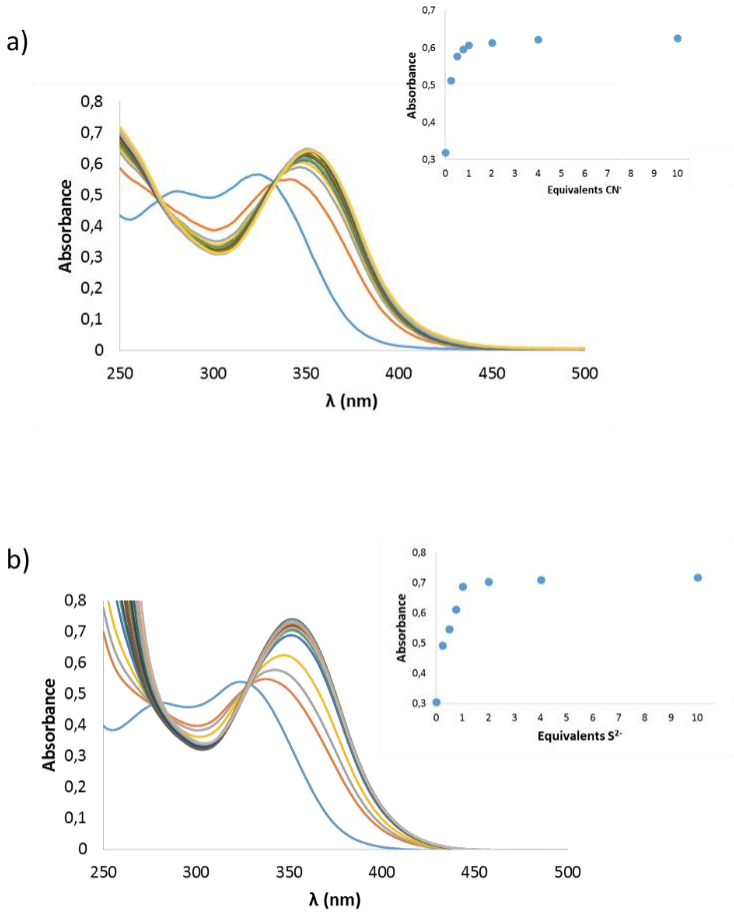

Figure 5.12 Changes in the absorption spectrum of **L_{32}** ($3.0 \cdot 10^{-5}$M) in H_2O/ MeCN (75:25 v/v) upon addition of increasing amounts (up to10 equivalents) of a) TBACN and b) Na_2S (0.1 M). Inset: Plot of absorbance (353 nm) vs. equivalents of CN^- and S^{2-} respectively. c) Naked-eye colour change. From left to right : L, CN^-, S^{2-}, BzO^-, Cl^-, $H_2PO_4^-$, I^-, Br^-,NO_3^-, AcO^-, HSO_4^-, ClO_4^- , SO_3^{2-}, F^-, HCO_3^-, SCN^- , Cit^{3-}.

By fitting the experimental data using Hypspec [21] we were able to calculate the stability constant for the formation of a 2:2 complexes (Log K_{22} = 15.5 (3) and 16.0 (4) respectively for S^{2-} and CN^-). The sulfide and cyanide LOD in these experimental conditions were 1.0 10^{-5} M and 9.8 10^{-6} M, respectively. Addition of all the other anions did not cause any change in the UV-Vis spectrum of the free receptor as confirmed by competitive studies reported in Figure 5.13 .

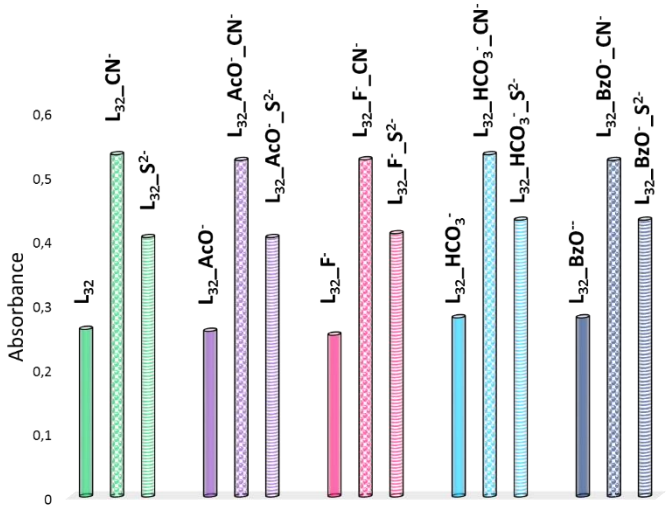

Figure 5.13 Anion competition study for **L_{32}** [3.0·10^{-5} M] in the presence of 1 equivalent of CN^- and S^{2-} and 1 equivalent of the other anions (0,1 M) in H_2O/ MeCN (75:25 v/v) (λ_{ABS}: 353 nm, ε = 25145 $M^{-1}cm^{-1}$).

5.5 $^{1}H,^{13}C,^{77}Se$-NMR spectroscopy

The dramatic changes observed in such a competitive solvent mixture described above cannot be ascribed by a simple hydrogen bond interaction between the anions and the NH groups of the receptor (see chapter 4), so in order to better understand the behaviour of receptor **L_{32}** in the presence of CN^- and S^{2-} in solution, we perform ^{1}H-, ^{13}C-, ^{77}Se-NMR spectroscopy experiments.

Proton NMR titrations of **L_{32}** in the presence of CN^- and S^{2-} were performed in DMSO-d_6/0.5% H_2O (a similar absorption spectrum to that observed in H_2O/MeCN (75:25 v/v) was observed in DMSO). The titration of the receptor with TBACN salt is reported in Figure 5.14. Upon addition of increasing amount of CN^-, the disappearance of the signal of the selenourea protons at 10.4 ppm and the formation of two new peaks were observed. These two new peaks were attributed to the formation of two amine NHs (at 4.2 ppm) according to the mechanism shown in Figure 5.14 b.

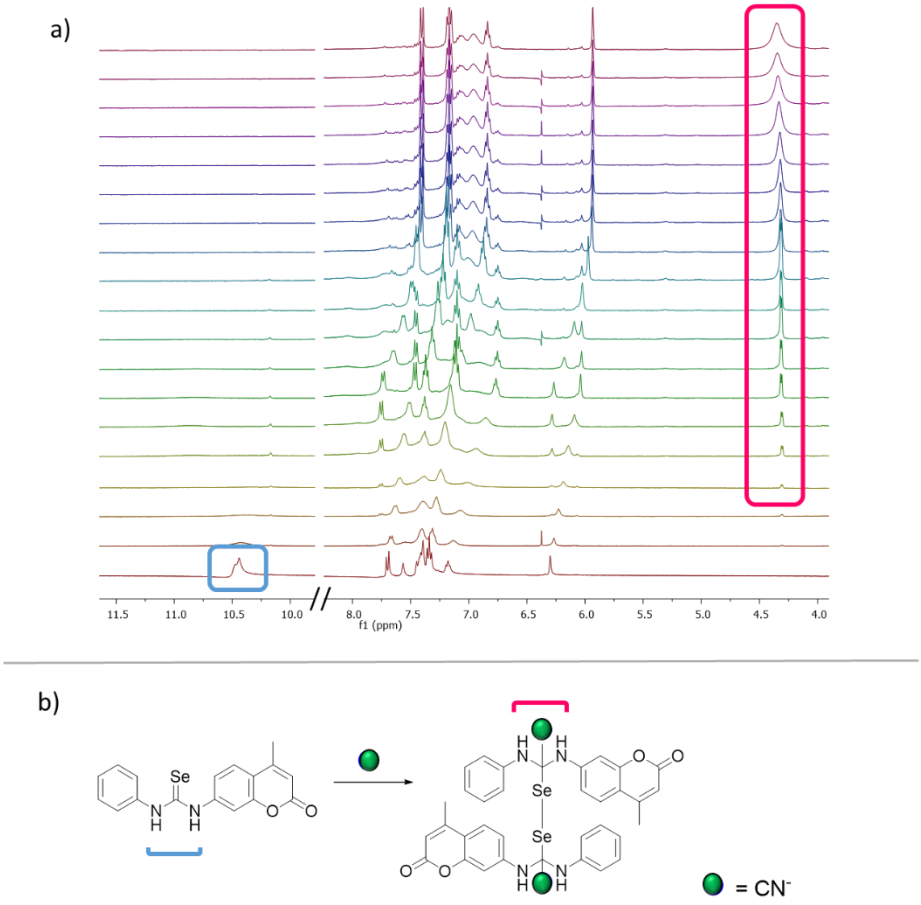

Figure 5.14 a) Stack plot of ^{1}H-NMR titration in DMSO-d_6 of **L_{32}** (0.005 M) upon addition of TBACN (0.075 M) in DMSO-d_6. b) Hypothesis of the interaction mechanism between the receptor and the anionic target.

In order to confirm the different behaviour of receptor **L_{32}** in the presence of cyanide with respect to the common complexation event observed in the case of urea-based receptors, the correspondent 1-(4-methylcoumarin)-3-phenylurea **L_{33}** was synthetized and the ^{1}H-NMR titration with CN^- was carried out (Figure 5.15). After the addition of the anion, only the deprotonation of the receptor was observed according to the well documented acidity of cyanide species. Also this

direct comparison between urea **L_{33}** and selenourea **L_{32}** remarks the radical difference between the receptors behaviours in terms of anion recognition.

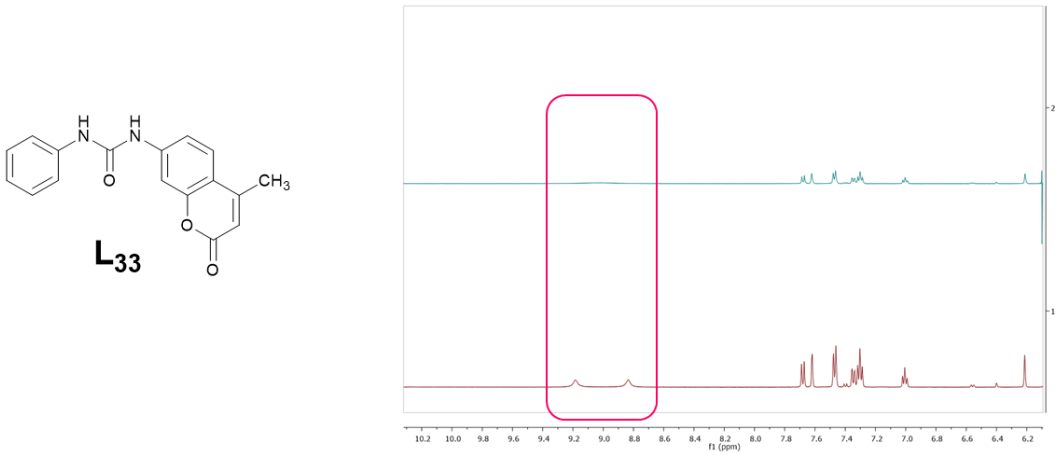

Figure 5.15 Changes in the ^{1}H-NMR spectra of a DMSO-d_6 solution of **L_{33}** (0.005 M) upon addition of one equivalent of TBACN (0.075 M) in DMSO-d_6.

As support of the proposed mechanism, ^{13}C- and ^{77}Se-NMR experiments were carried out. In the ^{13}C spectrum, upon addition of one equivalent of cyanide the peak at 179.01 ppm attributed to the C=Se disappear while new peaks at 129.00 and 111.66 ppm (attributed to the C-Se-Se and to the bound CN^- signals respectively), appear (see Figure 5.16 a). The result of the ^{77}Se-NMR experiment was in agreement with the ^{1}H and ^{13}C NMR spectra. An upfield shift of the Selenium signal of the free receptor was observed from 314 ppm to 243 ppm in the presence of one equivalent of CN^- (see Figure 5.16b). This behaviour was in accordance with the formation of a Se-Se bridge and a change of the hybridation of the Selenium atom from sp^2 to sp^3. [22,23,24,25,26]

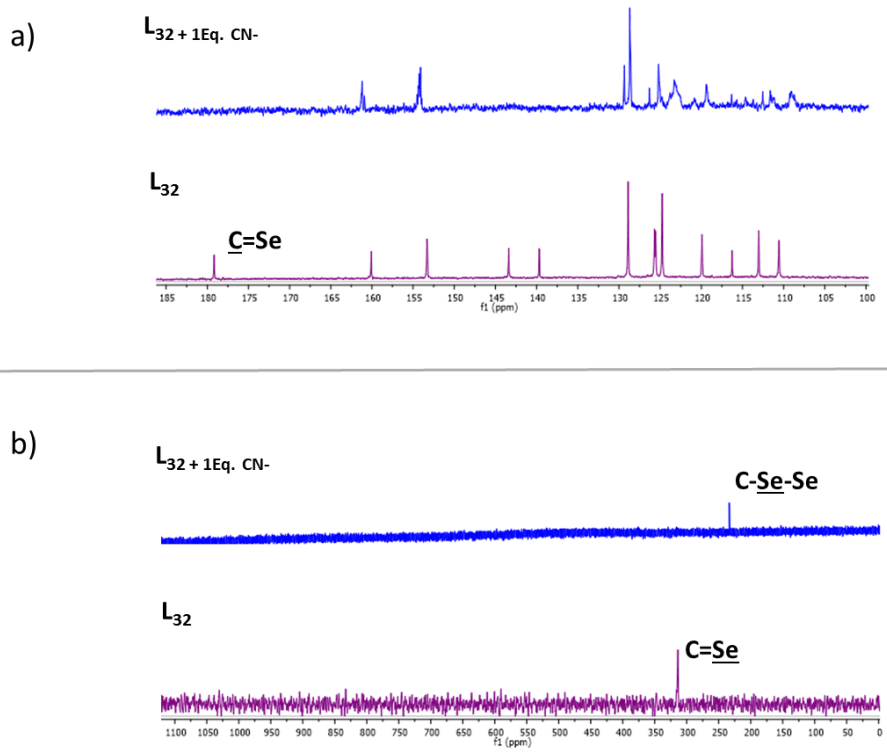

Figure 5.16: ^{13}C and ^{77}Se-NMR spectra (a and b, respectively) of a DMSO-d_6 solution of **L_{32}** (0.005 M) upon addition of a) 1 Eq. of CN^- (0.075 M) in DMSO-*d_6*.

A similar behaviour in terms of disappearance of the C=Se signal (in both ^{13}C and ^{77}Se NMR spectra) was observed in presence of S^{2-} (Figure 5.17) even if it was impossible to observe the new signal of the C-Se-Se bond due the decomposition (presumably with the formation of the correspondent thiourea as hypothesized in next paragraph) of the sample after the addition of S^{2-} .

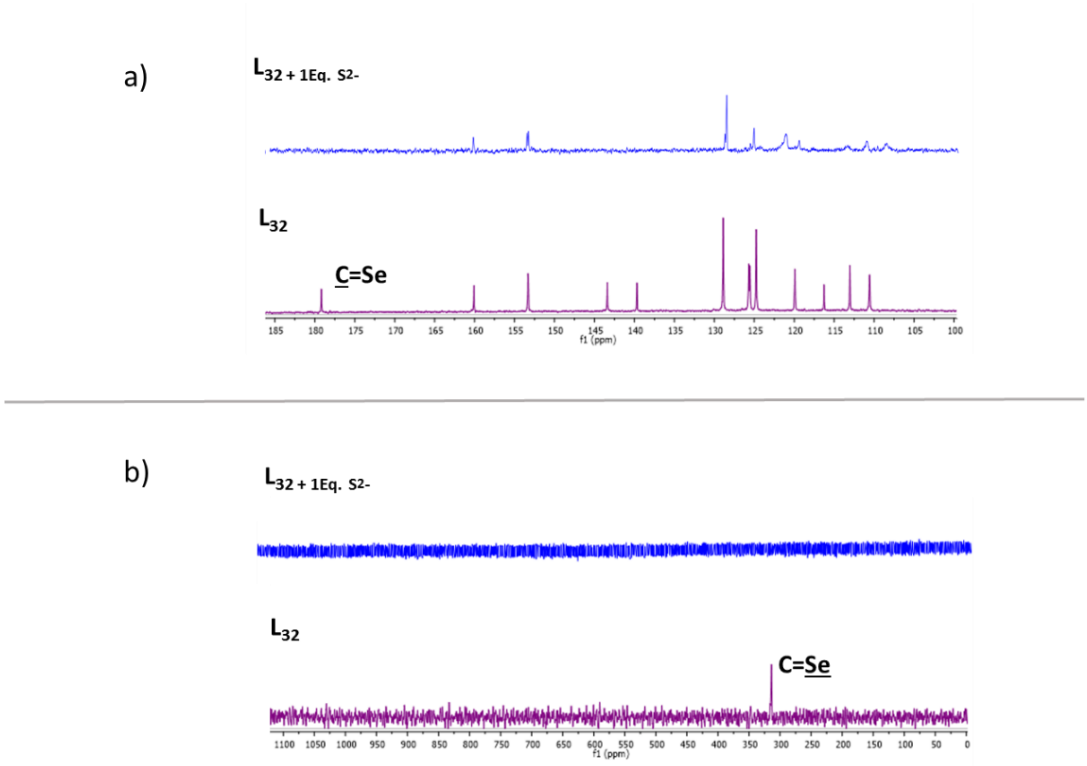

Figure 5.17 ^{13}C and ^{77}Se-NMR spectra (a and b, respectively) of a DMSO-d_6 solution of **L_{32}** (0.005 M) upon addition of 1Eq. of S^{2-} (0.075 M) in DMSO-*d_6*.

5.6 X-Ray Diffraction and ESI-MS

Single crystals suitable of X-ray diffraction analysis were obtained by slow evaporation of solution of **L_{32}** in H_2O/MeCN 75:25 (v/v) in the presence of an excess of TBACN. The structure obtained, reported in Figure 5.18, was a fragment of a decomposition species where cyanide is connected with the carbon atom of the urea site. It is possible theorized that CN^- interacts with the receptor on the C=Se bond via nuchephilic addition and then, after time, the loss of Selenium as black elemental Selenium (visible by naked-eye) leads into a space

rearrangement with a structure of the correspondent isolated nitrile. Principal bond lengths and angles are ported in Table 5.1

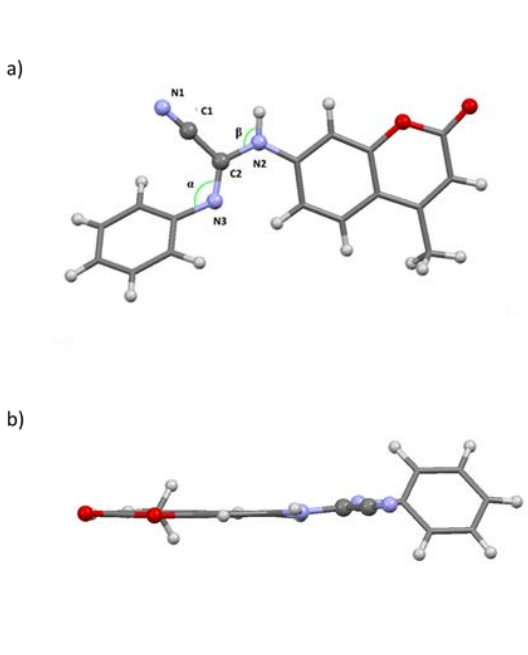

Figure 5.18 a) X-Ray crystal structure of the nitrile species obtained by reaction of $\mathbf{L_{32}}$ with CN^-. b) View of the staggered space disposal of the phenyl arm of $\mathbf{L_{32\text{-}CN^-}}$.

Table 5.1 Principal bond lengths and angles of the isolated nitrile species of $\mathbf{L_{32}}$ with CN^- .

Distance	Å	**Angle**	°
N1-C1	1.152	**N3C2N1**	123.78
C1-C2	1.456	**C2N2H**	113.04
C2N3	1.283		
C2-N2	1.385		

For analogy with the structure described above, we can hypothesize a similar reaction between S^{2-} and the receptor that involves the reactive selenourea site. On the base of this speculation, the analogue compound that should be formed after the host-guest interaction (and decomposition) is the correspondent 1-(4-methylcoumarin)-3-phenylthiourea as summarized in Scheme 5.6.

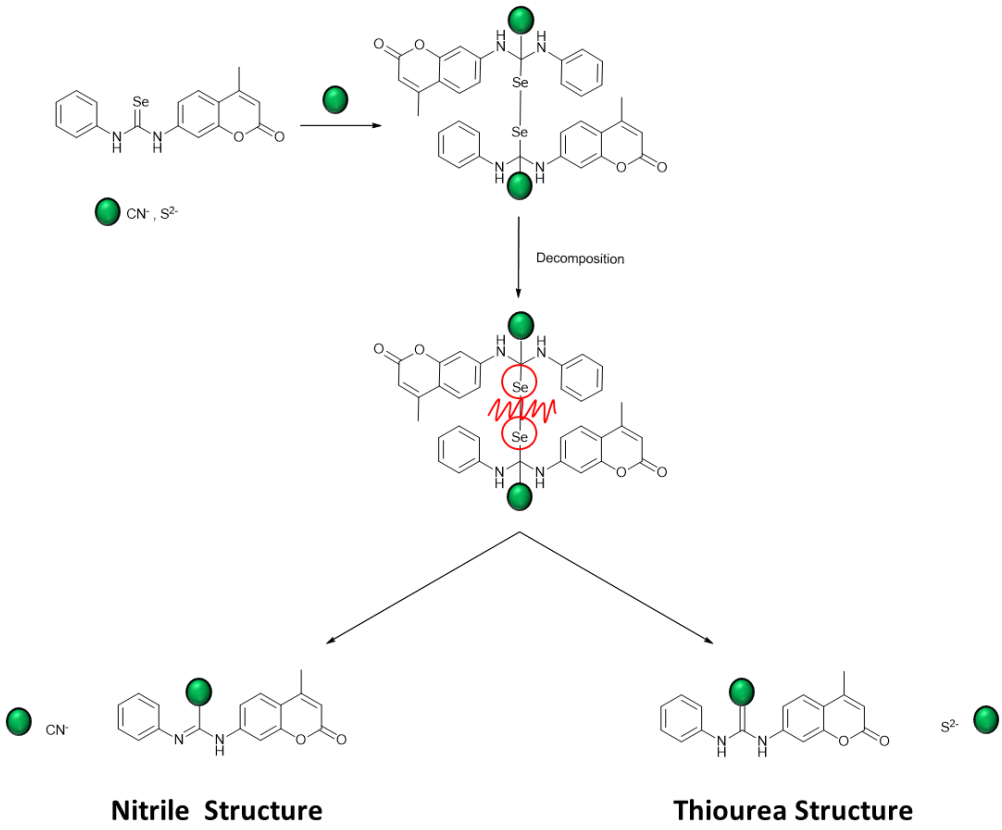

Scheme 5.6: Hypothesis of the decomposition species for the reaction between $\mathbf{L_{32}}$ CN^- and S^{2-}.

In order to confirm this theory, we decided to synthetize this thiourea derivative by reaction between phenyl-thioisocyanate and 7-amino-4-methylcoumarin. Unfortunately, although the formation of this compound was clearly observed, we were not able to isolate it as a pure product, but the diagnostic NHs signals of the thiourea function are compatible with those that were found in the ^{1}H-NMR spectra of the decomposed **L_{32}** with one equivalent of S^{2-} sample. Also this data were in agreement with the speculation about the interaction of the anion through the C=Se site.

ESI-MS spectrometry also corroborated the dimeric species formation mechanism reported in Figure 5.14. The ESI-MS spectrum of the 1:1 adduct of **L** with S^{2-} shows a peak at 356.9260 attributed to the free receptor and a peak at 745.2323 attributed to the dimer in the presence of SH. The isotopic pattern fits in agreement with the presence of one and two Selenium atoms, respectively.

5.7 Hybrid MCM-41 nanoparticles

Due the promising results obtained for **L_{32}** in a water mixture media in terms of recognition of cyanide and Sulfur species, we evaluated the possibility to use this chemosensor also in pure water environment. Because of the receptor insolubility in pure water, we decided to use MCM-41 nanoparticles as support scaffolds for the probe.[27] This material was designed according to the Scheme 5.7 using a variation of a functionalising silica nanoparticles procedure reported in literature. [27]

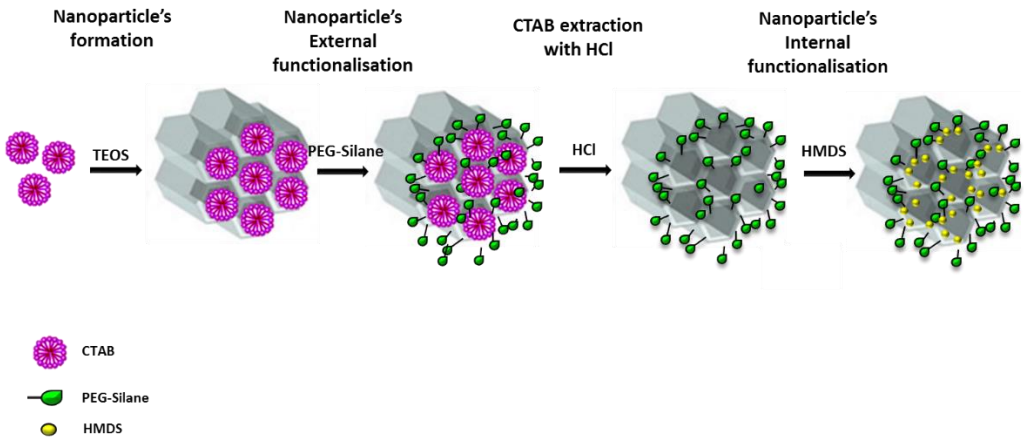

Scheme 5.7 Synthesis procedure of hybrid MCM-41 nanoparticles.

The key concept was to synthetize silica nanoparticles with a different hydrophobic agent for the external and internal surfaces (PEG-silane and hexamethyldisilazane HMDS respectively) obtaining a hybrid inorganic material. The scaffold in fact, should ideally be hydrophobic enough to maintain the probe in the nanopores but not too hydrophobic in order to obtain stable suspensions of the nanoparticles guaranteeing the reaction between the chemosensor and the target.

For this reason, the external surface of the nude MCM-41 nanoparticles was functionalized with PEG-silane and then, after the extraction of the structure-templating agent cetyltrimethylammonium bromide (CTAB) using hydrochloric acid, the inner sides of the pore walls were hydrophobized with HMDS.

These steps led to the formation of inorganic nanoparticles containing hydrophobic pockets. The probe loading of the scaffold was achieved by suspending the hybrid MCM-41 nanoparticles in a MeCN solution of sensor $\mathbf{L_{32}}$ (1.3 mM). Then, the mixture was stirred for 12 hours at room temperature.

0.47 mmol of sensor **L_{32}** per g SiO_2 were incorporated and as a consequence of the inclusion of the chemosensor into the hydrophobic cavities, through a simple adsorption process, a naked eye emission of the material was observed (Figure 5.19).

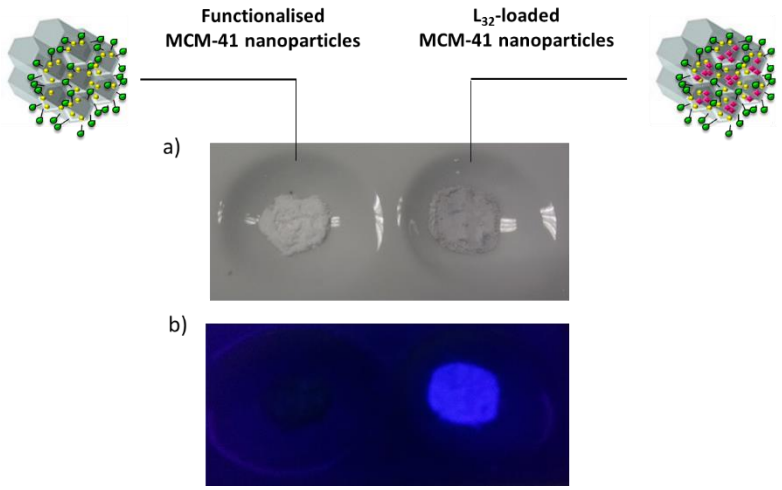

Figure 5.19 Fluorescence emission of the receptor-loaded MCM-41 nanoparticles.

All the nanoparticles obtained (nude, functionalised and loaded MCM-41) were characterized by Powder X-Ray diffraction (PXRD), thermogravimetric and elemental analysis, Porosimetry and TEM technique (see paragraph 5.9.3).

In order to evaluate the anion sensing and binding attitude of **L_{32}** embedded in the silica scaffolds, aliquots of CN^- and S^{2-} were added into a dispersion of MCM-41 loaded nanoparticles in water. As shown in Figure 5.20, a partial quenching of the emission of the **L_{32}**-loaded nanoparticles indicating the interaction between sensor and the anion target was observed also in pure water only after the

addition of S^{2-} . Any remarkable change in the photoemission properties of the system was observed in the case of cyanide.

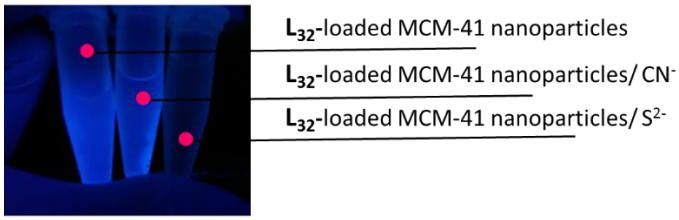

Figure 5.20 Fluorescence emission changes of **L**-loaded MCM-41 nanoparticles in water in the presence of CN^- and S^{2-} anions.

To quantify the quenching effect caused by S^{2-}, a fluorescence titration was carried out adding this anion into a water dispersion of **L_{32}**-loaded nanoparticles (12mg nanoparticles in 800 µl of water). After the addition of S^{2-} (up to 20 equivalents) a drastic decrease of the emission intensity of the sensing material at 394-427 nm (λ_{exc} = 330 nm) was observed as reported in Figure 5.21. This fluorescence response confirmed the affinity for S^{2-} of receptor **L_{32}** also within material scaffold and its real applicability as a chemosensor in water environment.

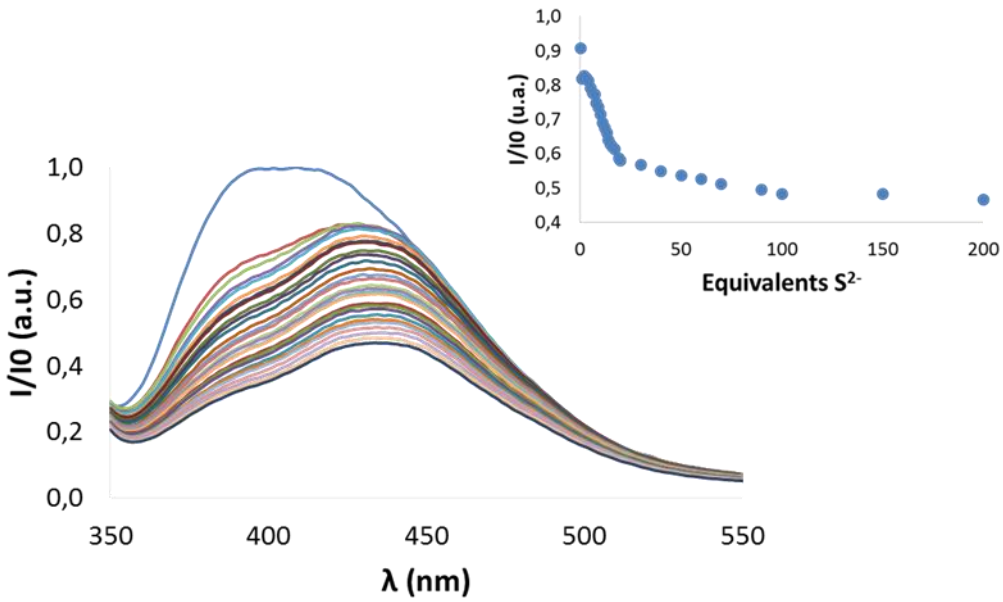

Figure 5.21 Changes in the emission spectrum of $\mathbf{L_{32}}$-loaded silica nanoparticles in H_2O (λ_{exc} = 330 nm) upon addition of increasing amounts (up to 200 equivalents) of Na_2S (0.05 M). Inset: Plot of emission (λ_{em} = 430 nm) vs. equivalents of S^{2-}.

5.8 Conclusion

In conclusion, we successfully designed receptors $\mathbf{L_{26}}$, $\mathbf{L_{27}}$ and $\mathbf{L_{32}}$. Ligand $\mathbf{L_{26}}$ showed a good affinity for CN^- with respect to the other anionic species under investigation in MeCN while in the case of $\mathbf{L_{27}}$ no selectivity in terms of complexation of specific anionic guest was found in the same media. The best results were obtained for receptor $\mathbf{L_{32}}$. This molecule can be used as colorimetric chemosensor for the selective detection of CN^- and S^{2-} in MeCN (LOD of 3.0 10^{-6} M and 6.0 10^{-6} M respectively) and also in more competitive H_2O/MeCN (75:25 v/v) environment (LOD of 9.8 10^{-6} M and 1.0 10^{-5} M respectively for cyanide and sulfide). In addition, the receptor is able to recognize S^{2-} species also when

embedded in hybrid inorganic MCM-41 nanoparticles in pure water working as an ON-OFF fluorescent chemosensor for the selective recognition of this species. ^{1}H, ^{13}C, ^{77}Se and HR-ESIMS techniques confirm the chemosensor nature of the receptor according with the Se-Se bridge formation between two different receptor units.

5.9 Experimental methods

All reactions were performed in oven-dried glassware under a slight positive pressure of nitrogen. ^{1}H-NMR (400 MHz, 500MHz) and ^{13}C NMR (100 MHz, 125MHz) spectra were determined on a Varian INOVA-400 spectrometer, and Varian INOVA-500 spectrometer. ^{77}Se spectra were determined on a Bruker Avance 400 MHz spectrometer. Chemical shifts for ^{1}H-NMR are reported in parts per million (ppm), calibrated to the residual solvent peak set, with coupling constants reported in Hertz (Hz). The following abbreviations are used for spin multiplicity: s = singlet, d = doublet, t = triplet, m = multiplet. Chemical shifts for ^{13}C NMR are reported in ppm, relative to the central line of a septet at δ = 39.52 ppm for deuterio-dimethylsulfoxide. Chemical shifts for ^{77}Se NMR are reported in ppm, relative to the singlet at δ = 446.44 for $(PhSe)_2$ in deuterio-dimethylsulfoxide. Microanalytical data were obtained using a Fisons EA CHNS-O instrument (*T* = 1000 °C). UV-visible spectra were recorded with a JASCO V-650 Spectrophotometer. Fluorescence spectra were recorded on a Cary Eclypse and JASCO FP-8500 spectrofluorimeters. HR-Mass spectra (HRMS) were carried out in a TRIPLETOF T5600 (ABSciex, USA) spectrometer. X-ray measurements were performed on a Seifert 3000TT diffractometer using Cu-Kα radiation. Thermo-gravimetric analysis were carried out on a TGA/SDTA 851e Mettler Toledo equipment, using an oxidant atmosphere (Air, 80 mL/min) with a heating program consisting on a heating ramp of 10 °C per minute from 393 K to 1273 K and an isothermal heating step at this temperature during 30 minutes. N2

adsorption-desorption isotherms were recorded on a Micromeritics ASAP2010 automated sorption analyser. The samples were degassed at 120 ºC in vacuum overnight. The specific surfaces areas were calculated from the adsorption data in the low pressures range using the BET model. Pore size was determined following the BJH method. Transmission electron microscope (TEM) images were performed in a Philips CM-10. All solvents and starting materials were purchased from commercial sources where available. Proton NMR titrations were performed by adding aliquots of the putative anionic guest (as the TBA salt, 0.075 M) in a solution of the receptor (0.005M) in DMSO-d_6/0.5% water to a solution of the receptor (0.005M). Phenylisoselenocyanate was synthesised following a literature procedure.[1]

[1]J. G. Fernández-Bolaños, Ó. López, V. Ulgar, I. Maya and J. Fuentes, *Tetrahedron Letters*, 2004, **45**, 4081-4084.

5.9.1 Synthetic probe procedure

Synthesis of L_{32}

A solution of phenylisoselenocyanate (0.25 g, 1.37 mmol) in dry DCM (3 ml) was added dropwise to a solution of 7-aminomethylcoumarin (0.241 g, 1,37 mmol) in ethanol absolute (5ml) in the darkness under N_2 atmosphere. The mixture was stirred for 3h at 40°C and then it was filtered to give the desired compound as a yellow solid. Yield 37 % (0.181 g, 0.51 mmol). ^{1}H-NMR (400 MHz,DMSO-d_6, 298K): δH: 10.50 (s, 1H); 10.45 (s, 1H); 7.71 (d, J= 8.6 Hz, 1H); 7.59 (s, 1H); 7.46 (d, J= 8.6 Hz, 1H); 7.42 (d, J= 7.9 Hz, 2H); 7.36 (t, J= 7.6 Hz, 2H); 7.20 (t, J= 7.3 Hz, 1H); 6.32 (s, 1H); 2.36 (s, 3H). ^{13}C-NMR (100 MHz, DMSO- d_6, 298 K), δC: 1780.94, 159.84, 153.10, 153.04, 143.17, 139.47, 128.65, 125.45, 125.31, 124.53, 119.69, 116.04, 112.80, 110.34, 18.08. $^+$HR-ESI-TOF MS: m/z 359.0316 $[M-H]^+$.

Synthesis of L_{33}

A solution of phenylisocyanate (0.068g, 0.57mmol) in MeCN (5 ml) was added dropwise to a solution of 7-aminomethylcoumarin (0.100g, 0.57mmol) in MeCN (2ml) under N_2 atmosphere. The mixture was stirred at room temperature overnight and then it was filtered to give the desired compound as a white solid. Yield 87% (0.146 g, 0.491 mmol). ^{1}H-NMR (500 MHz,DMSO-d_6, 298K): δH: 9.19 (s, 1H); 8.83 (s, 1H); 7.67 (d, J= 8.6 Hz, 1H); 7.62 (s, 1H); 7.46 (d, J= 8.6 Hz, 2H); 7.34 (d, J= 7.9 Hz, 1H); 7.30 (t, J= 7.6 Hz, 2H); 7.00 (t, J= 7.3 Hz, 1H); 6.21 (s, 1H); 2.40(s, 3H). ^{13}C-NMR (100 MHz, DMSO- d_6, 298 K), δC: 160.09, 153.93, 153.11, 152.13, 143.37, 139.14, 128.78, 126.13, 125.86, 122.27, 118.50, 114.28, 113.75, 111.41, 111.12, 107.43, 17.93.

5.9.2 Synthetic MCM-41 hybrid nanoparticles procedure

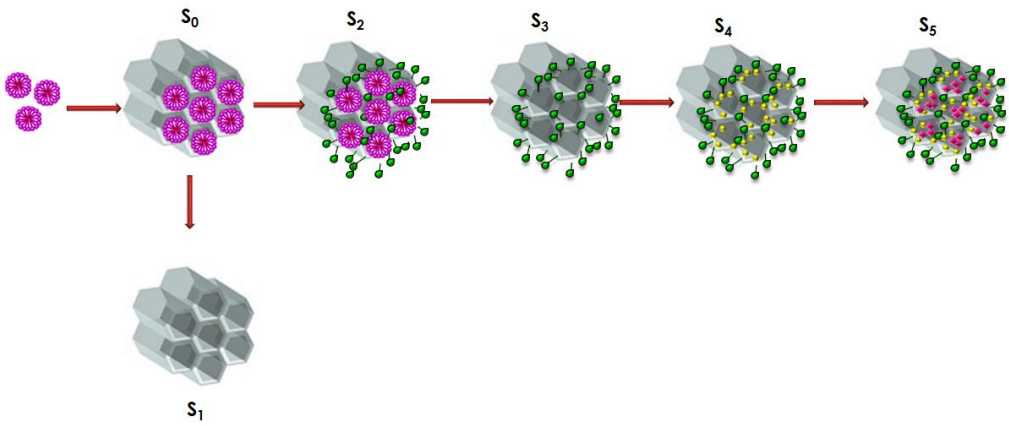

Synthesis of S_0

Mesoporous MCM-41 nanoparticles were synthesized following the procedure reported by Ramón Martínez-Máñez at All. [28] *N*-cetyltrimethylammonium bromide (CTAB, 1.00 g, 2.74 mmol) was first dissolved in deionized water (480

mL). Then, NaOH (3.5 mL, 2.00 M) in deionized water was added to the CTAB solution, followed by adjusting the temperature to 80 ºC. TEOS (5mL, 25.7 mMol) was then added dropwise. The mixture was stirred for 2 h to give a white precipitate. Finally, the solid product was centrifuged, washed with deionized water and ethanol, and dried at 60 ºC (MCM-41as-synthesized S_0).

A portion of the MCM-41 synthesized was calcined at 550 ºC using an oxidant atmosphere for 5 h in order to remove the template phase (S_1) .

Synthesis of S_2, S_3 and S_4

The hydrophobic MCM-41 nanoparticles were prepared as follows: 0.5 g of MCM-41 as-synthesized (S_0) was suspended in acetonitrile (40 mL) and 3-[Methoxy(polyethylenoxy) propyl] trimethoxy silane; 90%; 9-12 Pe units (PEG-Silane $_{[9\text{-}12]}$, 1,67 mL, 2,5 mmol) was added. The suspension was stirred for 5.5 h at room temperature with the aim of achieving the functionalization of the MCM-41scaffolding. Then, the solid (S_2) was isolated by centrifugation, washed with acetonitrile and abundant water, and dried at 37 °C for 12 h.

Then, in order to remove the CTAB excess, the extraction with HCl was carried out. At this respect, 0.5 g of this solid was suspended in 50 mL of hydrochloride acid solution in EtOH (1 M) and refluxed for 12h. This procedure was repeated 3 times, washing the solid (S_3) between each cycle with deionized water. To functionalize the internal surface, 0,341 g of the template-free solid was suspended in acetonitrile (50 mL) and hexamethyldisilazane (HMDS, 0,590 mL, 2.83 mmol) was added. The mixture was stirred 18 h at room temperature in order to achieve the maximum functionalization of the pores. Finally, the obtained solid (S_4) was isolated by centrifugation, washed with abundant water and dried at 37 °C for 12 h.

Preparation of S_5

For the preparation of loaded sensing solid S_5 , 0.06 g of solid S_4 were suspended in 5 mL of a solution of probe **L** (2.33 mg, 6.52 μmol) in acetonitrile. Then, the mixture was stirred for 12 hours at room temperature with the aim of achieving maximum loading of the pores of the MCM-41 scaffolding. Finally, the solid S_4 was isolated by centrifugation, washed with water and acetonitrile and dried under vacuum.

5.9.3 MCM-41 hybrid nanoparticles characterization

The power X-ray diffraction (PXRD) of the as-synthesised MCM-41 (S_0) (see **Figure** 5.22, curve A) shows the typical low-angle reflections that index as (100), (110), (200) and (210) Bragg peaks. From the PXRD data of the as synthesized MCM-41, a d100 spacing of 39.99 Å was calculated. A displacement of the peaks in the PXRD of the calcined MCM-41 was found corresponding to a cell contraction (Figure 5.22, curve b). This displacement and broadening are related to further condensation of silanol groups during the calcination step.

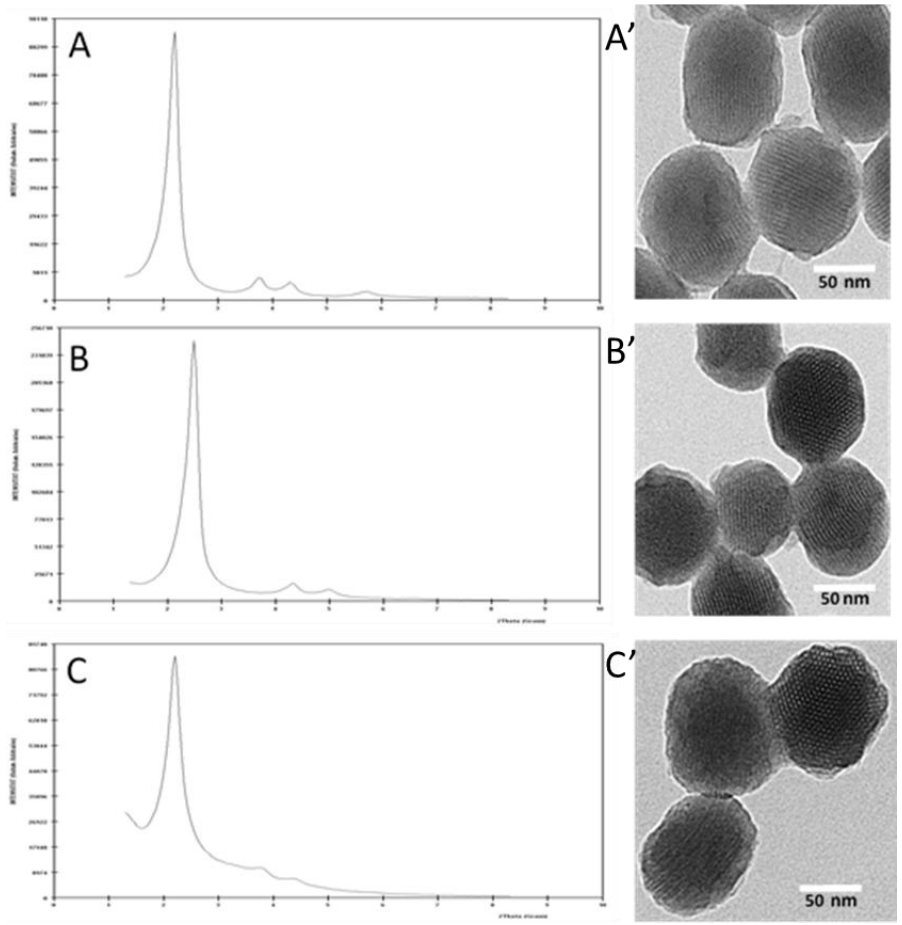

Figure 5.22 Powder X-ray patterns of the solids MCM-41 as synthesized S_0 (A), calcined MCM-41 S_1 (B) and functionalized MCM-41 S_4 (C). Right: TEM images of MCM-41 as synthesized S_0 (A'), calcined MCM-41 S_1 (B') and functionalized MCM-41 S_4 (C'), showing the typical hexagonal porosity of the MCM-41 mesoporous matrix.

By thermogravimetric and elemental analysis, a content of 0.136 g O.M./g SiO_2 (Organic material per g SiO_2) was determined for the functionalized nanoparticles S_4 while 0.169 g sensor/g SiO_2 was calculated for the loaded nanoparticles S_5.

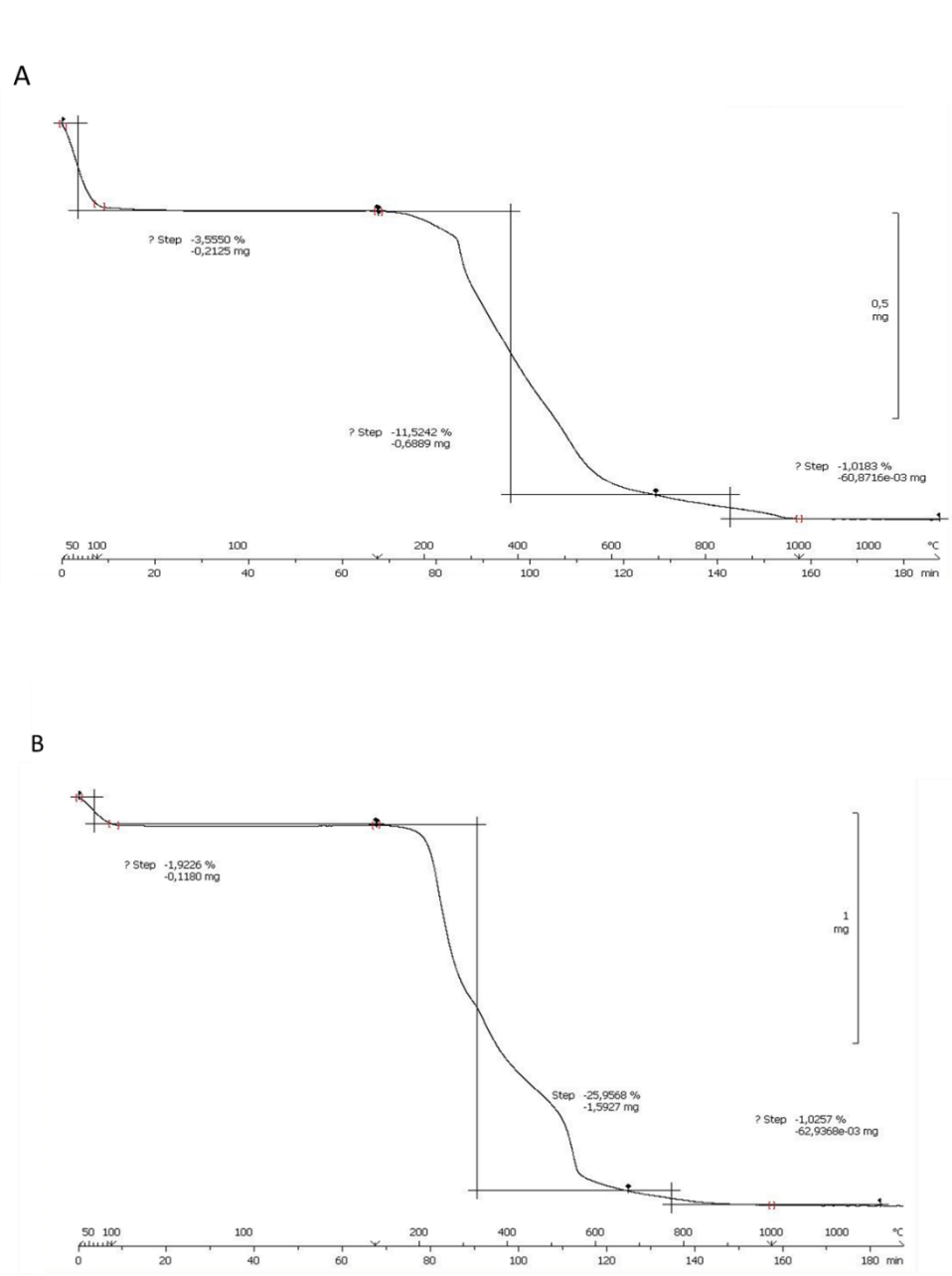

Figure 5.23 TGA results for A) functionalized nanoparticles S_4 and B) loaded nanoparticles S_5.

The N_2 adsorption-desorption isotherms of the calcined MCM-41 S_1 and functionalized nanoparticles S_4 show the typical curve for mesoporous solid; i.e. an adsorption step at intermediate P/P_0 value 0.3 (Figure 5.24, curves A and B). This step is related to the nitrogen condensation inside the mesopores by capillarity. The absence of a hysteresis loop in this interval and the narrow BJH pore distribution suggest the existence of uniform cylindrical mesopores.

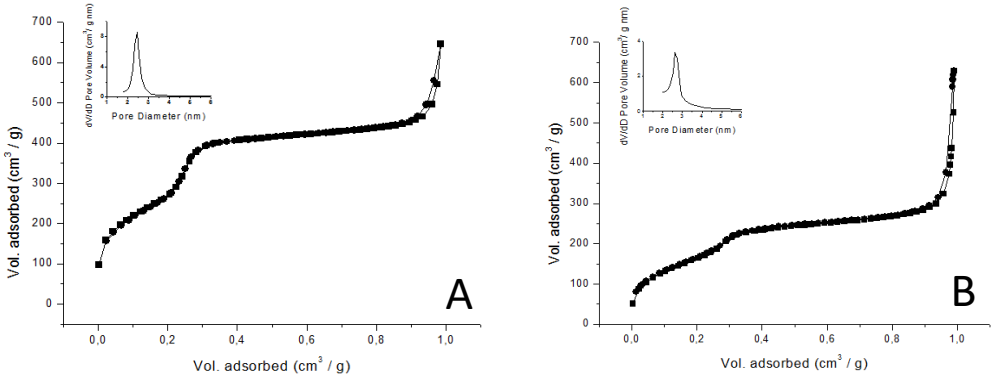

Figure 5.24 The N_2 adsorption-desorption isotherms for (A) the calcined MCM-41 mesoporous nanoparticles S1 and (B) functionalized nanoparticles S4. Inset: Pore size distribution.

N_2 adsorption-desorption isotherms for the solids S_1 and S_4 show a significant decrease in N_2 volume adsorbed as a consequence of functionalization. The pore size was estimated by using the BJH model applied on the adsorption band of the isotherm for $P/P_0 < 0.6$. Total pore volume was also calculated according to BJH model. BET specific values, pore volumes and pore sizes calculated from N_2 adsorption-desorption isotherms for selected materials are reported in Table 5.2.

Table 5.2 BET specific surface values, pore volumes and pore sizes calculated from N_2 adsorption-desorption isotherms for selected materials.

	S1 **Calcinated nanoparticles**	**S4** **Functionalized nanoparticles**
S_{BET} ($m^2\ g^{-1}$)	1004.5	0.764
Pore V [a] ($cm^3\ g^{-1}$)	0.764	0.460
Pore size [a] (nm)	2.53	2.65

[a] Pore volume and Pore size estimated by using the BJH model applied to the adsorption branch of the isotherm, for $P/P_0 < 0.6$, which can be associated with the surfactant-generated mesopores.

From the PXRD, porosimetry and TEM studies the a_0 cell parameter and a value for the wall thickness D_w reported in Table 5.3 can be calculated.

Table 5.3 The a_0 cell parameters and the values of wall thickness D_w calculated from PXRD, porosimetry and TEM studies for S_1 and S_4 MCM-41 nanoparticles.

	S1 **Calcinated nanoparticles**	**S4** **Functionalized nanoparticles**
a_0 (Å)	41.04	46.18
D_w (nm)	1.6	1.9

The thermal analysis of S_4 and S_5 shows a typical behaviour of functionalized mesoporous materials, that is, an initial weight loss between 50 and 150 °C related to solvent evaporation, a second loss between 150 and 800 °C due to the

combustion of organic material, and a final loss in the 800-1000 °C range related to the condensation of the silanol groups. The loading of the final solid S_5 was determined by elemental analysis and thermogravimetric studies. A ratio of 0,473 mmol **L**/g SiO_2 was calculated.

5.9.4 Crystallographic Data

Table 5.4 Crystal data and structure refinement details of $L_{32\text{-}CN}^-$

Empirical formula	C18H13N3O2
Formula weight	303.31
Crystal system	Monoclinic
Space group	P 21/n
Unit cell dimensions	a = 18.832(3) Å α = 90°
	b = 3.8846(6) Å β = 115.297(17) °
	c = 20.977(3) Å γ = 90°
Z	4
Crystal	prism; yellow.
θ range for data collection	4.1460- 74.6240°
Index ranges	$-22 \leq h \leq 20$, $-4 \leq k \leq 4$, $-16 \leq l \leq 25$
Reflections collected	5060
Independent reflections	2502 [R_{int} = 0.0935]
Completeness to θ = 66.97°	99.81%
Absorption correction	Multi-scan
Max. and min. transmission	0.74927and 0.76233
Refinement method	Full-matrix least-squares on F^2
Data / restraints / parameters	2502/ 0/ 213
Goodness-of-fit on F^2	1.076
Final *R* indices [$F^2 > 2\sigma(F^2)$]	*R1* = 0.0742, *wR2* = 0.1816
***R* indices (all data)**	*R1* = 0.0935, *wR2* = 0.1972

Equipment details: Single crystal X-ray diffractometer Rigaku Oxford Diffraction SuperNovaII; Atlas S2 CCD detector.

References

1. Fernandes, A. P.; Gandin, V., Selenium compounds as therapeutic agents in cancer. *Biochimica et Biophysica Acta (BBA)-General Subjects* **2015,** *1850* (8), 1642-1660.

2. Merino-Montiel, P.; Maza, S.; Martos, S.; López, Ó.; Maya, I.; Fernández-Bolaños, J. G., Synthesis and antioxidant activity of O-alkyl selenocarbamates, selenoureas and selenohydantoins. *European Journal of Pharmaceutical Sciences* **2013,** *48* (3), 582-592.

3. Panda, S.; Panda, A.; Zade, S. S., Organoselenium compounds as fluorescent probes. *Coordination Chemistry Reviews* **2015,** *300*, 86-100.

4. Zhu, B.; Zhang, X.; Jia, H.; Li, Y.; Liu, H.; Tan, W., A highly selective ratiometric fluorescent probe for 1, 4-dithiothreitol (DTT) detection. *Organic & biomolecular chemistry* **2010,** *8* (7), 1650-1654.

5. Lou, Z.; Li, P.; Pan, Q.; Han, K., A reversible fluorescent probe for detecting hypochloric acid in living cells and animals: utilizing a novel strategy for effectively modulating the fluorescence of selenide and selenoxide. *Chemical Communications* **2013,** *49* (24), 2445-2447.

6. Lou, Z.; Yang, S.; Li, P.; Zhou, P.; Han, K., Experimental and theoretical study on the sensing mechanism of a fluorescence probe for hypochloric acid: a Se⋯ N nonbonding interaction modulated twisting process. *Physical Chemistry Chemical Physics* **2014,** *16* (8), 3749-3756.

7. Li, Y.; He, S.; Lu, Y.; Zeng, X., Novel hemicyanine dye as colorimetric and fluorometric dual-modal chemosensor for mercury in water. *Organic & biomolecular chemistry* **2011,** *9* (8), 2606-2609.

8. Huang, S.; He, S.; Lu, Y.; Wei, F.; Zeng, X.; Zhao, L., Highly sensitive and selective fluorescent chemosensor for Ag+ based on a coumarin–Se 2 N chelating conjugate. *Chemical Communications* **2011,** *47* (8), 2408-2410.

9. Wang, B.; Yu, F.; Li, P.; Sun, X.; Han, K., A BODIPY fluorescence probe modulated by selenoxide spirocyclization reaction for peroxynitrite detection and imaging in living cells. *Dyes and Pigments* **2013,** *96* (2), 383-390.

10. Manjare, S. T.; Kim, S.; Heo, W. D.; Churchill, D. G., Selective and sensitive superoxide detection with a new diselenide-based molecular probe in living breast cancer cells. *Organic letters* **2013,** *16* (2), 410-412.

11. Goswami, S.; Hazra, A.; Chakrabarty, R.; Fun, H.-K., Recognition of carboxylate anions and carboxylic acids by selenium-based new chromogenic fluorescent sensor: A remarkable fluorescence enhancement of hindered carboxylates. *Organic letters* **2009,** *11* (19), 4350-4353.

12. López, Ó.; Maza, S.; Ulgar, V.; Maya, I.; Fernández-Bolaños, J. G., Synthesis of sugar-derived isoselenocyanates, selenoureas, and selenazoles. *Tetrahedron* **2009,** *65* (12), 2556-2566.

13. Kadam, S. A.; Martin, K.; Haav, K.; Toom, L.; Mayeux, C.; Pung, A.; Gale, P. A.; Hiscock, J. R.; Brooks, S. J.; Kirby, I. L., Towards the Discrimination of Carboxylates by Hydrogen-Bond Donor Anion Receptors. *Chemistry–A European Journal* **2015,** *21* (13), 5145-5160.

14. Kadam, S. A.; Haav, K.; Toom, L.; Haljasorg, T. i.; Leito, I., NMR Method for Simultaneous Host–Guest Binding Constant Measurement. *The Journal of organic chemistry* **2014,** *79* (6), 2501-2513.

15. Etter, M. C.; Urbanczyk-Lipkowska, Z.; Zia-Ebrahimi, M.; Panunto, T. W., Hydrogen bond-directed cocrystallization and molecular recognition properties of diarylureas. *Journal of the American Chemical Society* **1990,** *112* (23), 8415-8426.

16. Lu, A.; Wang, Z.; Zhou, Z.; Chen, J.; Wang, Q., Application of "hydrogen bonding interaction" in new drug development: Design, synthesis, antiviral activity, and SARs of thiourea derivatives. *Journal of agricultural and food chemistry* **2015,** *63* (5), 1378-1384.

17. Amendola, V.; Fabbrizzi, L.; Mosca, L., Anion recognition by hydrogen bonding: urea-based receptors. *Chemical Society Reviews* **2010,** *39* (10), 3889-3915.

18. Blažek Bregović, V.; Basarić, N.; Mlinarić-Majerski, K., Anion binding with urea and thiourea derivatives. *Coordination Chemistry Reviews* **2015,** *295*, 80-124.

19. Gale, P. A.; Caltagirone, C., Anion sensing by small molecules and molecular ensembles. *Chemical Society Reviews* **2015,** *44* (13), 4212-4227.

20. Bregović, V. B.; Basarić, N.; Mlinarić-Majerski, K., Anion binding with urea and thiourea derivatives. *Coordination Chemistry Reviews* **2015,** *295*, 80-124.

21. Gans, P.; Sabatini, A.; Vacca, A., Investigation of equilibria in solution. Determination of equilibrium constants with the HYPERQUAD suite of programs. *Talanta* **1996,** *43* (10), 1739-1753.

22. Wirth, T., Chiral selenium compounds in organic synthesis. *Tetrahedron* **1999,** *55* (1), 1-28.

23. Mukherjee, A. J.; Zade, S. S.; Singh, H. B.; Sunoj, R. B., Organoselenium Chemistry: Role of Intramolecular Interactions†. *Chemical reviews* **2010,** *110* (7), 4357-4416.

24. Metanis, N.; Hilvert, D., Strategic Use of Non-Native Diselenide Bridges to Steer Oxidative Protein Folding. *Angewandte Chemie International Edition* **2012,** *51* (23), 5585-5588.

25. Nascimento, V.; Ferreira, N. L.; Canto, R. F.; Schott, K. L.; Waczuk, E. P.; Sancineto, L.; Santi, C.; Rocha, J. B.; Braga, A. L., Synthesis and biological evaluation of new nitrogen-containing diselenides. *European journal of medicinal chemistry* **2014,** *87*, 131-139.

26. Sancineto, L.; Piccioni, M.; De Marco, S.; Pagiotti, R.; Nascimento, V.; Braga, A. L.; Santi, C.; Pietrella, D., Diphenyl diselenide derivatives inhibit microbial biofilm formation involved in wound infection. *BMC microbiology* **2016,** *16* (1), 220.

27. Climent, E.; Martínez-Máñez, R.; Sancenón, F.; Marcos, M. D.; Soto, J.; Maquieira, A.; Amorós, P., Controlled Delivery Using Oligonucleotide-Capped Mesoporous Silica Nanoparticles. *Angewandte Chemie* **2010,** *122* (40), 7439-7441.

28. Santos-Figueroa, L. E.; Giménez, C.; Agostini, A.; Aznar, E.; Marcos, M. D.; Sancenón, F.; Martínez-Máñez, R.; Amorós, P., Selective and sensitive chromofluorogenic detection of the sulfite anion in water using hydrophobic hybrid organic–inorganic silica nanoparticles. *Angewandte Chemie* **2013,** *125* (51), 13957-13961.